

**Electrical responses
of oligodendrocytes
to pathological stimuli**

Karolina Kołodziejczyk

A thesis submitted to University College London
for the degree of
Doctor of Philosophy

Department of Neuroscience, Physiology and Pharmacology
University College London
May 2011

Statement of the candidate's contribution to this thesis

All of the work in this thesis was carried out by Karolina Kołodziejczyk, with the single exception described below. She was responsible, with normal supervisory input, for planning the work, carrying out the electrophysiological, immunocytochemical and calcium imaging experiments, and analysing and interpreting all the data she collected.

In chapter 6, the experiments were conducted and data were collected and analysed together with Dr Nicola Hamilton. Karolina Kołodziejczyk carried out 60% of the work (this has been published, together with the data from Chapter 5, as Kołodziejczyk *et al.*, 2009, *Brain* 132 (Pt 6), 1496-1508).

Karolina Kołodziejczyk wrote the entire thesis.

Signed: David Attwell, Jodrell Professor of Physiology, PhD Supervisor

Karolina Kołodziejczyk

Abstract

The white matter is crucial for rapid transmission of information between different parts of the brain and spinal cord, and is damaged in diseases including the genetic leukodystrophies, stroke, spinal cord injury and multiple sclerosis. While damage in the grey matter of the CNS is well known to often involve over-activation of glutamate receptors, our understanding of white matter pathology is less advanced. The experiments in this thesis used patch-clamping and $[Ca^{2+}]_i$ imaging to examine the cerebellar white matter oligodendrocyte response to pathological insults mimicking those occurring in the leukodystrophies and in the ischaemia that occurs in stroke or after spinal cord injury.

Oligodendrocytes responded to simulated ischaemia with an inward current, which was triggered by glutamate release mediated by reversal of glutamate transporters, and not by exocytosis, NKCC1 or cystine/glutamate exchange. Surprisingly, this inward current was not mediated by glutamate receptors, nor by ASICs, gap junctional hemichannels, P2X receptors or GABA_A receptors, but reflected the closing of potassium channels. In current clamp mode this initial closing of K⁺ channels produced a depolarisation of the cells, followed by a repolarisation as other K⁺ channels activated. These data indicate, for the first time, a significant role for K⁺ channels in the response of oligodendrocytes to ischaemia.

In Canavan and Pelizaeus-Merzbacher-like leukodystrophies, elevated levels of N-acetylaspartylglutamate (NAAG) and N-acetylaspartate (NAA) occur. These compounds can activate or block neuronal NMDA receptors. Since oligodendrocytes are reported to express NMDA receptors, I tested their response to NAAG and NAA. NAAG, but not NAA, evoked a small inward NMDA receptor-mediated current in oligodendrocytes, but no $[Ca^{2+}]_i$ rise. Much of the inward current was a secondary effect of NAAG acting on neurons. Thus, actions of NAAG and NAA on oligodendrocyte NMDARs are unlikely to be a major contributor to white matter damage in the leukodystrophies.

Table of contents

Abstract.....	3
Table of contents.....	4
List of figures.....	10
List of tables.....	17
Acknowledgements.....	18
Dedication.....	19
Chapter 1: Introduction.....	20
1.1 White matter and its role in CNS function.....	20
1.2 Oligodendrocytes and their role in the white matter.....	20
1.2.1. Oligodendrocyte development.....	21
1.2.2. Neuron-glia interaction at the node of Ranvier.....	23
1.2.3. The classification of mature oligodendrocytes.....	24
1.2.4. The structure and role of cerebellum.....	25
1.3 Channel and receptor expression by oligodendrocytes.....	27
1.3.1. Ion channels.....	28
1.3.1.1. Voltage-gated sodium channels.....	28
1.3.1.2. Voltage-gated calcium channels.....	28
1.3.1.3. Potassium channels.....	29
1.3.1.4. Acid-sensing ion channels (ASICs).....	30
1.3.1.5. Transient receptor potential (TRP) channels.....	31
1.3.1.6. Gap junctions and hemichannels.....	32
1.3.2. Receptors expressed by oligodendrocytes.....	34
1.3.2.1. Glutamate receptors.....	34
1.3.2.1.1. AMPA/KA receptors.....	34
1.3.2.1.2. NMDA receptors.....	36
1.3.2.1.3. Metabotropic glutamate receptors.....	38
1.3.2.2. GABA receptors.....	39
1.3.2.3. Purinergic receptors.....	40
1.4 Pathology of white matter and the role of oligodendrocytes.....	41
1.4.1. Multiple sclerosis.....	42
1.4.2. The pathology of white matter ischaemia.....	44

1.4.2.1.	An overview of the grey matter ischaemia.....	45
1.4.2.1.1.	Energy failure.....	45
1.4.2.1.2.	Ionic imbalance.....	45
1.4.2.1.3.	Glutamate release and excitotoxicity.....	46
1.4.2.1.4.	Calcium influx.....	46
1.4.2.1.5.	Formation of reactive radicals.....	48
1.4.2.1.6.	Acidotoxicity.....	49
1.4.2.2.	The white matter oligodendrocyte response to ischaemia...	49
1.4.2.2.1.	The mechanism of ischaemic glutamate release in the white matter.....	50
1.4.2.2.2.	Oligodendrocyte glutamate receptor activation in ischaemia.....	52
1.4.2.2.3.	Ischaemia-induced calcium influx in oligodendrocytes..	53
1.4.2.2.4.	Additional factors that may influence the oligodendrocyte response to ischaemia.....	55
1.4.3.	Leukodystrophies.....	56
1.4.3.1.	Canavan and Pelizaeus-Merzbacher-like diseases.....	56
1.4.3.2.	The role of NAA and NAAG in CNS physiology and pathology.....	57
1.4.3.2.1.	The NAA and NAAG cycle in the brain.....	58
1.4.3.2.2.	Receptors for NAA and NAAG.....	59
1.4.3.2.3.	The physiological role of NAA.....	59
1.4.3.2.4.	The physiological role of NAAG.....	60
1.4.3.2.5.	The possible role of NAA and NAAG in the leukodystrophies.....	61
1.5	The aims of this thesis.....	61

Chapter 2: Materials and methods.....85

2.1	Preparation of cerebellar slices.....	85
2.2	Standard solutions used and model system for ischaemia.....	86
2.2.1	External solutions used.....	86
2.2.2	Internal solutions used.....	86
2.2.3	Ischaemic solution used.....	87
2.3	Pipettes and electrical set-up.....	87

2.4	Optical set-up for electrophysiology.....	88
2.5	Dye filling and cell identification.....	88
2.6	Patch-clamp recordings.....	89
2.7	Series resistance.....	90
2.8	Capacity transient analysis.....	91
2.9	Calcium imaging.....	93
2.9.1	Calcium imaging using acetoxymethyl ester dye loading.....	93
2.9.2	Calcium imaging of single cells.....	93
2.9.3	Optical set-up for calcium imaging.....	94
2.10	Cell death assay.....	94
2.11	Immunocytochemistry.....	95
2.11.1	Antibody labelling.....	95
2.11.2	Confocal imaging.....	95
2.12	Data analysis and statistics.....	96

Chapter 3: The electrical response of white matter oligodendrocytes to simulated ischaemia.....106

3.1	Introduction.....	106
3.2	Materials and methods.....	107
3.2.1	Brain slice preparation.....	107
3.2.2	Patch-clamping.....	107
3.2.3	Current and voltage analysis during anoxic depolarisation.....	107
3.2.4	Capacitance measurement.....	108
3.2.5	Membrane resistance and conductance measurements.....	108
3.2.6	Statistics.....	109
3.3	Results.....	109
3.3.1	Ischaemia evokes an inward current in mature oligodendrocytes.....	109
3.3.2	The amplitude of the ischaemia-evoked inward current depends on the developmental stage of the cell.....	110
3.3.3	Using K ⁺ instead of Cs ⁺ as the main intracellular cation does not affect the ischaemia-evoked current, but reduces the ischaemia-evoked voltage change.....	110

3.3.4	The time needed for ischaemia to alter the oligodendrocyte membrane current.....	112
3.3.5	The membrane resistance increases during ischaemia.....	113
3.3.6	Cell capacitance does not change significantly in mature oligodendrocytes during ischaemia.....	114
3.3.7	The membrane resistance increase reflects a loss of K ⁺ conductance.....	116
3.4	Discussion.....	118

Chapter 4: The role of glutamate in the oligodendrocyte response to ischaemia.....134

4.1	Introduction.....	134
4.2	Materials and methods.....	135
4.2.1	Brain slice preparation.....	135
4.2.2	Patch-clamping.....	136
4.2.3	Statistics.....	136
4.3	Results.....	136
4.3.1	Glutamate is a major trigger of the ischaemia-evoked current in white matter oligodendrocytes.....	136
4.3.2	Glutamate is released by reversed transport in white matter ischaemia.....	138
4.3.3	The contribution of gap junctional hemichannel opening and activation of P2X ₇ receptors to the ischaemia-induced current in oligodendrocytes.....	141
4.3.4	ASICs, GABA _A receptors and neuronal action potentials do not influence the oligodendrocyte response to ischaemia.....	142
4.3.5	Ionotropic glutamate receptor block does not inhibit the ischaemia-evoked current when applied after the start of ischaemic insult.....	143
4.3.6	The mechanism of the extended inward current in oligodendrocytes is different from that producing the END in neurons.....	144
4.4	Discussion.....	145

Chapter 5: Oligodendroglial and neuronal electrical responses to NAA and NAAG.....	178
5.1 Introduction.....	178
5.2 Materials and methods.....	179
5.2.1 Brain slice preparation.....	179
5.2.2 Patch-clamping.....	179
5.2.3 Statistics.....	180
5.3 Results.....	180
5.3.1 The effect of NAA and NAAG on oligodendrocyte and granule cell currents.....	180
5.3.2 Pharmacology of the NAAG-evoked current.....	181
5.3.3 Part of the oligodendrocyte NAAG response is produced by hydrolysis to glutamate.....	182
5.3.4 The NAAG response in oligodendrocytes is partly produced by neuronal action potentials.....	183
5.3.5 NAAG and NAA are not strong blockers of NMDA receptors.....	183
5.3.6 The effect of pathologically relevant levels of NAAG.....	184
5.4 Discussion.....	184
Chapter 6: Oligodendroglial and neuronal $[Ca^{2+}]_i$ changes in response to NAA and NAAG.....	198
6.1 Introduction.....	198
6.2 Materials and methods.....	199
6.2.1 Brain slice preparation.....	199
6.2.2 Patch-clamping.....	199
6.2.3 $[Ca^{2+}]_i$ imaging with Fluo-4-AM.....	199
6.2.4 Single cell $[Ca^{2+}]_i$ imaging.....	200
6.2.5 Cell death assay.....	200
6.2.6 Confocal microscopy.....	200
6.2.7 Statistics.....	200
6.3 Results.....	201
6.3.1 Effects of NAAG and NAA on $[Ca^{2+}]_i$ in the white matter and grey matter.....	201

6.3.2	Block of NAAG-evoked $[Ca^{2+}]_i$ rise in the white matter and grey matter.....	201
6.3.3	The effect of NAAG on $[Ca^{2+}]_i$ in oligodendrocytes and granule cells.....	202
6.3.4	The effect of pathologically relevant levels of NAAG.....	203
6.3.5	The effect of NAAG on cell death in white matter and grey matter.....	203
6.4	Discussion.....	204
Chapter 7: Discussion.....		213
7.1	The electrical response of white matter oligodendrocytes to simulated ischaemia.....	213
7.1.1	Discussion.....	213
7.1.2	Suggestions for the further work.....	214
7.2	The role of glutamate in the oligodendrocyte response to ischaemia..	215
7.2.1	Discussion.....	215
7.2.2	Suggestions for the further work.....	216
7.3	Oligodendroglial and neuronal electrical responses to NAA and NAAG.....	217
7.3.1	Discussion.....	217
7.3.2	Suggestions for the further work.....	218
7.4	Oligodendroglial and neuronal $[Ca^{2+}]_i$ changes in response to NAA and NAAG.....	218
7.4.1	Discussion.....	219
7.4.2	Suggestions for the further work.....	219
7.5	Conclusion.....	220
Chapter 8: Bibliography.....		224

List of figures

Figure 1.1	Coronal section of the human cerebral cortex.....	66
Figure 1.2	Confocal image of a mature Lucifer yellow-filled oligodendrocyte in the white matter of the cerebellum of a P12 rat.....	67
Figure 1.3	An electron micrograph showing myelinated axons in the optic nerve.....	68
Figure 1.4	Changes in morphology and expression of different antigenic markers at different developmental stages of oligodendrocytes.....	69
Figure 1.5	Oligodendrocyte interaction with axons at the node of Ranvier with the oligodendrocyte shown in blue and the axon in yellow.....	70
Figure 1.6	Drawing of white matter oligodendrocytes after staining with silver carbonate, by del Rio Hortega (1928) (see section 1.2.3).....	71
Figure 1.7	Synaptic organization of the cerebellar cortex.....	72
Figure 1.8	NMDA receptor subunits are expressed in the myelinating processes of cerebellar oligodendrocytes.....	73
Figure 1.9	Demyelination and remyelination in multiple sclerosis.....	74
Figure 1.10	The reversal of sodium-dependent glutamate transporters in ischaemia.....	75
Figure 1.11	Mechanisms of intracellular calcium concentration rise during ischaemia.....	76
Figure 1.12	The formation of the free radicals during ischaemia.....	77
Figure 1.13	During anoxia, in the white matter, axons and oligodendrocytes release glutamate by the reversal of sodium-dependent glutamate transporters.....	78
Figure 1.14	Ionotropic glutamate receptors on cerebellar oligodendrocyte lineage cells are activated during ischaemia.....	79
Figure 1.15	Ischaemia activates purinergic P2X ₇ receptors in cultured oligodendrocytes.....	80
Figure 1.16	Metabolic pathways of NAA and NAAG.....	81
Figure 1.17	NAA is transported from axons to oligodendrocytes where it is transformed into lipids in the myelin sheath.....	82
Figure 1.18	NAAG acts on neuronal NMDA receptors.....	83

Figure 1.19	NAAG can antagonize glutamate's action on NMDA receptors.....	84
Figure 2.1	Patch-clamping of a cerebellar white matter mature oligodendrocyte in a P12 rat.....	100
Figure 2.2	Confirmation of mature oligodendrocyte phenotype with immunostaining.....	101
Figure 2.3	A junction potential exists at any interface between different solutions, such as between the pipette solution and the bath solution.....	102
Figure 2.4	Capacity transient of a spatially compact cell such as a granule cell.....	103
Figure 2.5	Capacity transient of a complex cell such as a mature oligodendrocyte cell which is not voltage-uniform.....	104
Figure 2.6	Using the acetoxymethyl (AM) ester form of a Ca^{2+} -sensing dye...	105
Figure 3.1	Mature oligodendrocyte response to ischaemia.....	122
Figure 3.2	The size of the ischaemia-induced current in oligodendrocyte lineage cells depends on the developmental stage of the cell.....	123
Figure 3.3	The time course and amplitude of the ischaemia-induced current in mature oligodendrocytes is independent of the main ion used in the internal solution.....	124
Figure 3.4	The time course and amplitude of the ischaemia-induced voltage response in mature oligodendrocytes (recorded in current-clamp mode) depends strongly on the main ion used in the internal solution.....	125
Figure 3.5	The time to reach the peak of the ischaemia-evoked response in oligodendrocytes does not depend on the clamp mode used nor on the main ion present in the internal solution.....	126
Figure 3.6	Variability in the peak amplitude and the time to peak of the ischaemia-induced inward current in oligodendrocytes.....	127
Figure 3.7	The membrane resistance (R_m) increases in oligodendrocytes during ischaemia.....	128
Figure 3.8	Change in oligodendrocyte membrane capacitance (C_m) during ischaemia, measured by fitting a monoexponential decay to the capacity transient evoked by a 5 mV voltage step and deriving the parameters from the eqn. 2.6.....	129

Figure 3.9	Results of fitting the capacity current transients with the sum of two exponentials, a fast exponential with amplitude A_1 (mean initial value -206 ± 53 pA in 20 cells) and time constant τ_1 (mean initial value 657 ± 141 μ sec), and a slow exponential with amplitude A_2 (mean initial value -73 ± 13 pA) and time constant τ_2 (mean initial value 11 ± 2 msec).....	130
Figure 3.10	Membrane current response of a mature oligodendrocyte to voltage steps, using a Cs^+ -based internal solution.....	131
Figure 3.11	Membrane current response of a mature oligodendrocyte to voltage steps, using a K^+ -based internal solution.....	132
Figure 3.12	Ischaemia evokes a decrease in the oligodendrocyte membrane conductance.....	133
Figure 4.1	Combined application of the AMPA/KA receptor blocker NBQX ($25 \mu\text{M}$) and the NMDA receptor blocker AP5 ($50 \mu\text{M}$) significantly reduces the ischaemia-induced current in oligodendrocytes.....	149
Figure 4.2	Comparison of the mean values for the peak of the ischaemia-induced inward current (measured for each cell and then averaged over all cells in the same condition), for control cells and for cells with NBQX and AP5 applied, shows that ionotropic glutamate receptor blockers significantly reduced the ischaemia-induced current.....	150
Figure 4.3	Effect of the AMPA/KA receptor blocker, NBQX ($25 \mu\text{M}$), applied alone, on the ischaemia-induced current in oligodendrocytes.....	151
Figure 4.4	Effect of the NMDA receptor blocker, D-AP5 ($200 \mu\text{M}$), applied alone, on the ischaemia-induced current in oligodendrocytes.....	152
Figure 4.5	Comparison of the mean values for the peak of the ischaemia-induced inward current (measured for each cell and then averaged over all cells in the same condition), for control cells and for cells with either NBQX ($25 \mu\text{M}$) or AP5 ($200 \mu\text{M}$) applied alone, shows that these blockers did not significantly affect the size of the current.....	153
Figure 4.6	The metabotropic glutamate receptor blocker, MCPG (1 mM), significantly reduced the ischaemia-induced current in oligodendrocytes.....	154

Figure 4.7	MCPG (1 mM) significantly blocks the ischaemia-induced current in oligodendrocytes.....	155
Figure 4.8	Preloading with the Na ⁺ -dependent glutamate transporter antagonist, PDC (1 mM), significantly reduces the ischaemia-induced current in oligodendrocytes.....	156
Figure 4.9	The peak ischaemia-induced current is reduced by preloading with the glutamate transport blocker PDC (1 mM).....	157
Figure 4.10	Effect of the NKCC1 co-transporter blocker, bumetanide (50 μM), on the ischaemia-induced current in oligodendrocytes.....	158
Figure 4.11	Effect of the voltage-gated calcium channel blocker cadmium (Cd ²⁺ , 100 μM) which blocks exocytosis, on the ischaemia-induced current in oligodendrocytes.....	159
Figure 4.12	Effect of the cystine-glutamate exchanger (X _C ⁻) blocker, CPG (50 μM) on the ischaemia-induced current in oligodendrocytes....	160
Figure 4.13	Comparison of the mean values for the peak of the ischaemia-induced inward current (measured for each cell and then averaged over all cells in the same condition) for all the 179 control cells and for cells with the different blockers applied shows that bumetanide (50 μM), Cd ²⁺ (100 μM) and CPG (100 μM) had no effect on the peak ischaemia-evoked current.....	161
Figure 4.14	Comparison of the mean value for the peak of the ischaemia-induced inward current (measured for each cell and then averaged over all cells in the same condition) in the presence of various candidate drugs to block glutamate release and in interleaved control cells studied on the same day as each drug was studied. The blockers used were bumetanide (50 μM), Cd ²⁺ (100 μM) and CPG (100 μM).....	162
Figure 4.15	Effect of the gap junctional hemichannel blocker, lanthanum (100 μM) on the ischaemia-induced current in oligodendrocytes...	163
Figure 4.16	Effect of the P2X ₇ receptor blocker, BBG (10 μM) on the ischaemia-induced current in oligodendrocytes.....	164
Figure 4.17	Effect of the gap junctional hemichannel blocker La ³⁺ (100 μM) and the P2X ₇ receptor blocker BBG (10 μM) on the peak ischaemia-evoked current (measured in each cell and then averaged across cells).....	165

Figure 4.18	Effect of the ASIC blocker amiloride (100 μ M) on the ischaemia-induced current in oligodendrocytes.....	166
Figure 4.19	Effect of the action potential blocker TTX (1 μ M) on the ischaemia-induced current in oligodendrocytes.....	167
Figure 4.20	Effect of the GABA _A receptor blocker bicuculline (100 μ M) on the ischaemia-induced current in oligodendrocytes.....	168
Figure 4.21	Comparison of the mean peak ischaemia-induced inward current of all 179 control cells with the mean peak current with the blockers applied shows that amiloride (100 μ M), TTX (1 μ M) and bicuculline (100 μ M) had no effect on the size of the peak of the ischaemic response.	169
Figure 4.22	Comparison of the mean peak ischaemia-induced inward current in interleaved control cells (studied on the same day as the blockers) with the peak current evoked in the blockers shows that amiloride (100 μ M), TTX (1 μ M) and bicuculline (100 μ M) had no effect on the size of the peak ischaemia-evoked current.....	170
Figure 4.23	The AMPA/KA receptor blocker NBQX (25 μ M) and NMDA receptor blocker AP5 (50 μ M) do not block the ischaemia-induced current in oligodendrocytes once it has started. NBQX and AP5 were applied ~3.5 min after the start of ischaemia.....	171
Figure 4.24	Comparison of the averaged peak ischaemia-induced current in control cells and in cells with NBQX (25 μ M) and AP5 (50 μ M) applied ~3.5 min after the start of ischaemia shows that the ionotropic receptor blockers had no effect on the peak response.....	172
Figure 4.25	The extended neuronal depolarization (END) blocker, gadolinium (100 μ M), when applied from ~4 min after the start of ischaemia, does not block the ischaemia-induced current in oligodendrocytes.....	173
Figure 4.26	The extended neuronal depolarization (END) blocker, gadolinium (100 μ M), when applied throughout ischaemia, does not block the ischaemia-induced current in oligodendrocytes.....	174
Figure 4.27	The omission of calcium (with 50 μ M EGTA added to bind trace calcium) throughout ischaemia, which blocks the extended neuronal depolarization in neurons, does not block the ischaemia-induced current in oligodendrocytes.....	175

Figure 4.28	Average peak ischaemia-induced inward current for all 179 control cells and for 3 cells studied with Gd^{3+} present from ~4 min after the start of ischaemia, 7 cells studied with Gd^{3+} present throughout ischaemia and 6 cells studied in the absence of extracellular Ca^{2+} throughout ischaemia.	176
Figure 4.29	Comparing the peak ischaemia-induced inward current for manipulations that block the END and for interleaved control cells shows that Gd^{3+} (100 μ M) applied after the start or throughout ischaemia, as well as the omission of extracellular Ca^{2+} throughout ischaemia (with EGTA, 50 μ M), had no significant effect on the size of the peak ischaemia-evoked current.....	177
Figure 5.1	NAAG, NAA and NMDA-evoked whole cell currents at -74 mV in white matter oligodendrocytes and cerebellar granule cells.....	187
Figure 5.2	The NMDA receptor blocker, D-AP5 (100 μ M), significantly reduces the oligodendrocyte response to NAAG.....	188
Figure 5.3	The metabotropic glutamate receptor type 3 blocker, EGLU, does not block the NAAG-evoked current in white matter oligodendrocytes, but to a small extent blocks the current in granule cells.....	189
Figure 5.4	The NMDA receptor blocker, AP5, significantly blocked the response to NAA in cerebellar granule cells.....	190
Figure 5.5	The effect of blocking carboxypeptidases on the NAAG-evoked current at -74 mV in white matter oligodendrocytes.....	191
Figure 5.6	The carboxypeptidase blocker 2-PMPA does not significantly block the NAAG-evoked current at -74 mV in cerebellar granule cells...	192
Figure 5.7	The action potential blocker, TTX, partially blocks the NAAG-evoked current at -74 mV in white matter oligodendrocytes, but has no effect on the current in cerebellar granule cells.....	193
Figure 5.8	Test of block of the NMDA-evoked current at -74 mV by NAAG and NAA in white matter oligodendrocytes.....	194
Figure 5.9	Test of block of the NMDA-evoked current at -74 mV by NAAG and NAA in cerebellar granule cells.....	195

Figure 5.10	The current response of white matter oligodendrocytes and cerebellar granule cells to pathologically relevant concentrations of NAAG, 50 μ M, 200 μ M and 1 mM, in 0 mM Mg^{2+} solution.....	196
Figure 5.11	The current response of white matter oligodendrocytes to pathologically relevant concentrations of NAAG, 200 μ M and 1 mM, in 1 mM Mg^{2+} solution with no added glycine.....	197
Figure 6.1	Change in $[Ca^{2+}]_i$ in the white and grey matter on application of NAA (1 mM), NAAG (1 mM) and NMDA (60 μ M).....	206
Figure 6.2	Block of NAAG-induced rise in $[Ca^{2+}]_i$ in white and grey matter by D-AP5 (100 μ M).....	207
Figure 6.3	The group II mGluR blocker EGLU (200 μ M) did not reduce the NAAG-induced $[Ca^{2+}]_i$ rise in the white matter, but produced a small but significant decrease in the NAAG-evoked $[Ca^{2+}]_i$ rise in the grey matter.....	208
Figure 6.4	No detectable changes occurred in $[Ca^{2+}]_i$ in oligodendrocytes after NAAG (1 mM) application.....	209
Figure 6.5	NAAG-evoked changes in $[Ca^{2+}]_i$ in cerebellar granule cells mediated by NMDA receptors.....	210
Figure 6.6	$Ca^{2+}]_i$ rise in cerebellar granule cells, evoked by pathologically relevant concentrations of NAAG.....	211
Figure 6.7	The death of white matter (A) and grey matter (B) cells evoked by NAAG (1 mM; n=11 slices), NAAG+AP5 (1 mM and 100 μ M, respectively; n=6 slices), and NMDA (100 μ M; n=10 slices), compared with the death in control solution (n=10 slices).....	212
Figure 7.1	The possible sequence of events underlying the oligodendrocytes' response to ischaemia.....	223

List of tables

Table 1.1	List of outwardly-rectifying potassium channels expressed by oligodendrocytes and oligodendrocyte precursor cells (OPCs).....	63
Table 1.2	List of inwardly-rectifying potassium channels expressed by oligodendrocytes and oligodendrocyte precursor cells (OPCs).....	64
Table 1.3	List of two-pore domain potassium channels expressed by oligodendrocytes and oligodendrocyte precursor cells (OPCs).....	65
Table 2.1	List of the internal solutions and their composition used for the experiments presented in this thesis.....	97
Table 2.2	List of fluorophores, with the excitation, dichroic and emission wavelengths of filters when the fluorescence microscope on the patch-clamping rig was used.....	98
Table 2.3	List of fluorophores, with the excitation lines, and dichroic and emission wavelengths of filters when the confocal microscope was used.....	99

Acknowledgements

First and foremost, I would like to thank my supervisor, Prof. David Attwell, who patiently and with great perseverance guided me through my PhD. The task was, arguably demanding, required a lot of resilience and the results were often discouraging. I would like to assure him that his efforts, even though seemingly neglected at some times, were in fact deeply appreciated and the input helped me find the way through the winding path of science. I will always regard David's intelligence, knowledge and excellent mentoring skills as a shining example of a great scientist.

I would like to thank the members of the lab that, apart from their will to explain and teach me new tasks and techniques, built a unique atmosphere of support and understanding. My special thanks go to Dr Nicola Hamilton, who spent a lot of her time supervising my calcium-imaging experiments, was always enthusiastic about new findings and easily engaged in many scientific discussions we had.

To my family, for their constant encouragement, unconditional love and faith in me, even during the moments when I was losing this faith myself. *Dziękuję Wam z całego serca, Mamo i Tato!*

Last but not least, to all my friends, fellow PhD students, to whom this thesis is dedicated. We shared the same bright and 'dark days', and were always there for each other, to listen and to help. I would especially like to thank, Caroline Mestrallet and Anna Wade, who were not only my roommates, but also best friends, for their support, advice and optimism that helped me solve many of my scientific and non-scientific problems, and allowed me to enjoy all the years I spent in London.

Thank you!

Dedication

I dedicate this thesis to all my friends, fellow PhD students.

*I ask them to stand calm and firm, and united in his time of trial.
The task will be hard.
There may be dark days ahead (...).
But we can only do the right as we see the right (...).
If one and all we keep resolutely faithful to it,
then, with God's help,
we shall prevail.**

*King George VI, 3rd September 1939

Chapter 1: Introduction

This thesis describes experiments studying the response to pathological situations of oligodendrocytes, the myelinating cells of the central nervous system (CNS). In this introduction I will give the background information necessary to understand the importance of oligodendrocytes in CNS function, the disorders they are damaged in, and the possible role of ion channels and neurotransmitters in causing that damage.

1.1 White matter and its role in CNS function

White matter is a crucial part of the vertebrate CNS, particularly in higher mammals. The presence of myelin around axons (which is what makes the white matter white) greatly speeds the propagation of the action potential, and thus confers fast communication between distinct parts of the grey matter. For example, myelination allows action potentials to propagate between the two hemispheres of the human cerebral cortex (Fig. 1.1) approximately 60 times faster than would occur for unmyelinated axons (Bakiri *et al.*, 2009), reducing the conduction time from ~300 msec to ~5 msec, and thus speeding up cognition considerably. Indeed, segregation of the brain into grey matter where local processing occurs and white matter connecting tracts has been suggested to maximize the brain's information processing functionality (Wen and Chklovskii, 2005).

1.2. Oligodendrocytes and their role in the white matter

The white matter is composed of myelinated axons (and a certain fraction of unmyelinated axons in many tracts) and glial cells: astrocytes, oligodendrocytes and microglia. Oligodendrocytes, whose name stems from the Greek words *oligo* (few), *dendros* (branch) and *cytos* (cell), are highly specialized cells, the processes of which enwrap axons (Figs. 1.2 and 1.3), forming a multilayered myelin sheath of membranes (Fig. 1.3). The presence in series of all the myelin membranes decreases the effective axonal membrane capacitance, while increasing its resistance. This results in less charge

entry being needed to depolarise the cell and results in faster action potential conduction, which becomes saltatory because Na⁺ ions only enter at nodes of Ranvier.

1.2.1. Oligodendrocyte development

In the experiments described in this thesis I recorded from mature myelinating oligodendrocytes at a developmental stage of the cerebellum when there are also less mature oligodendrocyte lineage cells present. It is therefore useful to briefly review the development of these cells. Oligodendrocytes pass through three consecutive developmental stages: oligodendrocyte precursor cells (OPCs), immature cells and fully-myelinating mature cells.

Oligodendrocyte precursor cells are formed in distinct parts of the brain and spinal cord. In the spinal cord, OPCs are derived from progenitors present in the ventricular zone, initially from its ventral part (the first wave, at ~E12.5 of mouse development, provides 85% of all OPCs) and later from the dorsal part (this second wave, at ~E15 of mouse development, provides 15% of all OPCs). In the brain, oligodendrogenesis occurs in 3 different regions: first, in the ventral medial ganglionic eminence (MGE) at ~E12.5 of mouse development, then in the lateral ganglionic eminence (LGE) a few days after the first wave from the MGE, and finally in the cortex postnatally (Miller, 2002; Richardson *et al.*, 2006; Rowitch, 2004).

From their place of origin, OPCs migrate along radial glial cells and axonal tracts to populate different regions of the CNS. They are guided by soluble and membrane-bound molecular clues, such as (in the optic nerve) chiasm-derived chemorepellent signal netrin-1 (Sugimoto *et al.*, 2001) and platelet-derived growth factor (PDGF) (Armstrong *et al.*, 1990), produced by astrocytes and neurons. It is not clear what the 'stop signals' are that terminate the cells' migration: the most likely candidates are extracellular matrix molecules (such as tenascin-C and chemokine CXC1), but the involvement of yet uncharacterized axonal signals cannot be excluded (Miller *et al.*, 2002).

The precursor cells proliferate during migration and this proliferation is highly regulated by environmental factors provided by astrocytes and neurons, such as PDGF, fibroblast growth factor (FGF) and neuregulin (Barres and Raff, 1994; Barres and Raff, 1999; Miller, 2002). The axonal action potential also plays an important role in controlling OPC proliferation, since either axotomy or the application of TTX to the

optic nerve cause a significant decrease in the number of mitotic OPCs (Barres and Raff, 1993; Barres and Raff, 1999; Ueda *et al.*, 1999)

After arrival at their final destination, OPCs exit their cell cycle and differentiate into myelin-forming, mature oligodendrocytes. This process seems to be intrinsic to the cells' development, with a fixed number of cell divisions occurring before differentiation occurs (Raff *et al.*, 1985). However, oligodendrocyte differentiation is also influenced by axonal signalling molecules, such as the EGF-like growth factor neuregulin 1 (NRG1) and the Notch receptor ligand Jagged 1 (Wang *et al.*, 1998; Miller, 2002; Simons and Trajkovic, 2006). Neuronal activity also seems to play an important role in the process, since myelination can be inhibited by tetrodotoxin (Demerens *et al.*, 1996; but see also: Colello *et al.*, 1995), and this influence of activity might be linked to axonal release of promyelinating factors, such as adenosine and glutamate (Káradóttir and Attwell, 2007). Glutamate is a good candidate for an axon-derived differentiation-controlling molecule, because it has been shown that OPCs receive glutamatergic synapses from unmyelinated axons (Kukley *et al.*, 2007; Ziskin *et al.*, 2007), prompting the idea that synaptic transmission from unmyelinated axons to OPCs is a "myelinate me" signal.

In order to distinguish the three main phases of oligodendrocyte development, the cells can be characterized based on their morphology and the expression of specific antigenic markers (Fig. 1.4). OPCs are identified as bipolar (when migrating) or stellate (after migration) cells that express the proteoglycan NG2, a surface glycoside recognised by the antibody A2B5, GD3 ganglioside and PDGFR α (Kettenmann and Ransom, 2005). When differentiation occurs and the expression levels of NG2 and PDGFR α are downregulated, the change is accompanied by the cell becoming immunoreactive for the surface antigen O4 (expressed by late stage precursor cells, immature and early mature oligodendrocytes: Girolamo *et al.*, 2010) and GalC (Jackman *et al.*, 2009). This expression pattern is characteristic for immature, early myelinating oligodendrocytes that possess a small number of myelinating processes aligned parallel to axons, with the majority of the processes protruding in different directions, presumably because they are actively 'searching' for axons to myelinate. Differentiation is completed by the cell acquiring the fully mature phenotype, with the multiple processes aligned in parallel and myelinating up to 30 different axons. Mature cells express myelin basic protein (MBP), proteolipid protein (PLP) and myelin associated glycoprotein (MAG), which are localised in the myelin. In this thesis I used

both morphological criteria and immunostaining against MBP to distinguish mature oligodendrocytes from the population of precursors and immature cells (Trapp *et al.*, 1997; Kettenmann and Ransom, 2005), as described in later chapters.

Although most OPCs turn into myelinating oligodendrocytes (Zhu *et al.*, 2008) some OPCs, after arriving at their destination, remain as undifferentiated “adult OPCs” and preserve their proliferative capabilities (Dawson *et al.*, 2000; Miller, 2002). These cells stain positively for the OPC markers PDGFR α and proteoglycan NG2, and are found distributed throughout the grey and white matter of the adult brain (Dawson *et al.*, 2000). They represent approximately 5% of all the cells in the brain (~8% of cells in white matter and 3% in the grey matter; Dawson *et al.*, 2003) and are the main proliferative cell population (Dawson *et al.*, 2003). Their proliferation and migration rates are slower than for OPCs early in development, but these rates increase in response to injury and demyelination (Levine and Reynolds, 1999; Dawson *et al.*, 2000) probably to promote remyelination (Levine and Reynolds, 1999; Dawson *et al.*, 2000). A small proportion of OPCs has been reported to generate cells other than oligodendrocytes, i.e. astrocytes (Zhu *et al.*, 2008) and neurons (Rivers *et al.*, 2008), although this is controversial (Kang *et al.*, 2010).

1.2.2 Neuron-glia interaction at the node of Ranvier

The complex interplay between oligodendrocytes and axons leads, at the final stage of oligodendrocyte development, to the formation of myelin. Oligodendrocytes enwrap axons, dividing their structure into 4 different domains: the node, the paranode, the juxtaparanode and the internode itself (Fig. 1.5).

At the node of Ranvier, which is formed by the gap between two segments of myelin at regularly spaced intervals along the axon, the sodium channels that are initially continuously distributed along unmyelinated axons become clustered and anchored. The clustering depends on axon action potential activity, and can be promoted by either oligodendrocyte-conditioned medium (Kaplan *et al.*, 2001) or direct physical contact with oligodendrocyte processes (Kaplan *et al.*, 1997), underlining the necessity of the interaction between glia and axons in the process.

The paranode is the region of the axon-glia junction *per se*, with the myelin being directly anchored to the axonal membrane. This depends crucially on a complex interaction between oligodendrocyte-expressed (neurofascin-155) and axon-expressed

(contactin, Caspr and 4.1B) membrane proteins (Simons and Trajkovic, 2006; Jackman *et al.*, 2009). The anchoring is essential for the axonal action potential to propagate normally. Its disruption has been reported in various pathological conditions (Wolswijk and Balesar, 2003; Howell *et al.*, 2006; Fu *et al.*, 2009), and might occur during the experiments described in this thesis.

The juxtaparanode domain, which is slightly further away from the node than the paranodal region, is the final specialised region before the main part of the internode. Voltage-gated potassium channels on the axonal membrane, which may contribute to repolarization of the action potential, are located in the juxtaparanode (Wang *et al.*, 1993).

The main internode region consists of myelin wrapped around and tightly apposed to the axonal membrane. It is necessary that a highly restricted space exists between the myelin and axonal membrane in order to restrict extracellular current flow outside the axon and thus avoid short-circuiting of the capacitance-reducing effect of the myelin (because such short-circuiting would oppose rapid action potential propagation).

1.2.3 The classification of mature oligodendrocytes

A single mature oligodendrocyte can myelinate up to 30 different axons, with each cell process extending to form one internode (Fig. 1.2). The internodal processes are usually parallel to each other, and form myelin segments of a thickness and length that depends on the brain area and the diameter of the axon myelinated (Butt and Ransom, 1989). The properties of oligodendrocytes have been classified both morphologically and electrically.

Del Rio-Hortega first classified oligodendrocytes into four morphological types (denoted I-IV), depending on the shape and size of their soma, the number and size of the axons they myelinate, and their distribution within the CNS (Rio-Hortega, 1928) (Fig. 1.6). This classification was confirmed later with the use of immunohistochemistry assays (Butt and Ransom, 1989). Type I and II oligodendrocytes have a similar morphology, with small cell bodies and 4 or more primary processes that branch repeatedly to myelinate 10-30 axons of less than 2 μm in diameter. Type I oligodendrocytes, the most abundant of all types, have multiple branching processes supporting numerous myelin sheaths that need not to be parallel and are primarily found in the forebrain, cerebellum and spinal cord, while type II oligodendrocytes are distinguished by their processes forming parallel myelin sheaths and are present only in

the white matter, including the area that I studied in this thesis – the white matter of cerebellum. Type III oligodendrocytes have large cell bodies, myelinate up to five thick axons (4-15 μm), and are localized in the cerebral and cerebellar peduncles, the medulla oblongata and the spinal cord. Finally, type IV oligodendrocytes form a single long (up to 1000 μm) myelin sheath around large diameter fibres and are located exclusively near the entrance of the nerve roots into the CNS (Wood and Bunge, 1984; Kettenmann and Ransom, 2005).

Morphologically classified oligodendrocytes may differ functionally. For example, the properties of type II oligodendroglia differ depending on the region of the white matter they populate. Bakiri *et al.* (2011) reported that in the developing corpus callosum oligodendrocytes myelinate ~10 axons, whereas in the cerebellar white matter at the same age the average number of internodes formed by a single cell was ~7. In addition, oligodendrocytes in the corpus callosum formed shorter internodes than those in the cerebellar white matter. As a result of these differences, and the different diameter of the underlying axons, a computational model predicted the conduction speed for cerebellar axons to be twice that for corpus callosum axons. It was suggested that this difference may reflect a higher conduction speed being needed for axons conveying information to and from the cerebellum (in order to rapidly control motor output) than is needed for less time-critical movement of information between the cerebral cortices.

Thus, differences in oligodendrocyte morphology and electrical properties may stem from different functions that these cells perform in distinct parts of the brain, instead of being simply the result of their intrinsic developmental program. This notion is supported by a study showing that oligodendrocyte precursors purified from rodent optic nerve (which contains uniformly small-diameter axons) when transplanted into the spinal cord (containing both large- and small-diameter axons) myelinated both large and small axons in the host, rather than preferentially myelinating small axons (Fanarraga *et al.*, 1998).

1.2.4 The structure and role of the cerebellum

All the experiments that I performed for this thesis were carried out on cells in the rat cerebellum (Fig. 1.7). This brain region was chosen as it is well described in the literature, its microcircuits have been examined in depth, and it had been used previously to study oligodendrocyte properties by other workers in our lab, so my results could be directly compared with those previously obtained by the other members

of the lab. In this section I will give the background information on the cerebellum that is needed to understand the experiments that I performed. The anatomy and function of the cerebellar cortex can be summarised as follows (Kandel *et al.*, 2000).

The main function of the cerebellum is to store motor programmes and use them to provide fine motor control. The cerebellum does not initiate the movement *per se*, but it is important for the regulation of precise motor output to confer proper balance, posture and smooth motor movements. The cerebellum is located behind the cerebral cortex and has a highly organized and uniform structure. It can be divided into three lobes, denoted flocculonodular, anterior and posterior, of which the last two can be further divided into the central vermis and the two lateral cerebellar hemispheres. My experiments were carried out on cells in the vermis, which is composed of multiple folia, each of them characterized by the same layered structure (Fig. 1.7). Each folium comprises white and grey matter, with the grey matter surrounding centrally located white matter. The grey matter can be divided into three different layers: the granule cell, Purkinje cell and molecular layers.

The innermost granule cell layer is composed of a high number of densely packed granule cells and a smaller number of interneurons (Golgi cells), astrocytes and NG2 positive oligodendrocyte precursor cells. Granule cells are distinguished by their small cell body and 4-5 dendrites which receive excitatory synaptic input from the mossy fibers and inhibitory input from the Golgi cells (which also receive input from the mossy fibers). The mossy fibres are myelinated axons which provide information to the cerebellar cortex on the sensory environment (information derived from peripheral receptors) and on the desired motor output (information from the cortex and other brain areas). In the granule cell layer this input information is recoded into the firing of the granule cells. Each granule cell projects its axon (which is unmyelinated in rodents) vertically through the molecular layer where it splits into two branches which travel horizontally in opposite directions to form a so-called parallel fibre, which is approximately 4 mm long in the adult rat. The parallel fibre sends excitatory synapses onto the dendritic tree of ~130 Purkinje cells as well as onto the dendrites of interneurons, the basket and stellate cells, which inhibit the Purkinje cells. The Purkinje cells have their somata arranged in a thin layer – the Purkinje cell layer, which also contains the somata of radial glial cells (the Bergmann glia) which send long processes through the molecular layer. The elaborate Purkinje cell dendritic tree is flattened in a plane perpendicular to the cerebellar folds, so that the molecular layer mainly comprises

an array of these dendritic trees, with the parallel fibres running perpendicular to them, like telephone wires on poles. In addition to receiving excitatory synaptic input from the parallel fibres, the Purkinje cell also receives excitation from (myelinated) climbing fibres which arise in the inferior olive. This input may provide a teaching input to induce plasticity at the parallel fibre synapses and thus correct erroneous motor outputs. After integration of the information arriving on the approximately 100,000 synapses impinging on the Purkinje cell dendritic tree, the final output from the cerebellar passes *via* the Purkinje cell output axon (which is also myelinated) through the white matter to the deep cerebellar nuclei, whose cells are inhibited by the Purkinje cells. The deep cerebellar nuclear neurons then send axons to the premotor cortex, primary motor area and red nucleus to modulate the motor output of the body.

For the cerebellar cortex to process motor information rapidly, information has to arrive on the mossy and climbing fibres and leave on the Purkinje cell axons at high speed. This is achieved by these axons in the white matter of the cerebellum being myelinated. In addition to the myelinated axons, the white matter consists of oligodendrocytes, astrocytes, microglia and blood vessels. My experiments were performed mostly on mature oligodendrocytes in the white matter of the P12 rat vermis, at which age the cerebellum is to a large extent developed and it is easy to find mature myelinating oligodendrocytes. However not all axons are myelinated at this stage, and since myelin scatters light intensely, this makes it easier to see the cells' somata for whole-cell patch-clamp experiments.

1.3 Channel and receptor expression by oligodendrocytes

In the experiments described in this thesis I test the involvement of various receptors and ion channels in contributing to the membrane current response of oligodendrocytes to ischaemia and to agents like glutamate, N-acetyl-aspartate and N-acetyl-aspartyl-glutamate. This section provides background information on the receptors and ion channels that oligodendrocyte lineage cells express. The expression level of these proteins depends greatly on the cells' developmental stage, in part because many of them regulate important developmental processes such as cell migration, proliferation and maturation. However, overactivation of some of these receptors or channels in pathological conditions (e.g. in ischaemia as I investigate in Chapters 3 and

4), may lead to cell depolarization, a deleterious calcium or sodium influx and eventually cell death. In the following sections I focus in particular on the ion channels and receptors which I investigate the role of in this thesis.

1.3.1 Ion channels

1.3.1.1 Voltage-gated ion sodium channels

Voltage-dependent sodium channels are expressed by OPCs and may have an important role in axon-glia communication. Their characteristics are similar to those of neuronal sodium channels (i.e. they have rapid kinetics of activation, deactivation and inactivation, and a high sensitivity to TTX), but their density is much lower (Lin and Bergles, 2002). There is a progressive loss of these channels during cell maturation, which has been reported both at the mRNA (Cahoy *et al.*, 2008) and the functional level (Paez *et al.*, 2009a; De Biase *et al.*, 2010). It is possible, therefore, that sodium currents are involved in the mechanism through which OPCs sense electrically active axons in the environment (amplifying the depolarization produced by synaptic input, as suggested by Káradóttir *et al.* (2008)), a feature that is not required at later stages of development. Interestingly, sodium-channel-expressing OPCs are more vulnerable to dying in response to ischaemic insults, in comparison to NG2-expressing OPCs not expressing the sodium channels (Káradóttir *et al.*, 2008).

1.3.1.2 Voltage-gated calcium channels

The existence of voltage-dependent calcium channels (VDCCs) in oligodendrocytes was for a long time controversial. Sontheimer *et al.* (1989) and Barres *et al.* (1990) declared that these channels were absent from OPCs and oligodendrocytes in culture, but more recent studies reported the expression of these channels, specifically R-type and L-type VDCCs, in oligodendrocyte precursors and immature oligodendrocytes in brain slices (Chen *et al.*, 2000; Paez *et al.*, 2007; Paez *et al.*, 2009b). Their expression may be downregulated during developmental progression (Berger *et al.*, 1992a; Takeda *et al.*, 1995), although Agrawal *et al.* (2000) reported L- and N-type calcium channel expression by mature oligodendrocytes in spinal cord white matter.

The physiological function of oligodendrocyte VDCCs remains elusive. It was suggested that they might be preferentially localized to the cell processes and participate

in axon-glia signalling (Chen *et al.*, 2000), but others reported a possible role in the precursor cell migration and process extension (Paez *et al.*, 2009a). Additionally, and of potential relevance to my experiments, Agrawal *et al.* (2000) suggested that overactivated oligodendrocyte calcium channels might mediate deleterious calcium influx and damage to oligodendrocytes in a model of spinal cord injury.

1.3.1.3 Potassium channels

Oligodendrocytes express a wide range of potassium channels and their expression pattern depends strongly on the developmental stage of the cell. I will show in later chapters that K^+ channels play a key role in the cells' response to ischaemia, so this section reviews the properties of these channels in some detail.

OPCs express mainly voltage- and time-dependent potassium channels. Delayed rectifying channels (i.e. channels which are activated by depolarization and thus show an outward current at positive potentials after the channels have activated) in these cells have consistently been reported both in culture (Sontheimer *et al.*, 1989) and in brain slices (Berger *et al.*, 1991; Chvátal *et al.*, 1997), while A-type channels generating a transient outward current were initially claimed to be absent (Berger *et al.*, 1991), but subsequently found to be present (Chvátal *et al.*, 1997) in OPCs in CNS slices. In cultured cells some of the outward rectifying potassium channels are activated by calcium (Sontheimer *et al.*, 1989). Also, a transcriptome analysis by Cahoy *et al.* (2008) reported that OPCs express high levels of TASK-1, TREK-1 and TWIK-1, i.e. members of a newly-identified two-pore domain (K_2P) family of K^+ channels. Additionally, OPCs express inwardly rectifying potassium channels, including Kir4.1 (Olsen and Sontheimer, 2008) and ATP-sensitive channels (Butt and Kalsi, 2006). The primary function of the K^+ channels in the cell is to set a negative resting membrane potential but, possibly because of this, they may also be important for regulating cell proliferation and differentiation (Sontheimer *et al.*, 1989; Gallo *et al.*, 1996; Olsen and Sontheimer, 2008; Fogal *et al.*, 2010). For the full list of K^+ channels expressed by OPCs and mature oligodendrocytes, see Tables 1.1-3.

Mature oligodendrocytes express mainly “passive” potassium channels (also known as ‘background’ channels), with little apparent voltage- and time-dependence to their conductance, together with some voltage-activated outward rectifying channels (Gipson and Bordey, 2002). The passive conductance is partly mediated by weakly inwardly rectifying channels, mainly Kir4.1, the level of which increases during cell

development (Neusch *et al.*, 2001; Kalsi *et al.*, 2004; for a full list of inwardly rectifying K^+ channels in oligodendrocytes, see Table 1.2). However, an additional role could be played by THIK-1 channels (belonging to the K_2P family), the mRNA levels of which are also elevated in mature oligodendrocytes (Cahoy *et al.*, 2008). In another type of glial cell, astrocytes, whose membrane properties are also heavily dominated by passive potassium currents, a recent paper also suggests the involvement of the K_2P channels TWIK-1 (a weak inward rectifier) and TREK-1 (a weak outward rectifier) (Zhou *et al.*, 2009). These channels could also contribute to the passive potassium currents in oligodendrocytes, as their mRNAs are expressed by mature oligodendrocytes (though to a lower level than in OPCs; Cahoy *et al.*, 2008; for a full list of K_2P channels expressed by oligodendrocytes, see Table 1.3). The large permeability of the mature oligodendrocyte membrane mediated by passive potassium channels has been suggested to be important for spatial buffering of potassium by the oligodendrocyte (Berger *et al.*, 1991), just as Kir4.1 is important for spatial buffering of potassium in Müller glia (Kofuji *et al.*, 2002). In addition, or possibly because of this function, expression of Kir4.1 (possibly in OPCs: Olsen and Sontheimer, 2008) is necessary for myelination to occur *in vivo* (Neusch *et al.*, 2001).

No specific diseases have been assigned directly to potassium channel dysfunction in oligodendrocyte lineage cells, but many pathological conditions are associated with a downregulation of Kir4.1 channel expression, at least in astrocytes (Olsen and Sontheimer, 2008), suggesting that changes in the expression of these channels may occur in response to changes in the cells' environment and might thus contribute to pathology.

1.3.1.4 Acid-sensing ion channel (ASIC)

Acid-sensing ion channels are tetrameric cation channels activated by a decrease in extracellular pH (Waldmann *et al.*, 1999), which are predominantly permeable to Na^+ , but can also be permeable to K^+ and Ca^{2+} , depending on the subunits they are composed of (Baron *et al.*, 2002; Xiong *et al.*, 2004). They are widely expressed by neurons, in which cells they may be important in normal synaptic transmission, and contribute to pain sensation, mechanosensation, learning and memory, and the pathological response to ischaemia (Allen and Attwell, 2002; Xiong *et al.*, 2004; Feldman *et al.*, 2008).

It was shown recently that oligodendrocytes in culture and in brain slices express

transcripts for ASICs, including the calcium-permeable ASIC1a subunit, and that their level of expression decreases with cell development (Feldman *et al.*, 2008). Electrophysiological and calcium imaging studies confirmed the functionality of these channels (Feldman *et al.*, 2008). Their role in oligodendrocyte physiology remains unknown, but it is possible that they contribute to oligodendrocyte pathology. In a mouse model of multiple sclerosis (experimental autoimmune encephalomyelitis, EAE; Friese *et al.*, 2007), inflammatory lesions in the spinal cord were associated with an acidic shift of extracellular pH, and knock-out or blockade of ASIC channels were neuroprotective, suggesting that opening of ASIC channels, possibly in oligodendrocytes, contributes to cell damage. Since oligodendrocytes are highly vulnerable to ischaemic insult, and ischaemia is associated with an acid pH shift by ~1 unit as a result of an initial switch to anaerobic respiration (Kraig *et al.*, 1983; Silver and Erecińska, 1992), it is possible that Ca²⁺ entry caused by activation of ASICs contributes to a damaging rise in the intracellular calcium concentration ([Ca²⁺]_i) in these cells (in addition to that produced by AMPA and NMDA receptors: see section 1.3.2.1 below).

In Chapter 4 of this thesis I examine the contribution of ASIC channels to the response of oligodendrocytes to ischaemia.

1.3.1.5 Transient receptor potential (TRP) channels

Transient receptor potential channels are a large family of cation channels that are expressed in a variety of CNS regions. TRP channels are permeable to sodium and calcium (to varying degrees) and play an important role in sensory physiology, such as vision, taste, olfaction, hearing, nociception and thermo- and mechanosensation, and also in growth cone guidance, neurite outgrowth and synaptic activity (Venkatachalam and Montell, 2007). Broadly speaking, on the cellular level, they allow the individual cells to sense changes in their surrounding.

The expression of two particular calcium-permeable TRP channels – TRPC3 and TRPM3 - has been reported in oligodendrocytes using immunohistochemistry (Fusco *et al.*, 2004; Hoffmann *et al.*, 2010). TRPM3 expression in oligodendrocytes was found to start with the onset of myelination (Hoffmann *et al.*, 2010), so it is possible that its activation may contribute to triggering the differentiation process. TRPM3 is known to be activated by the lipid component sphingosine, which is a major component of myelin lipids, and Hoffmann *et al.* (2010) demonstrated a sphingosine-evoked Ca²⁺ influx into

oligodendrocytes, but the functional significance of this is uncertain. In neurons, it was shown that the opening of TRPs, specifically TRPM7, is involved in the acute response to ischaemia in culture (Aarts *et al.*, 2003), in slices (Lipski *et al.*, 2006) and *in vivo* (Sun *et al.*, 2009), however their role in pathologies affecting oligodendrocytes is unknown.

In Chapter 4 of this thesis I examine the contribution of TRP channels to the response of oligodendrocytes to ischaemia.

1.3.1.6 Gap junctions and hemichannels

Gap junctions are channels expressed on the membranes of two coupled cells that allow direct cytoplasm-cytoplasm communication through the exchange of intracellular metabolites and ions (e.g. ATP, NAD⁺ and glutamate) up to 1 kDa in size (Sáez *et al.*, 2005). In vertebrates they were originally thought to be formed of two families of proteins, the connexins and the pannexins, although now it is believed that only connexins form gap junctions between cells (Sosinsky *et al.*, 2011), while pannexins form so-called hemi-channels connecting the cytoplasm with the extracellular space (see below). In gap junctions, each cell contributes to the junction one connexon, which is made up of six connexin subunits. Connexons which are not coupled to a connexon on an apposed cell usually change conformation so that their intrinsic channel is closed, but under certain circumstances (e.g. low extracellular [Ca²⁺]), this may open (as also occurs for the pannexons), allowing an efflux of molecules like ATP and glutamate from the cytoplasm to the extracellular space (Sáez *et al.*, 2005).

Oligodendrocytes express 3 types of connexins (Cx29, Cx32 and Cx47) which are localized to the cell plasma membrane, and may form functional gap junctions between different oligodendrocytes, between oligodendrocytes and astrocytes, or between different lamellae of the myelin sheath within each oligodendrocyte (Pastor *et al.*, 1998; Orthmann-Murphy *et al.*, 2008; Maglione *et al.*, 2010; Wasseff and Scherer, 2011). There is controversy about the importance of gap junctions between oligodendrocytes and other cells. It was initially agreed that, unlike astrocytes, oligodendrocytes form gap junctions only occasionally, mostly with astrocytes and rarely with other oligodendrocytes (Pastor *et al.*, 1998; Orthmann-Murphy *et al.*, 2008), but two recent reports found extensive coupling between oligodendrocytes in the white matter (Maglione *et al.*, 2010; Wasseff and Scherer, 2011). In my experiments, however, gap junctions between oligodendrocytes and other cells were never detected

(i.e. dye entering the patch-clamped cell never passed to other oligodendrocytes) and a similar low incidence of coupling (3% and 9% of cells coupled in the corpus callosum and cerebellum, respectively) was reported by Bakiri *et al.* (2011). The reason for these differences is uncertain. Although the use of an intracellular medium with a more alkaline pH (7.4) would tend to promote the opening of gap junctions (Sáez *et al.*, 2005), the pH of my internal solution (7.3) was only slightly more acidic than that used in the other studies.

There are at least two examples of mutations in oligodendrocyte connexin genes leading to severe debilitating conditions (Kleopa *et al.*, 2010). Disruption of Cx32 expression leads to X-linked Charcot-Marie Tooth disease that mostly affects Schwann cells in PNS (causing peripheral neuropathy), but also affects oligodendrocytes, leading to cognitive dysfunctions. Mutation of another oligodendrocyte connexin, Cx47, was reported in some of the cases (~8%; Henneke *et al.*, 2008) of Pelizaeus-Merzbacher-like disease which causes severe mental disability and premature death of the affected individuals (see section 1.4.3.1 below). Furthermore, double knock-out of Cx32 in oligodendrocytes and Cx43 in astrocytes leads to white matter vacuolation, astrocyte loss and early mortality (Magnotti *et al.*, 2011).

Pannexins are structurally and functionally (though not evolutionarily) similar to connexins (MacVicar and Thompson, 2010). Pannexins are also expressed on the plasma membrane but, unlike connexins, they cannot form functional gap junctions with other pannexins (Sosinsky *et al.*, 2011; formation of gap junctions was found only when pannexins were overexpressed in oocyte: Bruzzone *et al.*, 2003, but this finding was criticised by: MacVicar and Thompson, 2010) and instead they serve as large-pore non-selective hemichannels. Like connexins, they are permeable to large molecules, such as ATP, glucose and glutamate, and it has been suggested that their main function is to allow the release of these metabolites, and to mediate an ion influx across the membrane upon NMDA receptor activation (Thompson *et al.*, 2006). Pannexins were found on astrocytes and neurons (Thompson and MacVicar, 2008), but their expression by oligodendrocytes is controversial. The transcriptome analysis by Cahoy *et al.* (2008) did not detect mRNA for pannexins in oligodendrocytes, however, another group found pannexin expression in mature oligodendrocytes, both at the mRNA and the protein level (Domercq *et al.*, 2010).

In neurons, hemichannel opening as a result of NMDA receptor overactivation was linked to such pathological conditions as epilepsy and ischaemia (Thompson *et al.*,

2006). Hemichannels were suggested to be activated by ischaemia, leading to a large inward current that evokes depolarization, but this has been criticised by Madry *et al.*, 2010. In oligodendrocytes it has been suggested that hemichannel opening in ischaemia leads to a release of ATP and a subsequent activation of P2X₇ receptors (Domercq *et al.*, 2010).

In Chapter 4 of this thesis I examine the contribution of hemichannels to the response of oligodendrocytes to ischaemia.

1.3.2 Receptors expressed by oligodendrocytes

In this section I will describe the three types of oligodendrocyte receptor that I studied during my PhD: ATP, GABA and glutamate receptors. Oligodendrocytes also express a variety of other receptors (such as serotonin, acetylcholine and glycine receptors), which I will not cover in this introduction as I did not examine their properties during my experiments.

1.3.2.1 Glutamate receptors

1.3.2.1.1 AMPA/KA receptors

AMPA receptors are formed from subunits GluR1-GluR4 (also known as GluA1-4; Collingridge *et al.*, 2009), while kainate receptors are made from GluR5, GluR6, GluR7, KA1 and KA2 (also known as GluK1-5, respectively; Collingridge *et al.*, 2009). AMPA/KA receptors are mostly permeable to sodium and potassium, with the permeability of AMPA receptors towards calcium being determined by the presence of GluR2 (which, when edited at the mRNA level, as normally occurs, suppresses the calcium permeability; Dingledine *et al.*, 1999).

Oligodendrocyte express GluR2-4, 6, 7, and KA1 and KA2, which permits them to form functional AMPA and KA receptors (Patneau *et al.*, 1994; Matute *et al.*, 1997; Itoh *et al.*, 2002). Indeed, a glutamate-evoked inward current in oligodendrocytes, mediated by AMPA/KA receptors, has been demonstrated both in culture (Barres *et al.*, 1990; Patneau *et al.*, 1994; Gallo *et al.*, 1996) and in brain slices (Berger *et al.*, 1992b). Although some studies reported a lack of GluR2 in functional AMPA/KA receptors in oligodendrocytes (Matute *et al.*, 1997), which would allow calcium to pass through the channel, others have suggested that the expression of this subunit varies with developmental stage, with GluR2 being present in mature oligodendrocyte and absent in

precursor and immature cells (Itoh *et al.*, 2002). This would explain the increased susceptibility of cells at these developmental stages to excitotoxic death (Back *et al.*, 2002; Deng *et al.*, 2003). Apart from subunit composition, it is not clear whether the overall expression level of AMPA/KA receptors changes during oligodendrocyte development. A transcriptome study found a downregulation of AMPA receptor expression with development (Cahoy *et al.*, 2008), but functional studies have given more varied results. While some researchers have reported that, in culture and in brain slices, the AMPA/KA-receptor mediated response to glutamate is larger in precursor and immature cells than in mature oligodendrocytes (Itoh *et al.*, 2002; Deng *et al.*, 2003), some studies in brain slices found a comparable size of response at different stages of development (Berger *et al.*, 1992b), and other researchers have reported that, both in culture and in slices, mature oligodendrocytes respond more to the application of AMPA than do OPCs (Patneau *et al.*, 1994; Káradóttir *et al.*, 2005).

AMPA/KA receptors have been proposed to play an important role in oligodendrocyte development, although the main function of these receptors remains to be resolved. Gallo *et al.* (1996) found that Na⁺ influx through AMPA receptors causes a rise of intracellular sodium concentration ($[Na^+]_i$) which blocks delayed rectifier potassium channels, and this leads to a block of cell proliferation and differentiation, while having no impact on cell migration. On the other hand, Wang *et al.* (1996) and Gudz *et al.* (2006) reported increased cell migration upon AMPA receptor activation, which correlated with calcium transients evoked in the cells and involved activation of G_i-coupled proteins (an effect that was not mediated by mGluRs).

AMPA/KA receptors are expressed on OPCs at the synapses these cells receive from axons in the grey (Bergles *et al.*, 2000) and the white matter (Kukley *et al.*, 2007; Ziskin *et al.*, 2007). These synapses are lost as the cells differentiate into mature myelinating oligodendrocytes (De Biase *et al.*, 2010; Kukley *et al.*, 2010), which further suggests a role for AMPA/KA receptors in cell maturation. In mature myelinating oligodendrocytes, the low number of AMPA/KA receptors present seems to be localized to their soma, with their functional role still unknown (Salter and Fern, 2005; Káradóttir and Attwell, 2007).

Oligodendrocyte AMPA/KA receptors are activated in pathological conditions, such as multiple sclerosis (MS) and ischaemia, as described in detail in later sections. In a mouse model of MS, glutamate (possibly released by activated immune cells) acts on mature oligodendrocyte AMPA/KA receptors causing cell damage and subsequent

damage to the underlying axon (Pitt *et al.*, 2000; Smith *et al.*, 2000). Similarly, during ischaemia, overactivation of AMPA/KA receptors leads to substantial oligodendrocyte death (McDonald *et al.*, 1998; Tekkök and Goldberg, 2001). It was suggested that the increased OPC vulnerability towards hypoxic/ischaemic insult (compared to mature cells) is caused by the calcium influx that results from their AMPA/KA receptor subunit composition, i.e. the lack of GluR2 described above (Fern and Möller, 2000; Deng *et al.*, 2003). However, the developmental change in the contribution of AMPA/KA receptors to ischaemia-evoked damage of axons is different to that for the overlying oligodendrocytes: McCarran and Goldberg (2007) reported that at early ages the AMPA/KA blocker NBQX protected oligodendrocyte lineage cells but not axons, while at later ages the axons were protected by AMPA/KA receptor block. More details on the role of AMPA/KA receptors in the response to ischaemic insult, both in the white and the grey matter, will be given below in section 1.4.2.

In Chapter 4 of this thesis I examine the contribution of AMPA/KA receptors to the response of oligodendrocytes to ischaemia.

1.3.2.1.2 NMDA receptors

NMDA receptors are composed of the following subunits: NR1 (also known as GluN1; Collingridge *et al.*, 2009), which binds glycine, NR2 (NR2A, NR2B, NR2C or NR2D, also known as GluN2A, 2B, 2C and 2D, respectively; Collingridge *et al.*, 2009), which binds glutamate and NR3 (NR3A and NR3B, also known as GluN3A and 3B; respectively; Collingridge *et al.*, 2009), which binds glycine. The receptors are composed of 4 subunits, thought usually to be two glycine-binding NR1 subunits and two glutamate binding subunits (i.e. NR2A-D), but it has also been shown that glycine-binding NR3A or NR3B can assemble with NR1 to form excitatory glycine receptors which are unaffected by glutamate (reviewed by Cull-Candy and Leszkiewicz, 2004), and heterotrimeric receptors containing NR1, NR2 and NR3 subunits are also formed and may be important in oligodendrocytes as described below.

NMDA receptors are permeable to sodium, potassium and calcium. For them to pass ions, in addition to the binding of extracellular glutamate and the co-agonist glycine (or D-serine), a depolarization of the cell membrane is required to release magnesium from the channel pore (Dingledine *et al.*, 1999; Wollmuth and Sobolevsky, 2004). The receptor sensitivity to magnesium depends on the NR2 and NR3 subunits involved in its structure, with a sensitivity ranging from the highest to the lowest in the

order: NR2A > NR2B > NR2C > NR2D; Kuner and Schoepfer, 1996), with the NR3 subunits conferring only a weak magnesium block (Sasaki *et al.*, 2002).

Even though mRNA for NMDA receptors was detected in oligodendrocyte cultures (Yoshioka *et al.*, 1996; Matute *et al.*, 1997), their functional expression in these cells was long denied based on a lack of current evoked by NMDA application, both in culture (Barres *et al.*, 1990; Patneau *et al.*, 1994) and in brain slices (Berger *et al.*, 1992b). Recently, however, many labs reported, based on immunocytochemistry, electron microscopy, electrophysiological and calcium-imaging studies, the presence of functional NMDA receptors at all three oligodendrocyte developmental stages, in brain slices and in the optic nerve (Káradóttir *et al.*, 2005; Salter and Fern, 2005; Micu *et al.*, 2006) (Fig. 1.8).

Oligodendrocyte NMDA receptors were found to have a very weak magnesium block, with 2 mM extracellular magnesium concentration (twice the normal extracellular level) reducing the current only 3 to 5-fold relative to that seen in a magnesium-free solution (in contrast, for neuronal receptors comprised of NR1 with either NR2A or 2B, or NR2C or 2D, expressed in oocytes, the reduction would be 70 to 20 fold respectively; Kuner and Schoepfer, 1996). This weak magnesium sensitivity, together with antibody labelling, suggested that the white matter oligodendrocyte NMDA receptors might be composed of NR1, NR2C and NR3 subunits (Káradóttir *et al.*, 2005; Salter and Fern, 2005; Micu *et al.*, 2006). Indeed, the co-assembly of NR1/NR2C/NR3A subunits in HEK cells leads to the formation of NMDA receptors with a magnesium block that closely resembles that seen in cerebellar oligodendrocytes (Burzomato *et al.*, 2010), consistent with this constitution being the one for oligodendrocyte NMDA receptors.

The physiological role of NMDA receptors in oligodendrocyte lineage cells still waits to be discovered: notably they do not seem to be activated by glutamate release at the synapses made from axons onto OPCs (Kukley *et al.*, 2007; Ziskin *et al.*, 2007), suggesting an extrasynaptic location in the OPCs (analogous to the extrasynaptic NMDA receptors found on neurons). Their preferential location on myelinating processes (detected by immunolabelling at both the light microscopy level, and also the EM level which showed expression of NR1 in the myelin: Káradóttir *et al.*, 2005; Salter and Fern, 2005; Micu *et al.*, 2006) suggests a possible role of these receptors in axon-glia signalling, probably during the myelination process (Káradóttir and Attwell, 2007). In pathological conditions, such as ischaemia, oligodendrocyte NMDA receptors were

shown to become overactivated, which has a detrimental effect on the cell, presumably by allowing calcium influx into the processes, resulting in myelin disruption and even a loss of the myelinating processes (Salter and Fern, 2005; Micu *et al.*, 2006), as described in more detail below in section 1.4.2.

In Chapter 4 of this thesis I describe experiments to investigate the role of NMDA receptors in the oligodendrocyte response to ischaemia.

1.3.2.1.3 Metabotropic glutamate receptors

Metabotropic glutamate receptors (mGluRs) can be divided into 3 groups, of which group I comprises mGluR1 and mGluR5, group II comprises mGluR2 and mGluR3, and group III comprises mGluR4 and mGluR6-8. Group I are G_q-coupled receptors, the activation of which stimulates phospholipase C (PLC) to generate IP₃ and diacylglycerol, and thus leads to the opening of endoplasmic reticulum calcium channels (raising [Ca²⁺]_i) and protein kinase C activation. Group II and III receptors are G_i-coupled proteins whose activation causes adenylyl cyclase inhibition and so decreases the intracellular cyclic AMP concentration (for a review see Conn and Pin, 1997).

OPCs in culture express a range of mGluRs, with mGluR3 and mGluR5 being the most commonly found, both at the mRNA and the protein level (Luyt *et al.*, 2003; Deng *et al.*, 2004; Luyt *et al.*, 2006; Cahoy *et al.*, 2008). The expression of mGluRs, apart from mGluR3 (Deng *et al.*, 2004; Cahoy *et al.*, 2008), seems to decrease with oligodendrocyte maturation, suggesting they may have a role in oligodendrocyte development (Luyt *et al.*, 2006). Activation of mGluR5 causes calcium oscillations in OPCs (Luyt *et al.*, 2003; Luyt *et al.*, 2006) and mGluR3 reduces intracellular cAMP concentration (Luyt *et al.*, 2006), both processes thought to enhance OPC migration (Othman *et al.*, 2003; Gudz *et al.*, 2006). Surprisingly, however, activation of these receptors alone failed to exert any effect on OPC motility (Luyt *et al.*, 2006). Activation of mGluR5 may decrease the cells' vulnerability to excitotoxic insults and apoptosis (Kelland and Toms, 2001; Deng *et al.*, 2004; Luyt *et al.*, 2006). Additionally, stimulation of group I mGluRs on oligodendrocytes has been recently found to cause a release of BDNF, an effect that may influence cell survival and development (Bagayogo and Dreyfus, 2009). However, to date, although mGluRs have been detected on OPCs in brain slices (Luyt *et al.*, 2003) there is no definite study proving a functional role for oligodendrocyte mGluRs *in situ*.

In Chapter 4 of this thesis I examine the contribution of mGluRs to the response of oligodendrocytes to ischaemia.

1.3.2.2 GABA receptors

GABA receptors are widely expressed in the CNS and can be divided into 3 subclasses: GABA_A, GABA_B and GABA_{A-ρ} (formerly GABA_C).

GABA_A receptors are ionotropic chloride-permeable receptors, the activation of which evokes a hyperpolarization in cells where the intracellular chloride concentration ($[Cl^-]_i$) is low (so the chloride reversal potential is more negative than their resting membrane potential), and a depolarization in cells with a high $[Cl^-]_i$ (so the chloride reversal potential is above their resting membrane potential). They are formed of 5 subunits: 2 α , 2 β and an auxiliary one (most commonly γ).

OPCs have been reported to express mRNA for 4 α (α_{2-5}) and 2 γ (γ_2, γ_3) subunits, while β subunits were not tested for (Williamson *et al.*, 1998). These cells are found to have a high $[Cl^-]_i$ that is maintained by NKCC1 co-transporter activity (Wang *et al.*, 2003) and so their reversal potential for chloride is shifted to a potential more positive than the resting potential (~ -43 mV; Lin and Bergles, 2004). Consequently, opening of GABA_A receptors causes an efflux of chloride, depolarizing the cell membrane, and GABA acts as an excitatory neurotransmitter at the synapses which OPCs receive from interneurons in the grey matter (Lin and Bergles, 2004; Vélez-Fort *et al.*, 2010).

The physiological role of GABA_A receptors in OPCs is uncertain. Lin and Bergles (2004) showed that activation of these receptors causes a transient inhibition of AMPA receptor currents in the OPCs, so it was suggested that GABA_A receptors may regulate cell development by modulating the efficacy of glutamate signalling (and hence presumably modulating glutamate's effects on OPC proliferation or migration). In the Attwell lab, Nicola Hamilton (unpublished) has shown that blocking GABA_A receptors in cultured cortical slices leads to a doubling of the number of oligodendrocyte lineage cells formed, but it is uncertain if this action of endogenous GABA is mediated *via* receptors on OPCs or on neurons..

The expression and importance of GABA_A receptors in mature oligodendrocytes is unclear: Vélez-Fort *et al.* (2010) reported decreasing GABAergic synaptic activity in OPCs during cell differentiation which implies either a loss of GABA release onto OPCs or a downregulation of their GABA_A receptors. However, Butt and Tutton (1992) recorded a small membrane depolarization (2-3 mV) evoked by GABA in optic nerve

mature oligodendrocytes, and similarly Pastor *et al.* (1995) reported a small inward current upon GABA application in spinal cord oligodendrocytes.

GABA_B receptors are G_i-protein coupled metabotropic receptors. In OPCs they are expressed both in culture and in the white matter of brain slices, and inhibition of these receptors increases OPC migration and differentiation (Luyt *et al.*, 2007). In mature oligodendrocytes, GABA_B receptors have only been found under culture condition (Charles *et al.*, 2003; Luyt *et al.*, 2007).

To date, GABA_{A-ρ} receptor expression has not been detected in oligodendrocyte lineage cells.

In Chapter 4 of this thesis I examine the contribution of GABA receptors to the response of oligodendrocytes to ischaemia.

1.3.2.3 Purinergic receptors

Purinergic receptors can be divided into two families: P1 (adenosine-activated) and P2 (ATP/ADP-activated) receptors. P2 receptors further subdivide into P2Y (metabotropic) and P2X (ionotropic) receptors (Burnstock, 2006). All of these types are expressed by oligodendrocytes.

All four subtypes of adenosine-activated P1 receptor (A1, A2a, A2b and A3) were found to be expressed in OPCs and in immature oligodendrocytes (defined by O4 expression, which does not allow for a rigid distinction between late precursors, immature and early mature oligodendrocytes, see Fig. 1.4) (Stevens *et al.*, 2002). They were found to be important for axon-glia communication, inhibiting cell proliferation and stimulating differentiation and myelination (Stevens *et al.*, 2002). Later studies showed that the A1a receptor (high-affinity A1 receptor variant; Ralevic and Burnstock, 1998) has a positive effect on migration, without exerting an influence on cell proliferation and differentiation (Othman *et al.*, 2003), suggesting that the effects observed by Stevens *et al.* (2002) on proliferation and myelination may have been mediated by adenosine receptors other than A1a receptors.

Although the role of adenosine receptors in mature oligodendrocyte physiology remains to be uncovered, Melani *et al.* (2009) have shown that blocking A2a receptors in ischaemia results in less damage occurring to myelin and a reduced death of OPCs and oligodendrocytes.

P2X receptors are classical cationic ligand-operated channels, permeable to sodium, potassium and calcium (Abbracchio *et al.*, 2009), of which oligodendrocytes

express many subtypes (such as P2X_{1-4,7}: Agresti *et al.*, 2005), with a most prominent role for P2X₇ receptors. P2X₇ receptors are reported to be responsible for producing an increase in intracellular calcium concentration upon ATP application, both in OPCs and in mature oligodendrocytes (Domercq *et al.*, 2010; Hamilton *et al.*, 2010). The physiological role of these receptors is unknown, but their overactivation leads to excitotoxic damage and death of oligodendrocytes during ischaemia and spinal cord injury (Wang *et al.*, 2004; Domercq *et al.*, 2010). Furthermore, blocking P2X₇ receptors in a mouse model of MS (EAE) reduced demyelination and ameliorated the EAE symptoms (Matute *et al.*, 2007).

P2Y receptors are classical G-protein coupled metabotropic receptors (Abbracchio *et al.*, 2009), of which subtypes 1, 2 and 4 are expressed by OPCs. Their activation leads to increased OPC migration and differentiation, and inhibits proliferation (Agresti *et al.*, 2005). Their expression by mature oligodendrocyte has not been yet investigated.

In Chapter 4 of this thesis I examine the contribution of P2X₇ receptors to the response of oligodendrocytes to ischaemia.

1.4 Pathologies of the white matter and the role of oligodendrocytes

As described in section 1.1, myelination of axons in the white matter greatly enhances the speed of signal transmission between distant parts of the CNS and so is crucial for the proper functioning of the nervous system. In many diseases affecting the white matter, the myelin sheath gets damaged (Levine *et al.*, 2001), causing a decrease of the conduction speed because of an increase in axon capacitance, and possibly also because of disruption of the protein organisation at the node of Ranvier (Howell *et al.*, 2006). Such processes eventually lead to axon atrophy (Papadopoulos *et al.*, 2006), probably because oligodendrocytes provide axons with trophic or energetic factors (Nave, 2010). If a significant fraction of axons in a tract are affected, this will inevitably lead to severe mental or physical disability. Such an outcome is seen in diseases such as multiple sclerosis, ischaemia (which occurs in stroke, spinal cord injury and in some cases of periventricular leukomalacia leading to cerebral palsy) and the genetic leukodystrophies. Prevention of myelin sheath damage and oligodendrocyte death, as well as restoration of destroyed myelin, is therefore a crucial aim of therapies for

pathological conditions affecting white matter.

In this section I will give an overview of oligodendrocyte pathologies, and their underlying mechanisms, some of which may also be involved in the particular pathologies that I am concerned with (ischaemia and the leukodystrophies).

1.4.1 Multiple sclerosis

Multiple sclerosis (MS; also known as *disseminated sclerosis* or *encephalomyelitis disseminata*) is an autoimmune demyelinating disease that affects young adults. It is characterized by the presence of large lesions in white matter that appear as a result of primary demyelination (Fig. 1.9A), and subsequent axonal dystrophy and loss of axonal function. In most cases, the early stages of multiple sclerosis have remission periods that are associated with remyelination of the primary lesions. Gradually, however, remyelination becomes less effective and a progressive loss of function of the affected tracts leads to a progressive deterioration of motor and cognitive functions, leading to permanent disability.

The origin of MS is unknown, but there are numerous hypotheses for possible causative agents, including genetic predisposition, and environmental and infectious factors (Hemmer *et al.*, 2002). At the cellular level, the primary demyelination is thought to be an autoimmune response mediated by T cells entering the CNS and failing to recognize myelin as being a normal part of the body, and subsequently attacking it, leading to inflammation, activation of microglia and macrophages, and release of cytokines and reactive oxygen species, all of which damage the myelin (Hemmer *et al.*, 2002). Afterwards the myelin debris is cleared. In the last 10 years it has been suggested that three ion channels on oligodendrocytes play a role in the pathological events of MS: glutamate receptors, ASIC channels and P2X₇ receptors. I will review these actions here since, in Chapter 4, I will investigate whether they also play a role in the oligodendrocyte response to ischaemia.

Glutamate release plays a role in multiple sclerosis. In the EAE mouse model of MS, activated immune cells were suggested to release glutamate that could act on oligodendrocyte AMPA/KA receptors, damaging the oligodendrocytes, and subsequently the underlying axons (Pitt *et al.*, 2000; Smith *et al.*, 2000). The evidence for this was that blocking AMPA/KA receptors resulted in a significant amelioration of the disease symptoms, increased oligodendrocyte survival and reduced dephosphorylation of neurofilament H, an indicator of axonal damage, without altering

immune system function or the amount of inflammation occurring (Pitt *et al.*, 2000).

ASIC1 channels also contribute to cell damage in EAE. In the ASIC knock out mouse there was a significant reduction in the clinical deficits and axonal degeneration evoked by EAE, when compared to the effects of EAE in control mice (Friese *et al.*, 2007). Further investigation, performed both on the EAE mice and on tissue samples from MS patients, showed an upregulation of ASIC1 channel expression on axons and oligodendrocytes and a co-localization of the axonal ASIC1 channel expression with the axonal injury marker beta amyloid precursor protein (Vergo *et al.*, 2011). Blocking ASICs with amiloride proved to be neuroprotective in nerve explants and protected both myelin and neurons from damage in EAE, an effect that was independent of activation of the immune system (Friese *et al.*, 2007; Vergo *et al.*, 2011). It is currently uncertain whether the main damaging action of ASICs is mediated by the ASICs on oligodendrocytes, or those on axons, or whether both are involved.

The purinergic P2X₇ receptor has similarly been proposed to play a role in MS, as prolonged activation of this receptor causes myelin damage and lesions similar to those found in MS, and its expression is elevated in MS patients (Matute *et al.*, 2007). Consistent with this, blocking P2X₇ receptors in mice with EAE proved to be beneficial, reducing the demyelination and restoring normal axon conduction velocity (Matute *et al.*, 2007).

It was reported that mature oligodendrocytes cannot form new myelin sheaths when transplanted into areas of demyelination (Targett *et al.*, 1996; Crang *et al.*, 2004) and that postmitotic oligodendrocytes that survive demyelination do not contribute to remyelination (Keirstead and Blakemore, 1997). This strongly suggests that mature oligodendrocytes are not involved in the restoration of myelin. The cells that are the most probable source of new myelin are adult NG2 cells (adult OPCs: Polito and Reynolds, 2005), which, in the absence of pathology, mostly differentiate into oligodendrocytes (Rivers *et al.*, 2008). It was found that, following lysolecithin-induced demyelination, OPCs that were labeled with BAG retrovirus (i.e. labeled by retrovirally-delivered beta-galactosidase, the activity of which leads to the emergence of intracellular blue staining) eventually transformed into BAG-labeled remyelinating oligodendrocytes (Gensert and Goldman, 1997), and that adult NG2 cells isolated from healthy white matter, when injected into a demyelinated area, can remyelinate it (Zhang *et al.*, 1999).

There are two main phases to the remyelination process: a recruitment phase

(which involves cell activation, proliferation and migration to the demyelinated area) and a differentiation phase (which is characterised by cells maturing into myelin-forming oligodendrocytes) (Franklin, 2002; Franklin and Ffrench-Constant, 2008) (Fig. 1.9B). Different growth factors play a role in both of these phases. PDGF and FGF were found to be involved in OPC recruitment, as they increase cell migration and proliferation (see section 1.2), while IGF and TGF β 1 were reported to be involved in the differentiation phase by regulating cell maturation (for a full review see: Franklin, 2002; Franklin and Ffrench-Constant, 2008; Fancy *et al.*, 2010).

It was also suggested that axons might play an active role in the remyelination process (as they do in primary myelination) both because their activity will release factors that regulate myelination, and because axonally expressed PSA-NCAM was found in demyelinating but not remyelinating areas, suggesting that this molecule prevents myelination (Charles *et al.*, 2002).

With time (and with increasing age of the affected individuals: Sim *et al.*, 2002) the remyelination process gradually becomes less efficient and its inadequacy results in the appearance of sustained lesions. The reason for this is unclear. It is supposed that either OPC recruitment or, more probably, their differentiation phase is disturbed (Fancy *et al.*, 2010).

The available therapies for MS involve mostly suppression of inflammation which decreases the speed of the demyelination. Remyelination treatments, which potentially include transplantation of adult OPCs, are still being developed (Windrem *et al.*, 2008).

1.4.2 The pathology of white matter ischaemia

Brain ischaemia is a critical reduction in cerebral blood flow that leads to irreversible brain damage in conditions such as stroke (one of the leading causes of death and disability in developed countries), traumatic brain injury, spinal cord injury and some cases of periventricular leukomalacia leading to cerebral palsy (Khwaja and Volpe, 2008; Taoufik and Probert, 2008). Neuronal cell death in the grey matter has a pivotal role in the loss of proper brain function, but the white matter also suffers greatly during ischaemia. Oligodendrocytes have been shown to be especially vulnerable to anoxic conditions and their damage has a deleterious effect on axonal action potential propagation, ultimately affecting proper communication between different brain areas. A comprehensive understanding of oligodendrocyte responses to the ischaemic insult

may therefore allow the occurrence of oligodendrocyte damage to be minimised. Since many of the experiments in this thesis investigate the electrical response of oligodendrocytes to simulated ischaemia, in the following sections I will review our current knowledge of ischaemia's effects, first on the grey matter (which is better studied) and then on the white matter.

1.4.2.1 An overview of the grey matter response to ischaemia

In the grey matter the greatly reduced supply of oxygen and glucose occurring in ischaemia results in various extracellular and intracellular changes that finally lead to an impairment of neuronal function and to cell death. In this overview I will highlight the main changes in cellular physiology affected by ischaemia in the grey matter, while a more detailed description of the effects of ischaemia on the white matter and on oligodendrocytes, a major focus of my PhD, will be given in section 1.4.2.2.

1.4.2.1.1 Energy failure

One of the most profound features of ischaemia is the energy failure due to the inhibition of oxidative phosphorylation. The lack of oxygen supply initially results in glycolysis becoming the major source of ATP production, but as this process is much less efficient than oxidative phosphorylation (producing 2 as opposed to 28 ATP molecules per molecule of glucose), and because local stores of glycolytic intermediates (and of astrocyte glycogen) are no longer being replenished by glucose arriving in the blood, the cell is soon deprived of sufficient energy levels (Lipton, 1999). That leads to an inhibition of cellular kinases and ATP-dependent pumps, notably the Na^+/K^+ -ATPase, on which 75% of brain energy is used (Attwell and Laughlin, 2001). This causes a severe ionic imbalance which results in membrane depolarization.

1.4.2.1.2 Ionic imbalance

Failure of the energy supply is the direct cause of the ion homeostasis disruption occurring in ischaemia. As mentioned above, the Na^+/K^+ -ATPase fails during ischaemia or anoxia due to ATP depletion. The block of the Na^+/K^+ pump results in the potassium efflux that occurs normally into the extracellular space (because cell resting potentials are more positive than the Nernst potential for K^+ so K^+ exits through the cells' resting K^+ conductance) not being pumped back, so the extracellular potassium concentration ($[\text{K}^+]_o$) rises. This depolarizes neurons and glia, leading initially to action potential

firing and also to excessive synaptic vesicle release that is action potential independent (Katchman and Hershkowitz, 1993). After several minutes a regenerative increase of $[K^+]_o$ occurs, resulting in $[K^+]_o$ rising to 40 mM in anoxia and ~55 mM in ischaemia (Hansen, 1985) and a fall of extracellular sodium concentration ($[Na^+]_o$) by a similar amount due to a sodium flux into the cell. These changes depolarize cells to about -20 mV, an event termed the anoxic depolarization.

1.4.2.1.3 Glutamate release and excitotoxicity

As mentioned above, the initial depolarization evoked by ischaemia, and the rise of $[Ca^{2+}]_i$ produced by this and by the inhibition of Ca^{2+} extrusion mechanisms occurring when ATP levels and ion gradients fall, causes excessive synaptic release of different neurotransmitters, among them glutamate. Nevertheless, the main mode of glutamate release in ischaemia is calcium-independent and mediated by glutamate transporters (Rossi *et al.*, 2000; Hamann *et al.*, 2005).

Under physiological conditions, glutamate transporters transport glutamate into the cell, removing it from the extracellular space (and, most importantly, from the synaptic cleft). The transport is Na^+ -dependent and electrogenic: for each glutamate anion entering the cell, three Na^+ ions and one proton enter, and one K^+ ion moves out of the cell (Fig. 1.10A). However, in ischaemia, the increase in $[Na^+]_i$, fall of $[Na^+]_o$, and rise of $[K^+]_o$ (and associated depolarization) cause the transporter to reverse and pump glutamate out of the cell (Rossi *et al.*, 2000) (Fig. 1.10B). This process generates a massive increase in the extracellular glutamate concentration, reaching up to ~100 μ M (Globus *et al.*, 1991; Phillis *et al.*, 1996), and leads to the overactivation of glutamate receptors, of which NMDA receptor opening is the most detrimental to the cell as it permits an excessive calcium influx, the effect of which is described below.

1.4.2.1.4 Calcium influx

A massive calcium influx from the extracellular space during ischaemia is triggered by multiple factors (Fig. 1.11). Predominantly, as mentioned above, it is caused by the activation of AMPA and NMDA receptors when the extracellular glutamate level increases (Rossi *et al.*, 2000; Hamann *et al.*, 2005; for a review see: Siesjö, 1988, and Lipton, 1999). However, activation of other channels and receptors may also contribute to the Ca^{2+} influx: ASICs (Xiong *et al.*, 2004), TRPs (Aarts *et al.*, 2003; Lipski *et al.*, 2006) and $P2X_7$ receptors (Domercq *et al.*, 2010) are all Ca^{2+} -

permeable and open during ischaemia. In addition, depolarization opens voltage-gated calcium channels, and the rise of $[Na^+]_i$ produced by glutamate-gated Na^+ entry reverses the action of the Na^+/Ca^{2+} exchanger, both of which result in a further increase in the intracellular calcium concentration (Hertz, 2008). At the same time, calcium extrusion from the cell by the ATP-dependent calcium pump is blocked because of ATP depletion (Nestler *et al.*, 2008).

The calcium concentration rise in the cell cytoplasm can also have an intracellular source (Fig. 1.11). In the ER, a process known as calcium-dependent calcium release (CIRC) occurs, where an increase in $[Ca^{2+}]_i$ activates (ryanodine receptor) channels on the ER, causing a calcium efflux into the cytoplasm (Lipton, 1999; Nestler *et al.*, 2008). Additionally, the action of inositol trisphosphate (a downstream product of group I mGluR activation) on its ER receptors causes opening of IP_3 receptor calcium channels in the ER membrane and a release of calcium (Nestler *et al.*, 2008). In addition the fall of ATP level in the cell inhibits the Ca^{2+} -ATPase that normally pumps Ca^{2+} into the endoplasmic reticulum, and the fall of energy supply to mitochondria will run down their membrane potential and reduce Ca^{2+} buffering by these organelles.

The intracellular calcium concentration is around 100 nM under normal conditions but during ischaemia rises to $\sim 2.5 \mu M$ (Lipton, 1999), causing an overstimulation of normally well-controlled Ca^{2+} -dependent processes. The increased activation of proteases, such as calpain, causes the irreversible activation of signalling pathways and may ultimately result in the break-down of the cytoskeleton and induction of apoptotic pathways. Elevated $[Ca^{2+}]_i$ leads also to the increased activation of lipases, such as phospholipase A (PLA) and C (PLC) (Raichle, 1983), whose action causes a breakdown of membrane phospholipids and may result in decreased membrane integrity. Activation of lipases also leads to the production of free fatty acids, including arachidonic acid, that in turn stimulate the production of eicosanoids, such as prostaglandins, thromboxanes and leukotrienes. Prostaglandin production may result in the formation of reactive oxygen species (described in the next section) and an increase in membrane permeability. Eicosanoids can additionally exacerbate the ischaemic insult by promoting vasoconstriction and platelet aggregation and in this way further block the supply of oxygen and glucose to the affected area (Raichle, 1983).

The promotion of reactive radical formation by Ca^{2+} is not restricted to the production of eicosanoids. Binding of nitric oxide (NO) synthase to the Ca^{2+} -calmodulin

complex initiates the production of NO from arginine (Lipton, 1999), which may result in the formation of the highly increased levels of reactive nitrogen species, described below.

1.4.2.1.5 Formation of reactive radicals

Excitotoxicity is frequently associated with the formation of reactive radicals (also known as free radicals or reactive oxygen and nitrogen species). Free radicals are molecules with an unpaired electron in an outer shell; this unpaired electron causes the molecule to be unstable and highly reactive, targeting membrane fatty acids with double bonds and protein sulphydryl groups, which greatly destabilizes their structures and leads to changes in their properties (Nestler *et al.*, 2008).

The production of reactive oxygen and nitrogen species (ROS and RNS, respectively) requires the presence of some oxygen, and greatly increases (i) in the penumbra of an ischaemic area where some oxygen is still provided by unblocked vessels nearby, and (ii) when blood flow is restored after ischaemia if an occluding clot is removed either spontaneously or by medical intervention with tissue plasminogen activator. Due to their high activity, free radicals (which may normally serve as second messengers in various signalling pathways) become detrimental to the cell, causing DNA damage, lipid peroxidation and severe protein oxidation, which lead to cell death (Raichle, 1983; Siesjö, 1988; Lipton, 1999).

The most damaging free radical, hydroxyl radical ($\cdot\text{OH}$) can be formed through different pathways (Fig. 1.12). The formation of superoxide anion, which may be initiated by phospholipase activation, is a prerequisite for the formation of other ROS, and it is also involved in the RNS pathway. Superoxide anion is transformed by superoxide dismutase (SOD) into hydrogen peroxide (H_2O_2), which may serve as a precursor for $\cdot\text{OH}$.

Excessive NO synthesis induced by the $[\text{Ca}^{2+}]_i$ rise occurring in ischaemia leads to the formation of RNS. Upon reaction of NO with superoxide anion, peroxynitrate is formed and that, together with H_2O_2 , may result in $\cdot\text{OH}$ and nitrogen dioxide formation. Peroxynitrate is also a precursor of other RNS radicals (e.g. nitrosoperoxy carbonate; Fig. 1.12).

In ischaemia, therefore, the greatly increased Ca^{2+} flux into the cell may lead to excessive ROS formation (through the activation of phospholipases; Raichle, 1983) and RNS formation (by NO synthase stimulation; Lipton, 1999).

Most of the free radicals, however, are formed during reperfusion after ischaemia. Upon a sudden increase in oxygen level, mitochondria drastically raise their level of superoxide production due to side reactions of electron carriers along the respiratory chain (mostly complexes I and III: Sugawara and Chan, 2003; Sugawara *et al.*, 2004). Additionally, radicals are formed during the autooxidation of many compounds (e.g. catecholamines) and in the xanthine oxidase reaction (Lipton, 1999).

The process of ROS and RNS formation leads to an increased membrane permeability, a prolonged inhibition of protein synthesis and promotion of DNA cleavage, including cleavage *via* the activation of pro-apoptotic signalling systems such as mitogen-activated protein kinases (MAPKs; Matsuzawa and Ichijo, 2005) which eventually cause extensive apoptotic cell death.

1.4.2.1.6 Acidotoxicity

Glycolysis, which is the main source of ATP in ischaemia (until the exhaustion, after a few minutes, of glucose and glycogen stores), produces large amount of pyruvate which is then transformed into lactate, because there is no oxidative phosphorylation to drive its consumption by the citric acid cycle. Lactate formation (and probably also the cessation of CO₂ clearance by the blood) greatly decreases the intra- and extracellular pH (to 6.0-6.5: Nedergaard *et al.*, 1991). The resulting fall of extracellular pH leads to the opening of ASICs (see section 1.3.1.4) and a further detrimental influx of Na⁺ and Ca²⁺ (Xiong *et al.*, 2004) which add to the ionic imbalance and to Ca²⁺-induced cell damage during ischaemia. Moreover, the intracellular pH change is suggested to interfere with many cellular processes, leading to an increase in protein degradation, a decrease in its synthesis and a loss of cell volume control (Rehncrona, 1985).

1.4.2.2 The white matter mature oligodendrocyte response to ischaemia

The white matter is vulnerable to anoxia and ischaemia. Oligodendrocytes, and especially their precursors at an early stage of development, suffer greatly from ischaemic insult, which may result in their death causing concomitant mental and physical impairment in stroke, spinal cord injury and periventricular leukomalacia leading to cerebral palsy (Park *et al.*, 2004; Stys, 2004; Khwaja and Volpe, 2008). The vulnerability of action potential propagation to anoxic disruption becomes greater as white matter tracts mature (Hamner *et al.*, 2011), but the response of mature oligodendrocytes to ischaemia is less studied than that of developing oligodendrocytes

and, in the adult when myelination is essentially complete, it is their damage that leads to axon dysfunction and the eventual loss of connectivity between different brain areas.

Just as for neurons, oligodendrocyte lineage cells are damaged by the glutamate that is released in anoxia and ischaemia. The following sections review the role of glutamate in damaging oligodendrocytes, its origin in the white matter and its actions on white matter ionotropic and metabotropic receptors, as well as additional factors and receptors that may add to the deleterious effect of ischaemia on mature oligodendrocytes.

1.4.2.2.1 The mechanism of ischaemic glutamate release in the white matter

In grey matter ischaemia, glutamate, which is the main trigger of neuronal damage, is mainly released *via* the reversal of glutamate transporters following a brief initial phase of increased vesicular release (see above). In the white matter, however, the origin of glutamate is still controversial.

Li *et al.* (1999) suggested that, as in the grey matter, the reversal of glutamate transporters is the main source of extracellular glutamate in white matter anoxia (Fig. 1.13). By immunolabelling glutamate, they showed it was predominantly released from axons and oligodendrocytes, but not from astrocytes (a result confirmed later by Li and Stys, 2001). Later, Fern and Möller (2000) also reported that cultured immature oligodendrocytes release glutamate in simulated ischaemia *via* reversal of glutamate transporters.

Immunostaining for glutamate transporters showed expression of EAAC1 on axons, GLAST on oligodendrocytes and astrocytes, and GLT1 on astrocytes (Li *et al.*, 1999), suggesting that EAAC1 and GLAST release the glutamate. However, the identity of the transporter primarily involved in glutamate release in white matter ischaemia is unclear, since Li *et al.* (1999) and Deng *et al.* (2003) found that dihydrokainate (DHK), a blocker that preferably inhibits GLT1, was neuroprotective in anoxia and OGD (oxygen-glucose deprivation) to a similar extent as the broad-spectrum glutamate transporter inhibitor, PDC. This result suggests a major involvement of GLT1 in glutamate release, and is surprising considering that GLT1 expression was confined to the astrocytes which apparently did not contribute to glutamate release (Li *et al.*, 1999; Stys, 2004). In comparison, in grey matter ischaemia, GLT1 and GLAST on Bergmann glia did not significantly contribute to the glutamate release, and the release was tentatively attributed to reversal of EAAC1 in neurons (Hamann *et al.*, 2005).

Another possible source of glutamate in white matter ischaemia is release of synaptic vesicles, at the synapses from axons to OPCs, which are described above (section 1.2.1). It was shown in grey matter that anoxia/ischaemia results in excessive vesicular release of neurotransmitters such as glutamate (Katchman and Hershkowitz, 1993) and GABA (Allen *et al.*, 2004) into the extracellular space. This release is independent of action potentials and probably reflects a rise of $[Ca^{2+}]_i$ occurring in the synaptic terminal when $[K^+]_o$ rises and depolarizes cells at the same time as Ca^{2+} extrusion is slowed. The increased vesicular release lasts several minutes until the anoxic depolarization occurs (Allen *et al.*, 2004). After the anoxic depolarization, Rossi *et al.* (2000) reported that glutamate release in grey matter ischaemia is predominantly by reversed uptake, but the role of exocytotic release in white matter ischaemia is unknown.

An additional potential mechanism for glutamate release in the white matter in response to ischaemic insult could be an overactivity of astrocyte NKCC1 co-transporters. NKCC1 co-transporters mediate the electroneutral transport of Na^+ , K^+ and $2Cl^-$ into the cell under physiological conditions and are expressed throughout the brain by neurons, astrocytes and oligodendrocytes (Chen and Sun, 2005). Their proposed role is to generate intracellular Cl^- accumulation, which results in GABA depolarizing (rather than hyperpolarizing) neurons especially early in development (Alvarez-Leefmans *et al.*, 1988; Sun and Murali, 1999). NKCC1 also plays a role in K^+ uptake and cell volume regulation in astrocytes (Mongin *et al.*, 1994). Under ischaemic condition, when $[K^+]_o$ rises (see above), the resulting increase of white matter astroglial NKCC1 activity (Su *et al.*, 2000) brings excessive K^+ , Na^+ , and Cl^- into the cell, followed by water, which causes cell swelling, membrane rupture and glutamate release (Su *et al.*, 2002). This leads to a sudden increase in extracellular glutamate concentration which directly damages oligodendrocytes (Wilke *et al.*, 2004).

Finally, another source of glutamate release in white matter has been suggested. Domercq *et al.* (2007) have shown that microglia activated by lipopolysaccharide (LPS, a constituent of bacterial walls) release glutamate through cystine/glutamate antiporters (system X_c^-). System X_c^- , which is especially abundant in macrophages and microglia, imports extracellular cystine in exchange for intracellular glutamate. Activated microglia produce and release large amounts of ROS, and in order to protect themselves from these molecules, they maintain high levels of ROS scavengers, such as glutathione (Watanabe and Bannai, 1987). Cystine is necessary for glutathione production and so

upon microglial activation there is an increase in cystine uptake and, consequently, more glutamate release through system X_c^- . This mechanism could occur during ischaemia, as microglia get activated under this condition (Yenari *et al.*, 2010), although Cavalier and Attwell (2005) have argued that the extracellular cystine concentration in the CNS is not high enough to allow significant glutamate efflux by this mechanism.

1.4.2.2.2 Oligodendrocyte glutamate receptor activation in ischaemia

Glutamate release in ischaemia has a detrimental effect on the white matter, especially on oligodendrocytes, which for a long time was attributed solely to the activation of their AMPA/KA receptors.

Fern and Möller (2000) found that the death of immature oligodendrocytes that occurs in culture during simulated ischaemia was mediated by a calcium influx through AMPA/KA receptors (and not due to the activation of voltage-gated calcium channels or NMDA receptors). Similarly, Tekkök and Goldberg (2001) concluded that hypoxic-ischemic white matter injury in adult mouse brain was due to AMPA/KA receptor activation, and McCarran and Goldberg (2007) found that blocking AMPA/KA receptors in ischaemia (applied to mimic one cause of periventricular leukomalacia) reduced axonal degeneration and oligodendrocyte loss (with oligodendrocytes being protected across a broader range of ages than axons were) while blocking NMDA receptors was not protective.

It is not clear which developmental stage of the oligodendrocyte lineage is more affected by AMPA/KA-mediated injury during ischaemia. Deng *et al.* (2003) reported that OPCs were more vulnerable to simulated ischaemia than were mature oligodendrocytes, while McCarran and Goldberg (2007) found that oligodendrocytes at postnatal days 10 and 21 (i.e. when a larger fraction are immature and mature oligodendrocytes) suffer more from AMPA/KA-receptor-mediated damage than cells at earlier ages (i.e. mostly OPCs). Considering that AMPA/KA receptors become downregulated with oligodendrocyte development (Cahoy *et al.*, 2008; De Biase *et al.*, 2010; Kukley *et al.*, 2010), it seems probable that OPCs and early immature oligodendrocytes are indeed more vulnerable than are the mature oligodendrocytes to the effects of hypoxic-ischaemic insult that are mediated by these receptors.

Although most of the studies performed so far on oligodendrocyte or white matter ischaemia did not show a beneficial effect of NMDA receptor blockers (Li and Stys, 2000; Fern and Möller, 2000; Tekkök and Goldberg, 2001; Tekkök *et al.*, 2007;

McCarran and Goldberg, 2007; Baltan *et al.*, 2008) recently Káradóttir *et al.* (2005) reported that NMDA receptors on white matter OPCs and mature oligodendrocytes are activated during ischaemic exposure (Fig. 1.14). Additionally, Salter and Fern (2005) and Micu *et al.* (2006) found that in the optic nerve during ischaemia there is an NMDA-receptor-mediated increase in intracellular calcium concentration in the myelinating processes of oligodendrocytes (but not in their somata), and that the myelinating processes are damaged in an NMDA-receptor-dependent manner. Consistent with this, Bakiri *et al.* (2008) found that NMDA receptor blockers reduced loss of the optic nerve compound action potential during ischaemia, while AMPA/KA receptor block was not protective. It is unclear why this study gave different results to that of the studies described above (e.g. Tekkök *et al.*, 2007; Baltan *et al.*, 2008), although the fact that Bakiri *et al.* (2008) studied rat optic nerve while the other two papers studied mouse optic nerve may account for the difference.

Salter and Fern (2005) and Micu *et al.* (2006) also found that in the optic nerve during ischaemia there is an AMPA/KA-receptor-mediated increase in intracellular calcium concentration in the somata of oligodendrocytes (but not in their myelinating processes), and AMPA/KA receptor blockers prevented soma damage (Salter and Fern, 2005), suggesting a preferential localization of AMPA/KA receptors on oligodendrocyte cell bodies, with NMDA receptors mainly located to the processes (as described above).

The lack of protective effect of NMDA receptor antagonists in some studies could be explained by the different models employed. For example, NMDA receptors may be downregulated in culture due to the lack of interaction with axons. Alternatively, the difference in developmental stage may play an important role, as Cahoy *et al.* (2008) have shown that the level of NMDA receptor mRNA decreases with cell maturation. Also, there might be regional and developmental variations of expression of NMDA receptors – for instance, oligodendrocytes in cerebellum were shown to respond with a larger current to NMDA application than those in corpus callosum (Káradóttir *et al.*, 2005).

1.4.2.2.3 Ischaemia-induced calcium influx in oligodendrocytes

A significant fraction of the damage occurring to oligodendrocytes in ischaemia is dependent on calcium entry from the extracellular space. Using a Ca^{2+} -sensitive dye Micu *et al.* (2006) showed that $[\text{Ca}^{2+}]_i$ rises both in the cell soma and the myelinating processes. Furthermore, calcium removal greatly reduces oligodendrocyte death and

somewhat reduces loss of their myelinating processes (Salter and Fern, 2005). It is thus important to assess the route by which Ca^{2+} enters oligodendrocytes in ischaemia.

AMPA/KA receptors were long considered solely responsible for the Ca^{2+} influx occurring in ischaemia (Fern and Möller, 2000; Tekkök and Goldberg, 2001; Deng *et al.*, 2003; Wilke *et al.*, 2004). However, most of these studies were conducted in culture (where the cells might change the proteins they express) and on immature cells, and it was found that the Ca^{2+} -permeability of oligodendrocyte AMPA/KA receptors depends strongly on the developmental stage of the cell. As noted above (section 1.3.2.1.1), OPCs and immature oligodendrocytes do not express the GluR2 subunit that is responsible for suppressing the Ca^{2+} permeability of AMPA/KA receptors, while this subunit is expressed by mature oligodendrocytes (Itoh *et al.*, 2002). What is more, as mentioned above, AMPA/KA receptors become downregulated with oligodendrocyte maturation (Cahoy *et al.*, 2008), which implies that the calcium influx into mature oligodendrocytes, which is evoked by ischaemia (Micu *et al.*, 2006), may be performed by other receptors or channels in addition to AMPA/KA receptors.

Recently, oligodendrocyte NMDA receptors were shown to mediate a Ca^{2+} influx into the cells' processes in ischaemia (Micu *et al.*, 2006). The presumed NR1/NR2C/NR3 subunit composition of these receptors should theoretically allow for some Ca^{2+} -permeability (although the presence of the NR3 subunit decreases the Ca^{2+} permeability, at least in neuronal receptors: Tong *et al.*, 2008). However, no direct studies were performed to prove this assumption and so it cannot be excluded that the depolarization or Na^+ influx evoked by these receptors' activation results in the opening of other channels that allow a Ca^{2+} influx, or reverses $\text{Na}^+/\text{Ca}^{2+}$ exchange to raise $[\text{Ca}^{2+}]_i$. In addition to NMDA and AMPA/KA receptors and voltage-gated calcium channels (which were suggested to cause calcium influx into oligodendrocytes in a model of spinal cord injury; Agrawal *et al.*, 2000), other receptors and channels that might contribute to the Ca^{2+} influx into mature oligodendrocytes include P2X_7 receptors, and TRP and ASIC channels.

Oligodendrocyte P2X_7 receptors are Ca^{2+} -permeable (as described in section 1.3.2.3) and their overactivation during ischaemia results in the induction of an inward current (Fig. 1.15), intracellular Ca^{2+} overload, ROS formation and a drop in mitochondrial potential, which together lead to the death of the cells (Matute *et al.*, 2007; Domercq *et al.*, 2010). During ischaemia there is a remarkable increase in the extracellular level of ATP (Domercq *et al.*, 2010), which may be caused by

hemichannel opening (as described previously in neurons by Thompson *et al.*, 2006). Accordingly, blocking oligodendrocyte hemichannels and P2X₇ receptors remarkably increased cell survival (Domercq *et al.*, 2010). Consequently, the activation of P2X₇ receptors by ATP released from hemichannels was proposed to be responsible for a substantial part of the Ca²⁺-induced damage to oligodendrocytes occurring in ischaemia.

TRP or ASIC channel opening is another possible cause of the [Ca²⁺]_i increase in oligodendrocytes during ischaemia. As described in sections 1.3.1.4 and 1.3.1.5, ASIC and TRP channels are expressed in oligodendrocytes, and in neurons their activation in ischaemia leads to a damaging Ca²⁺ influx. It is possible therefore that, as in neurons, ischaemia-evoked opening of these channels in oligodendrocytes leads to a detrimental Ca²⁺ influx into the cell.

Experiments described in Chapter 4 assess the contribution of AMPA/KA, NMDA, TRP and ASIC channels to the response of oligodendrocytes to ischaemia.

1.4.2.2.4 Additional factors that may influence the oligodendrocyte response to ischaemia

In the grey matter, during the first few minutes of ischaemia (as described in section 1.4.2.1.2), there is a massive increase in the spontaneous synaptic release of neurotransmitters into the extracellular space, and this includes a substantial rise in GABA release (Allen *et al.*, 2004). As a result, in neurons, ischaemic insult causes overactivation of GABA_A receptors which results in an excessive Cl⁻ entry and cell swelling (Allen *et al.*, 2004). GABA is also released into the white matter (in tracts including axons of inhibitory cells) during ischaemia (Shimada *et al.*, 1993), and so could activate the GABA_A receptors which are present on oligodendrocyte lineage cells (Gilbert *et al.*, 1984; Berger *et al.*, 1992a; Kirchhoff and Kettenmann, 1992; Pastor *et al.*, 1995). Although GABA_A receptor expression seems to be downregulated with oligodendrocyte development (Vélez-Fort *et al.* 2010), applying GABA to mature cells still evokes a response (Butt and Tutton, 1992; Pastor *et al.*, 1995), and so it is possible that GABA exerts an additional effect on mature oligodendrocytes during ischaemia.

Finally, a depolarizing membrane current may enter oligodendrocytes *via* potassium channels as a result of the ischaemia-evoked rise in extracellular potassium concentration: the extracellular potassium concentration ([K⁺]_o) in white matter ischaemia can rise to 14 mM (Ransom *et al.*, 1992). Additionally, Ca²⁺-activated potassium channels could be activated in ischaemia when [Ca²⁺]_i rises. We will see in

Chapter 3 that ischaemia does indeed evoke a change of oligodendrocyte membrane K^+ currents.

1.4.3 Leukodystrophies

Leukodystrophies (from the Greek: *leuko*, white, *dys*, lack of, and *troph*, growth) are a group of rare genetic disorders that are characterized by the lack of properly formed myelin (dysmyelination) or loss of once-formed myelin (demyelination), that lead to the white matter degeneration. Patients are mostly young children that exhibit normal early development, but then lose their previously acquired motor skills and regress as myelin deteriorates, with typical clinical symptoms of nystagmus, ataxia, spasticity and delayed mental development (although the severity of these symptoms and their onset depend greatly on the type of the leukodystrophy).

Although the specific genes whose mutation leads to leukodystrophy development are mostly identified, the reason for the myelin deterioration and oligodendrocyte death is still not well established. In some of the disorders (such as adrenoleukodystrophy, metachromatic leukodystrophy and Krabbe disease), the mutations cause a lack or decreased efficiency of the enzymes involved in the breakdown of long chain fatty acids (adrenoleukodystrophy), sulfatide lipids (metachromatic leukodystrophy) or terminal β -galactose-containing sphingolipids (Krabbe disease). This leads to the accumulation of unmetabolised lipids, which cannot be used for normal myelin formation, and ultimately causes the loss of oligodendrocytes. In many other types of leukodystrophy, however, the reason for the demyelination remains elusive. In this thesis I will focus on two leukodystrophies, Canavan disease and Pelizaeus-Merzbacher-like disease, in which there is a rise in the concentration of agents which might activate glutamate receptors on oligodendrocyte lineage cells.

The treatment for leukodystrophies is currently symptomatic, although new therapies, such as bone marrow and hematopoietic stem cell transplantation, are under investigation.

1.4.3.1 Canavan and Pelizaeus-Merzbacher-like diseases

Canavan disease (CD) and Pelizaeus-Merzbacher-like disease (PMLD) are two types of leukodystrophies where the reason for defects in myelin formation and

maintenance is not fully understood.

CD is an autosomal recessive disorder caused by a mutation in gene coding for the enzyme aspartoacylase (ASPA; Fig. 1.16), expressed solely by oligodendrocytes (Luyt *et al.*, 2007). ASPA breaks down N-acetylaspartylacetate (NAA), a molecule found in a high concentration in CNS (see section 1.4.3.2.5), into aspartate and acetate (Baslow, 2003). The resulting lack of acetate (which could disturb myelination: Fig. 1.17 and Chakraborty *et al.*, 2001), and high level of NAA (the elevated extrusion of which from oligodendrocytes in CD could result in damage to the cells due to excessive water efflux: Baslow, 2003) are proposed to be the reasons for the spongy degeneration of the white matter observed in CD.

Pelizaeus-Merzbacher disease (PMD) is caused by a mutation (duplication, missense or null mutation) in the gene for PLP protein, which is one of the main myelin proteins. However, around 20% of patients with symptoms indistinguishable from PMD do not have a mutation in PLP gene, and the aetiology of this disorder, named Pelizaeus-Merzbacher-like disease (PMLD), is unknown. In a minority of PMLD cases (around 8%: Henneke *et al.*, 2008), there is a mutation in the GJA12 gene that codes for oligodendrocyte connexin Cx47, which may mediate metabolic trafficking between different lamellae of the myelin sheath or between oligodendrocytes and astrocytes (see section 1.3.1.6). The majority of PMLD patients, however, do not carry this mutated allele and so the cause of the white matter deterioration in these cases is still obscure. PMLD is frequently associated with high levels (up to 200 μM : Wolf *et al.*, 2004) of N-acetylaspartylglutamate (NAAG), formed from NAA and glutamate, the reason for which is unknown.

1.4.3.2 The role of NAA and NAAG in CNS physiology and pathology

N-acetylaspartate (NAA) and its derivative, N-acetylaspartylglutamate, are highly abundant in the vertebrate CNS. NAA is the second most abundant metabolite in the brain after glutamate. Its concentration in neurons can be up to 20 mM (Wiame *et al.*, 2009), while it is present in the extracellular space at ~ 100 μM (Sager *et al.*, 1997; Chakraborty *et al.*, 2001). NAAG is the next most concentrated peptide in the brain with a concentration in neurons of up to 10 mM (Chakraborty *et al.*, 2001; Hanaya *et al.*, 2008) and in the extracellular space 5-8 μM (Faull *et al.*, 1999).

Although highly concentrated in the brain, the role of NAA and NAAG in various physiological and pathological conditions – including CD and PMLD

leukodystrophies - is still obscure.

1.4.3.2.1 The NAA and NAAG cycle in the brain

The formation and interconversion of NAA and NAAG in the brain is a complex process which involves three types of cells: neurons, oligodendrocytes and astrocytes (Fig. 1.16).

NAA is synthesized in neurons from aspartate and acetyl-CoA by aspartate N-acetyltransferase, NAT8L (Wiame *et al.*, 2009; Ariyannur *et al.*, 2010). There is a controversy over where NAT8L is localized in the cell, with the proposed compartments being either mitochondria (Madhavarao *et al.*, 2003; Ariyannur *et al.*, 2010), microsomes (Lu *et al.*, 2004) or endoplasmic reticulum (Wiame *et al.*, 2009). Once formed, NAA can then be transported to oligodendrocytes (Figs. 1.16, 1.17) *via* sodium-dependent dicarboxylate transporter 3, NaDC3 (Huang *et al.*, 2000) or transformed into N-acetylaspartylglutamate (NAAG). NAA which reaches oligodendrocytes is, at least in part, incorporated into myelin (Chakraborty *et al.*, 2001; Figs. 1.16, 1.17; see below)

NAAG is generated from NAA and glutamate by the cytosolic enzyme, NAAG synthetase (NAAGS; Becker *et al.*, 2010), and then released from neurons in synaptic vesicles in a calcium-dependent manner (Williamson and Neale, 1988a; 1988b; Williamson *et al.*, 1991). Once in the extracellular space, NAAG can be broken down to NAA and glutamate by glutamate-carboxypeptidases II (GCP II, also known as NAALADase; Bzdega *et al.*, 1997) and GCP III (Bzdega *et al.*, 2004), located on the extracellular membrane of astrocytes (Berger *et al.*, 1999). NAA is then transported to oligodendrocytes (Huang *et al.*, 2000), where it is broken down by ASPA into acetate and aspartate (Baslow, 2003).

Interestingly, astrocytes may also play an active role in NAA transport. Astrocytes do not express ASPA (Madhavarao *et al.*, 2003) and therefore are unable to catabolise NAA. However, these cells were found to express functional NaDC3 transporters (Fujita *et al.*, 2005) and, as they form a significant portion of the blood-brain barrier, they may be involved in NAA clearance from the brain (NAA is found normally in urine, perhaps indicating that there is a continuous NAA efflux from the brain: Kelley and Stamas, 1992). Another possibility is that NAA taken up from the extracellular space by astrocytes is transferred to oligodendrocytes *via* heterologous gap junctions (see section 1.3.1.6) composed of connexins Cx43 (expressed by astrocytes) and Cx47 (expressed by oligodendrocytes; Orthmann-Murphy *et al.*, 2008). It is

interesting that a mutation in the gene coding for Cx47 was linked to some of the cases of PMLD (see section 1.4.3.1).

1.4.3.2.2 Receptors for NAA and NAAG

Although the majority of NAA seems to be transported directly to oligodendrocytes and astrocytes by NaDC3 transporters (Huang *et al.*, 2000; Yodoya *et al.*, 2006), NAA also activates metabotropic glutamate receptors, causing neuronal depolarization (Yan *et al.*, 2003; Hanaya *et al.*, 2008), and NMDA receptors, evoking a rise in intracellular calcium concentration (Rubin *et al.*, 1995). The physiological role of these responses is unknown.

NAAG was also shown to bind to NMDA receptors (Westbrook *et al.*, 1986: Fig. 1.18), with a 25-fold lower affinity than glutamate (Valivullah *et al.*, 1994). Low levels of NAAG were suggested to antagonise NMDA-receptor mediated currents, decreasing the influx of calcium (Burlina *et al.*, 1994; Yourick *et al.*, 2003; Bergeron *et al.*, 2005; 2007; but see: Losi *et al.*, 2004), while at high levels NAAG seems to act as NMDA receptor agonist, increasing intracellular calcium levels (Yourick *et al.*, 2003). Another receptor proposed for NAAG is mGluR3 (Wroblewska *et al.*, 1997; Gafurov *et al.*, 2001; Losi *et al.*, 2004). By acting on mGluR3, NAAG was shown to block adenylate cyclase and decrease forskolin-stimulated cAMP levels (Wroblewska *et al.*, 1993; 1997).

1.4.3.2.3 The physiological role of NAA

NAA is thought to be involved in myelin formation, serving as a form of acetate 'storage' in the CNS and possibly being transported to oligodendrocytes when they experience increased demand for fatty acid production during myelination (Fig. 1.16). This hypothesis has been supported by the study of Chakraborty *et al.* (2001) which demonstrated that radiolabeled NAA was eventually transformed into lipids in the myelin sheath (Fig. 1.17). Also, Bhakoo *et al.* (2001), followed by Kirmani *et al.* (2003), showed that in the white matter ASPA activity strongly increases during the period of active myelination, and ASPA has been reported to be expressed solely in myelinating oligodendrocytes (Baslow *et al.*, 1999). However, the proposed role of NAA in myelination has been criticised on the grounds that in hypoacetylaspartia (caused by a mutation in NAT8L; Wiame *et al.*, 2009; Fig. 1.16), when NAA is deficient in the brain, there is only a moderate decrease in myelination efficiency

(Burlina *et al.*, 2006).

Another role that NAA could play in the CNS is serving as an osmolyte to act as a molecular water pump (Baslow, 2003), which allows the cotransport of water across a membrane against its gradient as NAA is transported down its own inter-compartmental gradient. NAA was calculated to transport 120 molecules of water per one molecule of NAA (Baslow, 2002). A different theory for NAA's role in the brain suggests its involvement in dopaminergic transmission, as the activity of the NAA synthetase, NAT8L (also called 'shati'), was found to be upregulated after D1 and D2 dopamine receptor activation by metamphetammine (Niwa *et al.*, 2007).

Finally, NAA plays a crucial role in NAAG formation.

1.4.3.2.4 The physiological role of NAAG

NAAG has been found to be a co-transmitter with several small neurotransmitters, including glutamate, GABA and acetylcholine, and is released from synaptic terminals in a calcium-dependent manner (Williamson and Neale, 1988a, 1988b; Williamson *et al.*, 1998). It has been suggested that upon NAAG binding to NMDA receptors, it antagonises the action of glutamate, reducing NMDA receptor mediated currents (Fig. 1.19) and blocking the induction of long-term potentiation. (Bergeron *et al.*, 2005; 2007). However, Yourick *et al.* (2003) reported that, with increasing concentration, NAAG becomes an NMDA receptor agonist. NAAG might therefore be better viewed as a modulator of glutamate's action on NMDA receptors, but whether it ever reaches extracellular concentrations high enough to significantly affect NMDA receptors is debatable.

NAAG was frequently found to be neuroprotective and this effect was mostly assigned to its activation of mGluR3 receptors. In ischaemia, application of low doses of NAAG increased cell survival (Thomas *et al.*, 2001; Cai *et al.*, 2002), while in a model of diabetic neuropathy, NAAG was found to protect neurons against glucose-induced programmed cell death and neurite degeneration (Berent-Spillson *et al.*, 2004). Also, inhibition of the peptidase GCP-II (which prevents NAAG from being cleaved into NAA and glutamate and so should increase the NAAG concentration in the CNS) was found to have an analgesic effect in animal models of pain (Zhang *et al.*, 2006; Yamamoto *et al.*, 2007), to delay the onset of symptoms and motor neuron loss in amyotrophic lateral sclerosis (Ghadge *et al.*, 2003), and to reduce the symptoms of schizophrenia (Olszewski *et al.*, 2004).

1.4.3.2.5 The possible role of NAA and NAAG in the leukodystrophies

As mentioned above, in CD and PMLD the concentrations of NAA and NAAG rise considerably. In CD, due to the lack of ASPA activity, the extracellular NAA levels can increase 10-fold, reaching up to 0.9 mM (Burlina *et al.*, 1999), and the extracellular concentration of NAAG rises as well (as a by-product of NAA) up to 20 μ M (Burlina *et al.*, 1999). In PMLD, the NAAG concentration was reported to be 50 μ M (Sartori *et al.*, 2008) and 200 μ M (Wolf *et al.*, 2004), and so greatly exceeds its normal levels in the CNS.

The reason for the heavy damage to myelin observed in both these leukodystrophies has not been determined yet. It is possible that both NAA and NAAG, acting on the recently discovered oligodendrocyte NMDA receptors, cause overactivation of these receptors and thus a detrimental calcium influx (similar to that observed for high, but not low, NAAG concentration in neurons: Yourick *et al.*, 2003). As oligodendrocyte NMDA receptors are most probably located on the cell processes (Salter and Fern, 2005; Micu *et al.*, 2006), the action of NAA and NAAG might cause preferential damage to newly formed myelin (a protective effect of NAAG acting on mGluR3 is highly unlikely as these receptors have not been described in oligodendrocytes *in vivo* yet).

The hypothesis that NAA and NAAG directly activate oligodendrocyte NMDA receptors and thus cause myelin loss in CD and PMLD is assessed in Chapters 5 and 6 of this thesis.

1.5 The aims of the thesis

The experiments performed in this thesis had four aims as follows:

The experiments in Chapter 3 investigated the electrical response of mature oligodendrocytes to ischaemia. They aimed to define the typical current time course and changes in cell membrane properties that occur in ischaemic condition, and the cause of the observed changes. Surprisingly, although ischaemia evokes an inward current in oligodendrocytes, as also occurs in neurons, the main component of this response turns out to be a decrease of membrane K^+ conductance rather than an opening of glutamate-gated channels as in neurons.

The experiments in Chapter 4 tested the idea that ischaemia-evoked glutamate

release was the main trigger of the electrical response described in Chapter 3, and the source of the glutamate released into the white matter was investigated. The idea of performing this work was to provide basic information which might help with developing therapies that increase oligodendrocyte survival during white matter ischaemia.

The experiments in Chapter 5 tested the hypothesis that two substances found at a high concentration in human brain, NAA and NAAG, exert a direct effect on oligodendrocyte NMDA receptors. The electrophysiological responses to NAA and NAAG were recorded and compared to neuronal ones in order to assess the possibility of NAA and NAAG affecting oligodendrocytes selectively, for example because of the unusual subunit composition of oligodendrocyte NMDA receptors.

The experiments in Chapter 6 explored the possibility of a Ca^{2+} influx being produced in mature oligodendrocytes by NAA- and NAAG-evoked NMDA receptor activation. Together, the experiments in Chapters 5 and 6 investigated the possible role that NAA and NAAG may play in myelin damage and oligodendrocyte loss in the two types of leukodystrophies, Canavan Disease and Pelizaeus Merzbacher-Like Disease, where the concentrations of these substances rise substantially.

In Chapter 7, a global summary of the experiments is provided and future directions for carrying the work forward are suggested.

Gene	Protein	Effect of hypoxia	Cs ⁺ permeability	Level of expression	References
Kcna1	Kv1.1, fast delayed voltage-gated potassium channel		No	Very high expression level in mature oligodendrocytes and in myelin; much lower in OPCs	Hille, 2001; Cahoy <i>et al.</i> , 2008; Ishii <i>et al.</i> , 2009
Kcna2	Kv1.2, fast delayed voltage-gated potassium channel		No		Duprat <i>et al.</i> , 1995; Hille, 2001; Ishii <i>et al.</i> , 2009
Kcna6	Kv1.6, fast delayed voltage-gated potassium channel		No	Similar expression in mature oligodendrocytes and OPCs	Hille, 2001; Cahoy <i>et al.</i> , 2008
Kcnc1	Kv3.1, fast delayed voltage-gated potassium channel		No	No expression in myelin; 4 x higher expression in OPCs than in mature oligodendrocytes	Hille, 2001; Cahoy <i>et al.</i> , 2008; Doyle <i>et al.</i> , 2008
Kcnd2	Kv4.2, transiently activated voltage-gated potassium channel		Yes	High expression in mature oligodendrocytes, but even higher in OPCs	Hille, 2001; Cahoy <i>et al.</i> , 2008; Wagner <i>et al.</i> , 2010
Kcnd3	Kv4.3, transiently activated voltage-gated potassium channel		Yes	High expression in mature oligodendrocytes, but even higher in OPCs	Hille, 2001; Cahoy <i>et al.</i> , 2008
Kcnma3	K(Ca)5.1, potassium large conductance calcium-activated pH-sensitive channel		Yes		Hille, 2001; Doyle <i>et al.</i> , 2008
Kcnmb4	BK channel, potassium large conductance calcium-activated channel	Conductance decreases after hypoxia, activation decreases neuronal damage in ischaemia	Yes	High expression in mature oligodendrocytes, but even higher in OPCs	Hille, 2001; Gao and Fung, 2002; Cahoy <i>et al.</i> , 2008; Zhang <i>et al.</i> , 2008
Kcnq1	KCNQ1, slow delayed voltage-gated potassium channel	Block by low pH	No	Small expression in mature oligodendrocytes, myelin and OPCs	Hille, 2001; Peretz <i>et al.</i> , 2002; Cahoy <i>et al.</i> , 2008

Table 1.1

List of outwardly-rectifying potassium channels expressed by oligodendrocytes and oligodendrocyte precursor cells (OPCs).

Gene	Protein	Effect of hypoxia	Cs ⁺ permeability	Level of expression	References
Kcnh8	Kv11.1 (hERG), rapid delayed voltage-gated potassium channel		No	Expressed by cerebellar oligodendrocytes	Smith <i>et al.</i> , 1996; Hille, 2001; Doyle <i>et al.</i> , 2008
Kcnj10	Kir4.1, potassium inwardly-rectifying channel	Decrease in channel conductance, loss of the channel expression	No	Very high expression in mature oligodendrocytes and in myelin, lower in OPCs	Hille, 2001; Pannicke <i>et al.</i> , 2004; Iandiev <i>et al.</i> , 2005; Cahoy <i>et al.</i> , 2008
Kcnj11	Kir6.2, ATP-dependent inwardly-rectifying potassium channel	Activation protective in hypoxia/ ischaemia	No	Moderate expression in mature oligodendrocytes, myelin and OPCs, mainly in white matter	Hille, 2001; Zhou <i>et al.</i> , 2002; Sun <i>et al.</i> , 2007; Cahoy <i>et al.</i> , 2008

Table 1.2

List of inwardly-rectifying potassium channels expressed by oligodendrocytes and oligodendrocyte precursor cells (OPCs).

Gene	Protein	Effect of hypoxia	Cs ⁺ permeability	I-V relation	Level of expression	References
Kcnk1	TWIK-1, two-pore domain potassium channel	Acid-sensitive	Yes, but very low	Weak inward rectifier	Moderate expression in mature oligodendrocytes, higher in OPCs	Cahoy <i>et al.</i> , 2008; Zhou <i>et al.</i> , 2009
Kcnk2	TREK-1, two-pore domain potassium channel	Mechano-sensitive, acid-sensitive	Yes, but low	Passive/outward rectifier	Low expression in mature oligodendrocytes, higher in OPCs	Maingret <i>et al.</i> , 1999; Cahoy <i>et al.</i> , 2008; Zhou <i>et al.</i> , 2009
Kcnk3	TASK-1, two-pore domain potassium channel,	Blocked by low pH and hypoxia		Outward rectifier	Moderate expression only in OPCs	Duprat <i>et al.</i> , 1997; Cahoy <i>et al.</i> , 2008; Meuth <i>et al.</i> , 2009
Kcnk13	THIK-1, two-pore domain potassium channel	Reversibly inhibited by hypoxia	Yes	Inward/moderately outward rectifier	Low expression only in myelin	Rajan <i>et al.</i> , 2001; Bushell <i>et al.</i> , 2002; Campanucci <i>et al.</i> , 2003; Cahoy <i>et al.</i> , 2008; Doyle <i>et al.</i> , 2008

Table 1.3

List of two-pore domain potassium channels expressed by oligodendrocytes and oligodendrocyte precursor cells (OPCs).

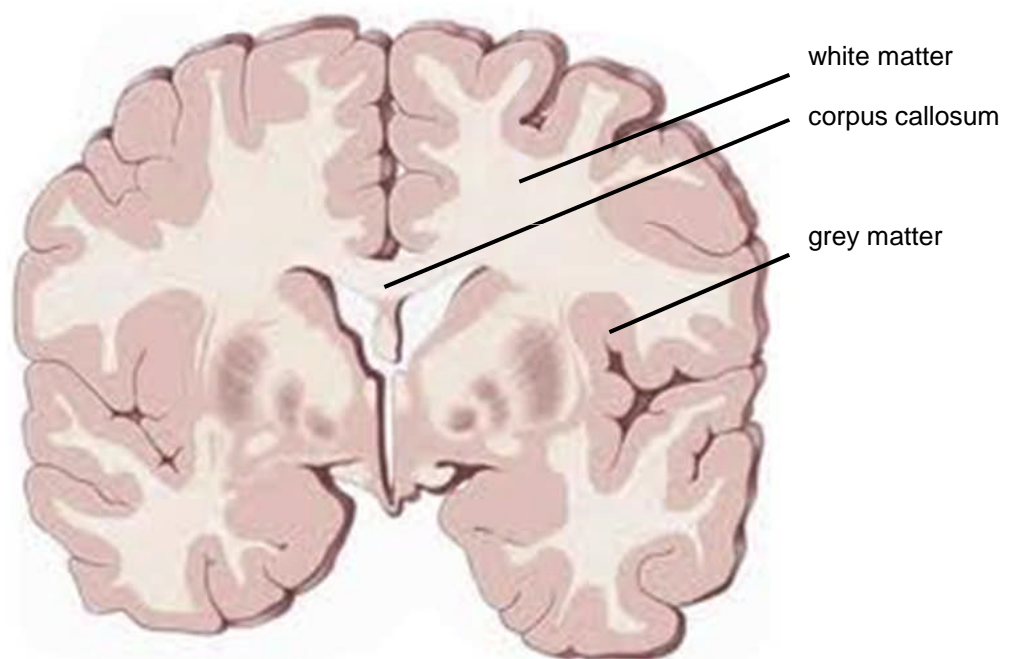
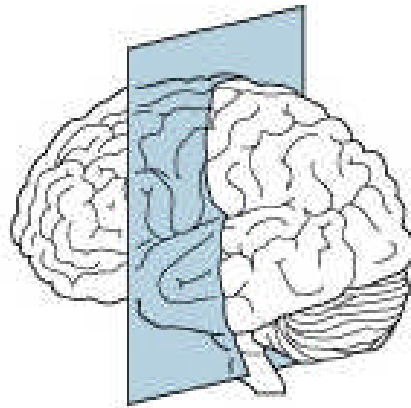


Figure 1.1

Coronal section of the human cerebral cortex. The white matter, which comprises over half of the human brain (Fields, 2008), underlies the grey matter and is largely composed of the myelinated neuronal axons. The corpus callosum is a large white matter tract, allowing fast signal transmission between the two cerebral hemispheres.

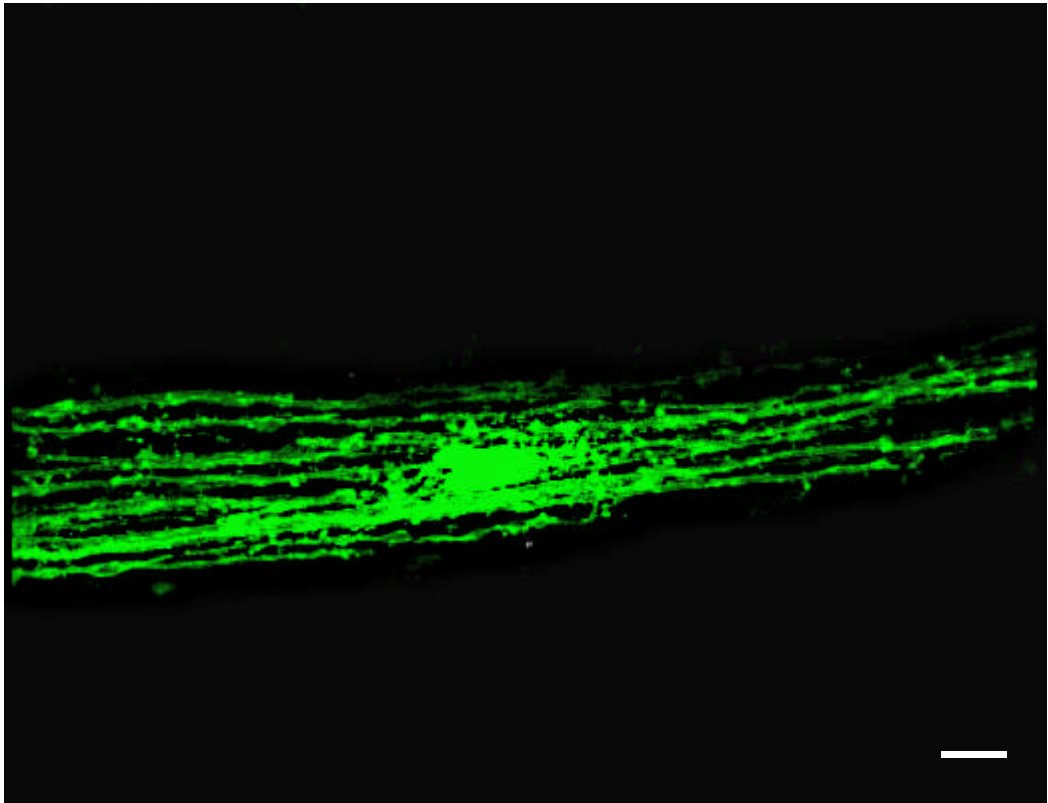


Figure 1.2

Confocal image of a mature Lucifer yellow-filled oligodendrocyte in the white matter of the cerebellum of a P12 rat. The cell has a characteristic oval soma and multiple parallel processes. Each process forms one internode on a different axon. Scale bar, 10 μm .

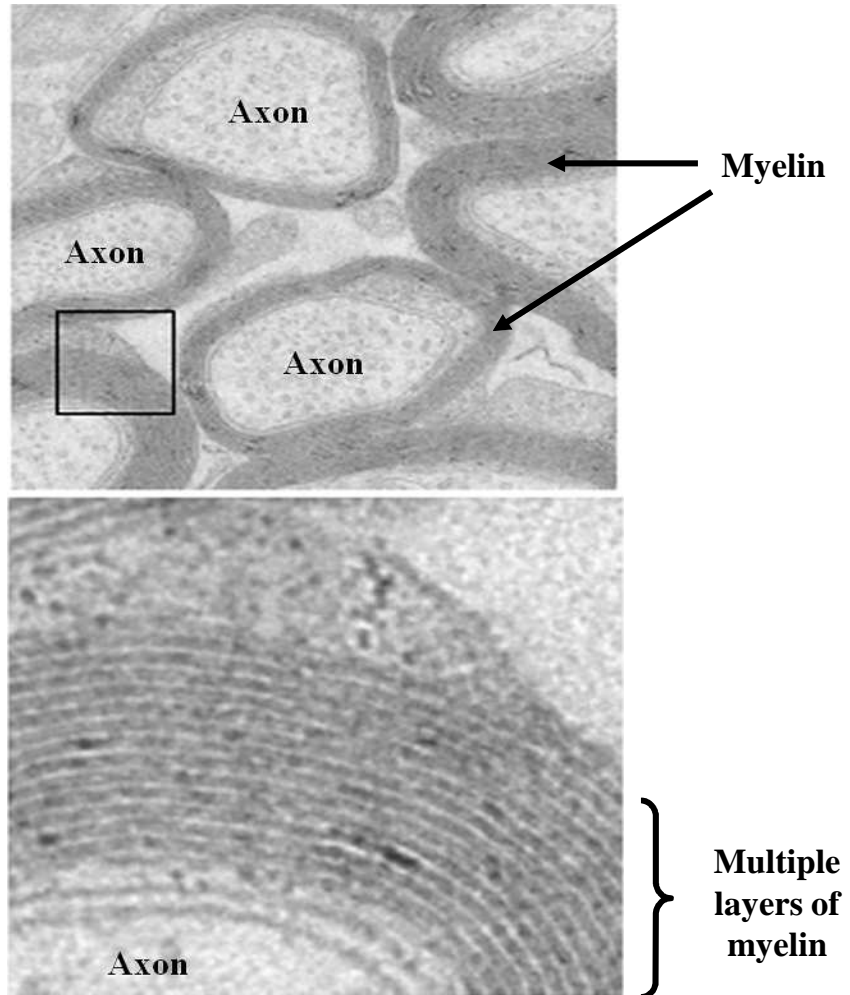


Figure 1.3
An electron micrograph showing myelinated axons in the optic nerve. The axons are surrounded by multiple layers of myelin. Adapted from Simons and Trajkovic (2006), scale not provided.

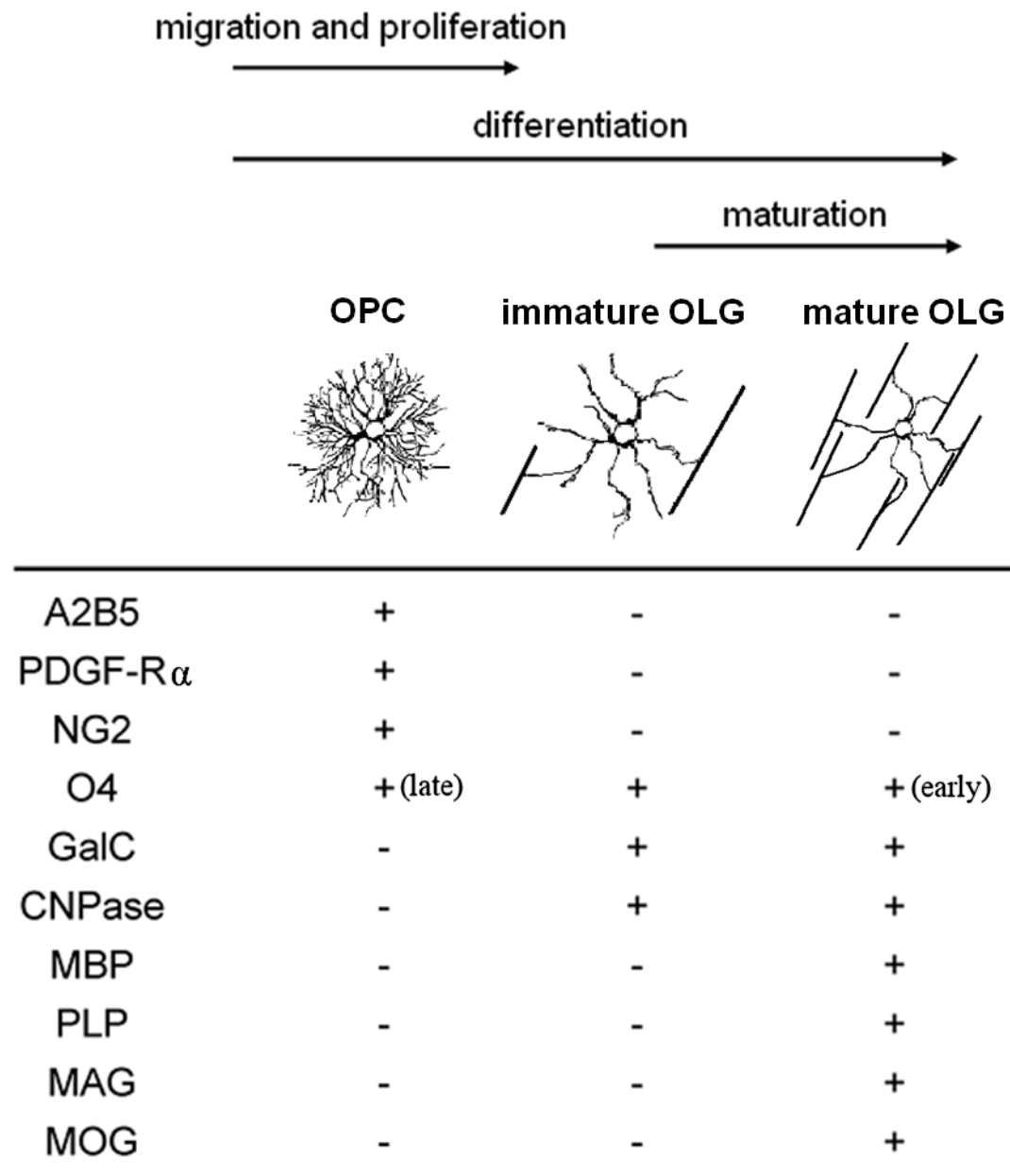


Figure 1.4

Changes in morphology and expression of different antigenic markers at different developmental stages of oligodendrocytes. Adapted from Arai and Lo (2009).

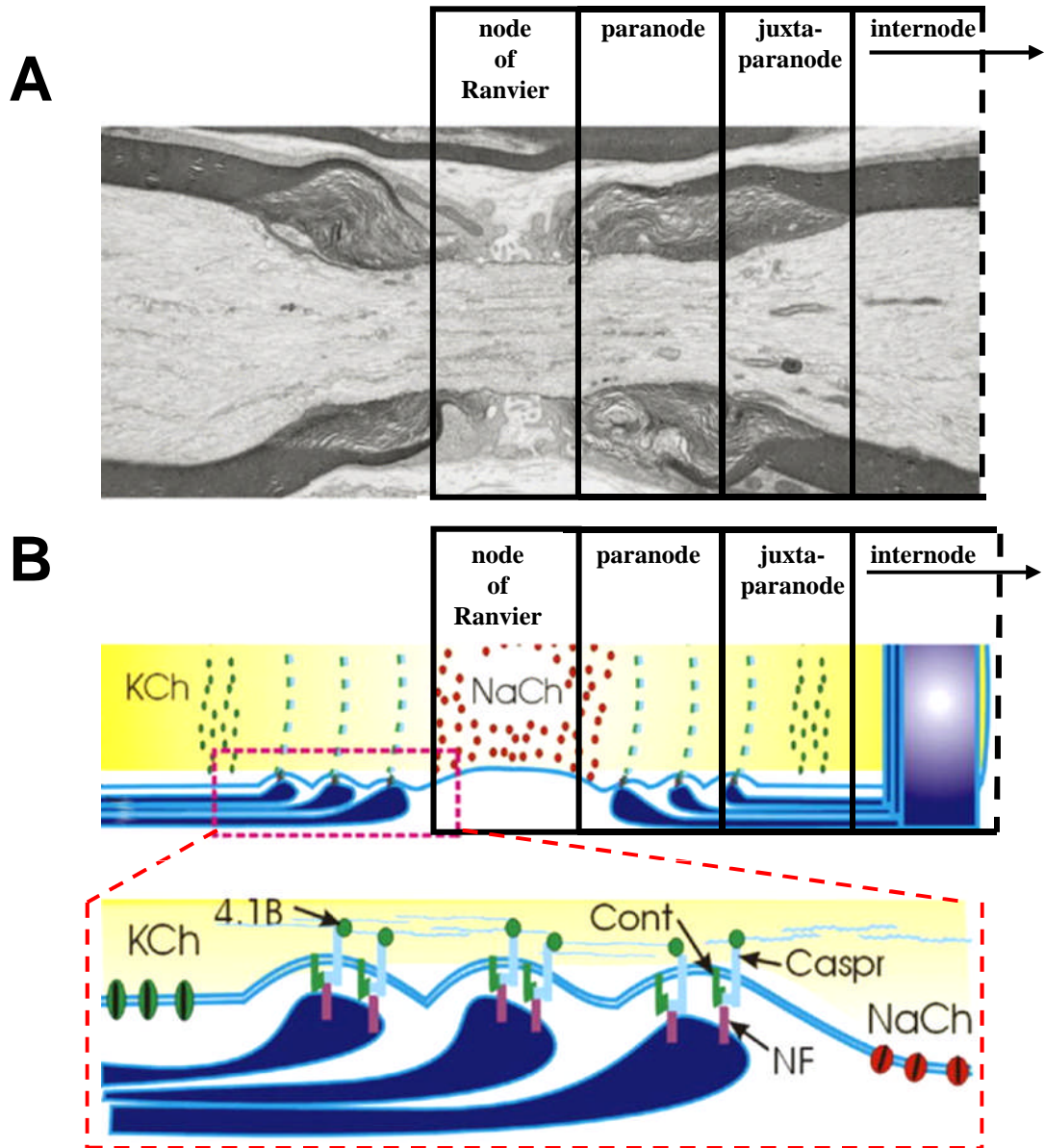


Figure 1.5

Oligodendrocyte interaction with axons at the node of Ranvier with the oligodendrocyte shown in blue and the axon in yellow. **A** An electron micrograph of a node of Ranvier and the adjacent oligodendrocyte domains: the paranode, the juxtaparanode and the internode (section from rat spinal dorsal root nerve). **B** Protein interactions and channel distribution at the node of Ranvier, with the oligodendrocyte shown in blue and the axon in yellow. The sodium channel (NaCh)-enriched node of Ranvier is adjacent to the paranode where the loops of myelin adhere to the axon through cell-adhesion molecules linked to the axon cytoskeleton: axonal contactin (Cont) and contactin-associated protein (Caspr), and oligodendroglial neurofascin-155 (NF). The juxtaparanodal domain contains clusters of potassium channels (KCh), and is followed by the internode, where compacted layers of myelin membrane restrict transmembrane ion currents to the nodal region. Adapted from Fields (2008), scale not provided.

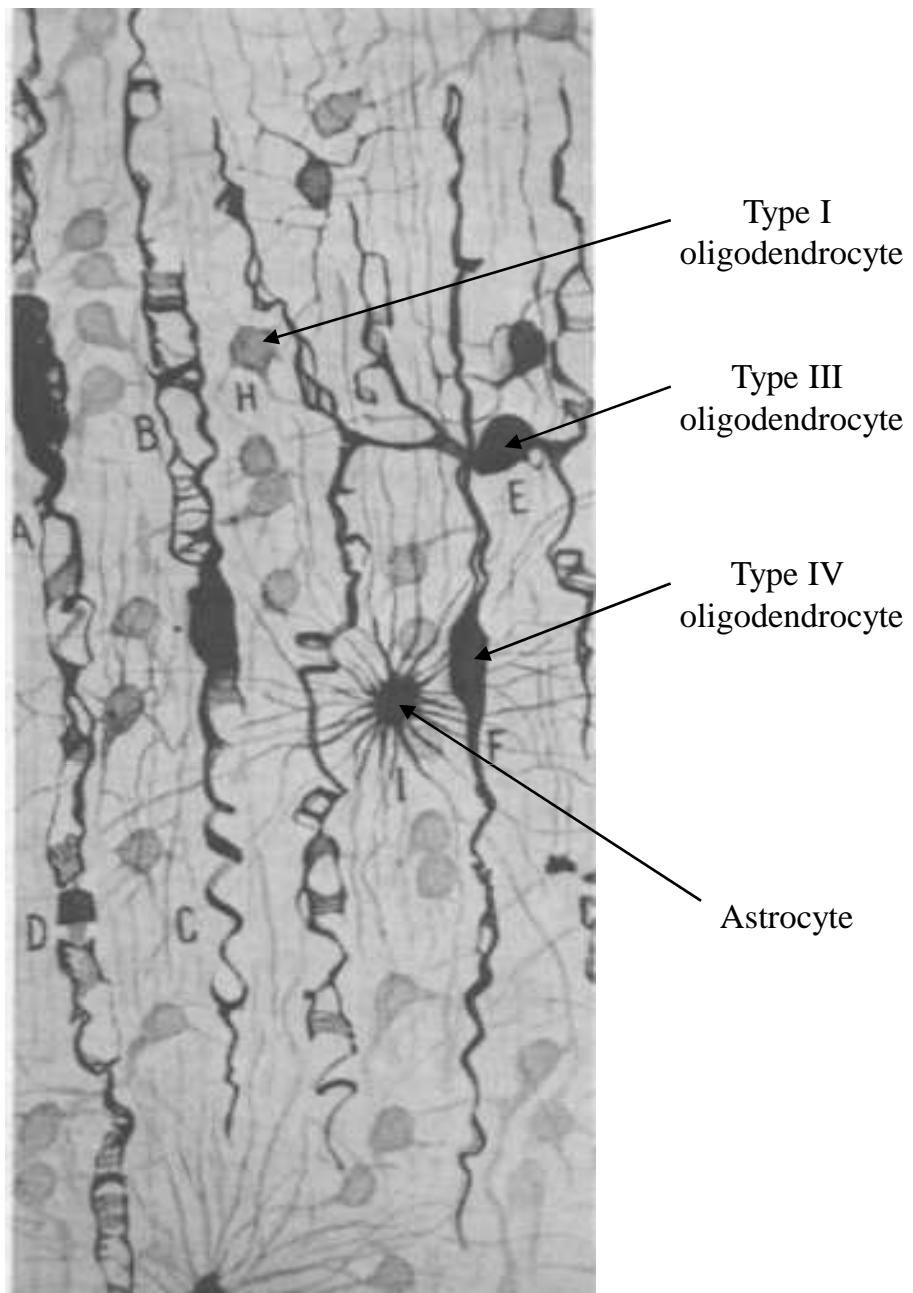


Figure 1.6

Drawing of white matter oligodendrocytes after staining with silver carbonate, by del Rio Hortega (1928) (see section 1.2.3). Three types out of the 4 classified by del Rio Hortega are found in the picture. Adapted from Wood and Budge (1984), scale not provided.

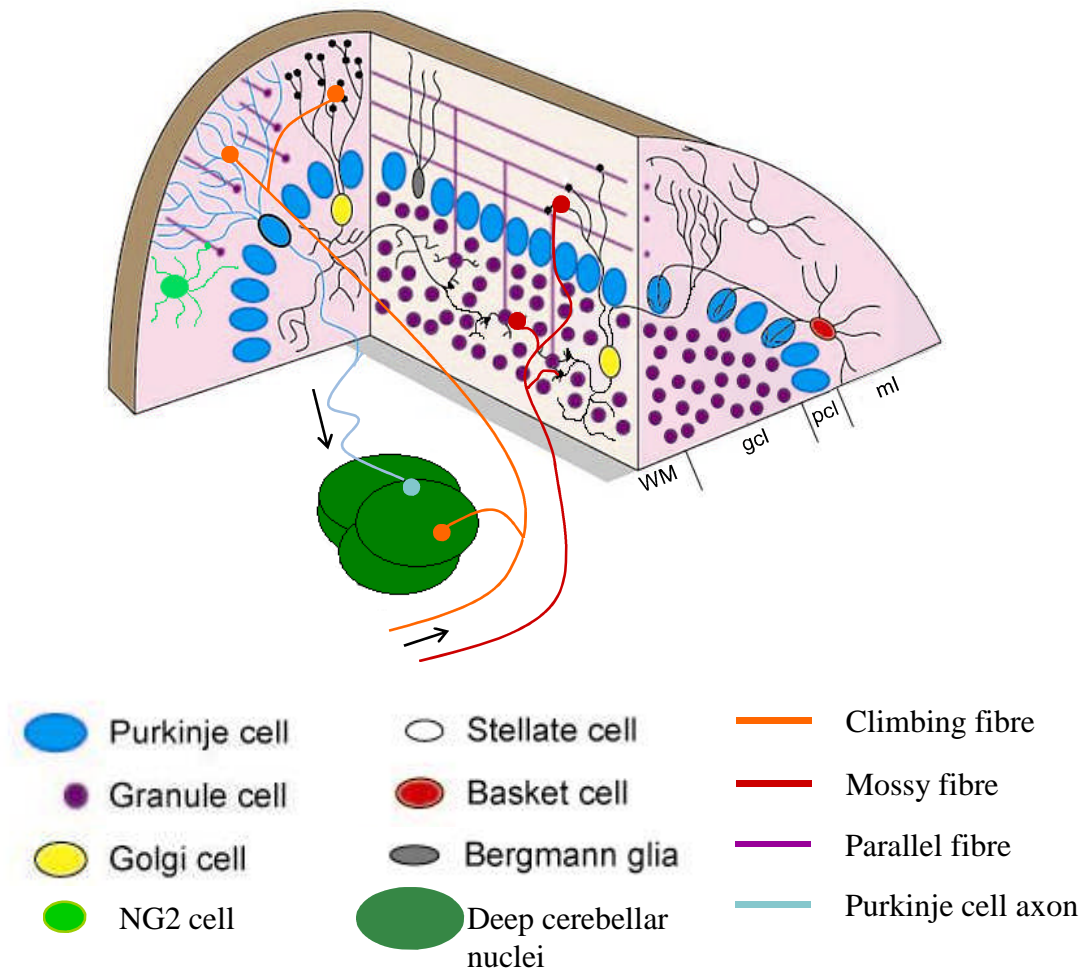


Figure 1.7

Synaptic organization of the cerebellar cortex. The diagram shows the cytoarchitecture of a single folium of the cerebellar vermis with each folium composed of 4 layers: the molecular layer (ml), the Purkinje cell layer (pcl), the granule cell layer (gcl) and the white matter (WM). The cerebellar cortex receives two types of excitatory afferents: mossy fibres originate from the neocortex, thalamus, vestibular system, brain stem nuclei and the spinal cord, and contact granule cells, deep cerebellar nuclear cells, OPCs (NG2 cells) and Golgi cells, while climbing fibres from the inferior olive directly synapse onto the Purkinje cells and NG2 cells (not shown), and also send collaterals to the deep cerebellar nuclei and the Golgi cells. The granule cells, through the parallel fibres, excite the Purkinje cells which send inhibitory axons to cells in the deep cerebellar nuclei. The deep cerebellar nuclei send excitatory axons via the thalamus and red nucleus to the spinal cord and multiple cortical areas (among them the premotor cortex). Adapted from Sillitoe and Joyner (2007).

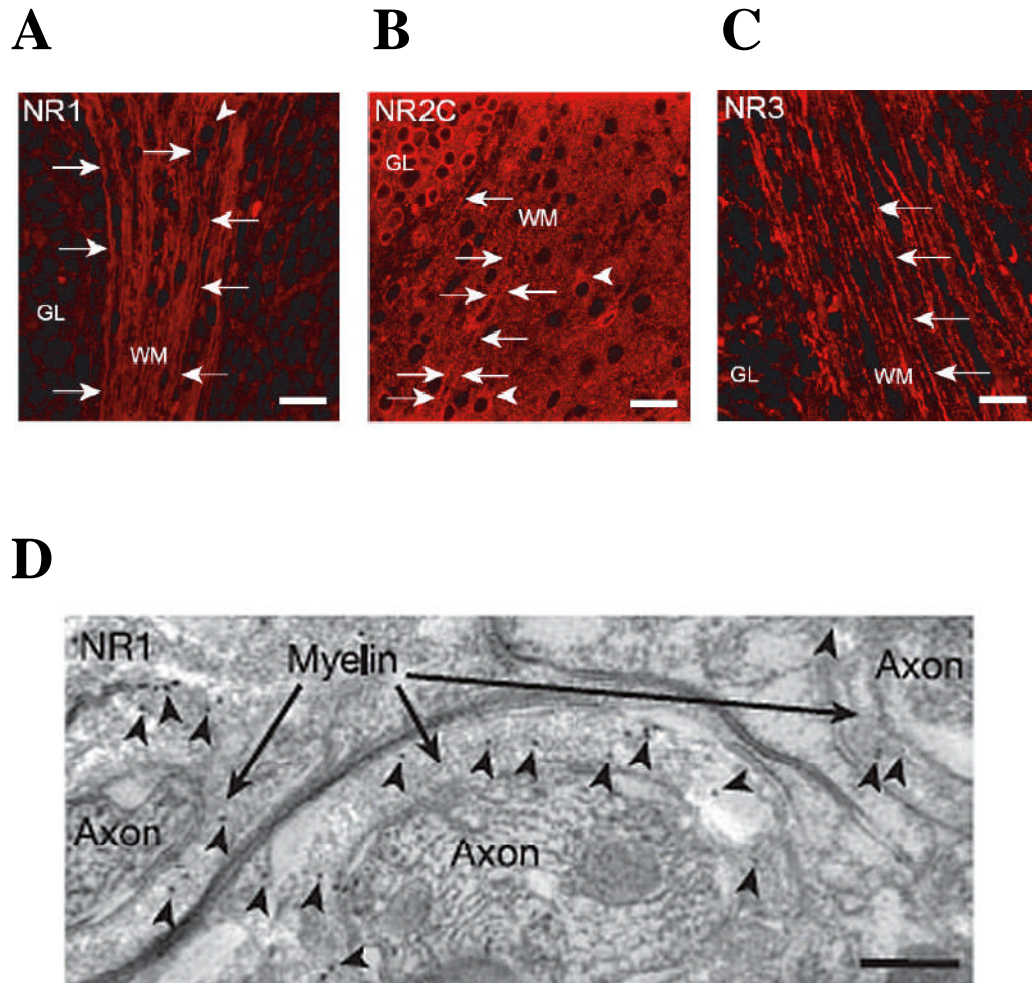
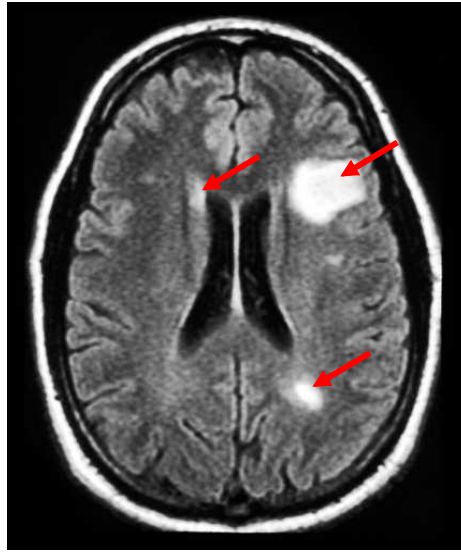
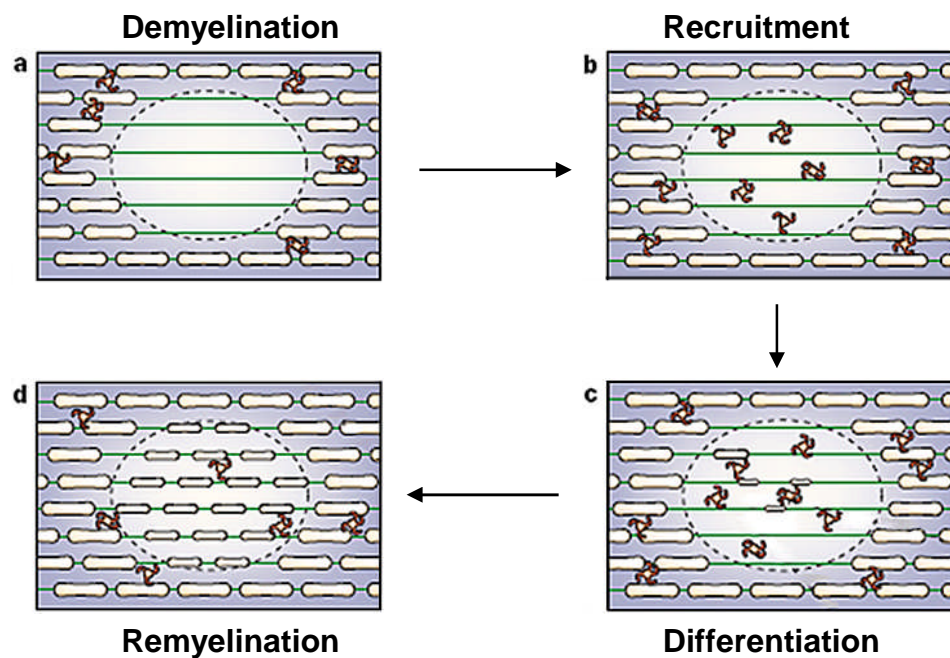
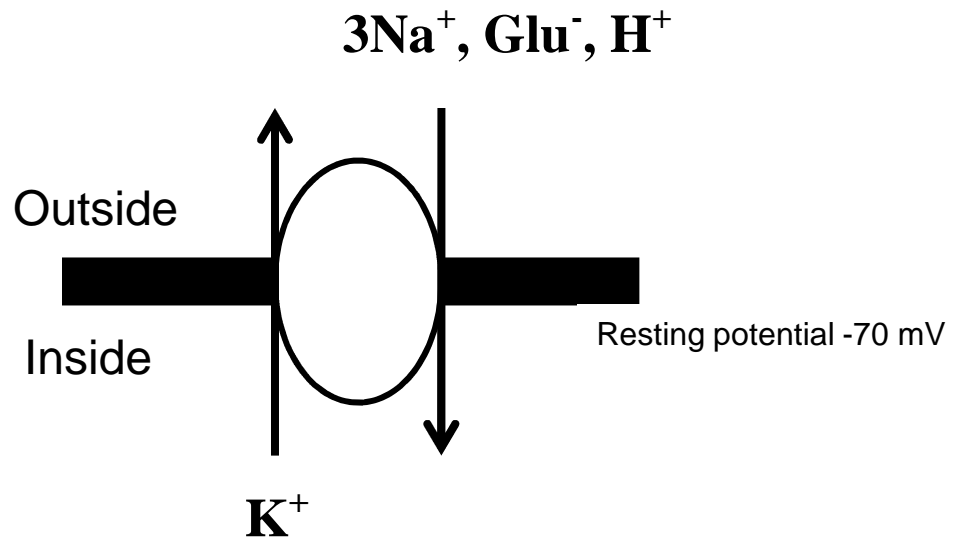
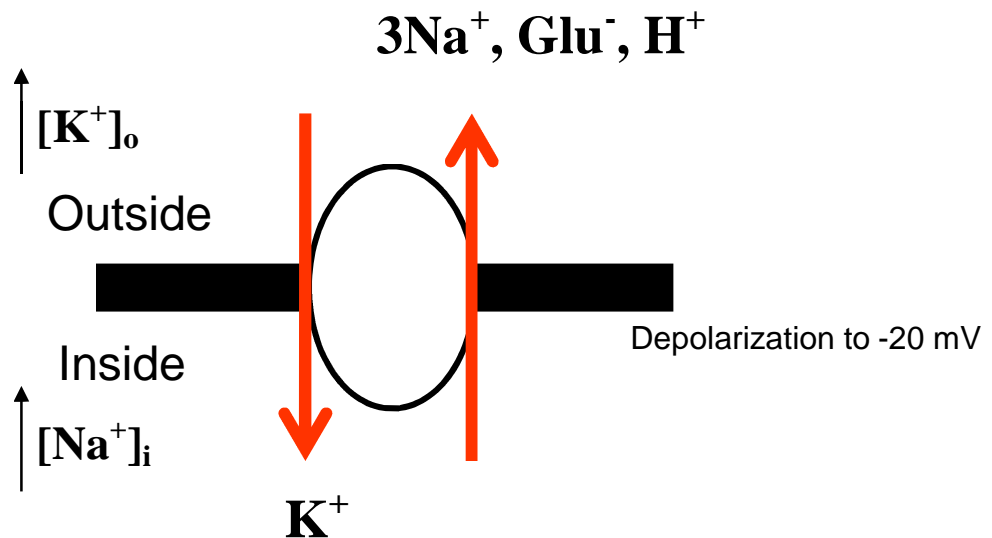


Figure 1.8

NMDA receptor subunits are expressed in the myelinating processes of cerebellar oligodendrocytes. **A-C** The myelinating processes of oligodendrocytes in the cerebellar white matter are labelled with an antibody against NR1 (**A**), NR2C (**B**; note that granule cells in the grey matter also strongly express NR2C) and NR3 (**C**; this antibody recognizes both NR3A and NR3B). The arrows indicate oligodendrocyte processes while the arrowheads indicate glial somata. WM: white matter; GL: granule cell layer. **D** NR1 subunits are present in the myelin of oligodendrocyte processes in the adult cerebellum, as indicated by immunogold staining with antibody recognizing NR1 subunit. Black dots (indicated with arrowheads) represent gold particles that antibodies were attached to. Scale bars, 20 μm (**A-C**), 0.25 μm (**D**). From Káradóttir *et al.* (2005).

A**B****Figure 1.9**

Demyelination and remyelination in multiple sclerosis. **A** Structural magnetic resonance image of the head of a patient with multiple sclerosis. Red arrows point at demyelinated lesions. **B** The main phases of the remyelination process. After demyelination, which results from an acute inflammatory episode, the myelin-forming oligodendrocytes are damaged and lost, leaving naked axons (green) (**a**). This is followed by the recruitment of OPCs (brown) from the neighbouring area: they proliferate and migrate to the affected brain region (**b**), where OPCs differentiate into mature oligodendrocytes (**c**). When the process is completed, the former lesion is fully remyelinated (**d**). Note that the newly-formed myelin sheath is thinner than the one that was originally destroyed. Adapted from Franklin (2002).

A**B****Figure 1.10**

The reversal of sodium-dependent glutamate transporters in ischaemia. **A** Under normal conditions, glutamate is transported into the cell by sodium-dependent, electrogenic glutamate transporters, which co-transport 3 Na^+ and an H^+ into the cell with each glutamate anion, while counter-transporting a K^+ anion. **B** In ischaemia, the rundown in ionic gradients and depolarization evoked by the fall of ATP level occurring results in the sodium-dependent glutamate transporters running backwards and therefore releasing glutamate into the extracellular space. Adapted from Rossi *et al.* (2000).

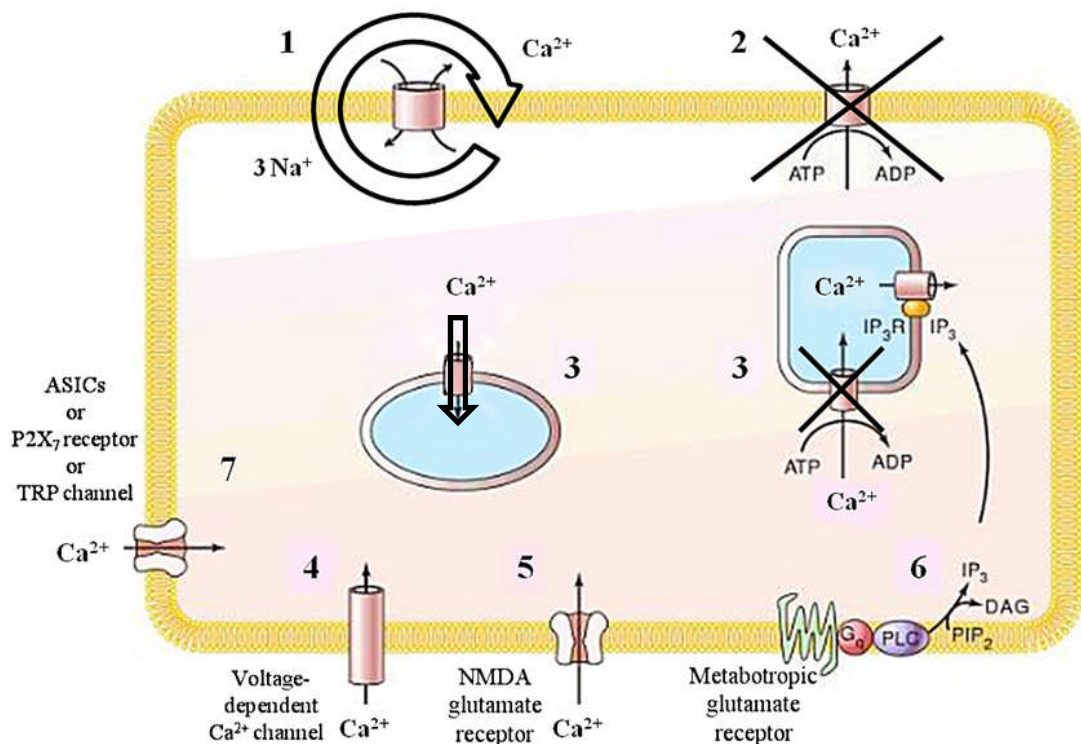


Figure 1.11

Mechanisms of intracellular calcium concentration rise during ischaemia. **1** Due to the change in ionic concentrations (i.e. increase in $[K^+]_o$ and $[Na^+]_i$), and associated depolarization, Na^+/Ca^{2+} exchangers reverse (large arrow) and transport Ca^{2+} into the cell. **2** ATP depletion leads to the inhibition of ATP-dependent Ca^{2+} pumps, blocking Ca^{2+} removal from the cell. **3** Similarly, Ca^{2+} pumps on the endoplasmic reticulum (ER) fail during ischaemia, while an excess of Ca^{2+} influx through Ca^{2+} uniporters leads to mitochondrium depolarization and a release of proapoptotic signals. **4** The depletion of the membrane potential leads to Ca^{2+} entry through voltage-dependent Ca^{2+} channels. **5** At the same time, a massive release of glutamate in ischaemia causes overactivation of NMDA receptors (and AMPA receptors, not shown in the picture) and permits excessive calcium influx. **6** Glutamate binds also to G_q -coupled metabotropic glutamate receptors that activate phospholipase C (PLC). PLC breaks down the phospholipid, phosphatidylinositol biphosphate (PIP_2), into diacylglycerol (DAG) and inositol trisphosphate (IP_3), which activates its receptors (IP_3R) on the ER and causes additional Ca^{2+} release. **7** In addition, an acid shift of extracellular pH activates Ca^{2+} -permeable ASICs, release of ATP activates a Ca^{2+} influx through $P2X_7$ receptors (Xiong *et al.*, 2004), and reactive oxygen and nitrogen species trigger transient receptor potential (TRP) channel opening and a further Ca^{2+} influx (Aarts *et al.*, 2003). ATP, adenosine triphosphate; ADP, adenosine diphosphate. Adapted from Nestler *et al.* (2008).

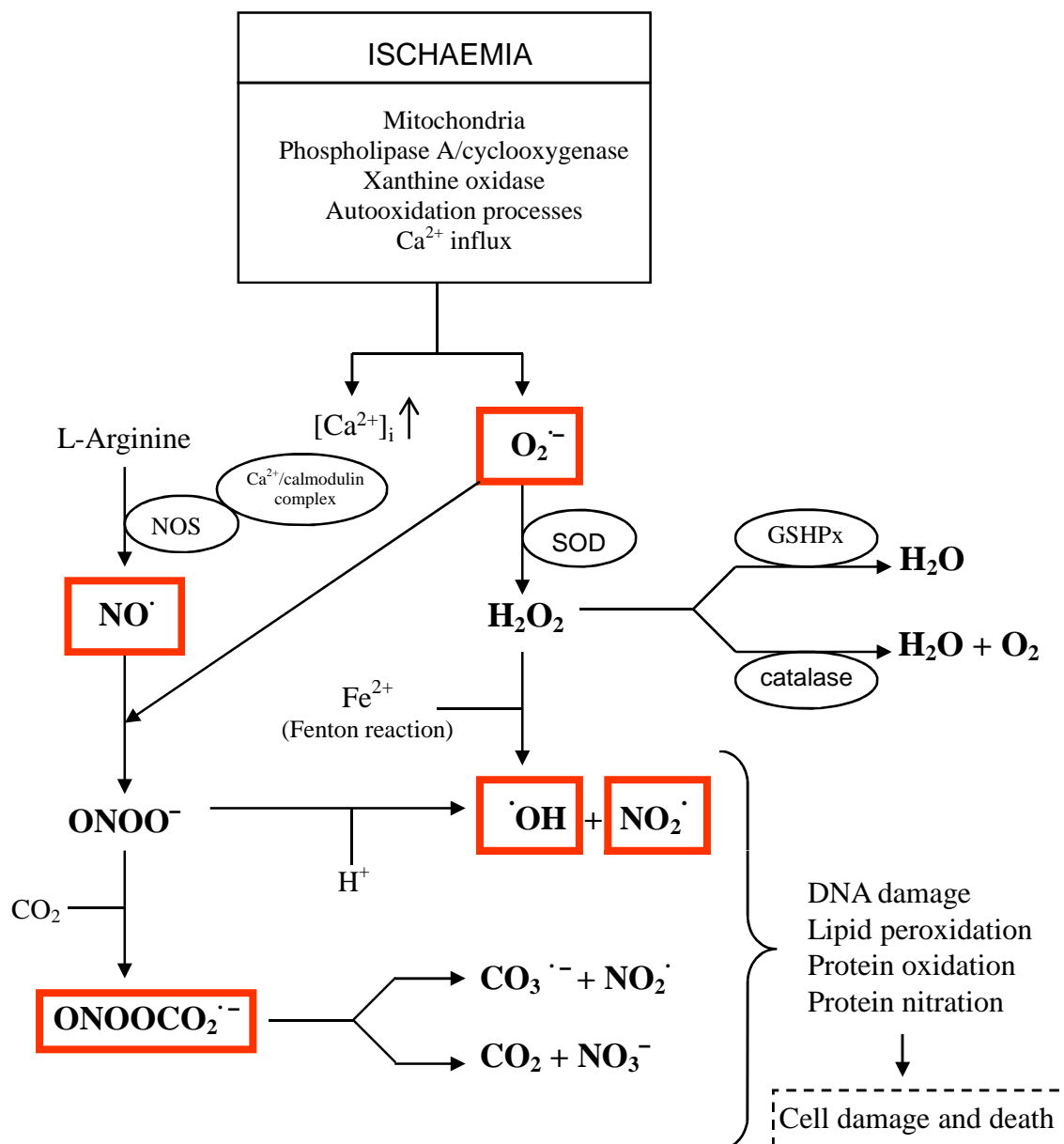


Figure 1.12

The formation of the free radicals during ischaemia. Various intracellular mechanisms induce the overproduction of reactive oxygen and nitrogen species in ischaemia, among them mitochondrial dysregulation, activation of phospholipases and oxidases, and autooxidation. The excess of superoxide anion ($O_2^{\cdot-}$) that is formed during these processes is transformed by superoxide dismutase (SOD) into hydrogen peroxide (H_2O_2) (which under normal condition is broken down into water by glutathione peroxidase, GSHPx, or to water and oxygen by catalase) and that results in an excessive formation of hydroxyl radical ($\cdot OH$). In parallel with this, the rise of $[Ca^{2+}]_i$ that occurs in ischaemia leads to the formation of Ca^{2+} /calmodulin complex, which binds to nitric oxide synthase (NOS), inducing overproduction of NO. This subsequently reacts with $O_2^{\cdot-}$ to form peroxynitrite ($ONOO^-$). Peroxynitrite can be later changed into $\cdot OH$ and nitrogen dioxide (NO_2^{\cdot}) or into nitrosoperoxycarbonate ($ONOOCO_2^{\cdot-}$), which leads to the further formation of other reactive species. All the free radicals react with many components of the cell, damaging them and eventually leading to the cell death.

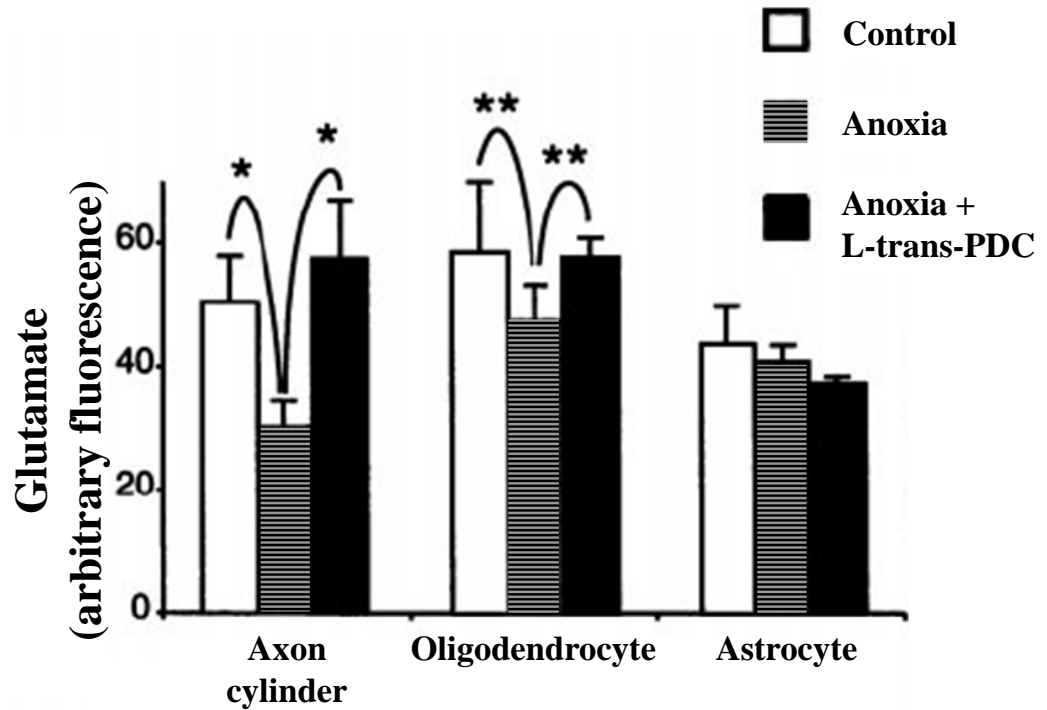
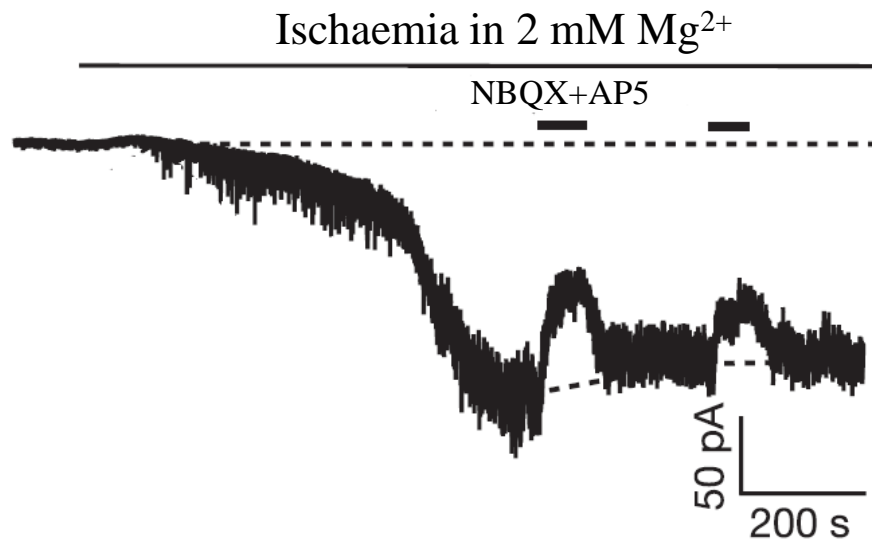
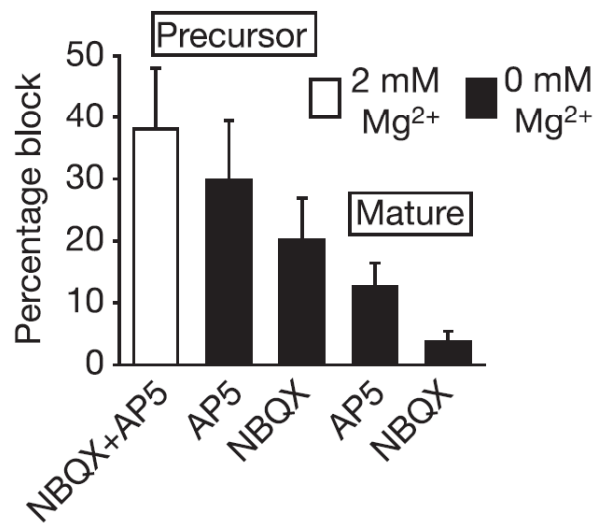
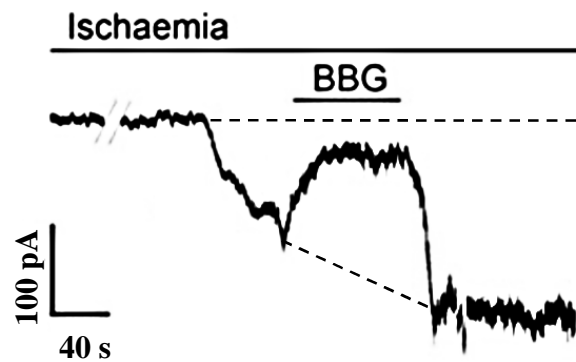
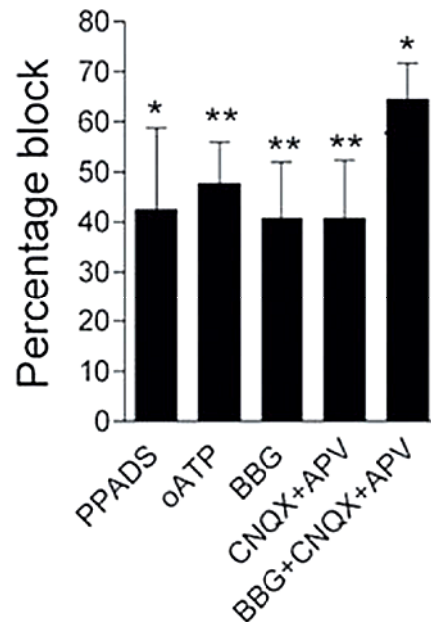


Figure 1.13

During anoxia, in the white matter, axons and oligodendrocytes release glutamate by the reversal of sodium-dependent glutamate transporters. Antibody labelling for glutamate showed that, in anoxic conditions, the glutamate concentration in axons and oligodendrocytes (but not in astrocytes) decreased, suggesting that these two components of the white matter released glutamate during anoxia. This release was inhibited by a specific blocker of sodium-dependent glutamate transporters, L-trans-pyrrolidine-2-4-dicarboxylic acid (L-trans-PDC), indicating that reversal of these transporters is the mechanism of glutamate release in anoxia (* $p < 0.01$, ** $p < 0.05$). From Li *et al.* (1999).

A**B****Figure 1.14**

Ionotropic glutamate receptors on cerebellar oligodendrocyte lineage cells are activated during ischaemia. **A** Ischaemia induces an inward current in an OPC (at -63 mV), which is partly blocked by AMPA and NMDA receptor blockers (NBQX and AP5, respectively) applied together, in 2 mM Mg²⁺. **B** Ionotropic glutamate receptor blockers, applied together (in 2 mM Mg²⁺, in OPCs) or separately (in 0 mM Mg²⁺, in OPCs and mature cells), block the ischaemia-induced current. The current is blocked in OPCs to a greater extent than in mature cells. Adapted from Káradóttir *et al.* (2005).

A**B****Figure 1.15**

Ischaemia activates purinergic P2X₇ receptors in cultured oligodendrocytes. **A** The ischaemia-induced current was blocked to a great extent by BBG, a specific P2X₇ receptor antagonist. The cell was held at -70 mV. **B** A broad-spectrum purinergic receptor blocker, PPADS, a preferential non-reversible antagonist of P2X₇ receptors (oATP) and the specific reversible antagonist of P2X₇ receptors (BBG), all blocked the ischaemia-induced current to a similar level as the ionotropic glutamate receptor blockers, CNQX and APV. There was an additive effect of simultaneous application of BBG and CNQX with APV. BBG, Brilliant Blue G; PPADS, pyridoxal phosphate 6-azophenyl-2,40-disulphonic acid; oATP, oxidized ATP. Adapted from Domercq *et al.* (2010).

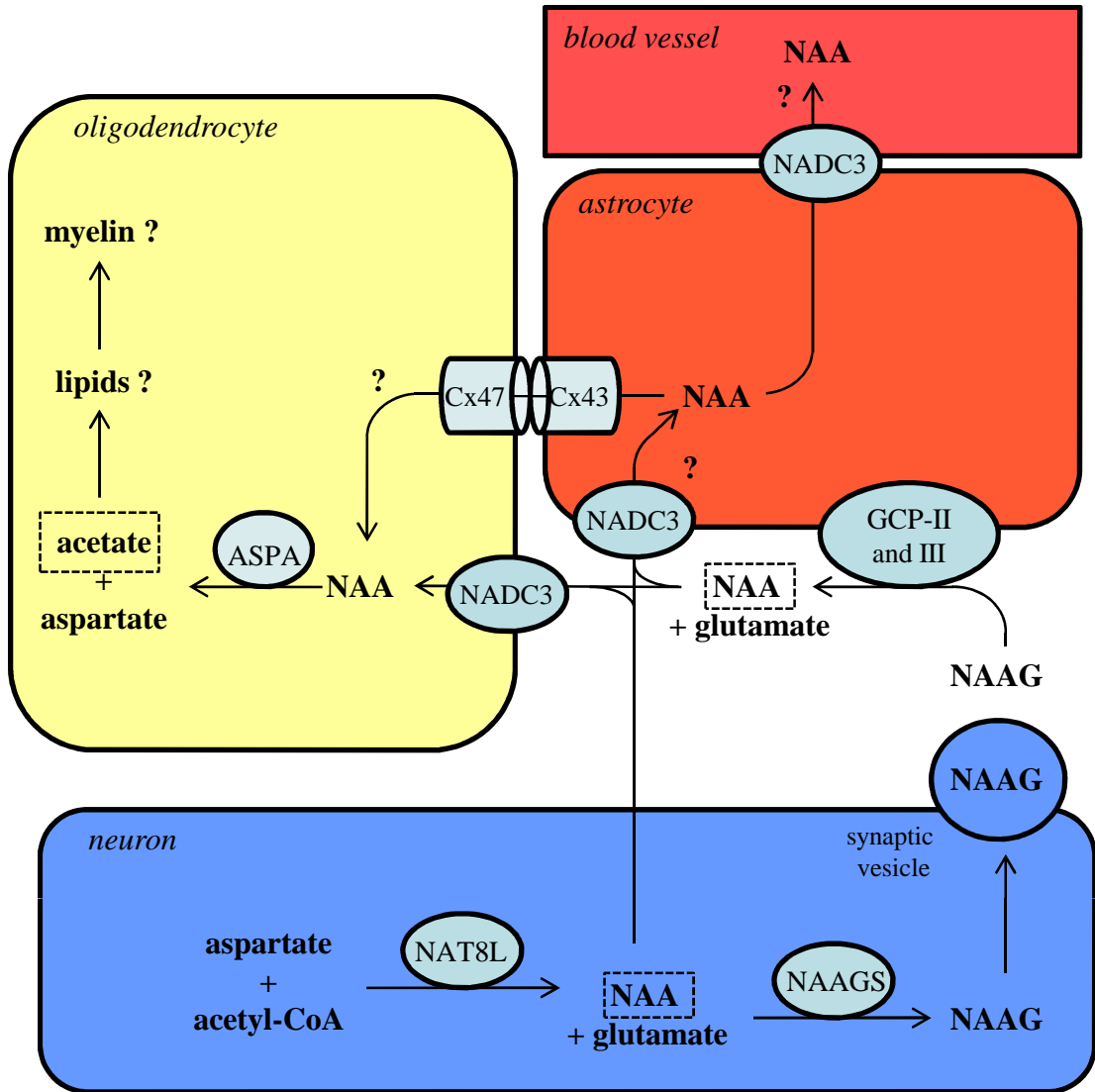


Figure 1.16

Metabolic pathways of NAA and NAAG. NAA is synthesized in neurons from aspartate and acetyl-CoA by the enzyme aspartate N-acetyltransferase (NAT8L) and may then be transported to oligodendrocytes through the Na^+ -dependent dicarboxylate transporter 3 (NADC3). In oligodendrocytes, NAA is converted to aspartate and acetate by aspartoacylase (ASPA, the enzyme lost in Canavan disease) and may thus be converted into lipids that form part of the myelin. Alternatively, NAA can be converted to NAAG in neurons by NAAG synthetase (NAAGS), and released (most probably, via synaptic vesicle release) to the extracellular space. There, NAAG is broken down to NAA and glutamate by glutamate carboxypeptidase II and III (GCP-II and III), expressed on the extracellular surface of astrocytes. NAA can be then taken up by oligodendrocytes or astrocytes. The role of NAA in astrocytes is unknown, but it is suggested that NAA may be transported to oligodendrocytes through gap junctions (formed by astrocytic Cx43 and oligodendrocytic Cx47, the latter being lost in some cases of Pelizaeus-Merzbacher-like disease). Alternatively, astrocytes may extrude NAA into the circulation.

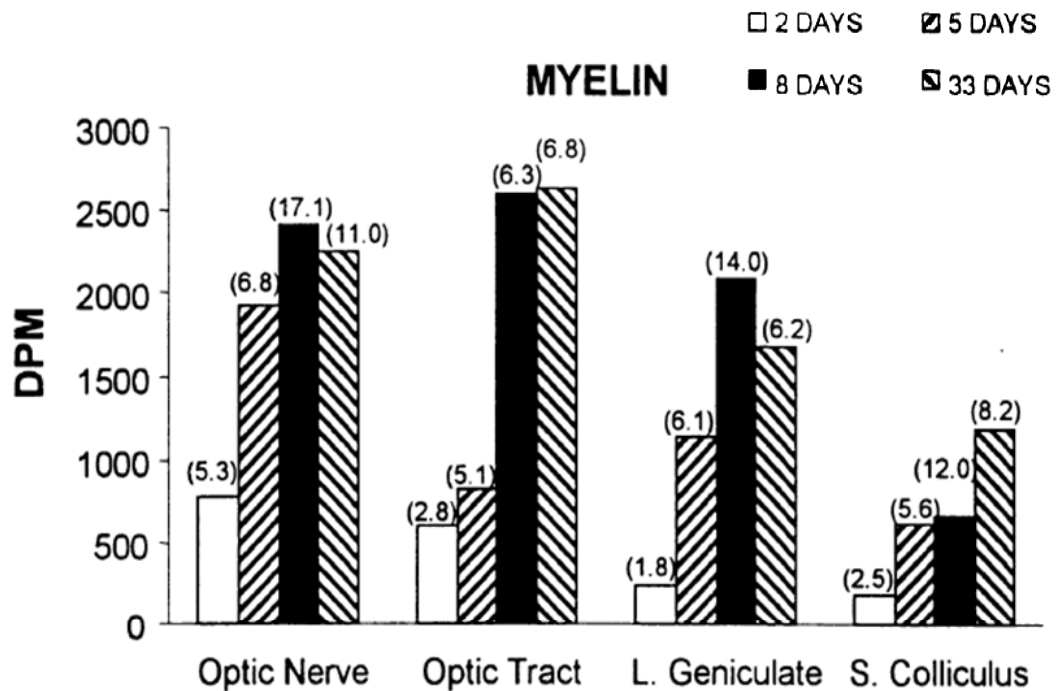


Figure 1.17

NAA is transported from axons to oligodendrocytes where it is transformed into lipids in the myelin sheath. Axonal transport and myelin incorporation of radiolabelled NAA ($[^{14}\text{C}]\text{NAA}$) was assessed using the rat optic nerve and tract, and the lateral geniculate and superior colliculus. $[^{14}\text{C}]\text{NAA}$ was administered into the right eye of six rats, and the four anatomical areas of the optic system were harvested at the times indicated, followed by tissue homogenization and myelin extraction. Then, myelin radioactivity was measured, and the results were corrected for the values from the control condition (which was the uninjected left eye, i.e. giving values for the left optic nerve, right optic tract, right lateral geniculate and right superior colliculus, since in the rat only a small percentage of optic nerve axons make ipsilateral projections to the lateral geniculate nucleus). Additionally, the ratio of radioactivity of the injected pathway vs. control was measured (numbers in brackets). Results indicate time-dependent axonal transport of NAA into oligodendrocytes and a subsequent incorporation of liberated acetyl groups into myelin lipids. DPM, disintegration per minute; L. Geniculate, lateral geniculate nucleus; S. Colliculus, superior colliculus. Adapted from Chakraborty *et al.* (2001).

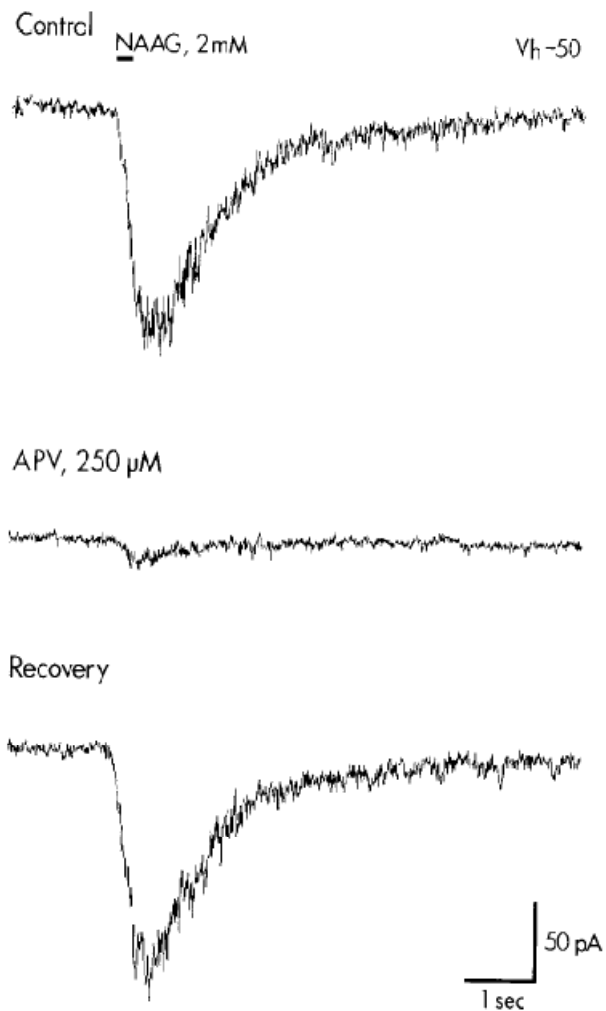


Figure 1.18

NAAG acts on neuronal NMDA receptors. The response of a cultured mouse spinal cord neuron to NAAG (2 mM) was reversibly blocked by the application of a specific NMDA receptor blocker, DL-2-amino-5-phosphoveneric acid (APV, 250 μM). The cell was voltage-clamped at -50 mV and NAAG was applied for 10 msec. Adapted from Westbrook *et al.* (1986).

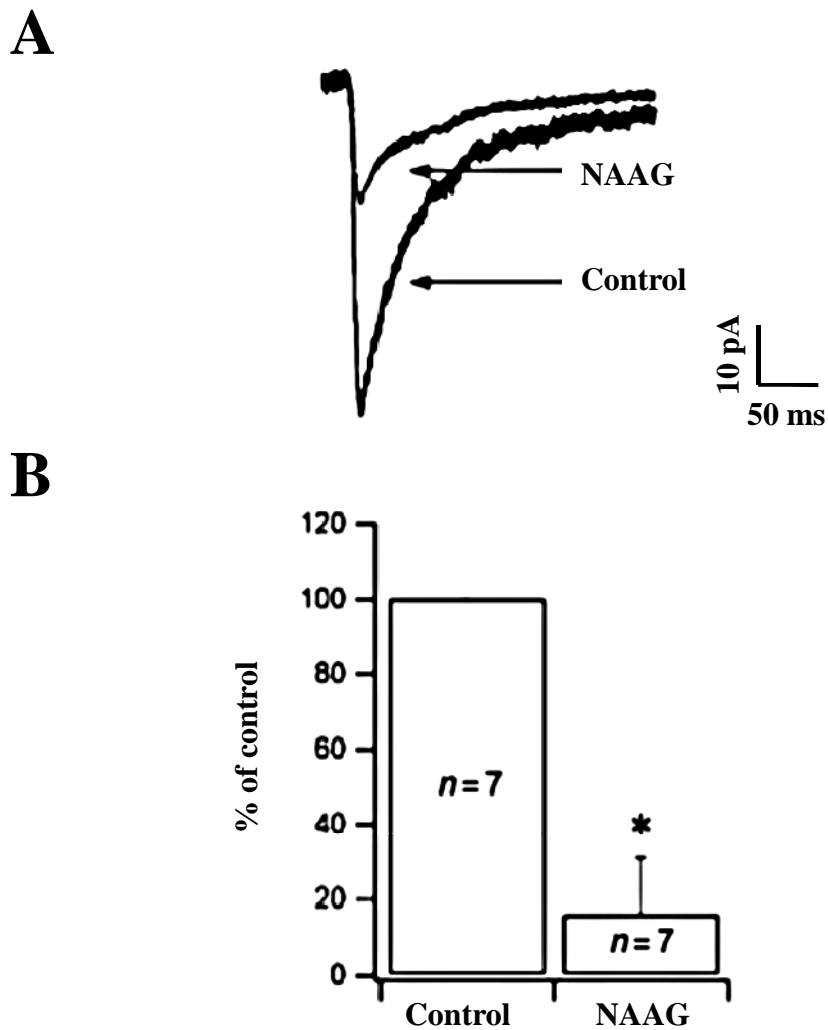


Figure 1.19

NAAG can antagonize glutamate's action on NMDA receptors. **A** Example of an NMDA receptor current (pharmacologically isolated from the total excitatory postsynaptic current, EPSC), and its inhibition by NAAG (20 μ M). **B** Mean NMDA current component in the absence (Control) and presence of NAAG application. EPSCs were recorded from CA1 pyramidal neurons following electrical stimulation of the Schaffer collaterals. N, number of cells; * $p < 0.05$. Adapted from Bergeron *et al.* (2007).

Chapter 2: Materials and methods

This chapter explains the general methods used for experiments throughout the thesis. All experiments were carried out in brain slices to allow patch-clamping and Ca^{2+} -imaging of oligodendrocytes, whilst applying pharmacological agents at a known concentration.

2.1 Preparation of cerebellar slices

Sprague-Dawley rats, aged postnatal day 12 (P12) were used for the preparation of the cerebellar brain slices employed for the experiments in Chapters 3-6. This age was chosen because at this stage of cerebellar maturation cells all the developmental stages of the oligodendrocyte lineage are present (Káradóttir *et al.*, 2005) and the relatively uncompacted white matter allows better visualization of the cells and easy access for patch clamping. Also, as the P12 cerebellum is routinely used by others in the laboratory, the results of my work could be directly compared with those obtained in related experiments. Animals were killed by cervical dislocation followed by decapitation, and the head was immediately immersed in ice-cold oxygenated slicing medium, composed of (in mM): NaCl 124, NaHCO_3 26, NaH_2PO_4 1, KCl 2.5, CaCl_2 2.5, MgCl_2 2, D-glucose 10 (gassed with 95% O_2 /5% CO_2), pH 7.4, and containing 1 mM kynurenic acid to block glutamate receptors during the slicing process and thus reduce damage to the cells. The scalp was removed and the skull was opened by cutting between the eyes, followed by lateral cuts on either side of the head from anterior to posterior. The excised region of the skull was lifted with forceps, and the whole brain was quickly removed and placed in ice-cold oxygenated slicing medium. To obtain parasagittal slices of the cerebellar vermis, cuts were made through the inferior colliculus and spinal cord (to separate the cerebellum from the rest of the brain) and the cerebellar hemispheres on either side of the vermis were removed (to isolate the vermis). The cerebellar block was then mounted on one of its cut surfaces on the stage of a vibrating tissue slicer (Vibratome) using Superglue and mechanically stabilised using an agar block attached to the Vibratome stage. The cerebellum was immersed in ice-cold oxygenated slicing medium throughout the cutting process. Sagittal slices of the cerebellar vermis, 225 μm thick, were cut and placed in oxygenated slicing medium

at room temperature until used for recording, which was less than 9 hours after the animal was killed. At the time of a recording the slice was placed in a recording chamber (volume ~1 ml) on the stage of an upright fixed stage microscope (Olympus BX50WI), and held in place by a “harp”, made of a parallel array of nylon threads (separated from each other by 0.5-1.0 mm) strung on a platinum frame (Fig. 2.1A).

2.2 Standard solutions used and model system for ischaemia

2.2.1 External solutions used

Oxygenated external solutions that mimic cerebrospinal fluid were used to maintain cells alive. In general a HEPES-based external solution was used for drug application experiments at room temperature (Chapters 5 and 6), since that allowed more rapid solution changes, and a bicarbonate-based external solution was used for ischaemia experiments at $33\pm 2^\circ\text{C}$ (Chapters 3 and 4).

The HEPES-based solution contained (in mM): 144 NaCl, 10 HEPES, 1 NaH_2PO_4 , 2.5 KCl, 2.5 CaCl_2 , 10 D-glucose (1 MgCl_2 was added where indicated), with pH adjusted to 7.3 using 1 M NaOH, and was oxygenated with 100% oxygen. The perfusion system consisted of containers (150 ml syringes) filled with the solution and connected to the recording chamber via tubing and valves to switch the flow on or off. The flow was driven by gravity, with the tubes from the syringes containing different solutions emerging near the bath at a rate of 2-4 ml/min. The bath volume was ~1 ml, giving a bath turnover time of 15-30 sec.

Bicarbonate-based solution contained (in mM): NaCl 124, NaHCO_3 26, NaH_2PO_4 1, KCl 2.5, CaCl_2 2.5, MgCl_2 1, D-glucose 10, and was bubbled with 95% O_2 /5% CO_2 , pH 7.4 (the same solution as described in section 2.1, but without the kynurenic acid). A peristaltic pump pumped the solution from its container to the recording chamber, passing through a heating block on the way to allow solution to reach close to physiological temperature ($33\pm 2^\circ\text{C}$). The temperature was set by adjusting the current through resistors attached to the heating block. It was chosen to be 33°C rather than 37°C , because slices lived longer at this temperature. The flow rate was 2-4 ml/min, giving a bath turnover time of 15-30 sec.

2.2.2 Internal solutions used

The whole-cell clamp experiments were performed using different intracellular (i.e. pipette) solutions appropriate for each experiment. A caesium-based internal solution was used for most voltage-clamp recordings in Chapters 3-6, as caesium does not pass well through most potassium channels and so increases the membrane resistance. Consequently, caesium increases the cell's electrical space constant and the voltage-clamp quality. However, to assess cell properties during ischaemia in Chapter 5, both caesium- and potassium-based internal solutions were used, the potassium-based solution being used to assess responses with the physiological cation present inside the cell. In each chapter the intracellular solutions used will be described, and these are collected for convenience in Table 2.1.

2.2.3 Ischaemic solution used

To mimic brain ischaemia *in vitro*, both glycolytic and mitochondrial ATP productions were blocked by removing glucose and O₂. In addition, because in open recording chambers oxygen from the room air can rapidly diffuse through the solution to the tissue, preventing the true inhibition of oxidative phosphorylation that would occur *in vivo*, metabolic blockers were added (Reiner *et al.*, 1990). To do this I used a bicarbonate-based solution with 7 mM sucrose (substituted for 10 mM D-glucose), bubbled with 95% N₂/5% CO₂, (substituted for 95% O₂/5% CO₂). Glycolysis was blocked with iodoacetate (2 mM) and oxidative phosphorylation was blocked with antimycin (25 μM) (Allen *et al.*, 2005).

2.3 Pipettes and electrical set-up

Patch pipettes were made from thick-walled filament-containing borosilicate glass capillaries (outer diameter 1.5 mm, inner diameter 0.86 mm, type GC150F-10 from World Precision Instruments), and they were produced using a two step vertical puller (Narishige PC-10). The electrode was then filled with the appropriate intracellular solution (see Table 2.1).

The recording electrode was inserted into the pipette holder of a patch-clamp headstage (Axopatch CV203BU, Axon Instruments), which was attached to and moved by an electric micro-manipulator (SM-5, Luigs and Neumann). The electrode had a resistance of 5-8 MΩ when placed in the bath. An Ag/AgCl pellet was placed in the

recording chamber to serve as the bath electrode. Membrane currents were recorded with an Axopatch 200B amplifier (filtered at 2 or 10 kHz, Axon Instruments), digitised at 1-10 kHz with a Digidata 1320 (Axon Instruments) and stored on a personal computer using pClamp9.2 and Axoscope9.2 (Axon Instruments). The data were analysed off-line using Clampfit 9.2 (Axon Instruments).

2.4 Optical set-up for electrophysiology

Slice experiments (Fig. 2.1) were carried out on a set-up equipped with an Olympus BX50WI upright microscope, with a fixed stage and microscope-moving table. Slices were viewed using an Olympus 4x objective or a 40x water immersion objective, with differential interference contrast (DIC) optics. The microscope was equipped with a Xenon arc lamp and a filter cube for viewing Lucifer yellow filled cells (excitation wavelength 425 ± 25 nm, dichroic mirror wavelength 460 nm, and emission above 515 nm; Chroma Technology; see Table 2.2). A CCD video camera (COHU, 2700 series) was attached to the microscope, so that the cells could also be visualized using a TV monitor, and their pictures were taken and stored on a computer using Dazzle Video Creator (Pinnacle Systems Inc.) with Pinnacle Studio software.

2.5 Dye filling and cell identification

Cells for the recording were chosen based on their position in the cerebellar slice (the granular layer for granule cells and the white matter for oligodendrocytes), their morphology under bright light (i.e. the size and apparent health of their soma), the size of their input resistance, and their morphology visualised with Lucifer yellow during and after recording. Fixable fluorescent Lucifer yellow dye was present in the pipette internal solution in Chapters 3-5 (Table 2.1) and as the dye diffused into the cell it revealed the cell's morphology (Fig. 2.1), allowing immediate cell identification. In addition, each cell was marked onto a map of the cerebellum, to simplify the later search for the cell in the confocal microscope when trying to image the morphology of cells that were recorded from. In Chapter 6, the Ca^{2+} -imaging dye, Fura-2, was used in the internal solution (Table 2.1), in which case the final identification of the cell was made at the end of the experiment, after the dye diffused into the cell. Sequential pictures of the cell were taken every 1 sec, with a progressively increasing depth for the

picture plane, starting from the top of the cell, which allowed the acquisition of a full picture of the cell body with processes attached.

Mature oligodendrocytes were distinguished from other cells in the white matter by their big, oval soma, low membrane resistance ($\leq 150 \text{ M}\Omega$) and multiple long parallel processes, each of which forms one internode (Figs. 1.2 and 2.1). White matter precursor cells (OPCs) were distinguished by their high membrane resistance ($\sim 1 \text{ G}\Omega$) and numerous processes spreading radially from the cell soma. Voltage step application revealed a transient inward current in a number of OPCs, which is mediated by voltage-gated sodium channels (Karadottir *et al.*, 2007). Immature oligodendrocytes in the white matter were identified by their intermediate membrane resistance ($>150 \text{ M}\Omega$ and $<1 \text{ G}\Omega$) and the presence of some cell processes forming parallel internodes while the rest were non-specifically oriented, possibly “looking” for an axon to myelinate. Granule cells were identified from their position in the granule cell layer, their small soma attached to approximately four dendrites and their high input resistance ($\geq 3 \text{ G}\Omega$).

After recording from an oligodendrocyte, some slices were fixed in 4% paraformaldehyde in phosphate-buffered saline (PBS) for an hour at room temperature with slight agitation. Then the slice was washed three times for 15 min in 0.1 M PBS. After the wash, the slice was kept in the fridge (with 0.05% NaN_3 added to the 0.1 M PBS solution) until being used for immunocytochemistry and imaging of the cell’s morphology to confirm the mature phenotype of the patch-clamped cell (as in Káradóttir *et al.*, 2005; Káradóttir and Attwell, 2006; see also section 2.11 and Fig. 2.2).

2.6 Patch-clamp recordings

All recordings were performed in the conventional whole-cell configuration (Hamill *et al.*, 1981; Edwards *et al.*, 1989).

After selecting the cell, the pipette was lowered into the bath, its resistance being monitored by application of 10 mV voltage step every 200 ms. A positive pressure was applied to keep the pipette tip clean, preventing the attachment of any debris flowing in the bath solution or of tissue when entering the slice. When closely approaching the cell soma, gentle suction was applied to produce a high resistance seal (usually 1-10 $\text{G}\Omega$) between the cell membrane and the tip of the glass patch pipette. The holding potential was then brought to -60 mV, i.e. a value close to the resting potential of oligodendrocytes and granule cells. The leak current in cell-attached mode (the

current that flows through the pipette while attached to the cell membrane, representing mainly an imperfect seal with the membrane) was less than -20 pA. At this stage, electronic compensation of the pipette capacitance transient was applied.

After formation of a high resistance seal in the cell-attached mode, further suction was applied to break through the piece of membrane at the tip of the pipette and thus gain diffusive and electrical access to the cell's interior (Fig. 2.1).

Owing to the different composition of the pipette solution and the bath solution, a junction potential (i.e. potential difference) exists at the end of the electrode before sealing onto the cell (Fig. 2.3), which is not present when the pipette solution has filled the cell in whole-cell mode (Fenwick *et al.*, 1982). For the gluconate-based pipette solutions used in the experiments, due to slower gluconate diffusion into the bath than chloride diffusion into the pipette, and due to sodium diffusing more slowly into the pipette than caesium and potassium diffuse out, a junction potential of -14 mV is present (Ng and Barry, 1995).

2.7 Series resistance

Pipette series resistance is the resistance between the cell's interior and the pipette's interior when in the whole-cell patch-clamp configuration, and can be measured as outlined below, in equation 2.1. A low series resistance (in the range of 4-20 M Ω , measured as described in section 2.8 below) implies a good electrical and diffusion pathway into the cell. A good diffusion pathway is essential for the efficient exchange of molecules between the pipette and the cell. A good electrical pathway to the cell interior is important because current flowing between the pipette and the cytoplasm will result in a voltage drop across the pipette tip, the value of which depends on the series resistance and the size of the current. A high series resistance or large current flow will result in a high voltage drop, and the real membrane potential in the soma will differ from the apparent membrane potential because of the voltage drop. Series resistance compensation (typically 50-70%) was employed to minimise such voltage errors in granule cells. In mature oligodendrocytes, series resistance compensation was not applied as the non-spherical shape of these cells, with thin and long processes, most probably results in a lack of uniformity of the voltage in the processes even when the soma voltage is well controlled (similar to CA1 neurons in hippocampus, where voltage control at most dendritic sites was shown to be extremely

poor: Major, 1993). The multiexponential decay of the capacity current discussed below supports this idea. There will therefore be a different resistance between the cell soma and different parts of the cell membrane, preventing accurate series resistance compensation of the whole cell.

For experiments on oligodendrocytes, the series resistance was typically $R_s \sim 10\text{-}20\text{ M}\Omega$. At the resting potential, where no current is flowing before a drug or ischaemia solution were applied, from the equation

$$V_{\text{error}} = IR_s \quad (2.1)$$

for a typical NMDA- or ischaemia-evoked current of $\sim 200\text{ pA}$, only a small voltage error of $V_{\text{error}} \sim 2\text{-}4\text{ mV}$ will occur, which can be neglected. Similarly, for experiments on granule cells, the series resistance of $10\text{-}20\text{ M}\Omega$, compensated by 50-70%, for a typical NMDA-evoked current of 50 pA at the resting potential, will cause a negligible voltage error of $0.15\text{-}0.5\text{ mV}$.

2.8 Capacity transient analysis

By analysing the current response to a voltage step, it is possible to measure the pipette series resistance, cell membrane resistance and conductance, and cell capacitance, and to assess whether the cell is uniformly voltage-clamped. Two cases were considered: first a spatially-compact voltage-uniform cell (such as the granule cells studied in Chapter 5), and a cell with long processes where the voltage is non-uniform (such as the mature oligodendrocytes studied in Chapters 3-6). The membrane acts as a capacitor and resistor connected in parallel, and the series resistance is in series with these elements (Figs. 2.4 and 2.5).

For a spatially-compact voltage-uniform cell (Fig. 2.4), the current flow, I , through this circuit in response to a voltage step, V_s , is predicted to be (Tessier-Lavigne *et al.*, 1988):

$$I(t) = \left(\frac{V_s}{R_m + R_s} \right) \cdot \left(1 + \frac{R_m \cdot e^{-t/\tau}}{R_s} \right) \quad (2.2)$$

where t is the time after the onset of the voltage step, R_m is the membrane resistance, R_s is the series resistance, and τ , the decay time constant of the current transient.

At the onset of the voltage step, at $t = 0$, the capacitor is uncharged and the voltage across it is zero. Consequently, just as the voltage step is applied, the voltage

across the series resistance is the applied voltage step, and the initial current flowing ($I(t = 0) = V_s/R_s$ from equation 2.2) allows calculation of the series resistance as:

$$R_s = \frac{V_s}{I(t = 0)} \quad (2.3)$$

In the steady state, i.e. at $t = \infty$, the capacitor is fully charged and no current flows through it. The membrane resistance can then be calculated from the voltage step and the current at $t = \infty$. Since $I(t = \infty) = V_s/(R_m + R_s)$ from equation 2.2,

$$R_m = \frac{V_s}{I(t = \infty)} - R_s \quad (2.4)$$

Similarly, the cell conductance, $G_m = 1/R_m$, at the steady state is calculated from the equation

$$G_m = \frac{(I(t = 0) \cdot I(t = \infty))}{V_s (I(t = 0) - I(t = \infty))} \quad (2.5)$$

and the membrane capacitance can be calculated as (Tessier-Lavigne *et al.*, 1988):

$$C_m = \tau \cdot \frac{R_s + R_m}{R_s \cdot R_m} \quad (2.6)$$

The time constant, τ , was obtained by fitting the current transient with a single exponential using Clampfit. An example of a fitted capacity transient is shown in Fig. 2.4. The current change at $t = 0$ was obtained by extrapolating this exponential back to the time of the voltage step.

This analysis assumes that the cell is isopotential, and predicts a monoexponential decay of the capacity current. This is the case for electrically compact cells such as cerebellar granule cells. For cells with complex morphology, however, such as mature oligodendrocytes, the resistance of the processes makes the cell non-uniform in voltage, and the capacity current decays as the sum of 2 or more exponentials (Fig. 2.5). The current response was then fitted with the sum of two exponentials:

$$I(t) = I(t = \infty) + I_1 \cdot e^{-t/\tau_1} + I_2 \cdot e^{-t/\tau_2} \quad (2.7)$$

where I_1 and τ_1 are the amplitude and time constant for the first exponential, I_2 and τ_2 are the amplitude and time constant for the second exponential, respectively, and $I(t = \infty)$ is the steady state current. For this model the series resistance is still given by equation 2.3, but it is not possible to derive the membrane resistance or capacitance in the different compartments of the cell without making further assumptions.

2.9 Calcium imaging

This technique allows the recording of intracellular calcium concentration ($[Ca^{2+}]_i$) changes by using specific calcium indicators (dyes). Calcium indicators can be generally divided into non-ratiometric and ratiometric ones.

For non-ratiometric dyes (e.g. Fluo-4), binding of calcium ions causes a change in dye conformation that results in increased brightness (increased efficiency of fluorescence emission) upon light excitation. This allows recording of a $[Ca^{2+}]_i$ increase, but cannot distinguish a change of $[Ca^{2+}]_i$ concentration from a change of dye concentration (e.g. due to cell damage or movement).

For ratiometric dyes (e.g. Fura-2), the change in conformation upon calcium ion binding results in a shift of the dye excitation wavelength. This allows recording of the change in $[Ca^{2+}]_i$ by taking the ratio of the emitted fluorescence evoked by two different exciting wavelengths. This provides a measurement of $[Ca^{2+}]_i$ change that is independent of the concentration of the dye, and thus less susceptible to artefactual errors.

2.9.1 Calcium imaging using acetoxymethyl ester dye loading

To image intracellular calcium changes in many cells of the grey and white matter without the need to load dye by patch-clamping, a slice was loaded with a cell-permeable calcium dye, the acetoxymethyl (AM) ester of Fluo-4 (Fluo-4-AM, Molecular Probes). Fifty micrograms of Fluo-4-AM were dissolved in 11.5 μ l of dimethyl sulfoxide (DMSO, Sigma) and 11.5 μ l of Pluronic acid (used to facilitate dye dispersion in aqueous media; Molecular Probes). This stock solution (2 mM) was diluted in the external solution in order to incubate the slice for 2 h in 5 μ M Fluo-4-AM. Before fluorescence measurements, the slice was washed in an indicator-free solution to remove any dye that was not taken up by the cells, and then incubated for at least 30 min to allow de-esterification of the intracellular AM esters to occur (Fig. 2.6). Regions of interest in the white and grey matter were identified from the morphology and anatomy of the slice. Fluo-4 was excited at 480 ± 10 nm, and the emitted light was collected at 535 ± 22 nm, using a dichroic at 505 nm (see Table 2.2).

2.9.2 Calcium imaging of single cells

To image intracellular calcium changes in a single cell, mature oligodendrocytes in the white matter or granule cells in the grey matter were patch-clamped with pipettes

containing a caesium-based internal solution with Fura-2 (free acid, not AM ester) as the calcium-sensing dye (Molecular Probes) (see Table 2.1). Fluorescence was excited sequentially at 340 ± 10 and 380 ± 10 nm, and the emitted light was collected at 510 ± 20 nm, using a dichroic at 415 nm (see Table 2.2). The ratio of the emission intensities (340 nm/380 nm) was used as a measure of $[Ca^{2+}]_i$ change. Only ratios that reflected both a decrease of fluorescence excited at 380 nm and an increase in fluorescence excited at 340 nm were used since if, for example, the signal decreased at both wavelengths, it suggests that dye has been lost from the cell due to membrane damage or dye bleaching, or the cell has moved partly out of the field of view.

2.9.3 Optical set-up for calcium imaging

The microscope (see section 2.4) was equipped with a xenon lamp and filter sets for viewing Fluo-4 or Fura-2 dyes (see sections above and Table 2.2). A CCD video camera (iXON, Andor) was attached to the microscope, and the cells were visualised on a computer screen. Data were acquired and analysed using Meta Imaging 6 software (Molecular Devices).

2.10 Cell death assay

Cell death was assessed by using propidium iodide (PI, Sigma). PI is a fluorescent molecule that binds to DNA by intercalating between its bases and, once bound, its fluorescence is enhanced 20- to 30-fold (using an excitation wavelength 543 nm, dichroic wavelength 488/543/633 nm, and an emission wavelength 570-600 nm see Table 2.3). PI is generally excluded from passing across the surface membrane of viable cells, so it can only reach the nucleus of cells if they have a permeable surface membrane which is generally associated with necrotic (and, in some cases, late apoptotic: Rieger *et al.*, 2011) cell death.

To perform the experiment, slices were bathed in an external solution containing appropriate drugs (see Chapter 6), or in control solution, at $36^{\circ}C$ for 6 hr, with propidium iodide ($37\ \mu M$) added from the beginning. After incubation, slices were fixed in 4% paraformaldehyde in PBS overnight, then washed three times for 15 min in 0.1 M PBS. After the wash, slices were kept in the fridge (with 0.05% NaN_3 added to the 0.1 M PBS solution) until being used for assessment of PI labelling and antibody labelling against myelin basic protein (MBP, see below) to quantify the (mainly

necrotic) death of cells in white matter identified as mature oligodendrocytes. During the mounting procedure, a mounting solution containing 300 nM DAPI (excitation wavelength 364 nm and emission wavelength above 385 nm, see Table 2.3; Fluoro-Gel II, EMS) to stain all cell nuclei was used, so that dead cells (stained with PI) could be quantified as a fraction of the pool of all the cells in the slice (stained with DAPI). Images were acquired using a confocal microscope.

2.11 Immunocytochemistry

2.11.1 Antibody labelling

Fixed slices (see section 2.5) were collected from the fridge and washed three times for 20 min with 0.1 M PBS. Then, slices were treated with a blocking and permeabilizing solution, containing 10% goat serum, 0.05% Triton X-100, 0.05% NaN₃ and 0.1 M PBS, for 4-6 hr at room temperature with slight agitation. This was followed by incubation with a primary antibody against myelin basic protein, a protein specific for mature oligodendrocytes (mouse anti-MBP, Chemicon), at a dilution of 1:200 in PBS containing 0.05% NaN₃ for 12-18 hr at room temperature with slight agitation. Then, slices were washed three times for 20 min with 0.1 M PBS. To reveal labelling with the primary antibody, a secondary antibody (goat anti-mouse IgG, conjugated to AlexaFluor 488, excitation wavelength 488 nm, dichroic wavelength 488 nm, and emission wavelength above 505 nm, see Table 2.3; Invitrogen) was used, diluted to 1:200 in 0.1 M PBS containing 0.05% NaN₃, for 8 hr at room temperature with slight agitation. Next, the slices were washed three times for 20 min and mounted on a microscope slide (BDH) with Citifluor (glycerol/PBS, Citifluor), covered with a 0.17 mm thick glass cover slip, and sealed with nail varnish (Boots, UK). A control experiment for antibody labelling was performed each time by omitting the primary antibody during the staining procedure.

2.11.2 Confocal imaging

All fixed slices were imaged with a confocal laser scanning microscope (LSM), either a Zeiss LSM 510 inverted microscope or a Zeiss LSM Pascal upright microscope. For high resolution images of single cells, a 63x oil DIC objective was used; for high resolution images of slices, a 40x DIC objective was used. All imaging with multiple

wavelengths was done with sequential scans at the different wavelengths (see Table 2.3 for excitation, dichroic and emission wavelengths), which reduces ‘bleed through’ of emitted fluorescence from one channel to another.

For single cell imaging, scanning was done in x-y and z directions, and averaged 2-4 times depending on the signal. The size of the z stack depended largely on the depth of the cell of interest, ranging from 15-90 μm , taken in $\sim 0.2 \mu\text{m}$ sections. The signal gain and zero offset were initially set for each image depending on the signal being detected, and those settings were then held constant for the control slices lacking primary antibody. Projections of images were made in LSM Examiner software, and control slices were treated in the same way with respect to brightness and contrast adjustments.

2.12 Data analysis and statistics

Data are presented as mean \pm s.e.m. and the significance of changes was normally assessed with 2-tailed Student’s t-tests. T-tests were either paired, as when analysing whether events within the same group of cells had altered over time or with a drug treatment, or were unpaired, as when comparing whether the mean responses of different groups of cells were significantly different. When comparing more groups than two in Chapters 3 and 4, a one-way ANOVA was used followed by a Holm-Bonferroni correction for multiple comparisons. Conventionally this is done as follows. For a desired level of significance such as $p < 0.05$, if N comparisons are made the most significant p value is compared with $0.05/N$ (rather than 0.05), the second most significant is compared with $0.05/(N-1)$, and the third most significant is compared with $0.05/(N-2)$, etc. In order to present p values on graphs in a form which could all be simply compared directly with 0.05, I calculated corrected p values by multiplying the most significant p value by N, the second most significant by N-1, the third most significant by N-2, etc. This procedure is formally equivalent to the Holm-Bonferroni correction, but has the advantage that any of the corrected p values which are shown on the graphs are significant if they are less than 0.05.

Type of internal solution	Cs-based	K-based	Ca²⁺-imaging
Main Ions	Cs-Gluconate 130 mM	K-Gluconate 130 mM	Cs-Gluconate 130 mM
NaCl	NaCl 4 mM	NaCl 4 mM	NaCl 4 mM
pH buffer	HEPES 10 mM	HEPES 10 mM	HEPES 10 mM
Calcium chelator	BAPTA 10 mM	BAPTA 10 mM	BAPTA 0.01 mM
Added calcium	CaCl ₂ 0.5 mM	CaCl ₂ 0.5 mM	
GTP	Na ₂ GTP 0.5 mM	Na ₂ GTP 0.5 mM	Na ₂ GTP 0.5 mM
ATP	MgATP 4 mM	MgATP 4 mM	MgATP 4 mM
Phosphocreatine			Phosphocreatine 10 mM
Fluorescent dye	Lucifer yellow 2 mM	Lucifer yellow 2 mM	Fura-2 1 mM
pH adjusted to 7.3 with	CsOH	KOH	CsOH

Table 2.1

List of the internal solutions and their composition used for the experiments presented in this thesis.

Fluorophore	Excitation wavelength (nm)	Dichroic wavelength (nm)	Emission wavelength (nm)	Light source
Fluo-4	488±10	505	535±22	Xenon arc lamp with monochromator
Fura-2	340±10 and 380±10	415	510±20	Xenon arc lamp with monochromator
Lucifer yellow	425±25	460	LP >515	Xenon arc lamp

Table 2.2

List of fluorophores, with the excitation, dichroic and emission wavelengths of filters when the fluorescence microscope on the patch-clamping rig was used. LP=Long Pass Filter.

Fluorophore	Excitation wavelength (nm)	Dichroic wavelength (nm)	Emission wavelength (nm)	Light source
Alexa Fluor 488	488	HFT 488	LP 505	Argon laser
DAPI	364		LP>385	UV laser
Lucifer yellow	458	HFT 458/514 NFT 545	BP 505-600	Argon laser
Propidium iodide	543	HFT 488/543/633	BP 570-600	HeNe laser

Table 2.3

List of fluorophores, with the excitation lines, and dichroic and emission wavelengths of filters when the confocal microscope was used. Abbreviations: BP=Band Pass Filter, LP=Long Pass Filter, HFT=Main Dichroic Beam Splitter, NFT=Secondary Dichroic Beam Splitter.

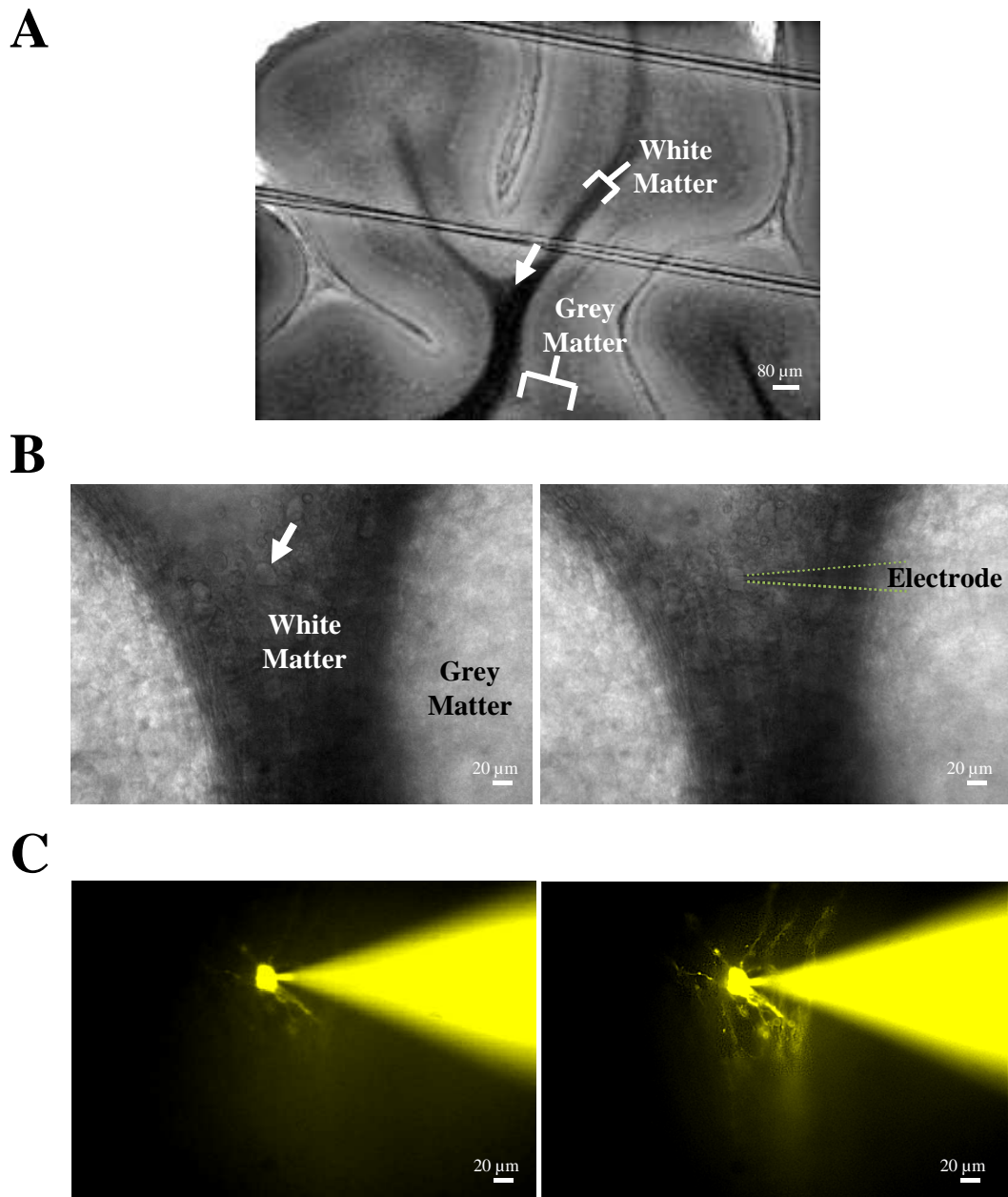


Figure 2.1

Patch-clamping of a cerebellar white matter mature oligodendrocyte in a P12 rat. **A** Low power picture of the cerebellum, where the white matter (darkest areas) is distinguishable from the grey matter. The arrow shows the area which is magnified in **B** and **C** (note that the strings are part of the harp which maintains the slice immobile in the bath). **B** Left: same picture at higher magnification: the arrow shows the cell about to be patch-clamped. Right: dotted lines show the position of an electrode, filled with Lucifer yellow, which was contacting the cell. **C** Left: Lucifer yellow labelling (pseudocolor): picture taken just after breaking through the cell membrane. Right: same cell 10 minutes later; the dye had diffused through the processes.

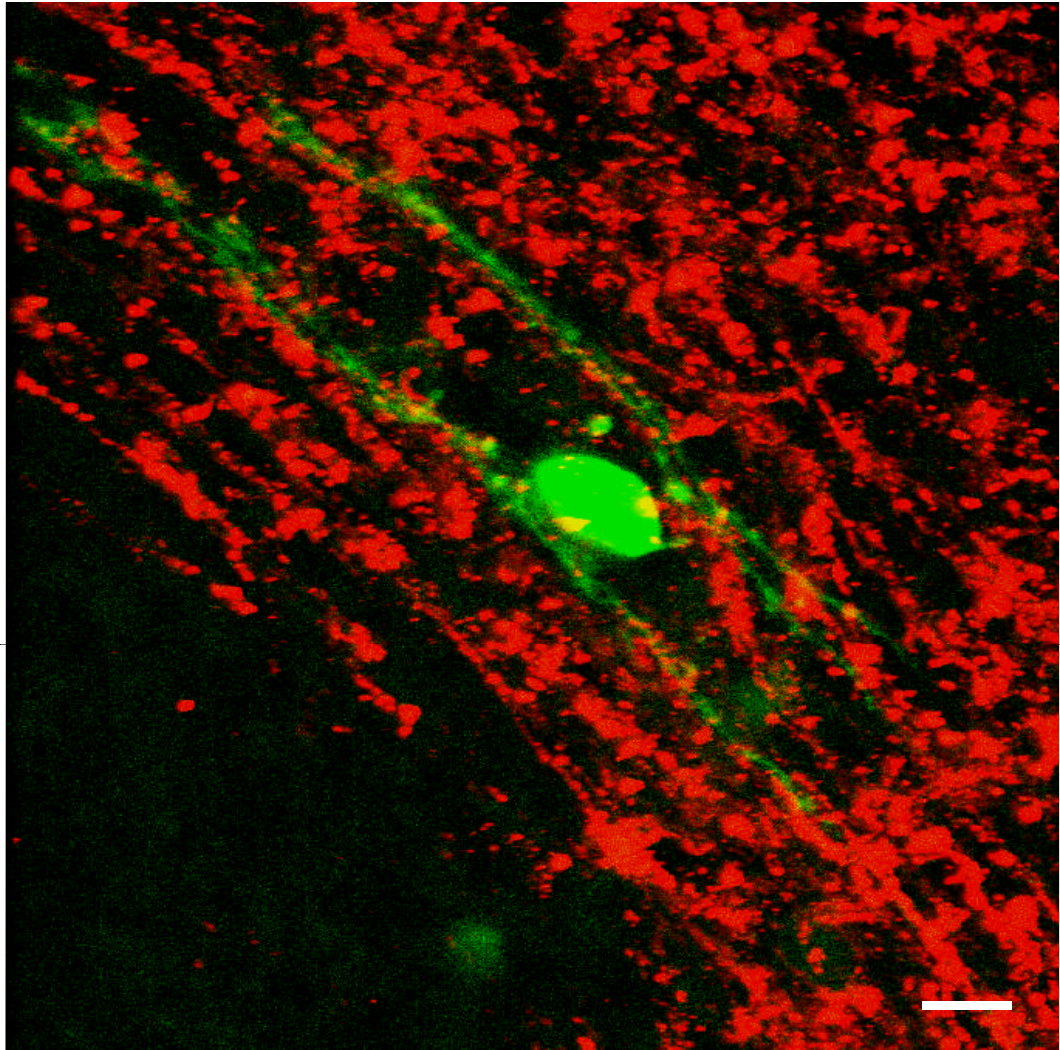


Figure 2.2

Confirmation of mature oligodendrocyte phenotype with immunostaining. A mature oligodendrocyte was filled with Lucifer yellow (green) during whole-cell patch-clamping and the slice was subsequently immunolabelled against myelin basic protein (MBP, red), which is expressed on oligodendrocyte processes. The merged image reveals an association between the patched cell's processes and the MBP staining. Scale bar, 10 μm .

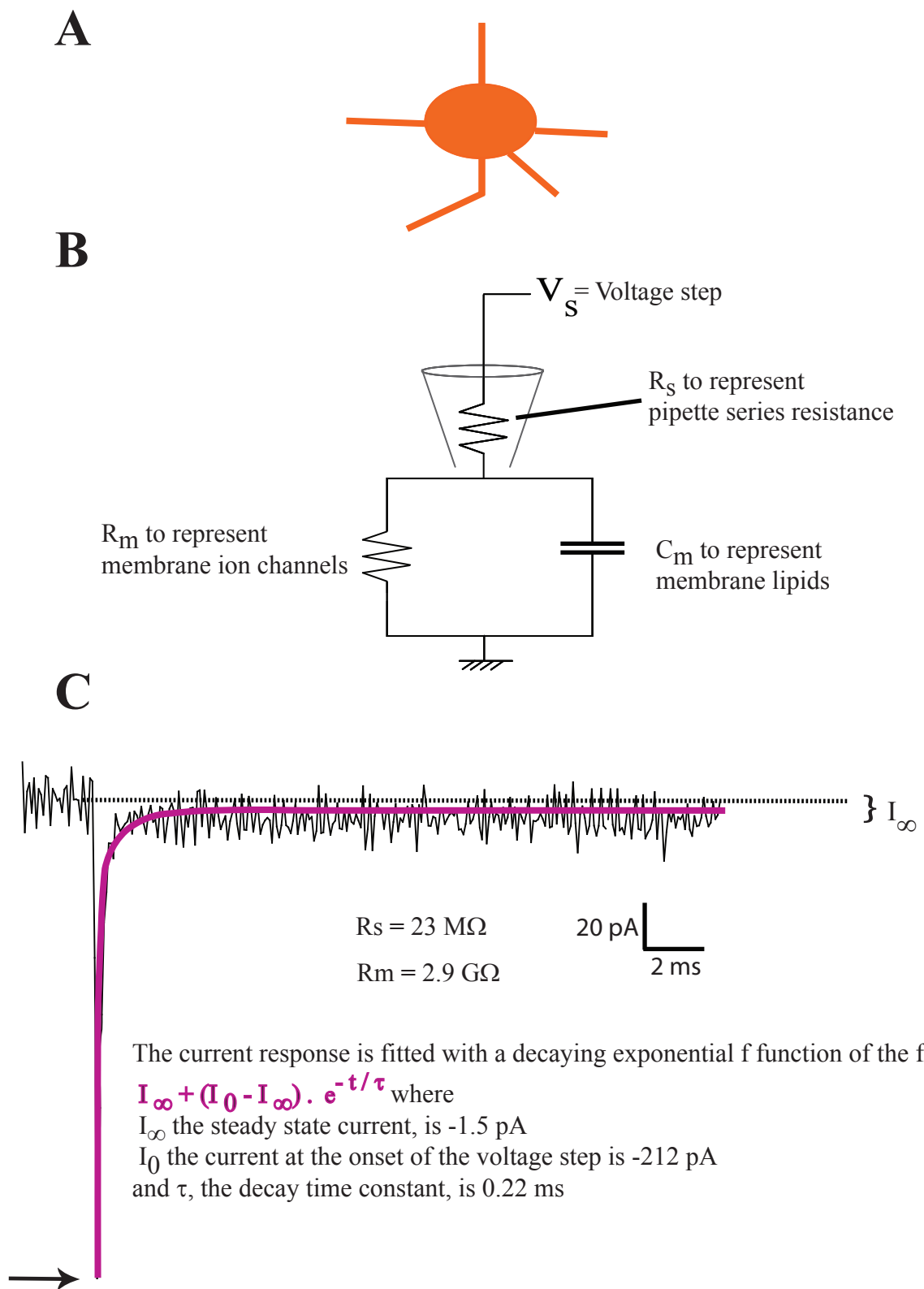


Figure 2.3

Capacity transient of a spatially compact cell such as a granule cell. A Schematic diagram of a granule cell with short electrically compact processes. B Effective circuit diagram of a whole-cell patch-clamped granule cell. C Trace shows the current response to a -5 mV pulse in a whole-cell patch-clamped cell. This could be fitted with a single decaying exponential (purple line). The series resistance is calculated from the peak current recorded when the voltage pulse is applied (see arrow) while the membrane resistance is obtained by measuring the current (I_∞) recorded after the membrane been charged, as described more detail in the text associated with equation 2.2.

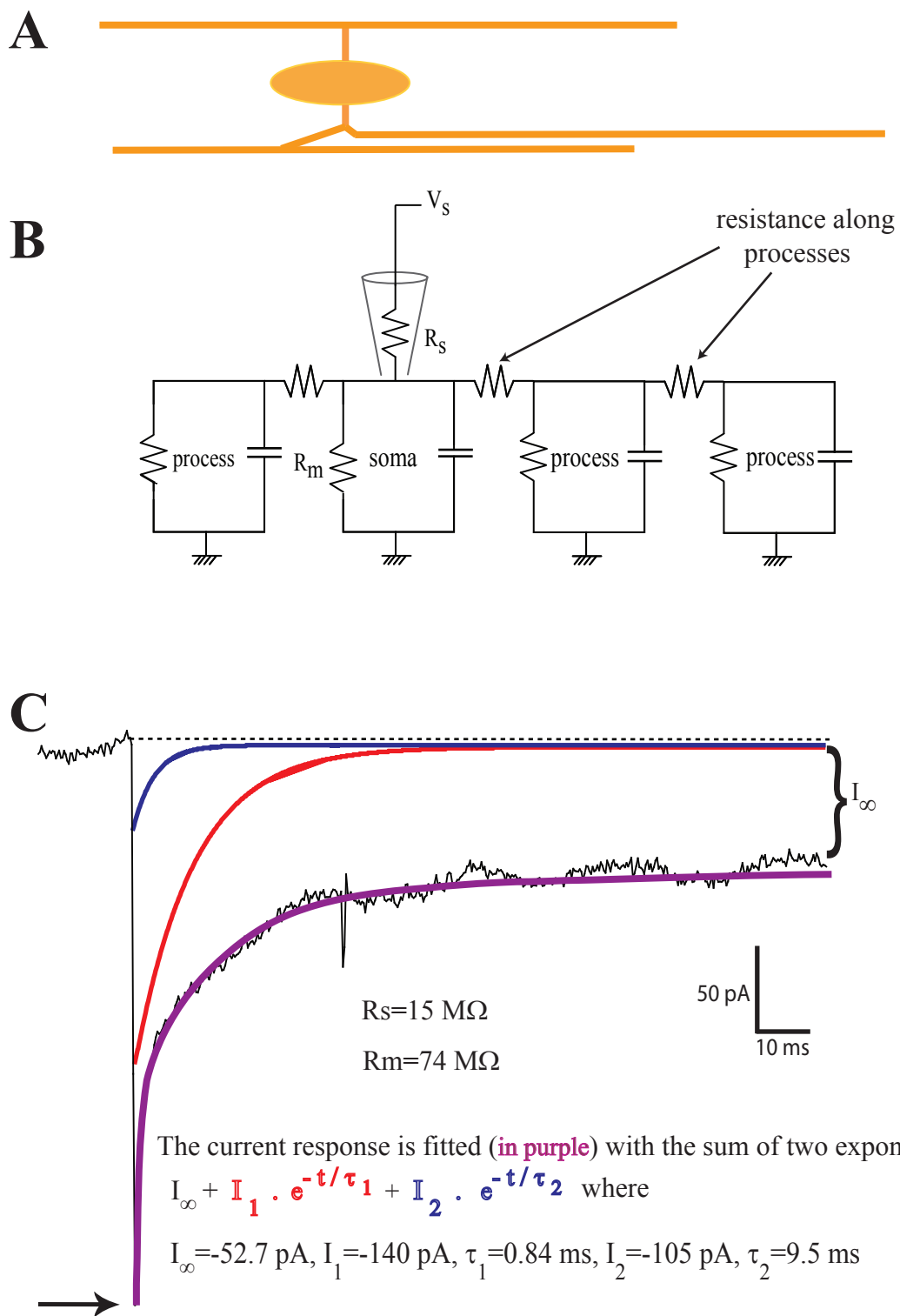


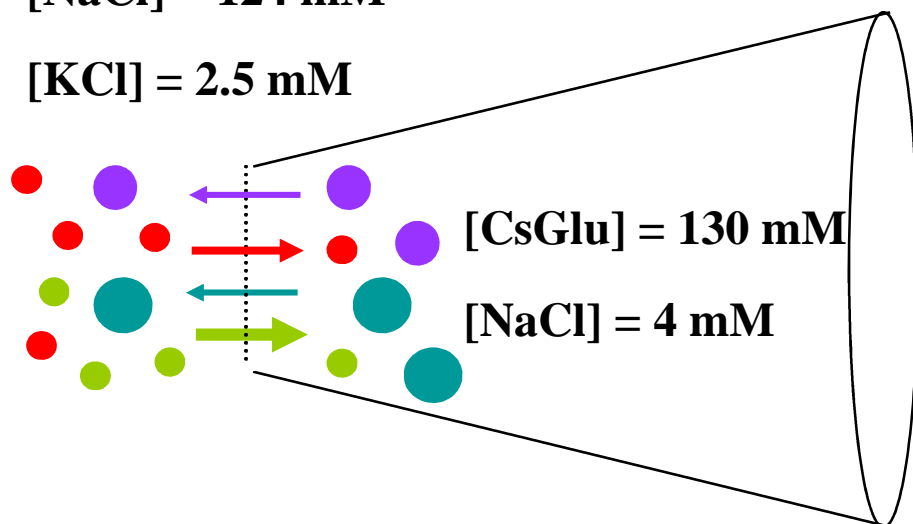
Figure 2.4

Capacity transient of a complex cell such as a mature oligodendrocyte cell which is not voltage-uniform. **A** Schematic diagram of a whole-cell clamped mature oligodendrocyte. Each process is treated as a series of electrical compartments. **B** Effective circuit diagram of a mature cell with numerous long processes. **C** Trace shows the current response to a -5 mV pulse in a whole-cell patch-clamped mature oligodendrocyte. This current could be fitted with the sum (purple line) of two exponentials (blue and red lines). The series resistance is calculated from the peak current recorded when the voltage pulse is applied (see arrow), while the input resistance of the cell is obtained by measuring the steady-state current recorded after the membrane has been charged.

$[\text{NaHCO}_3] = 26 \text{ mM}$

$[\text{NaCl}] = 124 \text{ mM}$

$[\text{KCl}] = 2.5 \text{ mM}$







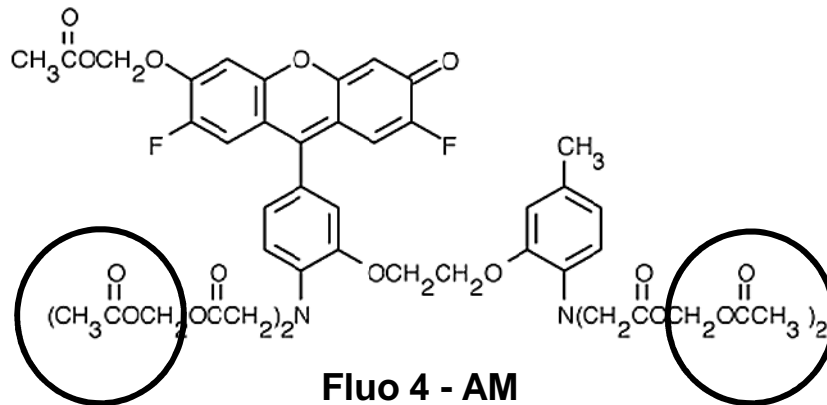
-  **Gluconate**
-  **Caesium**
-  **Chloride**
-  **Sodium**

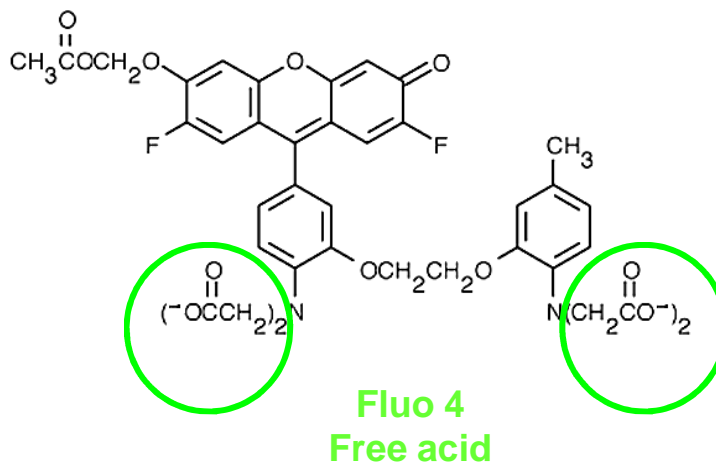
Figure 2.5

A junction potential exists at any interface between different solutions, such as between the pipette solution and the bath solution. It depends on the different diffusion coefficient values for the principal cations and anions, which cause them to diffuse at different rates (depending on their molecular weight and charge) across the interface. (Note that only the main ions are represented here).



**Cell permeant
Fluorescence is calcium-independent**

Esterases



**Cell impermeant
Fluorescence depends on $[Ca^{2+}]_i$**

Figure 2.6

Using the acetoxymethyl (AM) ester form of a Ca^{2+} -sensing dye. Slices were incubated in the presence of $5 \mu M$ of the cell permeant Fluo-4 dye for 60 minutes. Following the loading, the slice was washed and kept in medium without dye, while deesterification was taking place. The esterases inside the cell remove the ester group on Fluo-4 making it able to bind calcium (resulting in $[Ca^{2+}]_i$ -dependent fluorescence), and becoming membrane impermeant so it cannot leave the cell again.

Chapter 3: The electrical response of white matter oligodendrocytes to simulated ischaemia

3.1 Introduction

As reviewed in Chapter 1, the ischaemia, which occurs in stroke or when blood vessels are damaged in spinal cord injury, and possibly in conditions leading to periventricular leukomalacia, damages oligodendrocyte lineage cells in the white matter. It is conventionally assumed that, as for ischaemic damage to neurons, ischaemic damage to oligodendrocytes may in large part reflect a release of glutamate, and subsequent activation of an inward current across the cell membrane which includes damaging Ca^{2+} entry (see Chapter 1). Indeed, oligodendrocytes and their precursors have been reported to generate an inward current at the onset of ischaemia (Káradóttir *et al.*, 2005; Káradóttir *et al.*, 2008), which could be a prelude to the rise of $[\text{Ca}^{2+}]_i$ (Micu *et al.*, 2006) and loss of myelinating processes (Salter and Fern, 2005) that mature oligodendrocytes suffer in the first 30-60 min of ischaemia. However, previous studies of oligodendrocyte damage have mainly employed methods such as immunolabelling and biochemical assays which, although extending our knowledge about the long-term effects of ischaemia, do not provide information about the real-time response of oligodendrocytes to the ischaemic insult.

To investigate in more detail the initial membrane current response of oligodendrocyte lineage cells to ischaemia, I used whole-cell patch-clamping to record the membrane currents and voltage changes of white matter oligodendrocyte lineage cells in brain slices superfused with ischaemia-mimicking solution (in the rest of the text this will simply be denoted 'ischaemia'). The results show that, despite the fact that ischaemia evokes an inward current in oligodendrocytes, the mechanism of this current's generation is fundamentally different to that occurring in response to ischaemia in neurons.

3.2 Materials and methods

3.2.1 Brain slice preparation

Cerebellar slices were prepared from P12 rats as described in section 2.1. Slices were immersed and patch-clamped in a bicarbonate-based solution at room temperature with a flow rate of 2-4 ml/min. After obtaining the whole-cell patch-clamp recording mode, the temperature was elevated to 33°C and a stable baseline was recorded for ~5 min, before applying ischaemia-mimicking solution. The external solution and the ischaemic solution are described in sections 2.2.1 and 2.2.3, respectively.

3.2.2 Patch-clamping

White matter oligodendrocytes were whole-cell patch-clamped as described in section 2.6. Pipettes contained either Cs⁺ or K⁺-based internal solutions (for comparison see Table 2.1). These two different internal solutions were used because the Cs⁺-based solution permitted a better voltage clamp of the cell's membrane at depolarised potentials (since the K⁺ channels activated by depolarisation are impermeable to Cs⁺, so the membrane resistance and electrical space constant are higher), while the K⁺-based solution allowed physiologically-relevant recordings of the voltage changes occurring across the cell membrane when the cells were not voltage-clamped.

The series resistance was 10-20 MΩ, and was not compensated. For voltage-clamp experiments, the membrane voltage was held at -74 mV (including the junction potential of -14 mV, see section 2.6), while for the voltage recordings in current-clamp mode no current was applied.

3.2.3 Current and voltage analysis during anoxic depolarisation

For recordings in voltage-clamp mode, the ischaemia-evoked currents were measured relative to the current flowing at the start of ischaemic solution application. In current-clamp mode, voltage changes were measured from the resting potential that the cell assumed without injected current (the mean value of which was -73±2 mV with K⁺ inside, n=6, and -64±4 mV with Cs⁺ inside, n=6).

3.2.4 Capacitance measurement

For small and electrically compact cells (e.g. cerebellar granule cells or oligodendrocyte precursor cells), which show a monoexponential decay to their capacity current, the capacitance of the cells can be calculated from the current response to a small voltage step, using equation 2.6:

$$C_m = \tau \cdot \frac{R_s \cdot R_m}{R_s + R_m}$$

where τ is the decay time constant of the capacity current and R_s and R_m are given by equations 2.3 and 2.4. However, for myelinating oligodendrocytes the capacity current could not be well fitted by a single decaying exponential (see section 2.8), implying that the processes of the cell are not well voltage-clamped, but it could be approximately fitted by the sum of 2 exponential components as in equation 2.7:

$$I(t) = I(t = \infty) + I_1 \cdot e^{-t/\tau_1} + I_2 \cdot e^{-t/\tau_2}$$

The slower of these components was assumed to reflect charging of the more distant parts of the cell processes, which Salter and Fern (2005) have reported to be lost after 30-60 min ischaemia, so I examined whether the parameters of the slower exponential changed in ischaemia in a manner consistent with a loss of cell processes, i.e. whether its amplitude decreased or its time constant decreased. For this analysis, values were calculated from capacity current transients evoked by 5 mV voltage steps, which were applied every 1.5 min from 7.5 min before ischaemia until 7.5 min after the start of ischaemia, and again at 15 min and 21 min after the start of ischaemia.

3.2.5 Membrane resistance and conductance measurements

The apparent membrane resistance was calculated from equation 2.4:

$$R_m = \frac{V_s}{I(t = \infty)} - R_s$$

by subtracting the pipette series resistance from the total input resistance (note that for mature oligodendrocytes, which have imperfectly voltage-clamped processes, part of this resistance may be contributed by the internal resistance of the cells' processes).

The slope conductance of each measured I-V relation (ignoring the presence of the series resistance) was calculated, at the resting potential and at 0 mV, as the current change between two adjacent points of the I-V relation (bracketing either the resting

potential or 0 mV) divided by the voltage difference between the two points (i.e. 20 mV).

3.2.6 Statistics

Data are presented as mean \pm s.e.m. P values are from Student's 2-tailed t-tests or from ANOVA and post-hoc Student's 2-tailed t-tests. A Holm-Bonferroni correction was applied for multiple comparisons as described in Chapter 2, in such a way that differences are significant if the p values presented are less than 0.05.

3.3 Results

3.3.1 Ischaemia evokes an inward current in mature oligodendrocytes

I identified mature oligodendrocytes as described in section 2.5, and whole-cell voltage-clamped them at -74 mV with Cs⁺-based internal solution. Upon applying ischaemic solution (i.e. lacking oxygen and glucose, and with iodoacetate and antimycin added to block ATP production by glycolysis and oxidative phosphorylation, see section 2.2.3), the cells displayed an inward current which usually showed three characteristic phases (Fig. 3.1). After a few minutes of the current slowly becoming more inward (phase 1), the increase of inward current accelerated (phase 2) until the response reached a peak. This second component of the response has a time course similar to the anoxic depolarisation described in neurons (Hansen, 1985) and to the ischaemia-evoked current seen in cerebellar Purkinje cells (Hamann *et al.*, 2005). After this peak, the current became less inward (phase 3) and eventually tended towards a stable level that was more inward than before ischaemia (Fig. 3.1A).

The amplitude of the peak current evoked by ischaemia averaged over all the 179 mature oligodendrocytes studied was -209 ± 10 pA (Fig. 3.2C). However, when the time courses of the current responses from the different cells were averaged together, the different time of occurrence of the peak AD current in the different cells (ranging from 160 sec to 920 sec, average 439 ± 11 sec from the start of ischaemic solution application, see Fig. 3.5) led to an average current time course (Fig. 3.1B) that did not display a sharp peak as was seen in most cells, and which had a somewhat smaller

amplitude than that obtained (Fig. 3.2C) by averaging over the peak currents in the individual cells.

3.3.2 The amplitude of the ischaemia-evoked inward current depends on the developmental stage of the cell

I compared the ischaemia-evoked inward current displayed by mature oligodendrocytes to that induced in OPCs and immature oligodendrocytes, which were identified morphologically as described in section 2.5, and shown in Fig. 3.2A. Although the time course of the current response to ischaemia was broadly similar at all three developmental stages, the amplitude of the peak inward current increased with the stage of cell development, with OPCs displaying a peak current of -61 ± 10 pA ($n=15$), immature cells of -107 ± 25 pA ($n=8$) and mature cells of -209 ± 10 pA ($n=179$) (Fig. 3.2). The increase in peak inward current seen with development may suggest an increasing expression of the channels or receptors responsible for the generation of the ischaemia-evoked current, or could simply reflect the cells increasing in size with no change of the density of channels and receptors in the membrane.

3.3.3 Using K^+ instead of Cs^+ as the main intracellular cation does not affect the ischaemia-evoked current, but reduces the ischaemia-evoked voltage change

I mainly used a Cs^+ -based internal solution for voltage-clamp recordings, because Cs^+ does not permeate through many K^+ channels and thus increases cell membrane resistance. This will increase the cell's electrical space constant and the voltage-clamp quality. However, to investigate the cells' responses in a more physiological condition, I used a K^+ -based internal solution (see Table 2.1) and compared the results.

First, I compared data obtained when voltage-clamping mature oligodendrocytes with either Cs^+ or K^+ as the main ion in the internal solution. Upon application of ischaemic solution, with either of the internal solutions the cells displayed an inward current with a similar time course and amplitude (Fig. 3.3A): the average peak amplitude was -209 ± 10 pA ($n=179$) for Cs^+ - and -191 ± 41 pA ($n=10$) for K^+ -based solutions (not significantly different, $p=0.67$, Fig. 3.3B). Thus, the presence of Cs^+ rather than K^+ in the internal solution does not influence the oligodendrocyte current response to ischaemia when voltage-clamped to -74 mV.

Next, I investigated the oligodendrocyte voltage response to ischaemia in current-clamp mode. With Cs^+ in the internal solution, ischaemia caused an initial slow depolarisation of about 15 mV followed by a more rapid and large depolarisation of the cell membrane by ~ 50 mV (giving an overall depolarisation of 62 ± 7 mV, $n=6$) that lasted until the end of the recording (~ 15 min; Fig. 3.4A). In contrast, when a K^+ -based internal solution was used, the initial depolarisation of the cell membrane in ischaemia (by 18.7 ± 1.8 mV, $n=6$) was followed by a slow recovery of the cell membrane potential towards its pre-ischaemic baseline (Fig. 3.4B). The mean time course of the voltage response for these two conditions is shown in Fig. 3.4C, and the mean peak depolarisation (averaged over all the cells) is shown in Fig. 3.4D.

The much greater ischaemia-evoked depolarisation that occurs with Cs^+ in the cell than with internal K^+ suggests that, with K^+ (but not with Cs^+) present, outward K^+ currents are activated at depolarised potentials and oppose further depolarisation.

Many K^+ channels are blocked when K^+ is replaced by Cs^+ (Hille, 2001). Indeed, experiments presented below (Fig. 3.12A-C) show that this is true for the K^+ currents active in oligodendrocytes at depolarised potentials: around 0 mV the slope conductance of oligodendrocytes studied with internal Cs^+ was 3.8-fold ($p=7.45 \times 10^{-3}$) smaller than that seen with K^+ in the cell (Fig. 3.12C). However, near the resting potential the slope conductance with internal Cs^+ was only 2.2-fold smaller ($p=0.01$) than with internal K^+ (Fig. 3.12C). These data suggest that, as for astrocytes (Zhou *et al.*, 2009), the main ion channels open near the resting potential have a reasonably high permeability to Cs^+ as well as to K^+ , possibly because two-pore K^+ channels contribute to the resting conductance of the cells as in astrocytes (Zhou *et al.*, 2009).

According to this framework, once the membrane potential is displaced sufficiently positive from the resting potential, the inward current evoked by ischaemia (the origin of which is explored below, and in the next chapter) will depolarise cells more if they have Cs^+ inside than if they have K^+ inside, because the ion channels that pass large outward K^+ currents at depolarised potentials do not allow significant Cs^+ efflux. Complicating this picture, however, is the fact that the voltage response seen with K^+ inside the cell is not merely smaller than with Cs^+ inside, but after about 10 minutes returns towards the original resting potential (Fig. 3.4C). This suggests that, with K^+ (but not with Cs^+) inside the cell, late in the response to ischaemia there is an extra outward current produced, presumably as channels permeable to K^+ (but not to Cs^+) are either activated by ischaemia (e.g. as the result of a rise of $[\text{Ca}^{2+}]_i$ or a fall of

[ATP]_i in the distal parts of their processes despite the presence of ATP in the pipette) or their conductance increases as a result of the ischaemia-evoked accumulation of extracellular K⁺ (as is known to occur for inward rectifier channels: Hille, 2001).

3.3.4 The time needed for ischaemia to alter the oligodendrocyte membrane current

I first measured the time of the peak current reached by the cells in voltage-clamp mode, with caesium or potassium in the internal solution. There was no significant difference ($p=0.96$) in this parameter between the two internal solutions, which was 439 ± 11 sec in 179 cells studied using Cs⁺ and 442 ± 52 sec in 10 cells studied using K⁺ (Fig. 3.5). Similarly, when I compared the time of the peak depolarisation reached by the cells in current-clamp mode with Cs⁺ or K⁺ in the internal solution, this parameter also did not differ significantly ($p=0.15$) between the two internal solutions used: 670 ± 111 sec for 6 cells using Cs⁺ and 476 ± 44 sec for 6 cells using K⁺ (Fig. 3.5). There was also no significant difference between the time of the peak AD recorded in voltage- and current-clamp mode for either of the internal solutions used (Fig. 3.5). Thus, neither the composition of the internal solution nor the patch-clamp mode employed influenced the time to the peak of the ischaemia-induced response in oligodendrocytes.

These results closely resemble those obtained for the response of cerebellar Purkinje cells to ischaemia (Hamann *et al.*, 2005), where the clamp mode and the main ion used in the internal solution did not influence the time of the peak response of the neurons to the ischaemic insult.

As noted in section 3.3.1, the time to the peak of the current response varied greatly between cells, and this was also true for the amplitude of the peak current. To test whether the size of the peak current varied with the time of the peak, I analysed the distributions of the time and the size of the peak current in all the voltage-clamped cells that I studied (179 for Cs⁺- and 10 for K⁺-based internal solution, pooled together).

The distribution of the size of the peak current could be approximately fitted by a truncated Gaussian distribution ($r^2=0.56$) with the peak at an inward current of 152 ± 23 pA (Fig. 3.6A), slightly less than the mean inward current of 209 ± 10 pA reported in section 3.3.1. The distribution of the times to the peak of the current could also be approximately fitted by a Gaussian distribution ($r^2=0.75$), with the peak at 390 ± 9 sec (Fig. 3.6B), slightly less than the 439 ± 11 sec average time reported in section

3.3.4. Plotting the size of the peak current against the time of the peak for each cell (Fig. 3.6C), the time increased weakly with the size of the inward current. Although the data are scattered ($r^2=0.06$), the slope of the line in Fig. 3.6C is significantly different from zero ($p=0.001$, calculated from the t-statistic obtained from the mean and s.e.m. estimated for the slope).

In summary, the peak current varied significantly between different oligodendrocytes, perhaps correlating with differences in cell size (e.g. due to different numbers of axons being myelinated) or cells being recorded from at different depths in the slice which might result in a different amount of K^+ accumulation around the cell. In addition, there was a weak dependence of the time needed to reach the peak ischaemia-evoked current on the size of that current, which might reflect intrinsic differences in cell properties or differences in the depth of the cell in the slice.

3.3.5 The membrane resistance increases during ischaemia

In neurons, the membrane resistance decreases dramatically shortly after the start of ischaemia (Hansen *et al.*, 1982; Xu and Pulsinelli, 1996), mostly due to the activation of glutamate ionotropic receptors (Rossi *et al.*, 2000; Hamann *et al.*, 2005), although the cell's potassium conductance can also increase as a result of a rise in $[Ca^{2+}]_i$ activating calcium-activated K^+ channels (Liao *et al.*, 2010) and a fall of [ATP] leading to activation of ATP-gated K^+ channels (Kulik *et al.*, 2002). In oligodendrocytes it has been suggested that activation of glutamate receptors contributes to the ischaemia-evoked current (Káradóttir *et al.*, 2005) and rise of $[Ca^{2+}]_i$ (Micu *et al.*, 2006), so a decrease in membrane resistance might also be expected in these cells. To investigate how the membrane resistance of mature oligodendrocytes changes in simulated ischaemia, and how any change depends on the composition of the internal solution, the membrane resistance was calculated repeatedly from the current response to 5 mV depolarizing pulses from the holding potential of -74 mV, applied from 7.5 min before ischaemia until 21 min after the start of ischaemia.

Surprisingly, the membrane resistance (with either K^+ or Cs^+ in the internal solution) increased continuously after the start of ischaemia (Fig. 3.7). The change was more prominent for the Cs^+ -based internal solution. This may in part be due to a K^+ conductance being activated later in ischaemia and reducing the membrane resistance when K^+ is present inside the cell (see section 3.3.3), but to a large extent simply reflects the fact that the initial resistance is higher with Cs^+ inside the cell (as will be

explained in section 3.3.7). However, the significant increase in cell membrane resistance observed with the K^+ -based internal solution later in ischaemia indicates that the rise in resistance does not depend solely on having the non-physiological Cs^+ ion present in the internal solution. Thus, the membrane resistance change in ischaemia differs between oligodendrocyte and neurons.

The increase in the membrane resistance might be explained by two different phenomena. First, it has been suggested that during the first hour of exposure to ischaemic solution, oligodendrocytes lose some of their myelinating processes (Salter and Fern, 2005) and on exposure to glutamate (which is released in ischaemia: Li *et al.*, 1999; Káradóttir *et al.*, 2005) they retract their processes from the node of Ranvier (Fu *et al.*, 2009). If the membrane re-sealed after process loss, and/or if process retraction is achieved by endocytosis of the cell membrane, this would cause a loss of surface membrane area and conductance and hence produce an increase in resistance. To test this hypothesis I carried out the experiments described in section 3.3.6, measuring the membrane capacitance, since a loss of oligodendrocyte processes would also cause a loss of cell capacitance. An alternative explanation for the increase in membrane resistance observed in ischaemia could be a decrease in the number or conductance of the channels that are open in physiological conditions. To investigate the nature of the membrane current that might be modulated in ischaemia, I performed current-voltage relation measurements as described in section 3.3.7.

3.3.6 Cell capacitance does not change significantly in mature oligodendrocytes during ischaemia

To try to detect a loss of oligodendrocyte cell processes or process retraction at the node of Ranvier (Salter and Fern, 2005; Fu *et al.*, 2009), as a measure of the cell size I calculated the cell membrane capacitance from the current transient evoked by a small voltage step, as described in section 3.2.4. The membrane capacitance is generally assumed to be constant per unit area of the cell (and represents the amount of charge necessary to change the membrane potential by a certain amount). Thus, the capacitance is proportional to the cell area and so indirectly indicates the size of the cell. Furthermore, a correlation of the membrane conductance of cerebellar oligodendrocytes with the length of myelinating processes that they make has suggested that more than 80% of the cell conductance and capacitance are located in the cell processes (Bakiri *et*

al., 2011), indicating that an ischaemia-evoked loss of the processes (Salter and Fern, 2005) ought to be detectable as a change of the total capacitance of the cell.

First, I simplistically applied monoexponential fitting (see Fig. 2.3) to capacity current transients evoked by 5 mV pulses that were obtained continuously every 1.5 min from 7.5 min before ischaemia till 21 min after the start of ischaemia. Using monoexponential fitting assumes that the cell is well voltage-clamped (isopotential) without any voltage gradients along the cell processes (see Chapter 2, and below). According to this analysis the cell capacitance did not change significantly at any stage of the recording, compared to its pre-ischaemia value (Fig. 3.8). This analysis was, because of its time-consuming nature, only performed for a limited number of cells. However, even if the (statistically insignificant) ~17% decrease in capacitance shown in Fig. 3.8B became statistically significant with the addition of many more cells, and thus represented a ~17% loss of cell surface area, this could explain only a very small fraction of the ~4-fold increase in membrane resistance shown for the Cs⁺-filled cells in Fig. 3.7.

As described in Chapter 2, the fits of the mature oligodendrocyte capacity currents with single decaying exponentials were not very accurate, because the cells form more than a single electrical compartment: charging of the soma capacitance provides a fast decaying exponential to the current, while charging of the more distant membrane in the processes is limited by the axial resistance of the processes and contributes at least one more slower exponential component (see Fig. 2.4). I considered it possible that limitations in the accuracy of the single exponential fit were preventing me from detecting a change in the capacitance of the distant processes, and so fitted the capacity currents with the sum of two exponentials. Although the parameters of the two exponentials do not relate simply to the areas of the soma compartment and of the distant process compartment, changes in the membrane area of the latter compartment are expected to affect the amplitude (A_{slow}) and time constant (τ_{slow}) of the slower component more than those (A_{fast} , τ_{fast}) of the faster component. As shown in Fig. 3.9, none of these parameters changed significantly when ischaemic solution was applied. This suggests no changes in the surface membrane area of either the cell soma or the cell processes up to 21 min after the start of ischaemic insult.

These findings rule out the possibility that cell process loss is responsible for the early increase in membrane resistance during ischaemia. They also indicate that

oligodendrocytes remain physically intact during the initial 20 min of ischaemia, without major damage to their soma or processes. However, at the longest time period studied here, Salter and Fern (2005) reported only about a 20% loss of cell processes. In addition, I cannot rule out the possibility that whole-cell clamping the oligodendrocyte protects it from process loss (e.g. by maintaining the intracellular ATP level, or by providing the pipette as a route for the exit of water which enters across the cell membrane). Thus, my data do not contradict the observation of Salter and Fern (2005) that a more prolonged application of ischaemic solution to unclamped oligodendrocytes leads to process loss from the cells.

3.3.7 The membrane resistance increase reflects a loss of K⁺ conductance

The existence of an ischaemia-evoked inward current implies that ischaemia either increases a conductance with a reversal potential that is more positive than the holding potential used (-74 mV) or decreases a conductance with a reversal potential more negative than the holding potential. The increase of resistance documented in Fig. 3.7 implies that the latter of these scenarios is the cause of the inward current, but this cannot be attributed to an ischaemia-evoked loss of oligodendrocyte processes (see above). This suggests that ischaemia might decrease the activity of ion channels with a reversal potential more negative than -74 mV (i.e. K⁺, or possibly Cl⁻, channels)

In Müller glia, ischaemia causes a strong reduction of potassium conductance (Pannicke *et al.*, 2004; Pannicke *et al.*, 2005), which is probably mediated by a downregulation of the inwardly rectifying potassium channel Kir4.1 (Iandiev *et al.*, 2006). Kir4.1 is found in mature oligodendrocytes (Kalsi *et al.*, 2004; Cahoy *et al.*, 2008) and its knock-out causes a strong increase in oligodendrocyte membrane resistance (Neusch *et al.*, 2001). The loss of Müller cell K⁺ conductance reported by Pannicke *et al.* (2004) takes 1-3 days to occur after ischaemia, but Schwartz (1993) has reported that activation of metabotropic glutamate receptors (which might occur when glutamate is released in ischaemic conditions) reduces the conductance on a time scale of seconds to minutes. I therefore thought it worth investigating whether a down-regulation of K⁺ conductance is induced by ischaemia in oligodendrocytes.

Figures 3.10A and B show the membrane current response of a mature oligodendrocyte (using a Cs⁺-based internal solution) to voltage steps applied in 20 mV increments from a holding potential of -74 mV to potentials between -134 mV and +6 mV, in the control solution and after 4.8 min exposure to ischaemic solution. At

voltages positive to -60 mV and more negative than -120 mV the current in ischaemia is less than in the control solution. Subtracting the two I-V relations shows a current that reverses at around -95 mV (Fig. 3.10C). In Figs. 3.11A-C, similar data are shown for a cell studied with the K⁺-based internal solution. Again the subtracted current reverses around -110 mV, i.e. close to the calculated Nernst potential for K⁺ which is ~105 mV. Figure 3.12 presents the average I-V data obtained from experiments performed as in Figs 3.10 and 3.11.

Comparing first the pre-ischaemic I-V relations in Fig. 3.12A (for the Cs⁺ internal solution) and Fig. 3.12B (for the K⁺ internal solution), near the resting potential the slope conductance with internal K⁺ is about 2.2-fold greater than with internal Cs⁺ (Fig. 3.12C), implying that Cs⁺ permeates the cell membrane roughly 46% as well as K⁺ does. This is a surprisingly high Cs⁺ permeability, but a similar result has previously been reported for astrocytes ($P_{Cs}/P_K=0.43$: Zhou *et al.*, 2009). In comparison, around 0 mV, the slope conductance is 3.8-fold higher with K⁺ than with Cs⁺ inside the cell (Fig. 3.12C), reflecting the fact that Cs⁺ does not permeate well through the K⁺ channels that are activated at depolarised potentials, as was postulated in section 3.3.3 as an explanation for the different voltage response to ischaemia recorded with Cs⁺ and K⁺ as the main intracellular cation.

The current suppressed by ischaemia (obtained by subtracting the control and ischaemia I-V data for each cell and then averaging over all cells) is similar at -74 mV with Cs⁺ or K⁺ as the main internal cation (Fig. 3.12D). Furthermore, from the slope of the subtracted I-V data, ischaemia suppressed the same amount of conductance whichever ion was present (3.3 ± 1 nS for Cs⁺; 3.3 ± 0.9 nS for K⁺; $p=0.98$). The larger baseline conductance of the cell with intracellular K⁺ present explains why there is a much smaller fractional change of resistance in Fig. 3.7 for K⁺ inside the cell than for Cs⁺ inside. This can be seen as follows. For the cells studied in Fig. 3.12, Fig. 3.12C gives the initial conductance at the resting potential as being 6.9 nS with Cs⁺ and 15 nS with K⁺ inside. At 9 min into ischaemia when 3.3 nS of K⁺ conductance has been suppressed (either with Cs⁺ or with K⁺), the new conductance values will be $6.9-3.3 = 3.6$ nS with Cs⁺ and $15-3.3 = 11.7$ nS with K⁺. The normalised resistance will therefore become $6.9/3.3 = 2.09$, i.e. a 109% increase, for Cs⁺, and $15/11.7 = 1.28$, i.e. only a 28% increase for K⁺ (approximately 4-fold smaller than the percentage increase with Cs⁺ inside). These values are similar to those seen 9 min into ischaemia for a larger number of cells in Fig. 3.7A. Thus, suppression of the same magnitude of conductance by

ischaemia leads to a much smaller percentage rise of resistance with K^+ inside than with Cs^+ inside because the initial resistance is lower with K^+ inside.

3.4 Discussion

Ischaemia disrupts the function of the white matter, initially by impairing axonal action potential propagation and thus preventing neuronal signalling between different brain regions. Part of the inhibition of action potential propagation results from the run-down of ion gradients across the axonal membrane, but part also reflects ischaemia-evoked damage to the oligodendrocytes that surround axons and speed their conduction velocity by reducing their effective membrane capacitance. As reviewed in Chapter 1, ischaemia releases glutamate which activates oligodendrocyte glutamate receptors, it raises oligodendrocyte $[Ca^{2+}]_i$, and it produces physical disruption of the myelin sheath and a loss of myelinating processes (Dewar *et al.*, 2003; Káradóttir *et al.*, 2005; Salter and Fern, 2005; Micu *et al.*, 2006). The loss of myelin around axons may then lead to the axon dying (Nave, 2010; Pohl *et al.*, 2011).

Although many studies have employed electrophysiological techniques to study the neuronal response to ischaemia (Xu, 1995; Tanaka *et al.*, 1997; Rossi *et al.*, 2000; Allen *et al.*, 2004; Hamann *et al.*, 2005), only a few have investigated the changes in glial cell electrophysiology produced by this pathological condition (e.g. Xie *et al.*, 2008). Indeed, most of the previous studies of ischaemia's effects on oligodendrocyte lineage cells lacked the ability to record rapid changes occurring in oligodendrocyte membrane physiology and therefore did not describe a real-time cellular response to the ischaemic insult. A few previous studies of the electrical response to simulated ischaemia in oligodendrocytes have shown that these cells respond to the insult with an inward current (Káradóttir *et al.*, 2005; Bakiri *et al.*, 2008), but the nature of this current was not fully investigated, because it was assumed to be generated, as in neurons, by a cation influx through glutamate-gated channels. The work described in this (and the following) chapter is the first that aimed at giving a more comprehensive analysis of the oligodendrocyte electrical response to ischaemia. The main results obtained are: (i) the time course of the oligodendrocyte response to ischaemic insult; (ii) that although a similar ischaemia-evoked inward current is seen with Cs^+ or K^+ inside the cell, the

resulting voltage response differs significantly; and (iii) that the inward current evoked by ischaemia is the result of a decrease of K^+ conductance, rather than an increase in non-selective cation conductance as occurs in neurons. The implications of these results will now be discussed.

Ischaemia evokes an inward current in oligodendrocytes which develops over a period of 10 min with a characteristic shape (Fig. 3.1) and an amplitude which increased as the cells developed (Fig. 3.2). At -74 mV, neither the time course of the current nor its amplitude depended on whether the main ion used in the internal solution was Cs^+ or K^+ (Fig. 3.3), which, as discussed below, has implications for the identification of the underlying ionic channels. The time course of the current in Fig. 3.1, with a slowly developing inward current followed by (or with superimposed on it) a more rapidly developing transient inward current, might suggest that there are two components to the response, although my data provide no information on this. Notably, the fast phase of the response is similar to that recorded in neurons in the cerebellum during ischaemia (Hamann *et al.*, 2005), and it would be interesting to test whether, at the time of this current transient in the oligodendrocytes, there is a rise of $[K^+]_o$ produced in the white matter by the neuronal anoxic depolarisation.

Although the ischaemia-evoked current amplitude was unaffected by replacing intracellular K^+ by Cs^+ (Fig. 3.3), when not voltage-clamped, the cell depolarisation occurring was much larger with Cs^+ inside than with K^+ inside (Fig. 3.4), presumably because intracellular Cs^+ cannot permeate through K^+ channels that normally generate an outward current at depolarised potentials and thus limit depolarisation. Thus, *in vivo*, oligodendrocytes presumably only undergo an ischaemia-evoked depolarisation of less than 20 mV, much less than the 50-60 mV depolarisation that neurons undergo at the time of the anoxic depolarisation (Hansen, 1985; Hamann *et al.*, 2005). This may correlate with the smaller $[K^+]_o$ rise occurring in the white matter during ischaemia (14 mM: Ransom *et al.*, 1992) than occurs in the grey matter (50-60 mM: Hansen, 1985).

It is well established that a large release of glutamate by reversal of uptake carriers during ischaemia leads to the generation of a massive inward current in neurons by activation of ionotropic (AMPA and NMDA) glutamate receptors (Olney and de Gubareff, 1978; Choi *et al.*, 1987; Choi, 1988; Rossi *et al.*, 2000; Arundine and Tymianski, 2004). Similarly, glutamate release by reversed uptake (Li *et al.*, 1999) and activation of similar receptors on oligodendrocytes has been assumed to account for the inward current evoked in these cells by ischaemia (Káradóttir *et al.*, 2005). It was

surprising to find, therefore, that the inward current was associated with a conductance decrease rather than a conductance increase (Fig. 3.7) and, furthermore, that the reversal potential of the suppressed current was close to that for K^+ ions (Fig. 3.12). Thus, the origin of the ischaemia-induced response in oligodendrocytes is not dominated by an opening of sodium- or calcium-permeable channels and so differs significantly from the anoxic depolarisation observed in neurons.

Capacitance measurements (Figs. 3.8 and 3.9) were used to demonstrate that the decrease of conductance was not a result of a loss of cell processes induced by ischaemia (Salter and Fern, 2005) implying that ischaemia reduces the number of ion channels open (or the conductance per channel) to below the normal value. The resting conductance of the cell is only ~2-fold larger with K^+ inside than with Cs^+ inside (Fig. 3.12C), and the conductance decrease evoked by ischaemia had a similar magnitude and reversal potential (Fig. 3.12) with either Cs^+ or K^+ inside the cell. This suggests that the resting conductance that is being suppressed by ischaemia is not highly selective for K^+ over Cs^+ . It is also worth bearing in mind that some of the current changes induced by ischaemia might not be due to changes in the number of ion channels open, but could reflect a rise of extracellular $[K^+]$ evoked by ischaemia (Hansen, 1985). This will increase the inward current through ohmic K^+ channels, but can increase the outward current (at voltages more positive than the Nernst potential for K^+) through inward rectifier channels by increasing their conductance (Nichols and Lopatin, 1997).

The molecular identity of the potassium channels that are open at the resting potential (and thus are candidates for being closed by ischaemia) is uncertain for oligodendrocytes (Gipson and Bordey, 2002), though it seems likely to include Kir4.1 inward rectifying channels (Poopalasundaram *et al.*, 2000; Neusch *et al.*, 2001; Kalsi *et al.*, 2004), as well as some two-pore domain potassium channels, such as TREK-1 and TWIK-1 which have a relatively high Cs^+ -permeability (Zhou *et al.*, 2009) and have been found to contribute significantly to the potassium conductance of astrocytes along with Kir4.1 (Skatchkov *et al.*, 2006; Seifert *et al.*, 2009; Zhou *et al.*, 2009). Since the I-V relation of oligodendrocytes shows little inward rectification, the two-pore channels may be more dominant. Interestingly, inhibition of the activity of the two-pore channel THIK-1 by low oxygen levels has been suggested to contribute to the anoxic depolarisation of neurons (Campanucci *et al.*, 2003) and THIK-1 is expressed in myelinating oligodendrocytes (Cahoy *et al.*, 2008). The fact that some of the two-pore channels are suppressible by pharmacological agents such as halothane (Campanucci *et*

al., 2003) suggests future experiments that might be able to identify the main channel type whose conductance is suppressed by ischaemia.

To summarize, my results suggest that the ischaemia-evoked depolarisation in mature oligodendrocytes is generated not by the activation of a non-specific (e.g. glutamate-gated) cation conductance, but by the closing of potassium channels that are open at the resting potential and are quite permeable to Cs⁺. The repolarisation that follows presumably depends on voltage-gated potassium channels that are very slowly activated by depolarisation, on activation of ATP-gated K⁺ channels when intracellular [ATP] falls, or on a rise of [K⁺]_o increasing the outward current through inward rectifier channels. These findings demonstrate that the oligodendrocyte response to ischaemia is strikingly different to that observed in neurons. Consequently, if the membrane current changes that I have characterised are found to contribute to damage to the oligodendrocytes, for example by evoking a Ca²⁺ influx through voltage-gated Ca²⁺ channels, then therapeutic modulation of this response to try to rescue oligodendrocytes from the damage caused by ischaemic insult may require a different therapeutic approach to that needed for neuronal protection. This raises the question of the role of glutamate in all of these events, since glutamate's activation of its ionotropic receptors has been suggested to contribute to damaging both oligodendrocytes and their precursors in conditions of energy deprivation (Agrawal and Fehlings, 1997; Wrathall *et al.*, 1994; McDonald *et al.*, 1998; Fern and Möller, 2000; Follett *et al.*, 2000; Volpe, 2001; Tekkök and Goldberg, 2001; Dewar *et al.*, 2003; Stys, 2004; Káradóttir *et al.*, 2005; Salter and Fern, 2005; Micu *et al.*, 2006; Fu *et al.*, 2009). This is investigated in the next chapter.

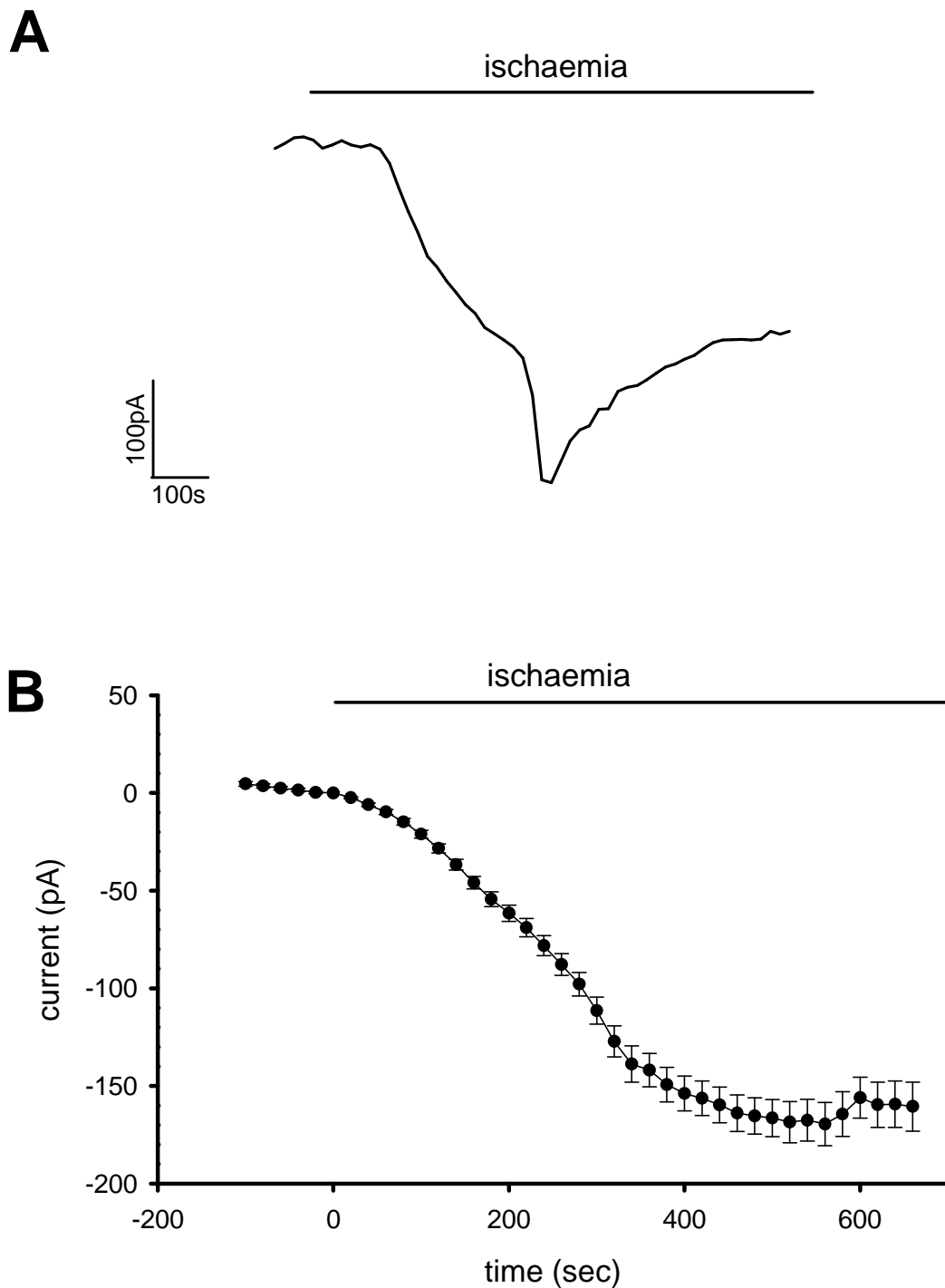


Figure 3.1

Mature oligodendrocyte response to ischaemia. **A** The specimen response of one cell to ischaemia can be divided into three phases. In phase 1, the cell develops a slow inward current which then becomes inward more rapidly and reaches a peak - the anoxic depolarisation current - in phase 2. Then, in phase 3, the current recovers and reaches a stable plateau that is more inward than the starting baseline level. **B** The average response of 179 mature oligodendrocytes to ischaemia lacks a clear distinction between these three phases as the peak current was reached by each cell at a different time (see Fig. 3.5). The start of ischaemia is denoted by $t=0$. The internal solution was Cs^+ -gluconate based.

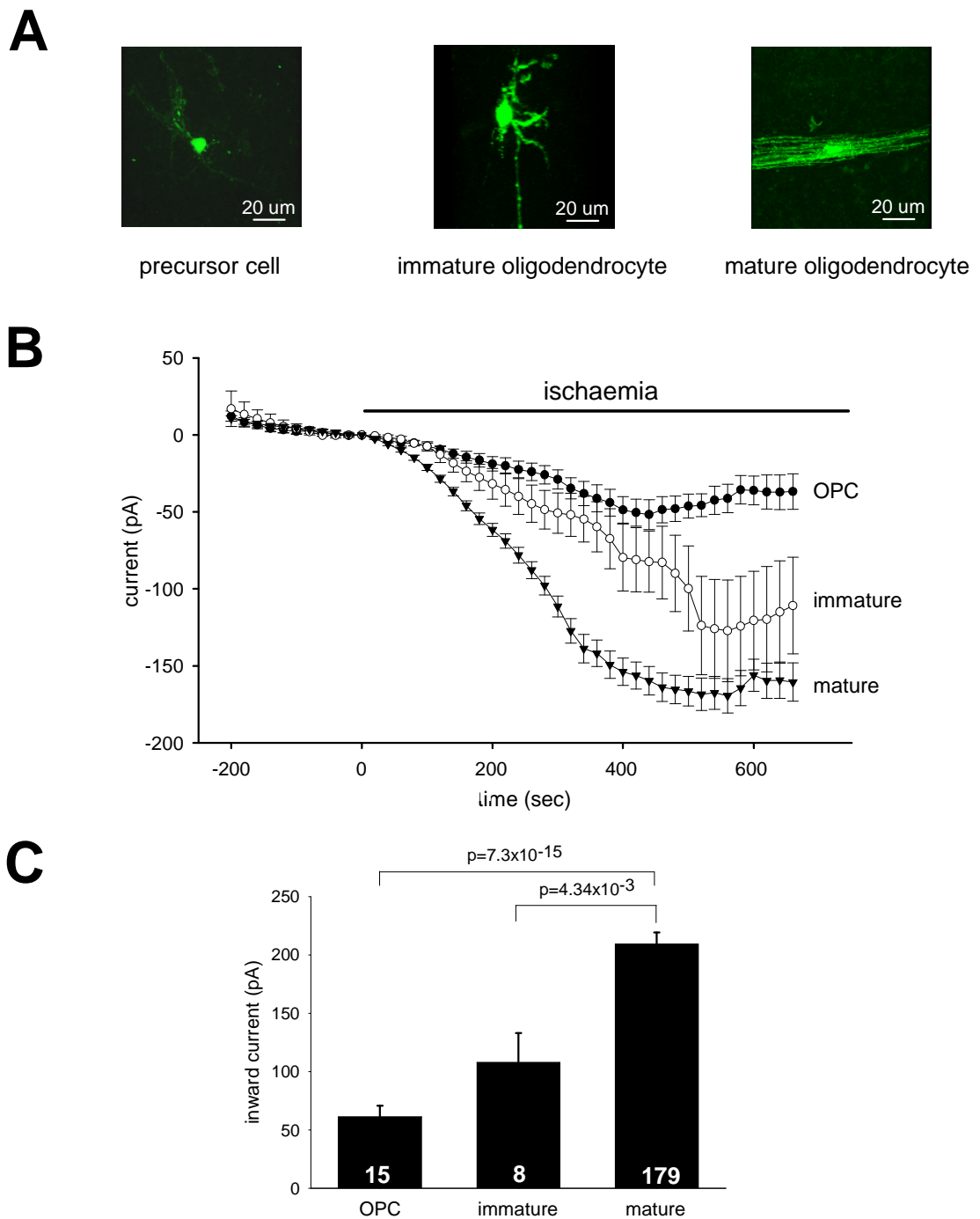


Figure 3.2

The size of the ischaemia-induced current in oligodendrocyte lineage cells depends on the developmental stage of the cell. **A** Representative pictures of a whole-cell patch-clamped oligodendrocyte precursor cell (OPC), immature and mature oligodendrocyte filled with internal solution containing Lucifer Yellow fluorescent dye. **B** The average ischaemia-induced current time course in OPCs ($n=15$), immature ($n=8$) and mature ($n=179$) oligodendrocytes. The time course for the mature cells is reproduced from Fig. 1B for ease of comparison. The start of ischaemia is at $t=0$. **C** The amplitude of the inward current induced by ischaemia increased with the developmental stage of the oligodendrocytes. The current was measured at the peak of the response in each cell, and then averaged over the cells of each class (in contrast to panel B which shows the time course averaged over all the cells recorded from. Cells were held at -74 mV and the Cs^+ -based internal solution was used.

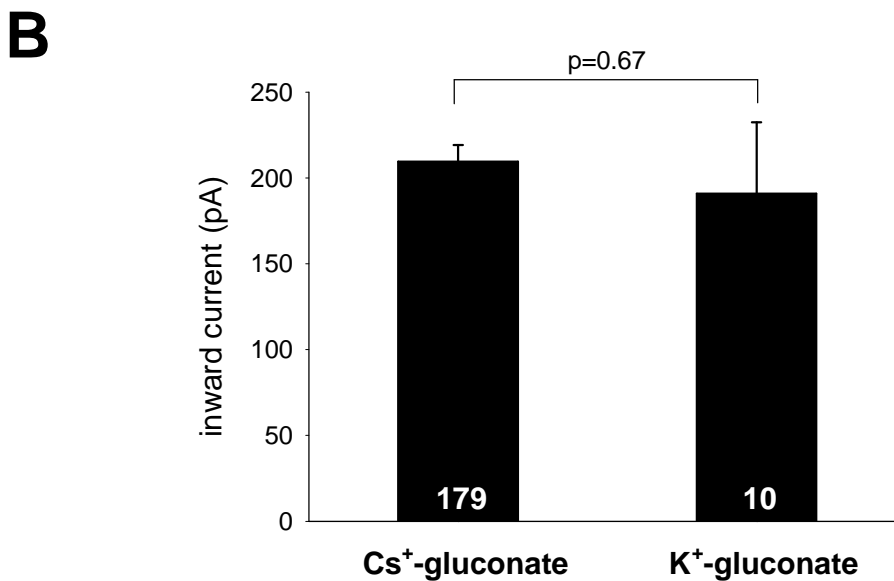
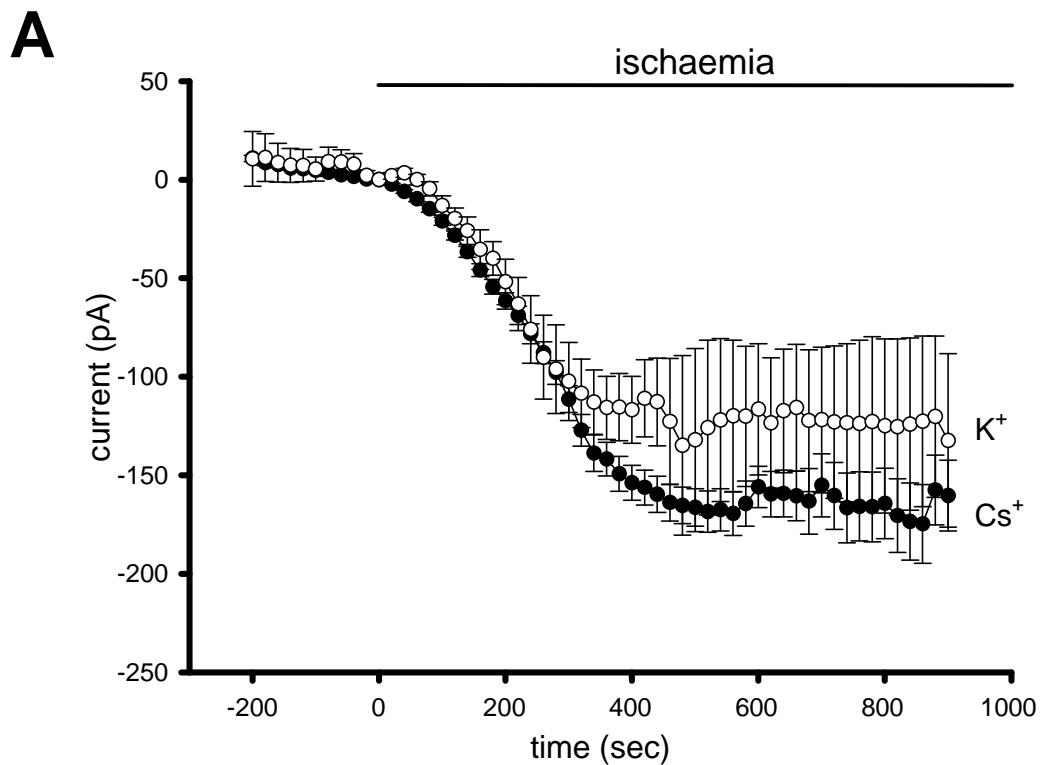


Figure 3.3

The time course and amplitude of the ischaemia-induced current in mature oligodendrocytes is independent of the main ion used in the internal solution. **A** Average over all the cells recorded from of currents evoked at -74 mV by ischaemia in cells filled with Cs⁺- or K⁺-based internal solutions. Independent of whether the internal cation was mainly Cs⁺ or K⁺, the currents showed a similar time for the start of the response, and a similar subsequent time course. **B** The peak of the ischaemia-evoked current, measured in each cell and then averaged over the different cells, was not significantly different between cells filled with Cs⁺- or K⁺-gluconate based internal solutions.

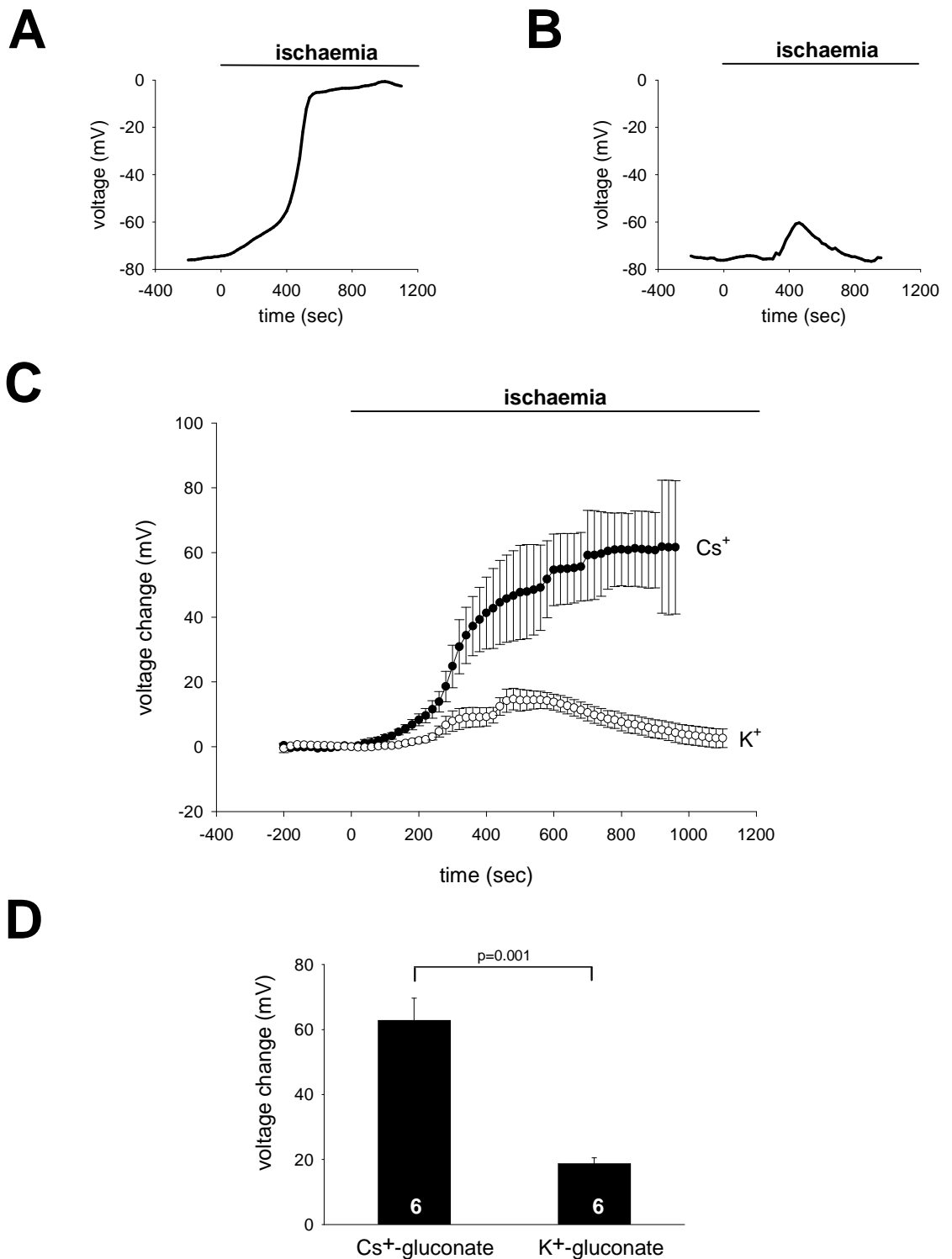


Figure 3.4

The time course and amplitude of the ischaemia-induced voltage response in mature oligodendrocytes (recorded in current-clamp mode) depends strongly on the main ion used in the internal solution. **A** Representative trace of voltage change in a cell filled with Cs⁺-based internal solution. **B** Representative trace of voltage change in a cell filled with K⁺-based internal solution. **C** Averaged time courses of voltage changes evoked by ischaemia in cells filled with Cs⁺- or K⁺-based internal solutions. **D** The peak of the ischaemia-evoked depolarisation, measured in each cell and then averaged over all the recorded cells, was significantly different between cells filled with Cs⁺- or K⁺-based internal solutions.

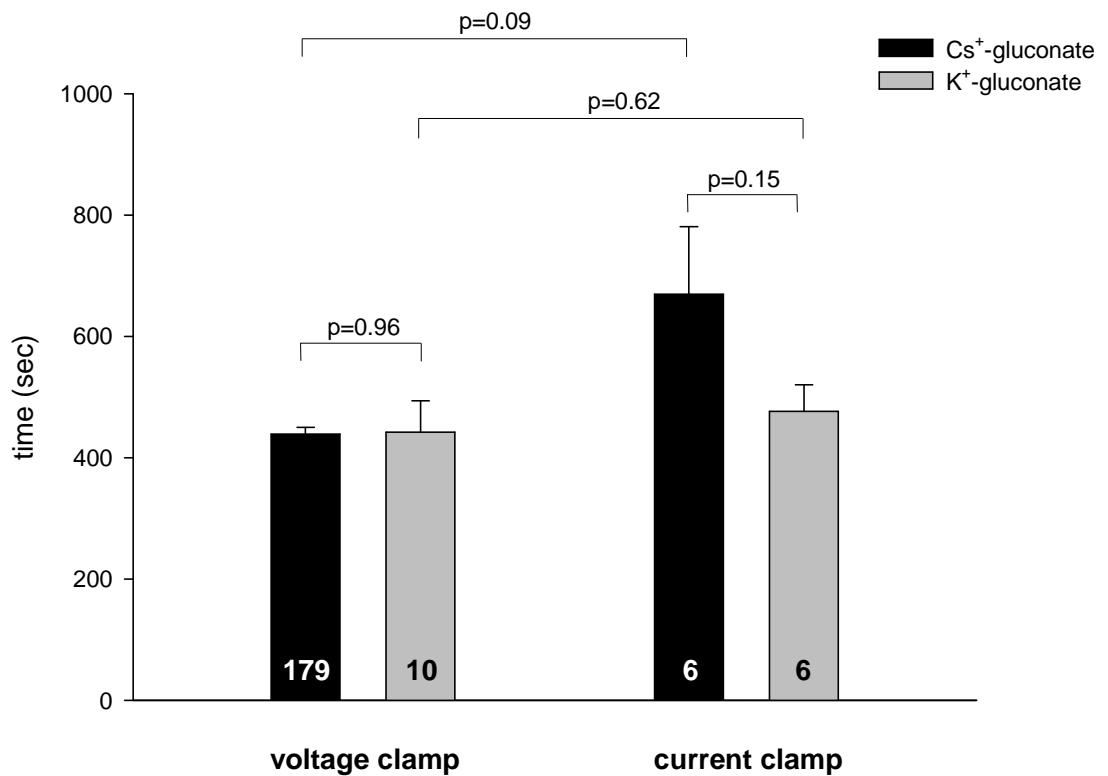


Figure 3.5

The time to reach the peak of the ischaemia-evoked response in oligodendrocytes does not depend on the clamp mode used nor on the main ion present in the internal solution. Bars show the time to the peak of the response to ischaemia, measured in each cell and then averaged over all cells. There was no significant difference in the time of the response peak between the cells in voltage-clamp or current-clamp configurations, nor between the cells filled with Cs⁺- or K⁺-based internal solutions.

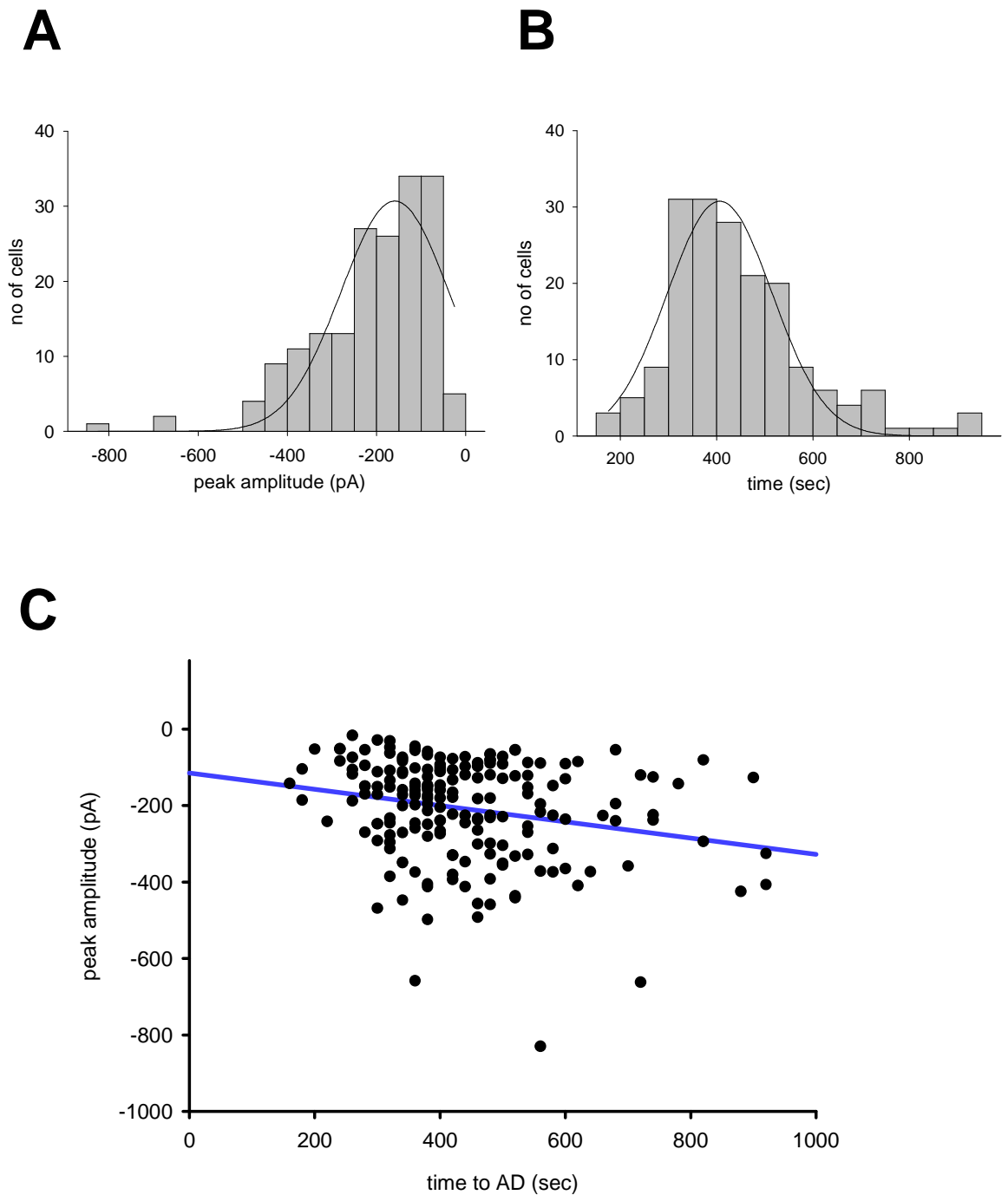


Figure 3.6

Variability in the peak amplitude and the time to peak of the ischaemia-induced inward current in oligodendrocytes. **A** The amplitude (plotted as a negative number to denote inward current) can be fitted by a truncated Gaussian distribution ($r^2=0.56$) with a peak value at -152 ± 23 pA. **B** The time to reach the peak of the current can be fitted by a Gaussian distribution ($r^2=0.75$) with a peak value at 390 ± 9 sec. **C** The amplitude of the inward current evoked by ischaemia plotted as a function of the time to the peak current: each point is a separate cell. Although the data are scattered ($r^2=0.06$), the slope of the line is significantly different from zero ($p=0.001$, calculated from the t-statistic obtained from the mean and s.e.m. estimated for the slope). All the cells were held at -74 mV and include those filled with Cs^+ ($n=179$) or K^+ ($n=7$) based internal solutions.

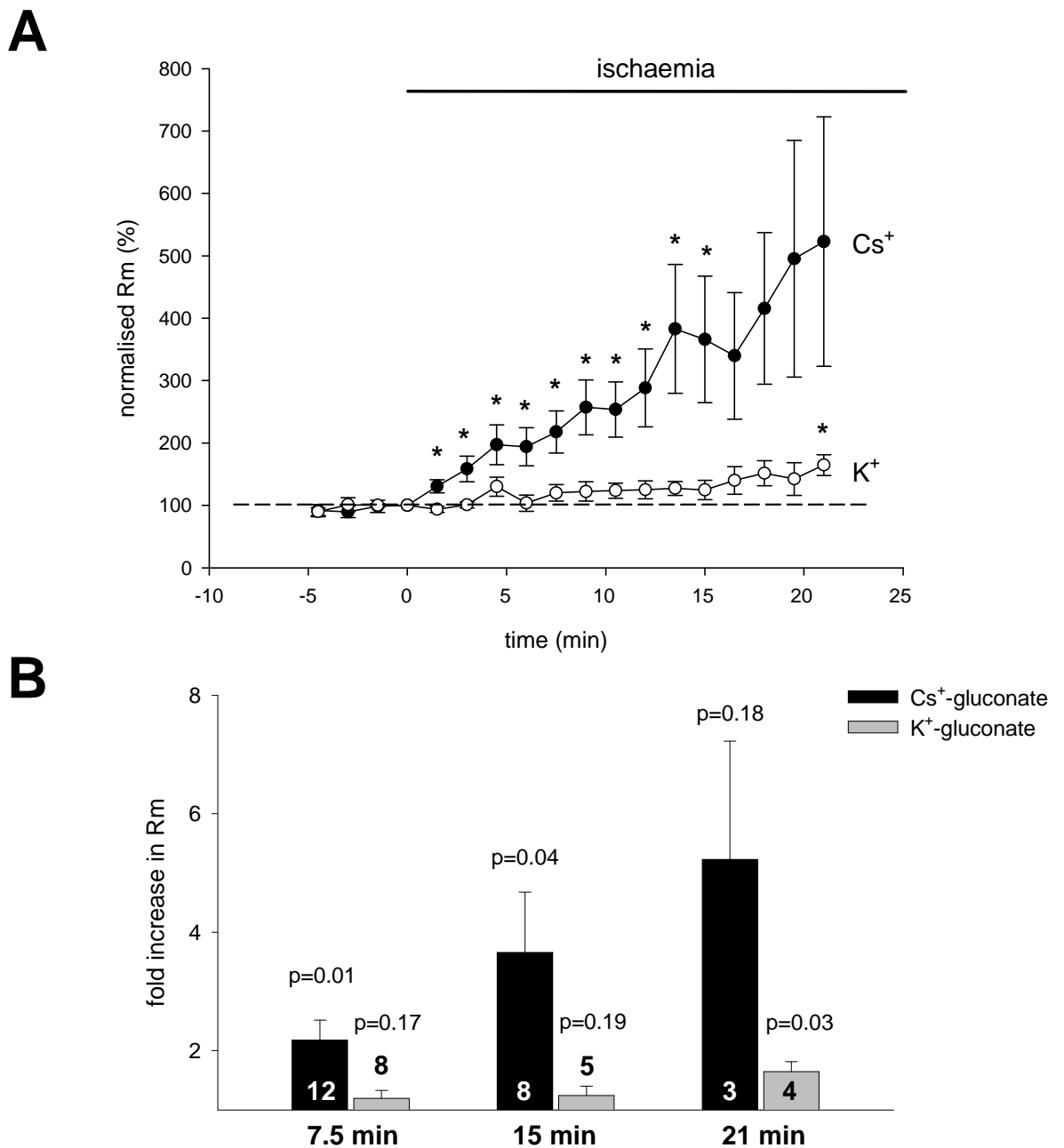
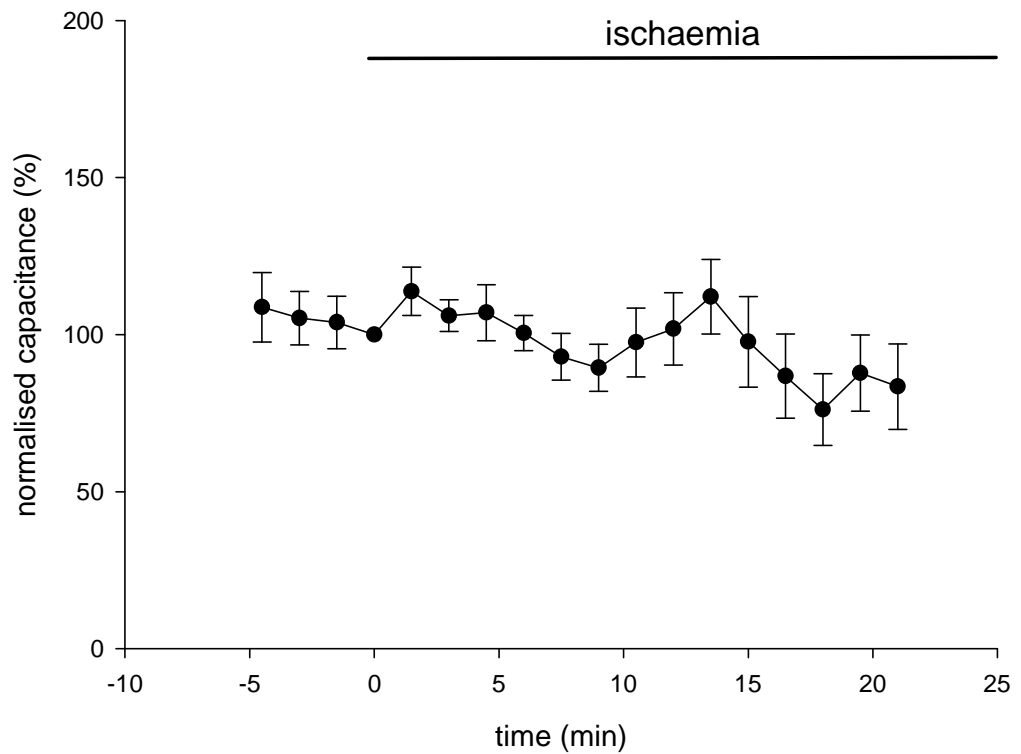
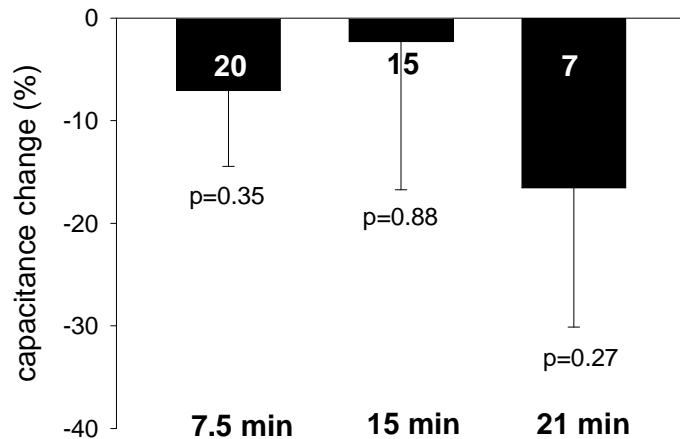


Figure 3.7

The membrane resistance (R_m) increases in oligodendrocytes during ischaemia. **A** During ischaemia the value of R_m (normalised to its pre-ischaemic value) increases by a small amount in cells filled with K^+ -based internal solution, but much more in cells filled with Cs^+ -based internal solution. **B** The increase in R_m measured at 7.5 min (the approximate time of the peak AD current), at 15 min and at 21 min after the start of ischaemia shows a statistically significant change in R_m for the cells filled with Cs^+ -based internal solution at all the three time intervals. The change in R_m for the cells filled with K^+ -based internal solution is statistically significant at 21 min after the start of ischaemia. The cells were held at -74 mV. * indicates statistically significant difference ($p < 0.05$) in comparison to the pre-ischaemic values.

A**B****Figure 3.8**

Change in oligodendrocyte membrane capacitance (C_m) during ischaemia, measured by fitting a monoexponential decay to the capacity transient evoked by a 5 mV voltage step and deriving the parameters from the eqn. 2.6. **A** The normalised C_m changes during ischaemia show no significant decrease of this parameter with time. The greater variability at later times is due to the earlier cessation of the experiment for several cells, which resulted in a decreasing number of cells contributing data at late times. **B** The changes in C_m measured at 7.5 min (the approximate time of the peak inward current), 15 min and 21 min after the start of ischaemia indicate no statistically significant decrease at any of these times. There was no difference in the (lack of) capacitance change between Cs^+ - and K^+ - based internal solutions (12 and 8 cells respectively, data not shown), and therefore the data shown in this figure are pooled from both internal solutions. The cells were held at -74 mV.

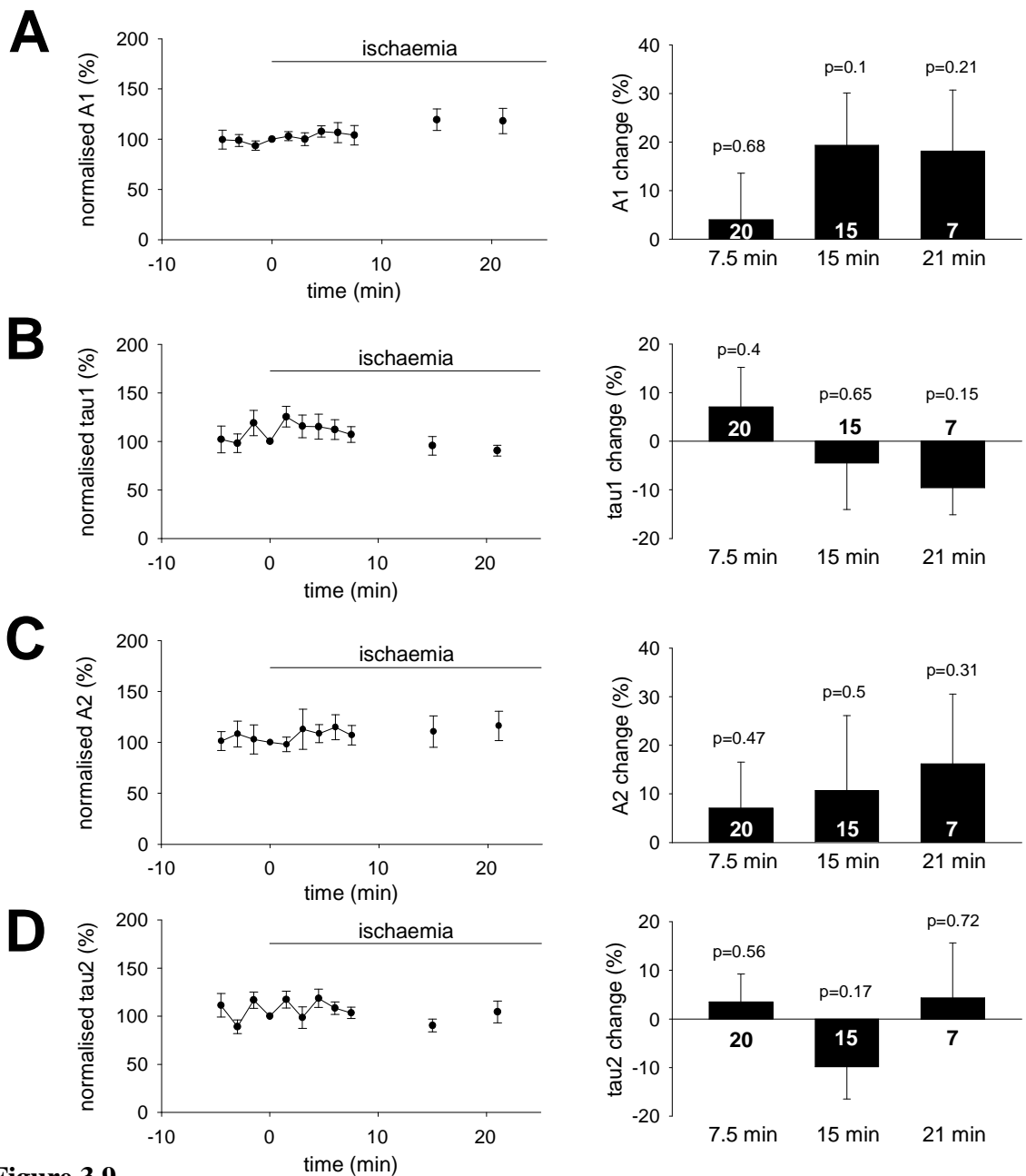


Figure 3.9

Results of fitting the capacity current transients with the sum of two exponentials, a fast exponential with amplitude A_1 (mean initial value -206 ± 53 pA in 20 cells) and time constant t_1 (mean initial value 657 ± 141 μ sec), and a slow exponential with amplitude A_2 (mean initial value -73 ± 13 pA) and time constant t_2 (mean initial value 11 ± 2 msec). For each panel the left hand graph shows the time course of the parameter normalised to its value at the start of ischaemia, averaged over all the cells, while the right hand graphs show the fold change in the average values at 3 times (7.5 min which is the approximate time of the peak inward current, 15 min and 21 min after the start of ischaemia), and p values assessing whether the change from the pre-ischaemic value is significant. **A, B** The amplitude (A) and time constant (B) of the fast component, A_1 , do not change during ischaemia. **C, D** The amplitude (C) and time constant (D) of the slow component, A_2 , do not change during ischaemia. There was no difference in the (lack of) capacitance change between CS^{+} - and K^{+} - based internal solutions (12 and 8 cells respectively, data not shown), and therefore the data shown in this figure are pooled from both internal solutions. The cells were held at -74 mV.

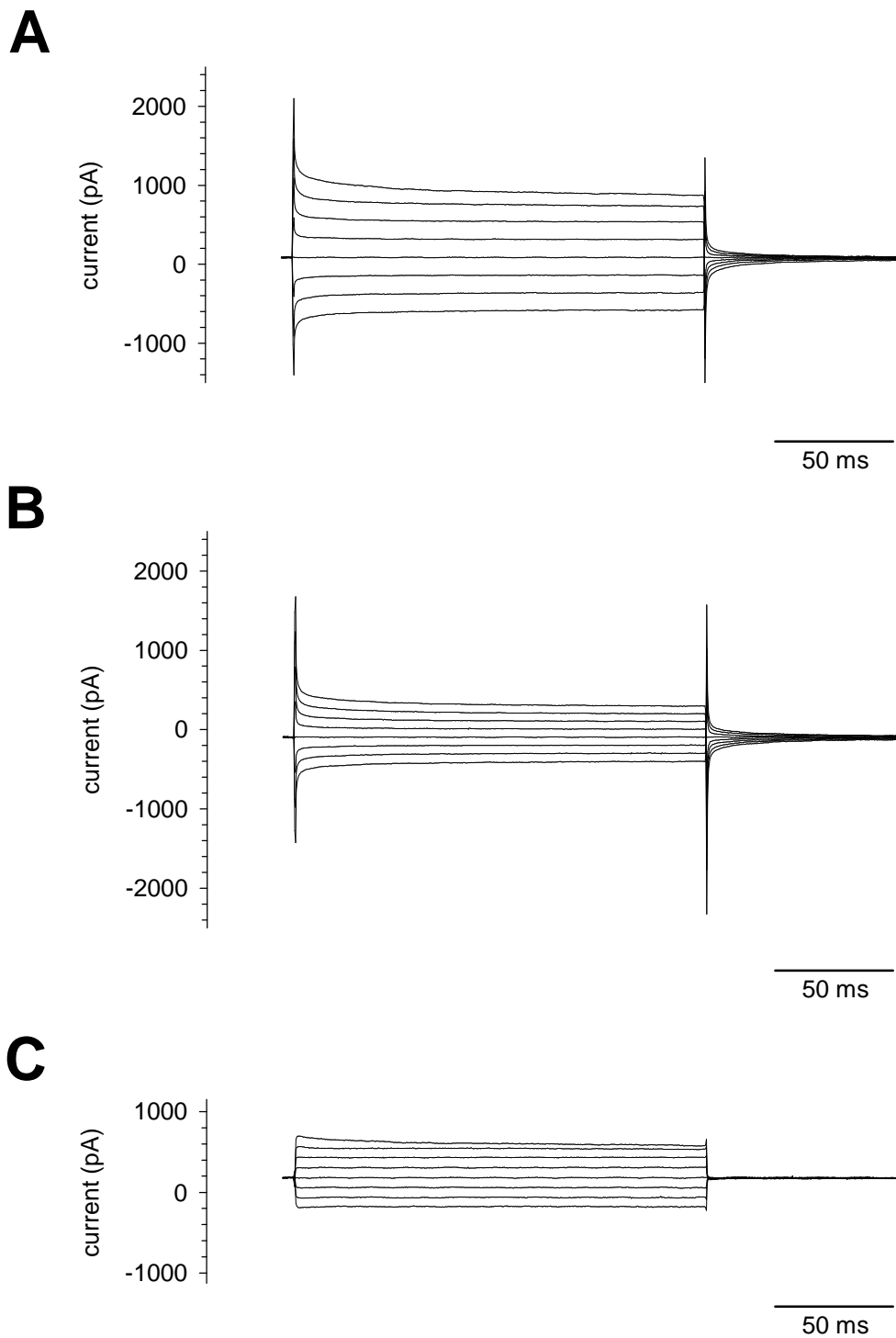


Figure 3.10

Membrane current response of a mature oligodendrocyte to voltage steps, using a Cs^+ -based internal solution. Voltage steps of 200 ms duration were applied from -134 mV to +6 mV in 20 mV increments from a holding potential of -74 mV. **A** In the control solution, the voltage steps induced large passive currents. **B** After 4.8 min exposure to the ischaemic solution, the passive currents were substantially reduced, indicating an increase in the membrane resistance. **C** Subtraction of the currents in ischaemic solution (**B**) from the currents in control solution (**A**) shows that the increase in membrane resistance is due to the closing of channels with a reversal potential at ~ -95 mV.

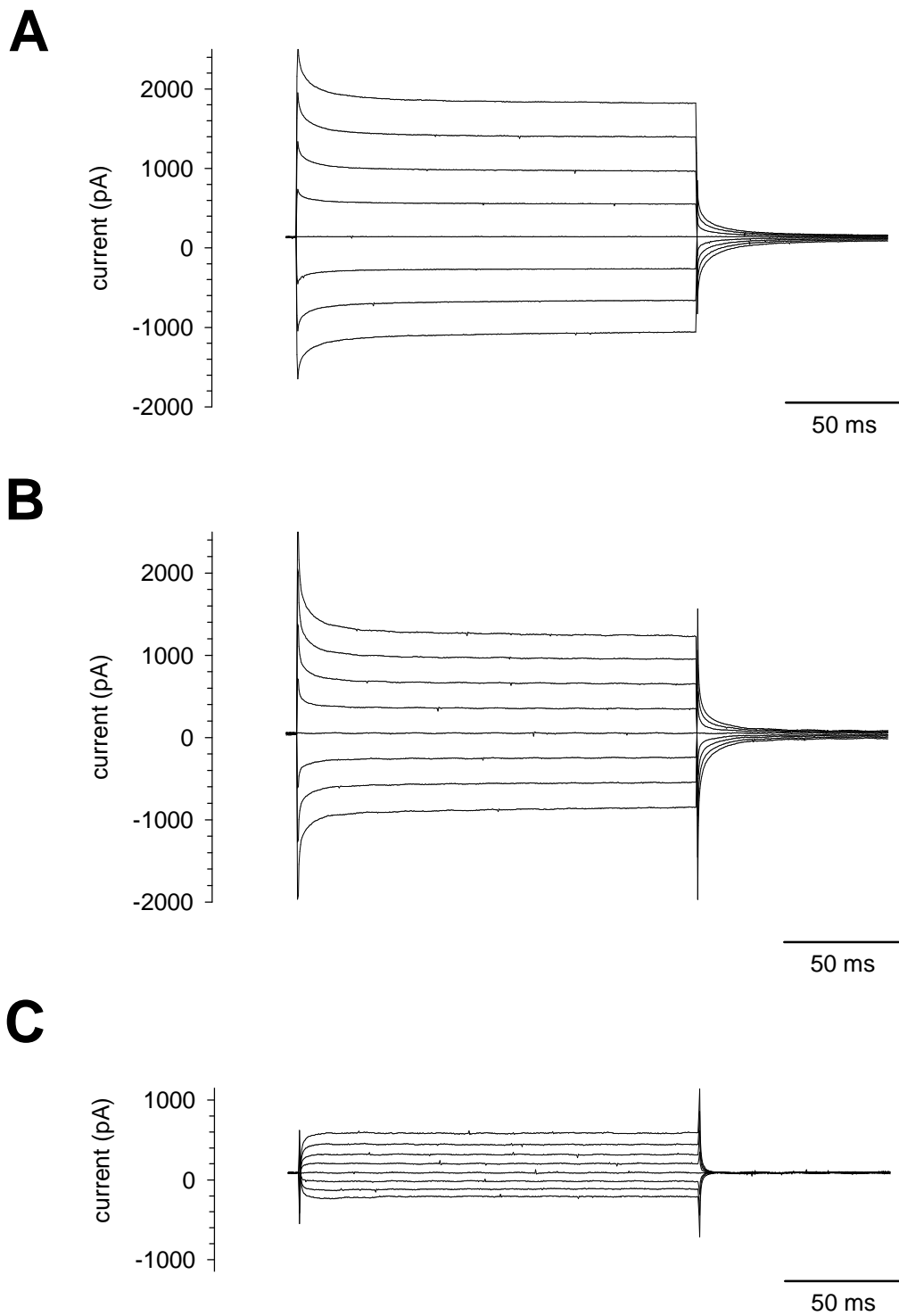


Figure 3.11

Membrane current response of a mature oligodendrocyte to voltage steps, using a K^+ -based internal solution. Voltage steps of 200 ms duration were applied from -134 mV to +6 mV in 20 mV increments from a holding potential of -74 mV. **A** In the control solution, the voltage steps induced large passive currents. **B** After 3.1 min exposure to the ischaemic solution, the passive currents were substantially reduced, indicating an increase in the membrane resistance. **C** Subtraction of the currents in ischaemic solution (**B**) from the currents in control solution (**A**) shows that the increase in membrane resistance is due to the closing of channels with a reversal potential at ~ -110 mV.

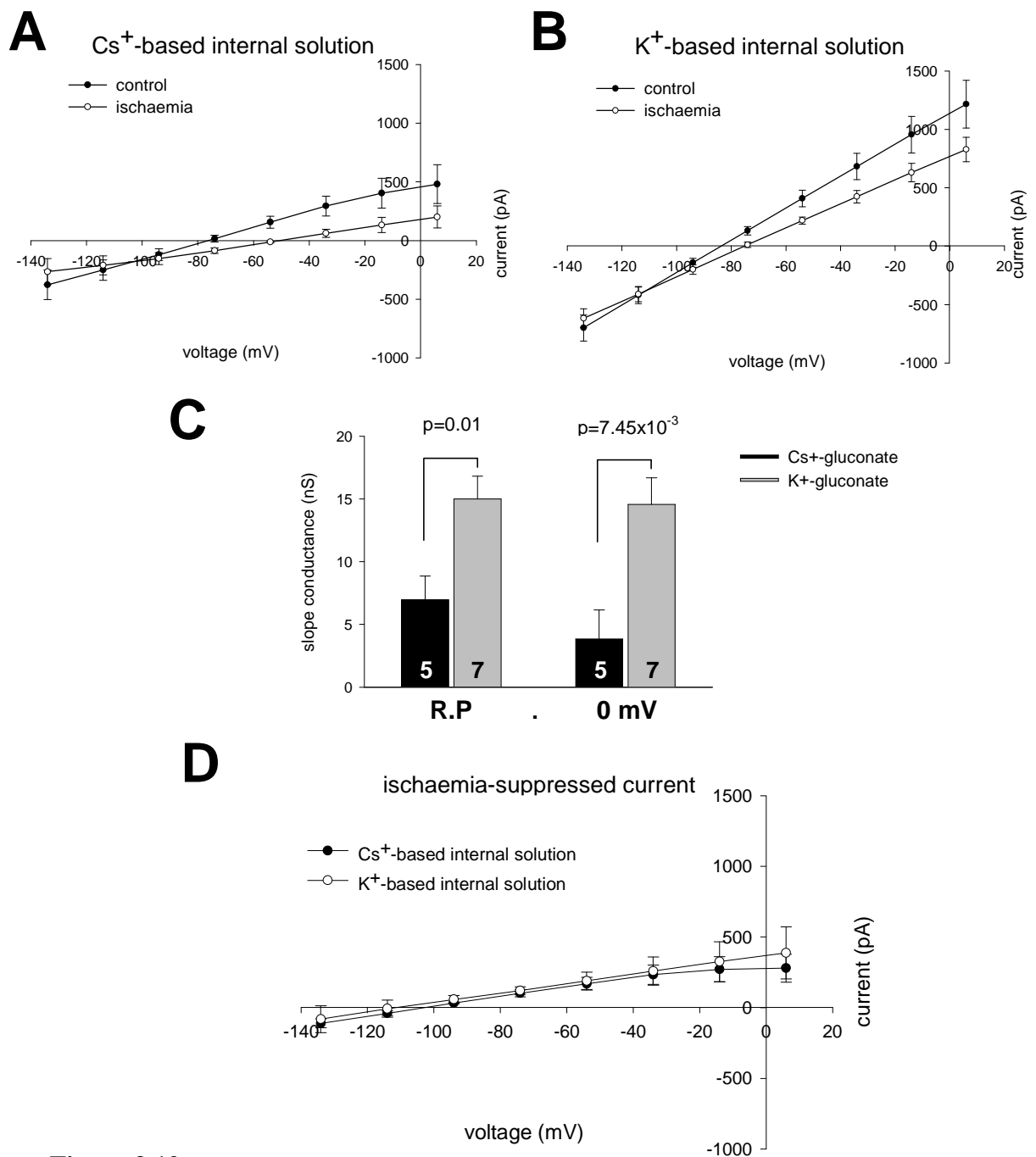


Figure 3.12

Ischaemia evokes a decrease in the oligodendrocyte membrane conductance. **A, B** Mean current-voltage (I-V) relations measured at the end of 200 msec pulses from experiments as in Fig. 3.10 (**A**, using Cs⁺ internal solution; n=5) and Fig. 3.11 (**B**, using K⁺ internal solution; n=7). Graphs show the steady state I-V relations before ischaemia (control; filled circles), and after ~9 min ischaemia (ischaemia; open circles). **C** Slope conductance of the I-V relations in control solution at the resting potential (R.P.) and 0 mV for Cs⁺- and K⁺-based internal solutions. The slope conductance for K⁺ is significantly higher than for Cs⁺ in both of the conditions, but the relative permeability to Cs⁺ is higher at the R.P. than at 0mV. **D** The I-V relations of the current suppressed in ischaemia (current before ischaemia minus current in ischaemia), using Cs⁺- (filled circles) or K⁺-based internal solution (open circles), show no difference between the two internal solutions. The current suppressed shows characteristic of a passive conductance with a reversal potential at ~100 mV.

Chapter 4: The role of glutamate in the oligodendrocyte response to ischaemia

4.1 Introduction

As described in Chapter 3, oligodendrocytes respond to ischaemia with an inward current that reflects a closing of potassium channels. The experiments in this chapter investigate the mechanism of this phenomenon. Ischaemia could cause a reduction in potassium channel open probability by directly altering a factor affecting the channels, for example lowering the level of intracellular ATP or raising the intracellular calcium concentration (although normally these changes would increase the conductance, by opening ATP- or Ca^{2+} -gated K^+ channels), or causing cell swelling and membrane stretch. Alternatively, the effect could be more indirect, and be a secondary consequence of the activation of another receptor or channel expressed by oligodendrocytes.

Various factors have been reported to be released during white matter ischaemia, among them: glutamate (Tekkök *et al.*, 2007), GABA (Lee *et al.*, 1993; Fern *et al.*, 1995) and ATP (Domercq *et al.*, 2010). An abnormally increased level of glutamate has been suggested to be the main damaging agent during white matter ischaemic insult (Stys, 2004; Jensen, 2005; Matute *et al.*, 2007), but the mechanism by which this neurotransmitter is released by ischaemia in the white matter remains controversial. As reviewed in Chapter 1, it has been suggested that, as in the grey matter (Rossi *et al.*, 2000), loss of the energy supply to the white matter causes glutamate transporters to reverse and release glutamate (Li *et al.*, 1999), but increased exocytosis induced by a rise of $[\text{Ca}^{2+}]_i$ is also a possibility since there are synapses from unmyelinated axons to oligodendrocyte precursor cells (Kukley *et al.*, 2007; Ziskin *et al.*, 2007). Alternative mechanisms include astrocyte swelling and rupture (releasing intracellular glutamate) caused by an activation of astrocytic NKCC1 co-transporters (Su *et al.*, 2000; Wilke *et al.*, 2004), microglial cystine-glutamate antiporters (Domercq *et al.*, 2007), or gap junctional hemichannel opening (reported in grey matter ischaemia: Thompson *et al.*, 2006). In this chapter I investigate the role of

glutamate in the current response of oligodendrocytes to ischaemia, and assess the likely release mechanism.

As reviewed in Chapter 1, glutamate is a major damaging agent in white matter ischaemia, acting through AMPA/KA and NMDA receptors and causing calcium overload, loss of cell processes and later cell death (McDonald *et al.*, 1998; Tekkök and Goldberg, 2001; Li *et al.*, 1999; Káradóttir *et al.*, 2005; Salter and Fern, 2005; Micu *et al.*, 2006). As a result of these actions, myelinated axons lose their sheath and the action potential fails (Li *et al.*, 1999; Tekkök and Goldberg, 2001; Bakiri *et al.*, 2008). In addition, high levels of ATP have been reported to overactivate oligodendrocyte purinergic receptors, especially P2X₇ receptors, and cause severe cell damage by generating a calcium influx in ischaemic condition (Domercq *et al.*, 2010). It is also possible that GABA, the concentration of which rises fivefold in ischaemia (Shimada *et al.*, 1993), acts on oligodendrocytes GABA_A receptors, resulting in Cl⁻ influx and cell swelling, as was reported for gray matter neurons (Allen *et al.*, 2004). Finally, in neurons, the low pH level that occurs in ischaemia (Siesjö, 1988; Lipton, 1999) was found to activate acid-sensing ion channels (ASICs) leading to cell damage and death (Xiong *et al.*, 2004), and these channels are also expressed by oligodendrocytes (Feldman *et al.*, 2008). I therefore tested whether any of these factors may have an influence on the closing of oligodendrocyte potassium channels evoked by ischaemia with the aim of establishing a possible mechanism for the oligodendrocyte current response to the ischaemic insult.

4.2 Materials and methods

4.2.1 Brain slice preparation

Cerebellar slices were prepared from P12 rats as described in section 2.1. Slices were immersed and patch clamped in a bicarbonate-based solution for most of the mechanism-blocking drugs studied, or in a HEPES-based solution for experiments with Gd³⁺ which binds to bicarbonate. The solution was initially at room temperature and had a flow rate of 2-4 ml/min. After obtaining the whole-cell patch clamp mode, the temperature was changed to 33°C and a stable current baseline was recorded for 5 min.

The external solutions and the ischaemic solution are described in section 2.2.1 and 2.2.3, respectively.

4.2.2 Patch-clamping

White matter oligodendrocytes were whole-cell patch-clamped as described in section 2.6. Pipettes contained a Cs⁺-based internal solution (see Table 2.1) to provide a better voltage-clamp quality. The series resistance was 10-20 MΩ, and was not compensated. The membrane potential was held at -74 mV (including the junction potential of -14 mV, see section 2.6). During recording drugs were usually added ~2 min before the application of ischaemic solution, which is an approach similar to that taken by Hamann *et al.* (2005). For preloading of L-*trans*-pyrrolidine-2,4-dicarboxylic acid (PDC, a slowly transported antagonist of Na⁺-dependent transporters) into the cells, slices were incubated in this drug (1 mM) at room temperature for 30 min (with 1 mM Na⁺-kynurenate present to prevent activation of ionotropic glutamate receptors when the extracellular glutamate concentration rises in the presence of PDC: Volterra *et al.*, 1996), before recording from the cells. PDC was omitted from the recording solution.

4.2.3 Statistics

Data are presented as mean±s.e.m. P values are from Student's 2-tailed t-tests or by ANOVA and post-hoc Student's 2-tailed t-tests. A Holm-Bonferroni correction was applied for multiple comparisons, as described in Chapter 2, in such a way that differences are significant if the p values presented are less than 0.05.

4.3 Results

4.3.1 Glutamate is a major trigger of the ischaemia-evoked current in white matter oligodendrocytes

An excessive glutamate level has been reported to exert an excitotoxic effect on cells in the white matter (Wrathall *et al.*, 1994; Agrawal and Fehlings, 1997), especially on oligodendrocytes (Oka *et al.*, 1993), through activation of ionotropic glutamate receptors (Li *et al.*, 1999; Káradóttir *et al.*, 2005; Salter and Fern, 2005; Micu *et al.*, 2006). However, the experiments in the previous chapter showed that the ischaemia-

induced current in oligodendrocytes is caused by a closing of potassium channels. This raises the question of whether the effect of glutamate seen by previous workers somehow precedes this response, e.g. by generating an agent that decreases the activity of potassium channels.

To test if the ischaemia-induced current in oligodendrocytes is triggered by ionotropic glutamate receptors, I applied the AMPA/KA receptor blocker NBQX (25 μ M), together with the NMDA receptor blocker AP5 (50 μ M), from the start of ischaemia, to block both types of ionotropic glutamate receptor. A significant decrease in the ischaemia-evoked current was observed, confirming that these receptors play an important role in the response to ischaemia (Fig. 4.1).

To quantify this effect, I measured the peak ischaemia-evoked current in each cell and averaged this value over cells from control and from glutamate receptor blocker-treated slices. The mean peak current was reduced by $51\pm 11\%$ in 12 NBQX and AP5-treated cells ($p=6.3\times 10^{-4}$, Fig. 4.2A) when compared with all 179 control cells, or by $68\pm 4\%$ ($p=0.1$, Fig. 4.2B) when comparing 6 NBQX and AP5 treated cells with 6 interleaved control cells recorded on the same day as NBQX and AP5 were studied (the insignificant p value most probably occurs due to the increased variability of the control group).

I attempted to test which ionotropic glutamate receptor class contributes more to triggering the ischaemia-evoked current, by applying NBQX (25 μ M) and AP5 (200 μ M) separately. Although NBQX, an AMPA/KA receptor blocker, reduced the ischaemia-evoked current (Fig. 4.3), the reduction of the peak response (measured for each cell and then averaged over cells) did not reach statistical significance. The mean peak current in 10 cells studied in NBQX was reduced by $23\pm 21\%$ compared with all the 179 controls ($p=0.63$, Fig. 4.5A), and by $43\pm 16\%$ compared with 11 interleaved control cells recorded on the same day ($p=0.09$, Fig. 4.5B). Despite the reduction in the peak current not reaching significance, examination of the time course of the averaged current in Fig. 4.3A and B shows that NBQX does significantly reduce the current ($p<0.05$, indicated with stars on the graphs) over much of the 10 minute period studied. This suggests that activation of AMPA/KA receptors does play a significant role in triggering the ischaemia-evoked current in oligodendrocytes, but that not enough cells were recorded from to convincingly demonstrate a reduction of the peak current.

D-AP5 (200 μ M), an NMDA receptor blocker, applied from the start of ischaemia, did not significantly alter the time course of the ischaemia-evoked current (Fig. 4.4). Similarly, AP5 did not significantly alter the mean value for the peak ischaemia-evoked current (measured for each cell and then averaged over cells), which was increased by $32\pm 36\%$ in 5 AP5-treated cells compared with all 179 control cells ($p=0.51$, Fig. 4.5A), and was reduced by $5\pm 26\%$ compared with 3 interleaved control cells recorded on the same day ($p=0.89$, Fig. 4.5C).

These results suggest that AMPA/KA receptors play the more important role in triggering the ischaemia-evoked current. However, since NBQX+AP5 gives a more convincing block of the current than does NBQX alone, they leave open the possibility that to fully trigger the ischaemia-evoked current the simultaneous activation of both AMPA/KA and NMDA receptors is needed.

To assess the possible role of metabotropic glutamate receptors in triggering the ischaemia-evoked current, I applied MCPG (1 mM), a broad spectrum metabotropic glutamate receptor antagonist. The ischaemia-evoked current was significantly reduced (Fig. 4.6). Measuring the peak ischaemia-evoked current for each cell, and then averaging over cells, the mean peak current was reduced by $50\pm 6\%$ in 6 MCPG-treated cells compared with all 179 controls ($p=9.7\times 10^{-5}$, Fig. 4.7A) and by $63\pm 5\%$ compared with 6 interleaved control cells recorded on the same day ($p=2.3\times 10^{-3}$, Fig. 4.7B). This reduction is comparable to that produced by the combined block of AMPA/KA and NMDA classes of ionotropic glutamate receptors.

These experiments, together with those in the previous chapter, show that glutamate is the major trigger of the oligodendrocyte current response to ischaemia, acting both on its ionotropic and metabotropic receptors and causing the closing of oligodendrocyte potassium channels. In the remainder of this chapter I investigate the mechanism of glutamate release, study when glutamate has to be present to trigger the ischaemia-evoked current in oligodendrocytes, and assess the possible contribution of other ion channels to the response.

4.3.2 Glutamate is released by reversed transport in white matter ischaemia

To assess whether the glutamate, which triggers the ischaemia-evoked current, is released by a reversal of glutamate transporters, as occurs in the anoxic spinal cord (Li *et al.*, 1999), I preloaded slices with PDC (1 mM), a broad-spectrum Na^+ -dependent

glutamate transporter antagonist. PDC is transported on glutamate transporters at only ~25% the rate of glutamate (Sarantis *et al.*, 1993). During exposure to PDC, cells take up this substance and accumulate it in their cytoplasm (glutamate receptors were blocked with 1 mM Na⁺-kynurenate during this loading to prevent damage by the rise of extracellular glutamate concentration that occurs due to heteroexchange with PDC on the carrier: Volterra *et al.*, 1996). When the transmembrane ion gradients run down in ischaemia, promoting transporter reversal (Szatkowski *et al.*, 1990), the preloaded intracellular PDC occupies the transporters and prevents glutamate release (Roettger and Lipton, 1996; Li *et al.*, 1999; Rossi *et al.*, 2000). As shown in Fig. 4.8, PDC preloading reduced the ischaemia-evoked current in oligodendrocytes. To quantify this, I measured the peak ischaemia-evoked current in each cell and averaged this value over cells from control and from PDC-treated slices. The mean peak current was reduced by 72±6% in 5 PDC-treated cells ($p=1.2\times 10^{-7}$), when compared with all 179 control cells, or by 62±12% ($p=6.8\times 10^{-3}$), when compared with 7 interleaved control cells recorded on the same day as the PDC was studied (Fig. 4.9).

Next, I tested three other possible mechanisms of glutamate release that could add to the rise of extracellular glutamate concentration produced by the reversal of glutamate transporters. Astrocytic NKCC1 co-transporters have been proposed to release glutamate upon ischaemia by generating an excessive ionic flux into the cells which leads to astrocyte swelling and death, and thus the release of intracellular glutamate (Su *et al.*, 2000; Wilke *et al.*, 2004). After application of bumetanide (50 µM, Wilke *et al.*, 2004) to inhibit NKCC1 co-transporters in 10 slices, the ischaemia-evoked current showed a later onset and smaller amplitude when compared with all the 179 control cells (Fig. 4.10A), but showed an indistinguishable onset time course and amplitude when compared with 10 interleaved control cells recorded on the same day (Fig. 4.10B). This difference from the data for all 179 control cells presumably reflects day to day variation in the amplitude and time course of the response to ischaemia. The mean value of the peak current amplitude was reduced by 31±11% in 10 cells in bumetanide-treated slices compared with the mean for all 179 control cells ($p=0.08$, Fig. 4.13), but not significantly reduced when compared with the data from 10 interleaved control cells recorded on the same day (reduced by 2%±15%, $p=0.93$, Fig. 4.14A). This suggests that there is little or no influence of NKCC1 co-transporters on the early ischaemia-evoked release of glutamate in the white matter (and hence on the suppression of oligodendrocyte K⁺ current that ischaemia produces).

I also investigated the possibility of exocytosis from unmyelinated axons being involved in white matter glutamate release. Recently, unmyelinated axons in the white matter have been shown to release glutamate at synapses onto oligodendrocyte precursor cells (Kukley *et al.*, 2007; Ziskin *et al.*, 2007) and this release may increase in ischaemia, as has been reported for glutamate and GABA in the grey matter (Katchman and Hershkowitz, 1993; Allen *et al.*, 2004). However, after application of Cd^{2+} (100 μM , Kukley *et al.*, 2007), an exocytosis blocker, there was no significant change in the time course or magnitude of the ischaemia-induced current in oligodendrocytes (Fig. 4.11). The mean value of the peak current amplitude was insignificantly increased by $24\pm 30\%$ in 13 cells in Cd^{2+} -treated slices compared with the mean for all 179 control cells ($p=0.87$, Fig. 4.13), while comparing the Cd^{2+} data with that from 8 interleaved control cells on the same day a non-significant decrease of $15\pm 23\%$ ($p=0.71$) was seen (Fig. 4.14B).

Finally, I ruled out activation of cystine-glutamate antiporters as another possible mechanism of ischaemia-induced glutamate release. It has been suggested that microglial cystine-glutamate antiporters can release excessive glutamate during exposure to lipopolysaccharide, causing oligodendrocyte death (Domercq *et al.*, 2007), so I examined whether this also occurs in ischaemia. However, application of the cystine-glutamate exchange blocker (S)-4-carboxyphenylglycine (CPG, 50 μM , a concentration demonstrated to be effective by Cavelier and Attwell (2005)) did not have any significant effect on the time course of the ischaemia-induced current in these cells (Fig. 4.12). The mean value of the peak current amplitude was insignificantly increased by $6\pm 42\%$ in 5 cells in CPG-treated slices compared with the mean for all 179 control cells ($p=0.90$, Fig. 4.13), while comparing the CPG data with that from 4 interleaved control cells on the same day an insignificant increase of $58\pm 63\%$ ($p=0.42$) was seen (Fig. 4.14C).

In conclusion, these experiments demonstrate that a reversal of glutamate uptake transporters is the main mechanism of glutamate release early in ischaemia of the white matter, excluding a significant contribution to this process from NKCC1 co-transporter overactivation, exocytosis from unmyelinated axons or activation of microglial cystine-glutamate antiporters.

4.3.3 The contribution of gap junctional hemichannel opening and activation of P2X₇ receptors to the ischaemia-induced current in oligodendrocytes

Despite its importance, glutamate is not the only factor that affects cell survival during ischaemic insult, and it has been shown that gap junctional hemichannel opening and activation of ATP-gated P2X₇ receptors can also contribute to the ischaemia-evoked damage. A recent study in oligodendrocytes linked these two phenomena, showing that the activation of P2X₇ receptors in ischaemia is directly caused by a release of intracellular ATP mediated by hemichannel opening (Domercq *et al.*, 2010).

Hemichannels can open during ischaemia, possibly releasing agents (such as glutamate and ATP) responsible for ionic dysregulation, and decreasing the intracellular levels of ATP and glucose (Ye *et al.*, 2003; Thompson *et al.*, 2006). I therefore investigated the effect of blocking hemichannel opening with La³⁺ (100 μM, Ye *et al.*, 2003). Lanthanum decreased the amplitude of the peak ischaemia-evoked current in 11 cells from La³⁺-treated slices when compared with all 179 control cells (reduced by 40±10%, p=6.7x10⁻³, Figs. 4.15A and 4.17A), but not when compared with 12 interleaved control cells recorded on the same day (reduced by 10±16%, p=0.65, Figs. 4.15B and 4.17B). This difference presumably reflects day to day variation in the amplitude of the ischaemia-evoked current: on the days that La³⁺ was studied, the ischaemia-evoked currents in the control cells were smaller than average. Although more experiments are needed to confirm the result, the lack of effect of La³⁺ when compared with control cells studied on the same day suggests that La³⁺ does not have a significant effect on the glutamate release mechanism.

ATP, released from cells upon injury and acting through P2X₇ receptors, causes excessive neuronal firing, an irreversible calcium overload and death of spinal cord neurons (Wang *et al.*, 2004). The expression of P2X₇ receptors is significantly upregulated as a consequence of ischaemic insult (Franke *et al.*, 2004) and P2X₇ receptors are also found in oligodendrocytes (Agresti *et al.*, 2005). Nevertheless, blocking P2X₇ receptors with BBG (10 μM, Domercq *et al.*, 2010) did not significantly affect the initial time course nor the average peak value for the ischaemia-evoked current (Fig. 4.16). The mean peak current was reduced by 22±17% in 6 BBG-treated cells when compared to all 179 control cells (not significant, p=0.27, Fig. 4.17A), and by 6±21% when compared with 7 interleaved control cells recorded on the same day (p=0.85, Fig. 4.17B).

These results suggest that, compared to glutamate, hemichannel opening and P2X₇ receptor activation make a negligible contribution to the oligodendrocyte response to ischaemia.

4.3.4 ASICs, GABA_A receptors and neuronal action potentials do not influence the oligodendrocyte response to ischaemia

In addition to a release of glutamate, an acid extracellular pH shift activating acid sensitive ion channels (ASICs), a release of GABA that activates GABA_A receptors, and excessive neuronal firing, have also been described as general features of grey matter ischaemia (see Chapter 1 and section 4.1 above), so I investigated whether any of these factors contributed to the generation of the ischaemia-evoked current in oligodendrocytes

Acidotoxicity may contribute to ischaemic damage, as neuronal ASIC channels open in ischaemia (Xiong *et al.*, 2004), their block reduces the size of the infarct *in vivo* (Pignataro *et al.*, 2007) and oligodendrocytes also express ASICs (Feldman *et al.*, 2008). However, blocking ASIC channels with amiloride (100 µM, Feldman *et al.*, 2008) did not significantly affect either the time course (Fig. 4.18) or the magnitude of the ischaemia-evoked current in oligodendrocytes: the averaged peak current in 6 cells studied with amiloride was reduced by 17±15% compared to all 179 control cells (p=0.64, Fig. 4. 21) and was increased by 8±20% compared with 6 interleaved control cells studied on the same day (p= 0.76, Fig. 4.22A).

Action potentials occurring in neurons at the start of ischaemia (Hamann *et al.*, 2005) may lead to an excessive vesicular release of neurotransmitter from synapses made in the white matter onto OPCs (Kukley *et al.*, 2007; Ziskin *et al.*, 2007). In the cerebellar white matter this could include glutamate released from afferent mossy and climbing fibres, and GABA released from Purkinje cell axons. Action potentials could also generate extracellular K⁺ accumulation. However, blocking action potentials with TTX (1 µM) had no significant effect on the time course of the ischaemia-evoked current in oligodendrocytes (Fig. 4.19), nor on its mean magnitude (which in 13 cells studied in TTX was reduced by 19±13% compared to that in all 179 control cells (p=0.59, Fig. 4.21), and increased by 7±17% compared to 10 interleaved control cells recorded on the same day (p=0.75, Fig. 4.22B)).

During ischaemic insult in the grey matter, neurons release GABA which activates GABA_A receptors, causing a Cl⁻ influx and cell swelling (Allen *et al.*, 2004)

that might lead to cell membrane rupture and the release of intracellular agents. To investigate the possible contribution of such a GABA effect to the ischaemia-induced current in white matter oligodendrocytes, I applied bicuculline (100 μ M), a GABA_A receptor blocker. Bicuculline did not alter the time course of the ischaemia-evoked current (Fig. 4.20). It also did not alter the averaged peak inward current produced by ischaemia in 5 bicuculline-treated cells (reduced by $7\pm 19\%$ compared with all 179 controls ($p=0.74$, Fig. 4.21) and by $6\pm 19\%$ compared with 4 interleaved controls studied on the same day ($p=0.80$, Fig. 4.22C)).

4.3.5 Ionotropic glutamate receptor block does not inhibit the ischaemia-evoked current when applied after the start of ischaemic insult

Although previous studies that examined the effect of blocking ionotropic receptors on the oligodendrocyte response to ischaemia reported a protective effect (described above and in Chapter 1), there are still no effective therapies using these blockers to treat white matter injury after ischaemic insult. This may be explained by the fact that all the laboratory studies were performed by applying AMPA/KA and NMDA receptor blockers 20 min to 1 h before the exposure to ischaemia (Li and Stys, 2000; Tekkök and Goldberg, 2001; Micu *et al.*, 2006; McCarran and Goldberg, 2007; Bakiri *et al.*, 2008), while a medical treatment needs to be effective during or after the exposure to the ischaemic insult. I therefore tested the efficiency of ionotropic glutamate receptor blockers for inhibiting the ischaemia-evoked current when applied after the initiation of white matter ischaemia.

Surprisingly, unlike in neurons where the ischaemia-evoked current is largely produced by an ion influx through ionotropic glutamate receptors (Rossi *et al.*, 2000; Hamann *et al.*, 2005), when NBQX (25 μ M) and AP5 (50 μ M) were applied from 3-4 min after the start of ischaemia, they did not block the already developing ischaemia-evoked current (Fig. 4.23). The peak inward current evoked by ischaemia occurred on average at 439 ± 11 sec after the start of ischaemia for control cells (as described in Chapter 3) and at 487 ± 52 sec after the start of ischaemia (not significantly different, $p=0.4$) for the 6 cells to which NBQX and AP5 were applied 3-4 min after the start of ischaemia. In contrast to the 51-68% reduction in ischaemia-evoked current seen when NBQX and AP5 were applied together from before the ischaemia started, in the cells to which NBQX and AP5 were applied 3-4 min after the start of ischaemia the mean peak current was insignificantly reduced by $1\pm 16\%$ ($p=0.95$) compared to all 179 control

cells and was increased by $17\pm 19\%$ ($p=0.55$) compared to 5 interleaved control cells studied on the same day (Fig. 4.24).

The fact that ionotropic glutamate blockers inhibit the ischaemia-evoked current when applied before ischaemia, but not when applied after the start of ischaemia closely resembles a neuronal phenomenon called the extended neuronal depolarisation (END) - an inward current observed in neurons upon prolonged exposure to glutamate that is maintained even when the initial trigger, glutamate, is removed (Coulter *et al.*, 1992; Limbrick *et al.*, 2003).

4.3.6 The mechanism of the extended inward current in oligodendrocytes is different from that producing the END in neurons

In neurons, the END is induced by excessive activation of glutamate receptors and largely depends on the duration of the exposure to glutamate. It is mediated by an influx of extracellular calcium and causes delayed neuronal cell death. As such, END can be linked to the pathophysiology of stroke or traumatic brain injury (Coulter *et al.*, 1992; Limbrick *et al.*, 2003). A similar phenomenon has not been reported in oligodendrocytes so far, but the results from the previous experiments mimic many of those observed in END, namely a dependence on an initial activation of ionotropic glutamate receptors, a failure to abolish the response (once initiated) with ionotropic receptor blockers, and an insensitivity to block by TTX and amiloride (Coulter *et al.*, 1992; Limbrick *et al.*, 2003; Deshpande *et al.*, 2007).

In neurons, the END was found to be blocked by $100\ \mu\text{M}\ \text{Gd}^{3+}$, or by the omission of extracellular calcium (Coulter *et al.*, 1992; Limbrick *et al.*, 2003), even when these manipulations were applied after the depolarisation was established, and so its effect is most probably exerted through calcium-permeable channels. However, Gd^{3+} ($100\ \mu\text{M}$) did not block the ischaemia-evoked inward current in oligodendrocytes, either when added from ~ 4 min after the start of ischaemia (Fig. 4.25) or when present from before the start of ischaemia (Fig. 4.26). When Gd^{3+} was applied after the start of ischaemia in 3 cells the mean peak ischaemia-evoked current was $61\pm 45\%$ larger than that in all 179 control cells ($p=0.31$, Fig. 4.28) and $38\pm 39\%$ larger than in 3 interleaved control cells studied on the same day ($p=0.47$, Fig. 4.29A). When Gd^{3+} was applied throughout ischaemia to 7 cells the mean peak current was reduced by $30\pm 19\%$ compared with all 179 control cells ($p=0.57$, Fig. 4.28) and increased by $4\pm 28\%$ when

compared with 6 interleaved control cells studied on the same day ($p=0.19$, Fig. 4.29B).

Similarly, removing extracellular calcium (and with trace calcium chelated by the addition of 50 μM EGTA to the external solution) did not prevent or reduce the ischaemia-evoked current (Fig. 4.27). In the absence of calcium the mean peak ischaemia-evoked current in 6 cells was $43\pm 35\%$ larger than the mean for all 179 control cells ($p=0.55$, Fig. 4.28) and $48\pm 36\%$ larger than the mean for 10 interleaved control cells recorded on the same day ($p=0.26$; Fig. 4.29C). The lack of an effect of Ca^{2+} removal is interesting in that previous data suggested that an excessive influx of calcium exerts a damaging effect on white matter oligodendrocytes during ischaemia (Deng *et al.*, 2003; Salter and Fern, 2005; Micu *et al.*, 2006; Domercq *et al.*, 2010). This result implies that the suppression of K^+ conductance that is evoked by ischaemia does not depend on Ca^{2+} entry.

These data show that the mechanism of the extended depolarisation evoked by glutamate in neurons differs from that induced by ischaemia in oligodendrocytes.

4.4 Discussion

The white matter is vulnerable to anoxia or ischaemia, particularly in the immature brain (McCarran and Goldberg, 2007; Hertz, 2008), and the energy supply failure occurring in conditions such as stroke, perinatal asphyxia leading to periventricular leukomalacia, and spinal cord injury causes a loss of oligodendrocytes or their precursors (Park *et al.*, 2004; Stys, 2004; Ludwin, 2006; Khwaja and Volpe, 2008). Since oligodendrocytes are crucial for proper propagation of neuronal action potentials in the white matter, it is of critical importance to identify the causative agents responsible for their damage in such pathological conditions.

In the previous chapter I showed that the oligodendrocyte membrane current response to ischaemia is dominated by an inward current that is caused by the closing of potassium channels. In this chapter I investigated the possible mechanism of this response and demonstrated that its main trigger is glutamate, released into the white matter by the reversal of glutamate transporters (and not by the activation of NKCC1

co-transporters, cystine-glutamate antiporters or synaptic release), and that glutamate acts on oligodendrocytes through its ionotropic and metabotropic receptors.

Other factors, such as ATP activating P2X₇ receptors, hemichannel opening, GABA acting on GABA_A receptors, low pH activating ASICs, or neuronal action potentials, had a negligible influence on the ischaemia-evoked current. It should, however, be born in mind that it may be necessary to study a larger number of cells for each drug condition than was possible in the finite time of this PhD to establish small effects on the ischaemia-evoked current: consequently, although glutamate seems to have the dominant influence, I cannot rule out the possibility that some of the other agents which gave insignificant effects might show small effects if a much larger number of cells were studied.

The response to ischaemia in oligodendrocytes was strongly reduced by the application of either ionotropic glutamate receptor blockers (by ~50%) or of a metabotropic glutamate receptor blocker (~50%), and so it is likely that the combined application of these inhibitors together would completely abolish the current. Further experiments are needed to investigate this possibility.

The lack of a significant contribution of oligodendrocyte NMDA receptors to the ischaemia-induced current was surprising, as Káradóttir *et al.* (2005) have demonstrated previously that NMDA receptor blockers inhibit the current evoked in oligodendrocytes in ischaemia. However, in that paper the block in mature cells was shown to be only ~15% and so the variability of my responses might have concealed such a small reduction in the current. In order to definitely reject such a possibility, the experiment would have to be repeated on a considerably larger number of cells.

It is surprising that although glutamate triggers the ischaemia-evoked current, the current is not mediated by an ion flux through ionotropic glutamate receptors, but by a suppression of potassium conductance (see previous chapter). However, activation of glutamate receptors has previously been reported to exert a suppressive effect on potassium channels in glia. Gallo *et al.* (1996) found that delayed rectifier K⁺ channels in oligodendrocyte precursors can be closed by the activation of AMPA/KA receptors (the mechanism being an influx of Na⁺ ions which blocks the channels from the inside: Knutson *et al.*, 1997), while in Müller glial cells Schwartz (1993) described potassium channel inhibition by glutamate metabotropic receptors. It is plausible therefore, that glutamate induces a similar effect in myelinating oligodendrocytes, acting both through ionotropic and metabotropic receptors.

Surprisingly, ionotropic glutamate receptor blockers were effective only when applied before ischaemia, not once the ischaemia-evoked current had been activated. It would be interesting to test whether this is also the case for the effect of mGluR blockers. This result was unexpected, as it differs from that obtained in neurons, where the ischaemia-evoked current can be immediately abolished by AMPA/KA and NMDA receptor blocker application even after the current has been activated (Rossi *et al.*, 2000; Hamann *et al.*, 2005). Although in oligodendrocytes, like in neurons, ionotropic glutamate receptor blockers also blocked the majority of the ischaemia-evoked current if present throughout ischaemia, the current could not be abolished by these blockers once it had been established. This phenomenon appears similar to one described in neurons, in which exposure to glutamate for more than a certain duration leads to the irreversible activation of a depolarizing current (termed the extended neuronal depolarisation, or END: Sombati *et al.*, 1991; Coulter *et al.*, 1992; Limbrick *et al.*, 2003; Deshpande *et al.*, 2007). However, the hypothesis that the events in oligodendrocytes were identical to the END phenomenon in neurons had to be excluded based on the fact that Gd^{3+} and calcium removal did not reduce the ischaemia-evoked current in oligodendrocytes, while in neurons they block the END even when applied after it has been activated.

The experiments with La^{3+} and Gd^{3+} , used as blockers of hemichannels and of the END effect, respectively, also excluded the possibility of transient receptor potential (TRP) channels being involved in the induction of the ischaemia-evoked current. It was shown in neurons that TRPM7 (which is blocked by La^{3+} and Gd^{3+}) is responsible for a death mechanism in ischaemia, allowing Ca^{2+} influx and ROS production even when ionotropic glutamate receptor blockers were applied (Aarts *et al.*, 2003; Lipski *et al.*, 2006). This effect was also shown *in vivo* (Sun *et al.*, 2009). However, my results rule out an important role for TRP channel activation in the white matter oligodendrocytes' current response to ischaemia.

In conclusion, my results indicate that in white matter ischaemia glutamate is released through a reversal of glutamate transporters and acts on ionotropic and metabotropic glutamate receptors, evoking a membrane current response in oligodendrocytes that is dominated by the closing of potassium channels. I show for the first time that the majority of ischaemia-evoked current in oligodendrocytes is caused, but not maintained, by the activation of glutamate receptors, as blocking these receptors did not reduce the inward current once it was established. This phenomenon,

although similar to the neuronal END effect, has a different and as yet obscure mechanism. All of the above results indicate that the oligodendrocyte response to ischaemia is a complex phenomenon that differs substantially from the one described in neurons.

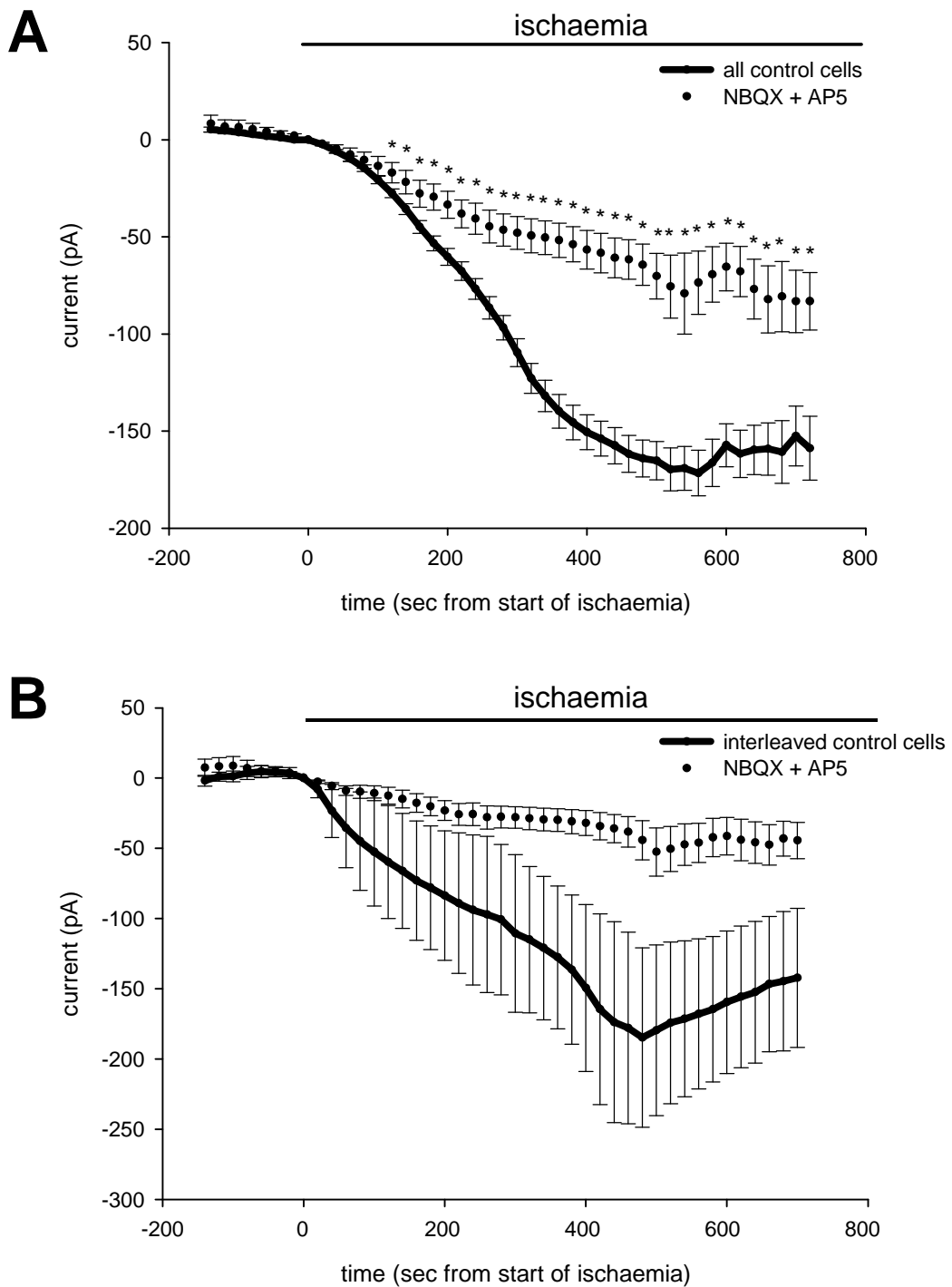


Figure 4.1

Combined application of the AMPA/KA receptor blocker NBQX (25 μ M) and the NMDA receptor blocker AP5 (50 μ M) significantly reduces the ischaemia-induced current in oligodendrocytes. **A** Comparison between the averaged time course of the ischaemia-evoked current from 12 cells in slices treated with NBQX and AP5 and from all 179 control cells shows a significant decrease of the current amplitude in the presence of NBQX and AP5. **B** Comparison between the averaged time course of the ischaemia-evoked current in 6 cells studied with NBQX and AP5 and in 6 interleaved control cells (i.e. recorded on the same day) shows a decrease of the current in the presence of the blockers (although not significant due to the high variability in the amplitude of the control cell responses). Ischaemia starts at $t=0$. * indicates statistically significant difference at the time point indicated ($p<0.05$).

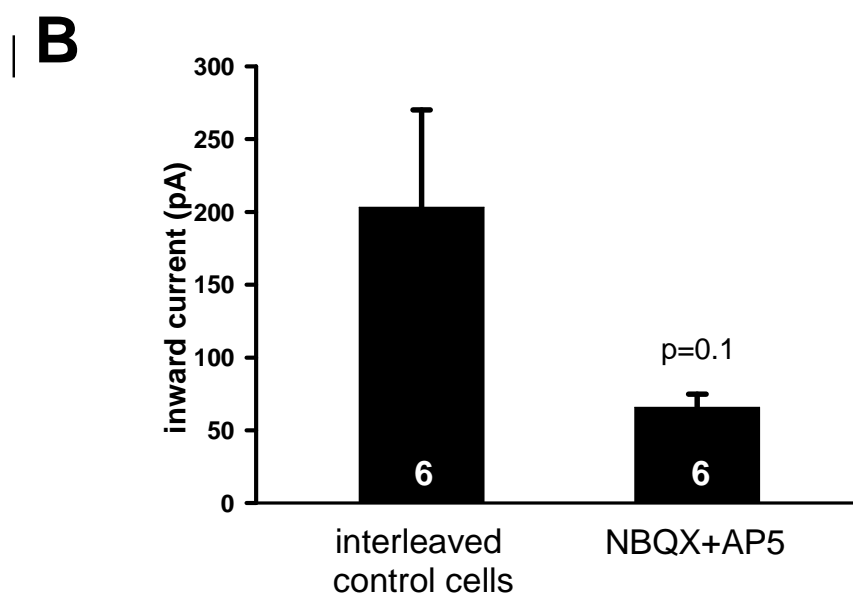
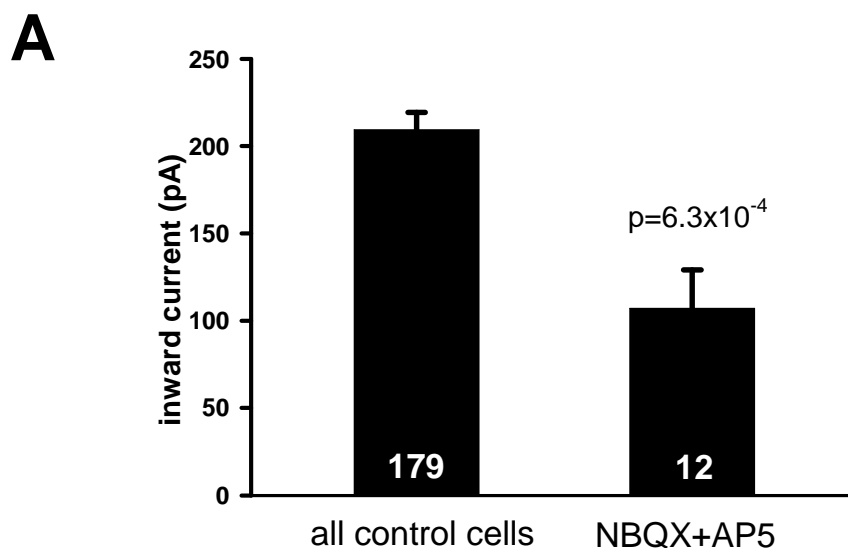


Figure 4.2

Comparison of the mean values for the peak of the ischaemia-induced inward current (measured for each cell and then averaged over all cells in the same condition), for control cells and for cells with NBQX and AP5 applied, shows that ionotropic glutamate receptor blockers significantly reduced the ischaemia-induced current. **A** Comparison between the average peak current in 12 cells studied in NBQX and AP5 and the current in all 179 control cells shows a significant decrease of the current amplitude when the blockers were applied. **B** Comparison between the average peak current in 6 cells with NBQX and AP5 and in 6 interleaved control cells studied on the same day also shows a decrease of the current amplitude when the blockers were applied (although not significant due to the high variability in the amplitude of the control cell responses).

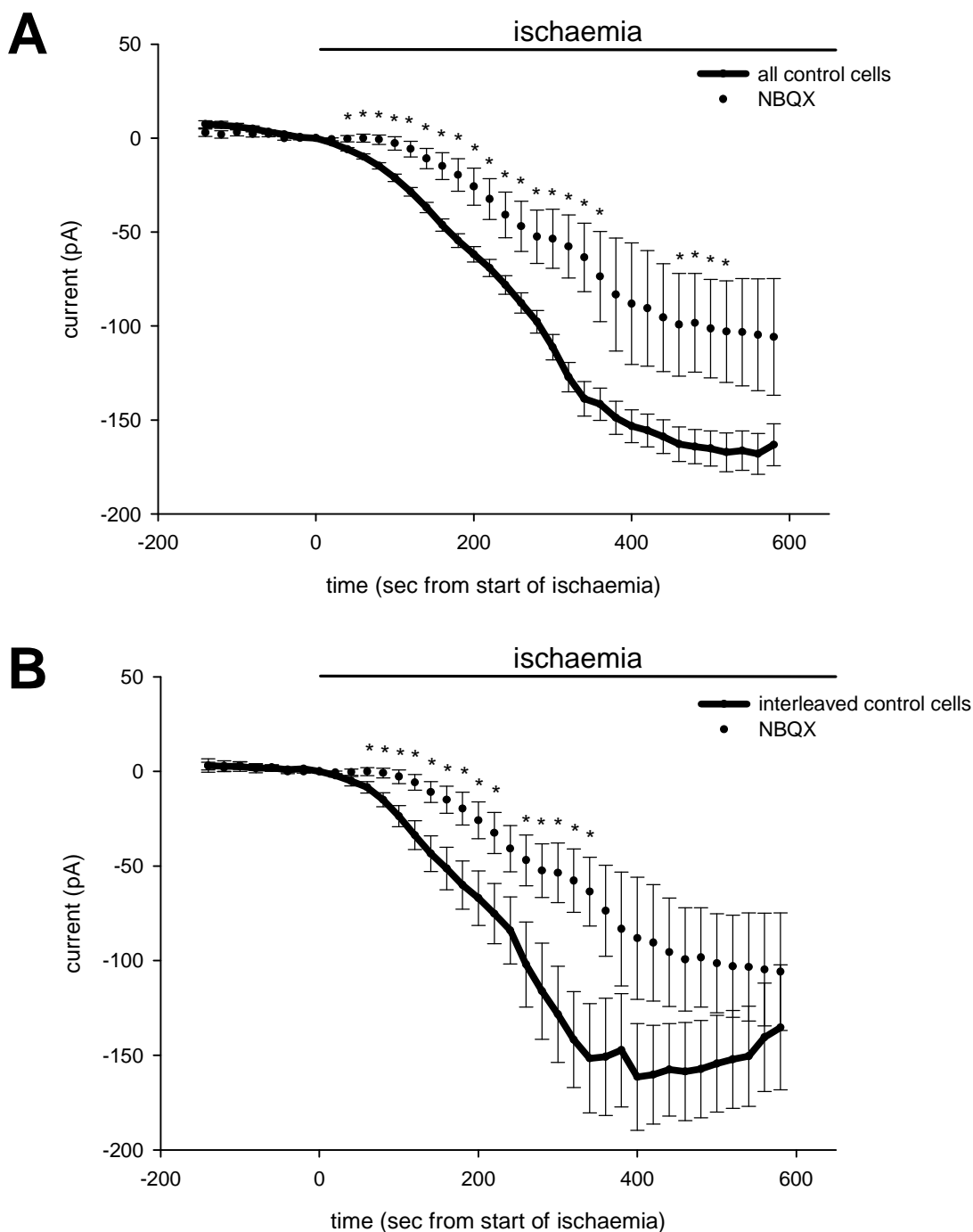


Figure 4.3

Effect of the AMPA/KA receptor blocker, NBQX (25 μ M), applied alone, on the ischaemia-induced current in oligodendrocytes. **A** Comparison between the averaged time course of the ischaemia-evoked current from 10 cells in slices treated with NBQX and from all the 179 control cells shows a delay in the current response to ischaemia and a reduced amplitude before 600 sec in the presence of NBQX. **B** Comparison between the averaged time course of the ischaemia-evoked current in 10 cells in slices treated with NBQX and in 12 interleaved control cells (studied on the same day as application of NBQX) shows a delay in the response but a similar amplitude in the presence of NBQX. Ischaemia starts at t=0. * indicates statistically significant difference at the time point indicated (p<0.05).

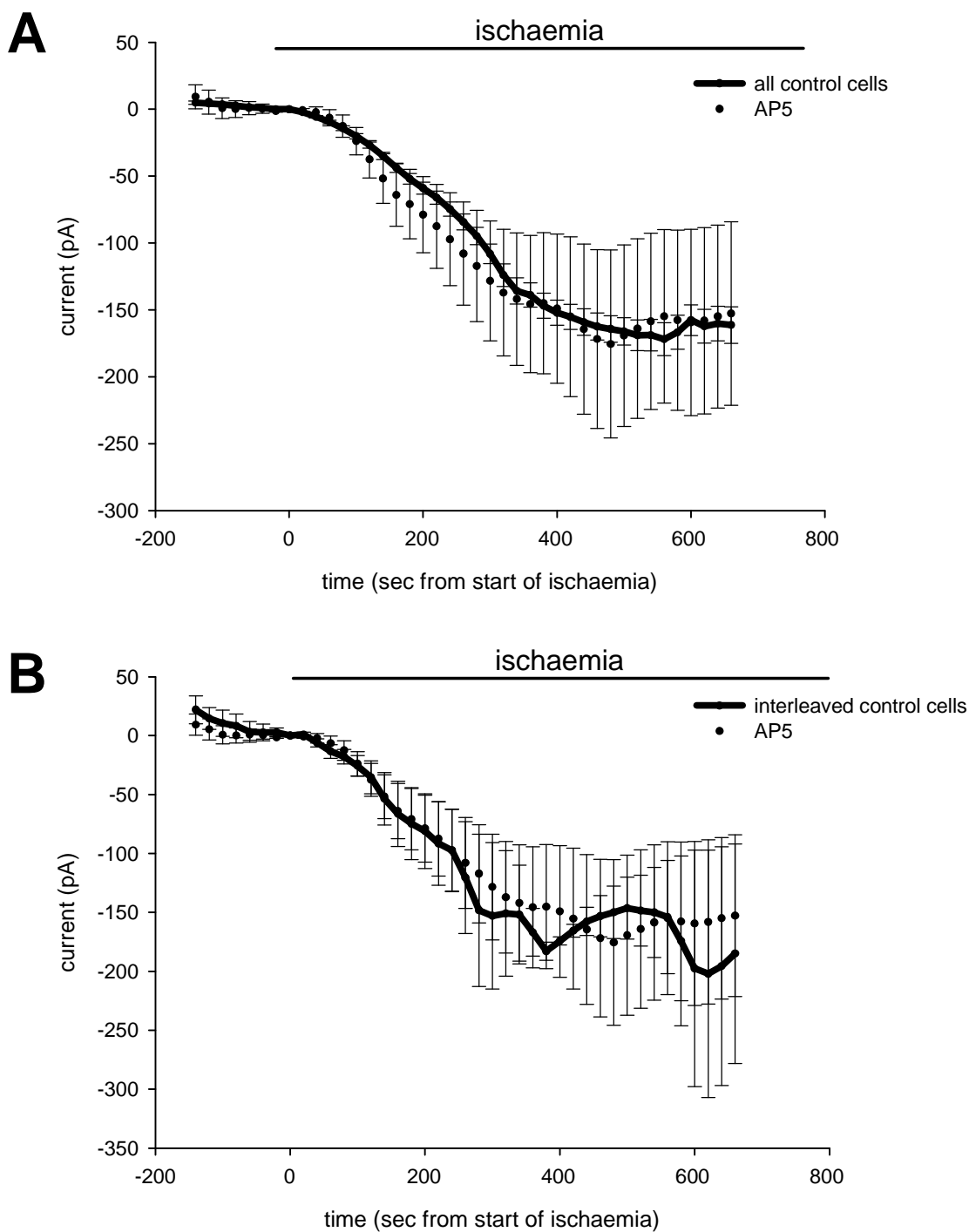


Figure 4.4

Effect of the NMDA receptor blocker, D-AP5 (200 μ M), applied alone, on the ischaemia-induced current in oligodendrocytes. **A** Comparison between the averaged time course of the ischaemia-evoked control current from 5 cells in slices treated with AP5 and from all 179 control cells, $n=179$) and the current with AP5 ($n=5$) shows little difference between them. **B** Comparison between the averaged time course of the ischaemia-evoked current from 5 cells in slices treated with AP5 and from 3 interleaved control cells (studied on the same day as application of AP5) shows little difference between them. Ischaemia starts at $t=0$.

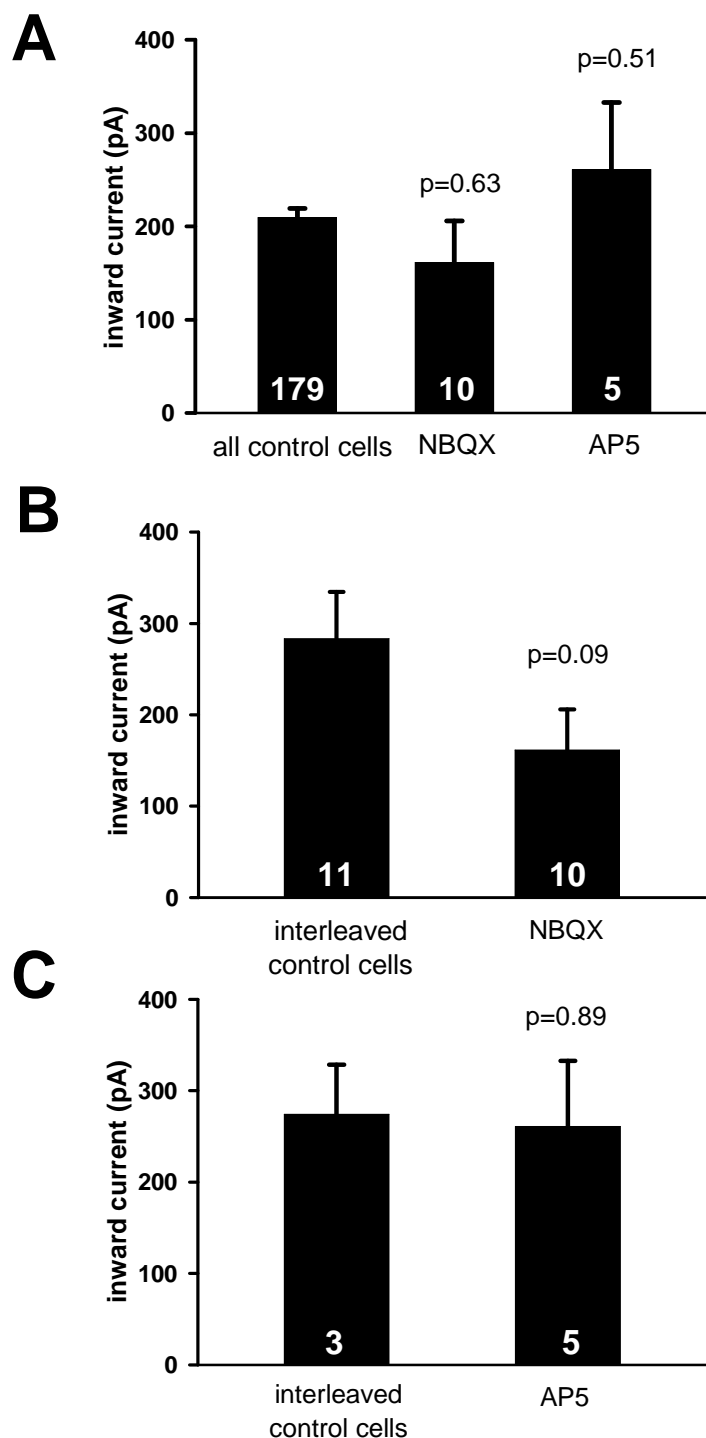


Figure 4.5

Comparison of the mean values for the peak of the ischaemia-induced inward current (measured for each cell and then averaged over all cells in the same condition), for control cells and for cells with either NBQX (25 μ M) or AP5 (200 μ M) applied alone, shows that these blockers did not significantly affect the size of the current. **A** Comparison between the average peak current from all 179 control cells and from 10 cells in NBQX and 5 cells in AP5 shows no significant effect of the blockers. **B** Comparison between the average peak current in 10 cells in NBQX and in 11 interleaved control cells (studied on the same day as NBQX). **C** Comparison between the average peak current in 5 cells studied in AP5 and in 3 interleaved control cells shows no significant effect of the blocker.

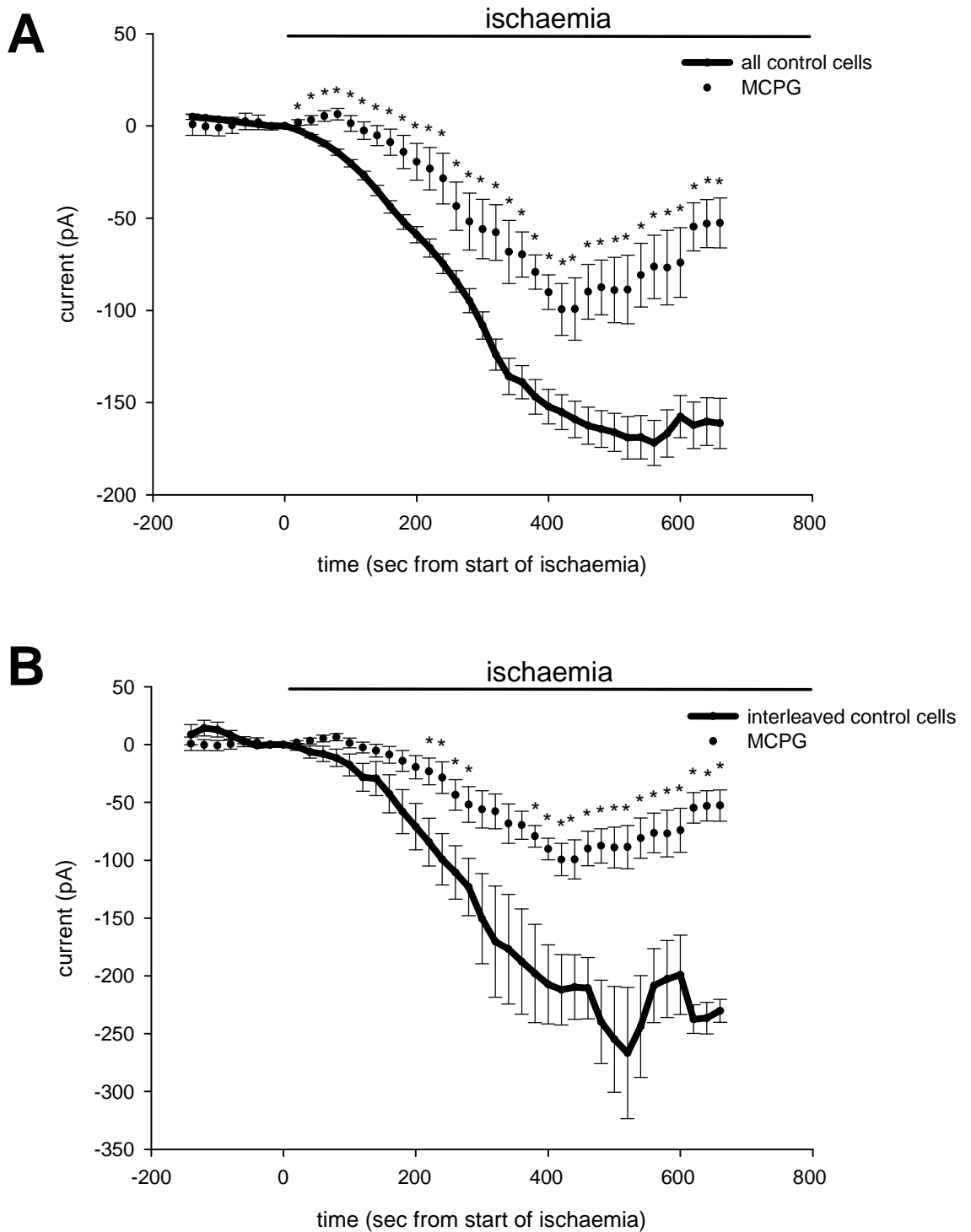
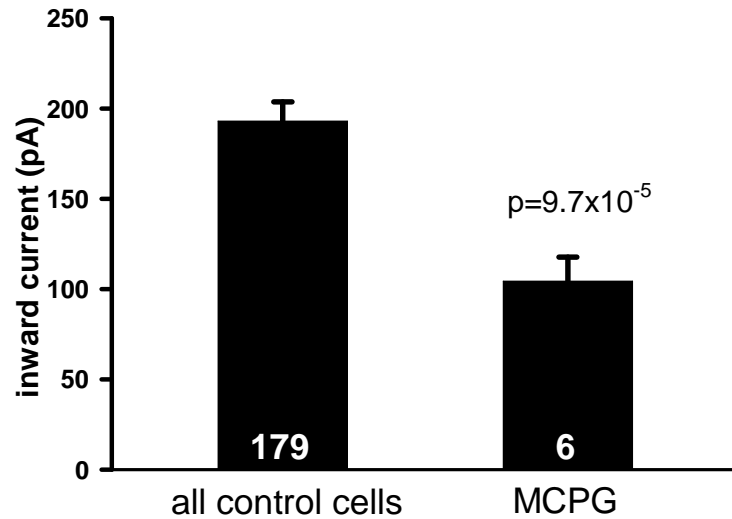
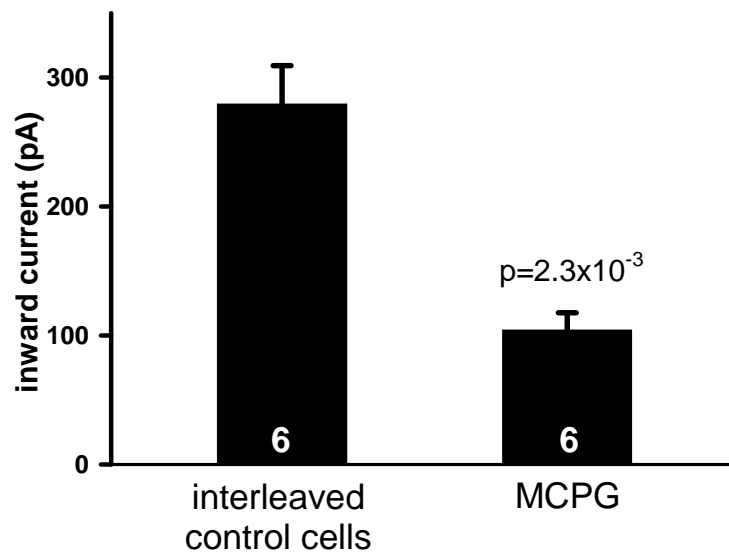


Figure 4.6

The metabotropic glutamate receptor blocker, MCPG (1 mM), significantly reduced the ischaemia-induced current in oligodendrocytes. **A** Comparison between the average time course of the ischaemia-evoked current in 6 cells studied with MCPG and in all 179 control cells shows a significant decrease of the current when the blocker was applied. **B** Comparison between the average time course of the ischaemia-evoked current in 6 cells studied with MCPG and in 6 interleaved control cells (studied on the same day as MCPG) shows a significant decrease of the current when the blocker was applied. Ischaemia starts at $t=0$. * indicates statistically significant difference at the time point indicated ($p<0.05$).

A**B****Figure 4.7**

MCPG (1 mM) significantly blocks the ischaemia-induced current in oligodendrocytes. **A** Comparison of the mean values for the peak of the ischaemia-induced inward current (measured for each cell and then averaged over all cells in the same condition), for all 179 control cells and for 6 cells with MCPG present shows a significant decrease of the current when the blocker was applied. **B** Comparison between the average peak current in 6 cells with MCPG and in 6 interleaved control cells (studied on the same day as MCPG) shows a significant decrease of the current when the blocker was applied.

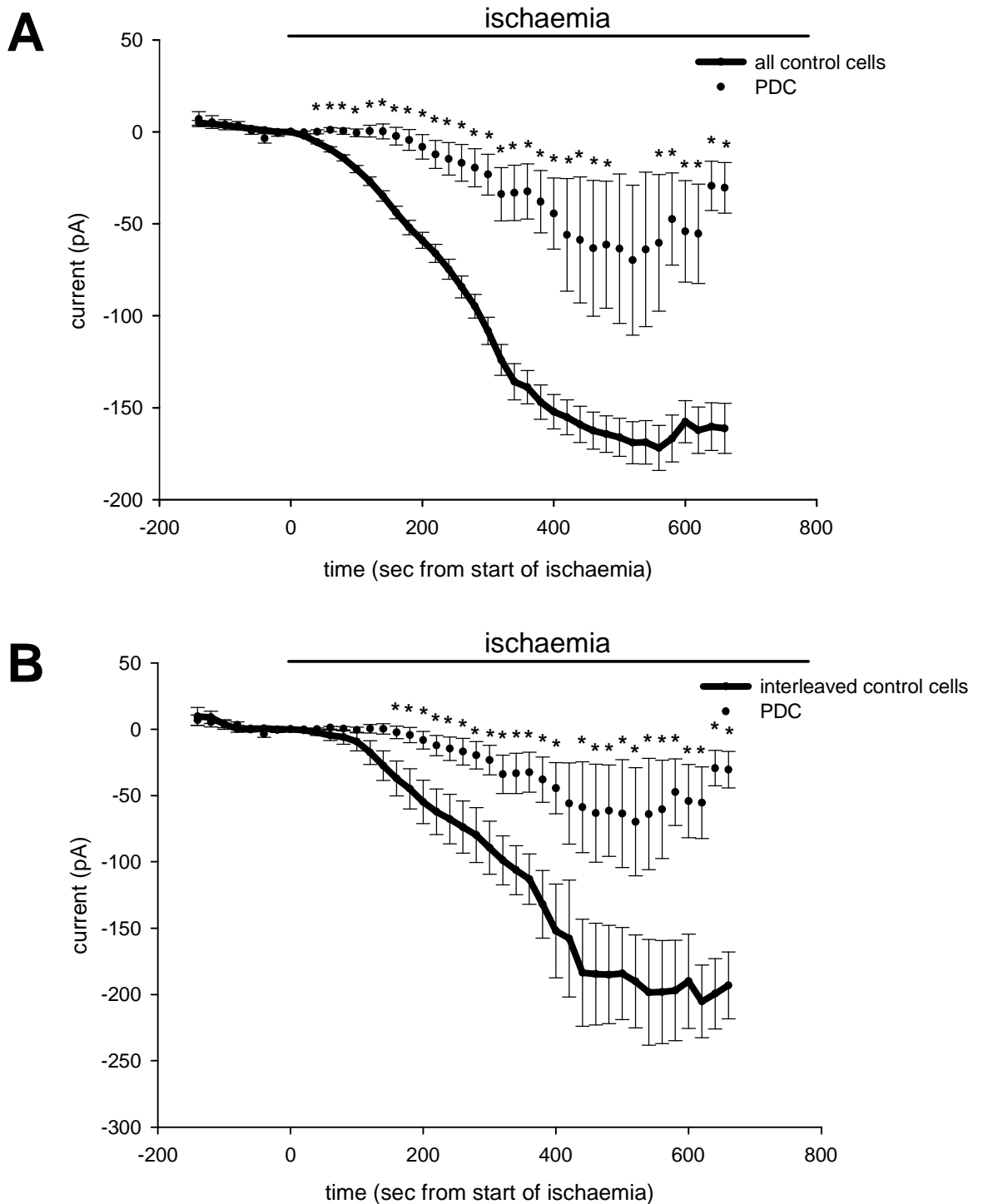
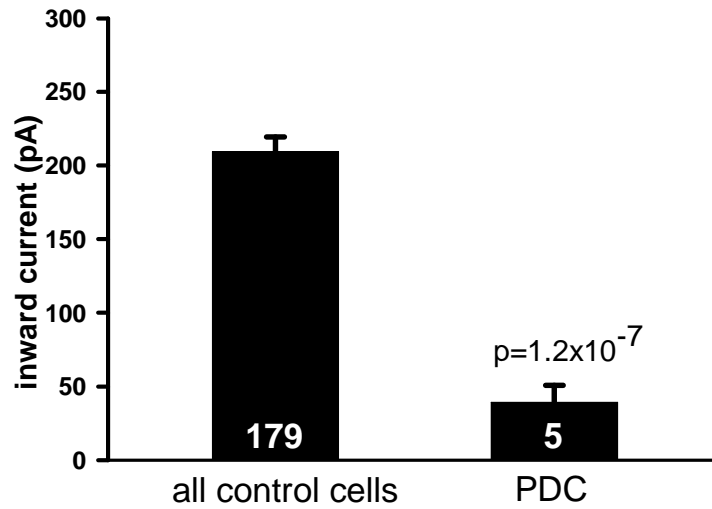
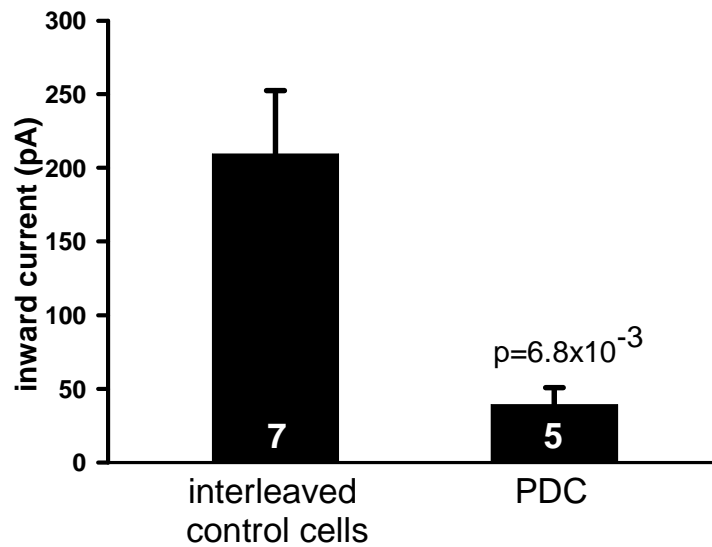


Figure 4.8

Preloading with the Na^+ -dependent glutamate transporter antagonist, PDC (1 mM), significantly reduces the ischaemia-induced current in oligodendrocytes. **A** Comparison between the averaged time course of the ischaemia-evoked current from 5 cells in slices preloaded with PDC and from all 179 control cells shows a significant decrease of the current amplitude when the slice was preloaded with the antagonist. **B** Comparison between the averaged time course of the ischaemia-evoked current in 5 cells studied with PDC-preloading and in 7 interleaved control cells (i.e. recorded on the same day) also shows a significant decrease of the current when the slice was preloaded with the antagonist. Ischaemia starts at $t=0$. * indicates statistically significant difference at the time point indicated ($p < 0.05$).

A**B****Figure 4.9**

The peak ischaemia-induced current is reduced by preloading with the glutamate transport blocker PDC (1 mM). **A** Comparing the average value of the peak of the ischaemia-induced current in all 179 control cells, and the average peak current in 5 cells in slices preloaded with PDC (n=5) shows a significant decrease of the current amplitude when the cells were preloaded with the antagonist. **B** Comparing the average peak ischaemia-induced control current in 7 control cells interleaved with 5 cells in slices preloaded with PDC also shows a significant decrease of the current when the cells were preloaded with the antagonist.

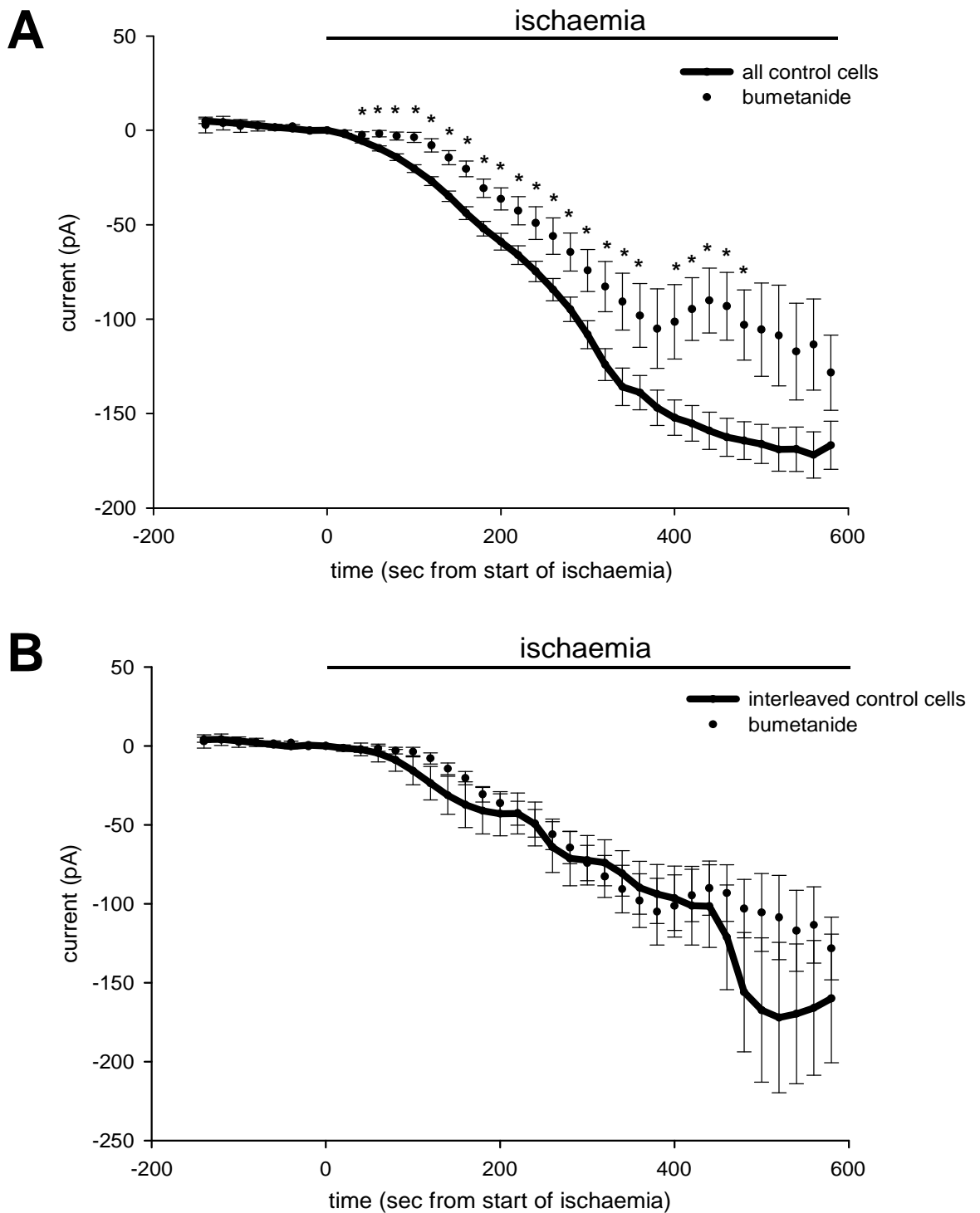


Figure 4.10

Effect of the NKCC1 co-transporter blocker, bumetanide (50 μ M), on the ischaemia-induced current in oligodendrocytes. **A** Averaged time course of the ischaemia-evoked control current from all 179 control cells and from 10 cells in slices treated with bumetanide. **B** Averaged time course of the ischaemia-evoked current in 10 cells in slices treated with bumetanide and in 10 control cells interleaved with the bumetanide-treated cells. Ischaemia starts at $t=0$. * indicates statistically significant difference at the time point indicated ($p<0.05$).

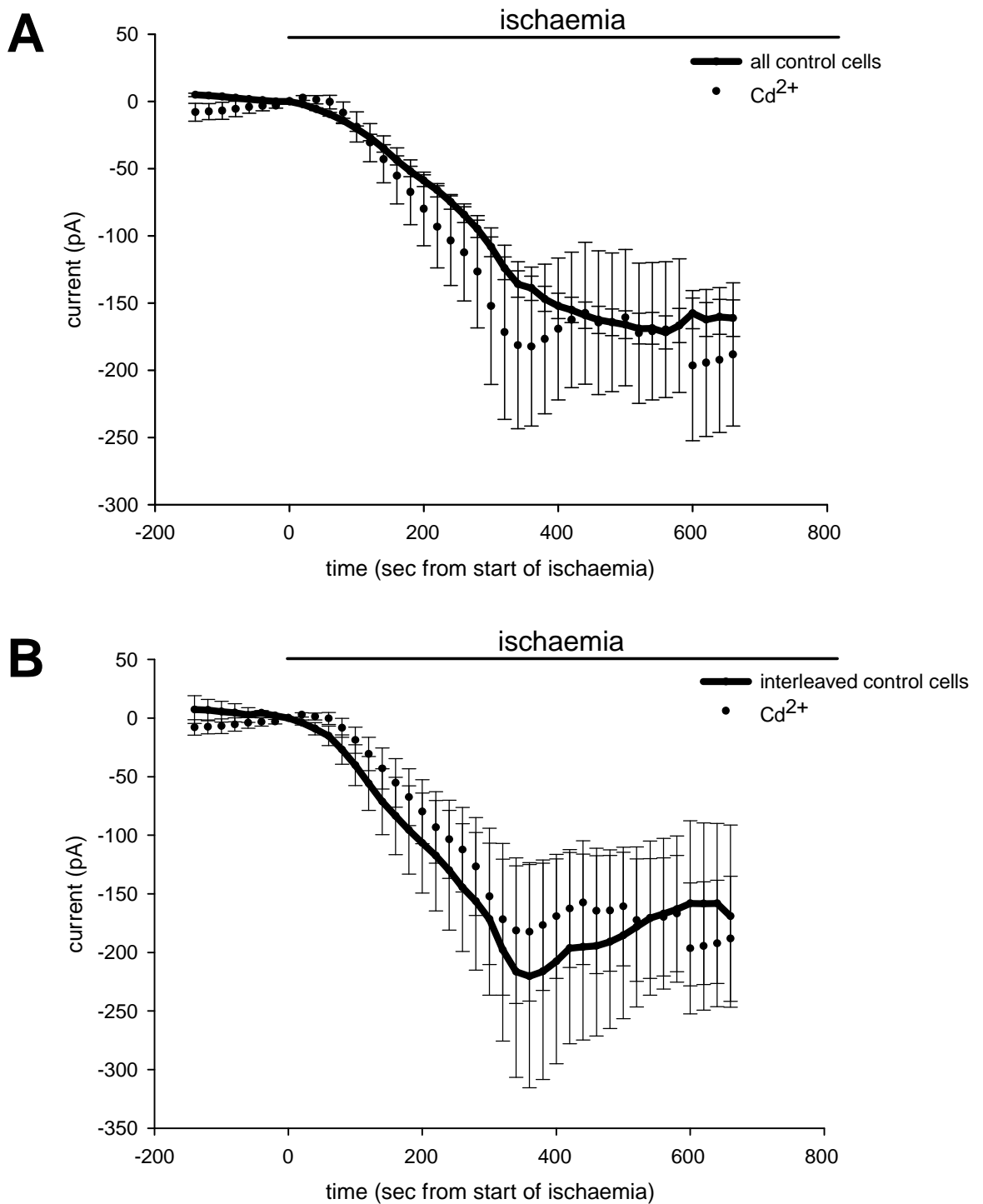


Figure 4.11

Effect of the voltage-gated calcium channel blocker cadmium (Cd^{2+} , 100 μM) which blocks exocytosis, on the ischaemia-induced current in oligodendrocytes. **A** Averaged time course of the ischaemia-evoked current from all 179 control cells and from 13 cells in slices treated with Cd^{2+} . **B** Averaged time course of the ischaemia-evoked current in 13 cells in Cd^{2+} and in 8 interleaved control cells. Ischaemia starts at $t=0$.

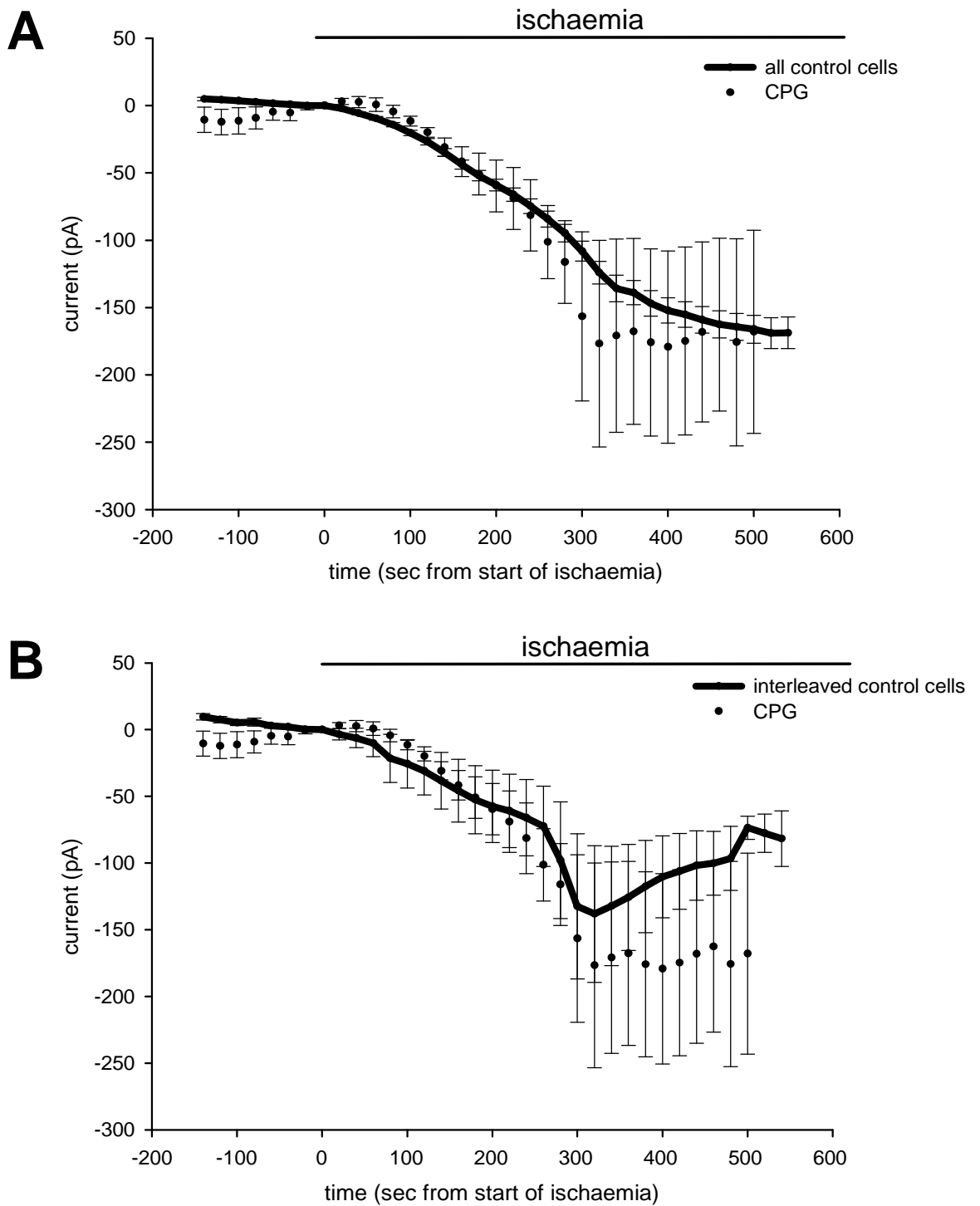


Figure 4.12

Effect of the cystine-glutamate exchanger (X_C^-) blocker, CPG (50 μM) on the ischaemia-induced current in oligodendrocytes. **A** Averaged time course of the ischaemia-evoked current in all 179 control cells, and in 5 cells from CPG-treated slices. **B** Averaged time course of the ischaemia-evoked current in 5 cells from slices treated with CPG and in 4 interleaved control cells. Ischaemia starts at $t=0$.

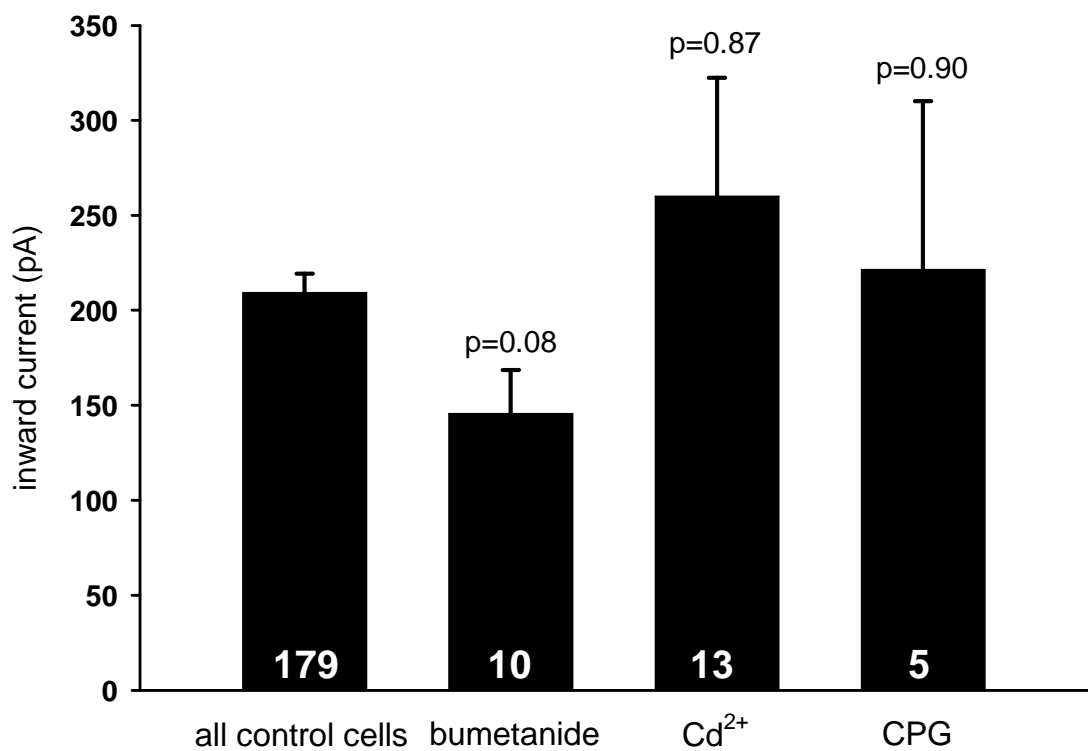


Figure 4.13

Comparison of the mean values for the peak of the ischaemia-induced inward current (measured for each cell and then averaged over all cells in the same condition) for all the 179 control cells and for cells with the different blockers applied shows that bumetanide (50 μ M), Cd²⁺ (100 μ M) and CPG (100 μ M) had no effect on the peak ischaemia-evoked current.

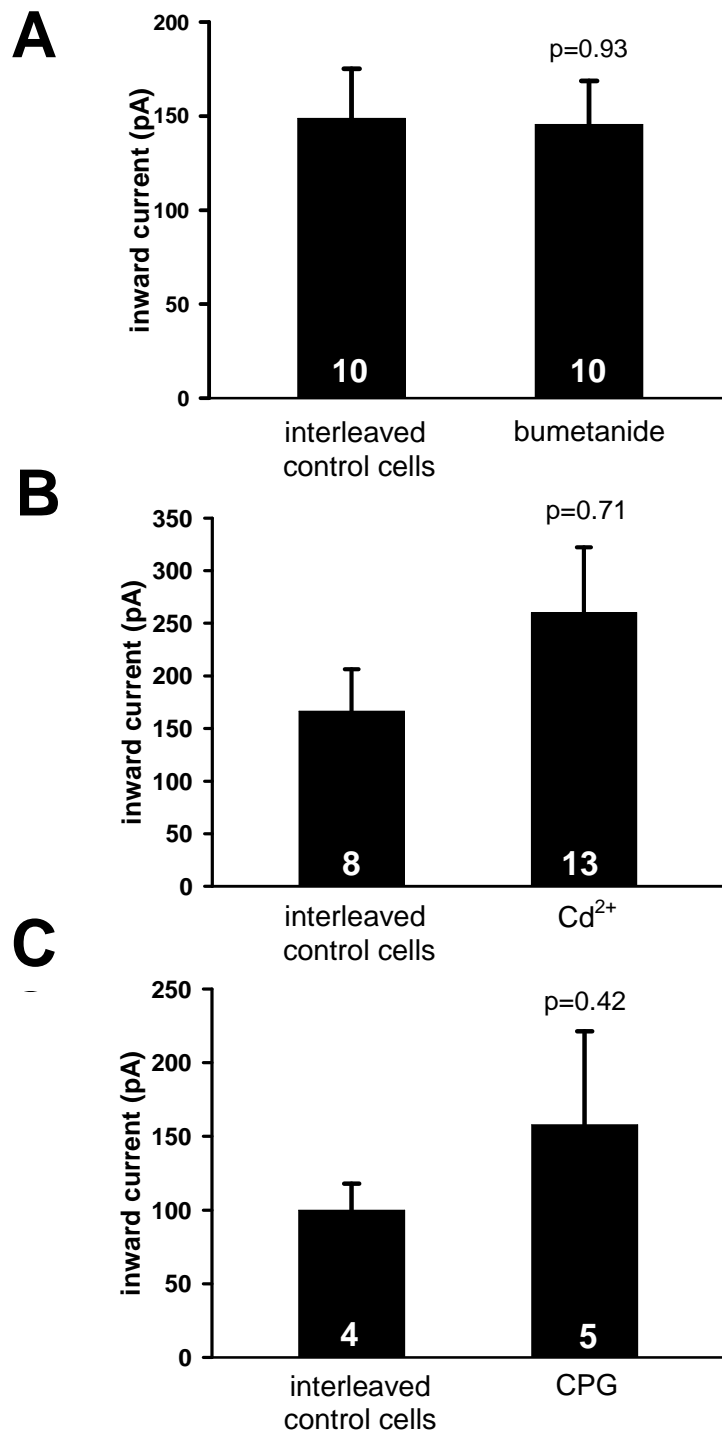


Figure 4.14

Comparison of the mean value for the peak of the ischaemia-induced inward current (measured for each cell and then averaged over all cells in the same condition) in the presence of various candidate drugs to block glutamate release and in interleaved control cells studied on the same day as each drug was studied. The blockers used were bumetanide (50 μ M), Cd²⁺ (100 μ M) and CPG (100 μ M). **A** Comparison between the average peak current in 10 cells studied in bumetanide-treated slices and in 10 interleaved control cells shows no significant effect of the blocker. **B** Comparison between the average peak current in 13 cells studied in Cd²⁺ and in 8 interleaved control cells shows no significant effect of the blocker. **C** Comparison between the average peak current in 5 cells studied in CPG and in 4 interleaved control cells shows no significant effect of the blocker.

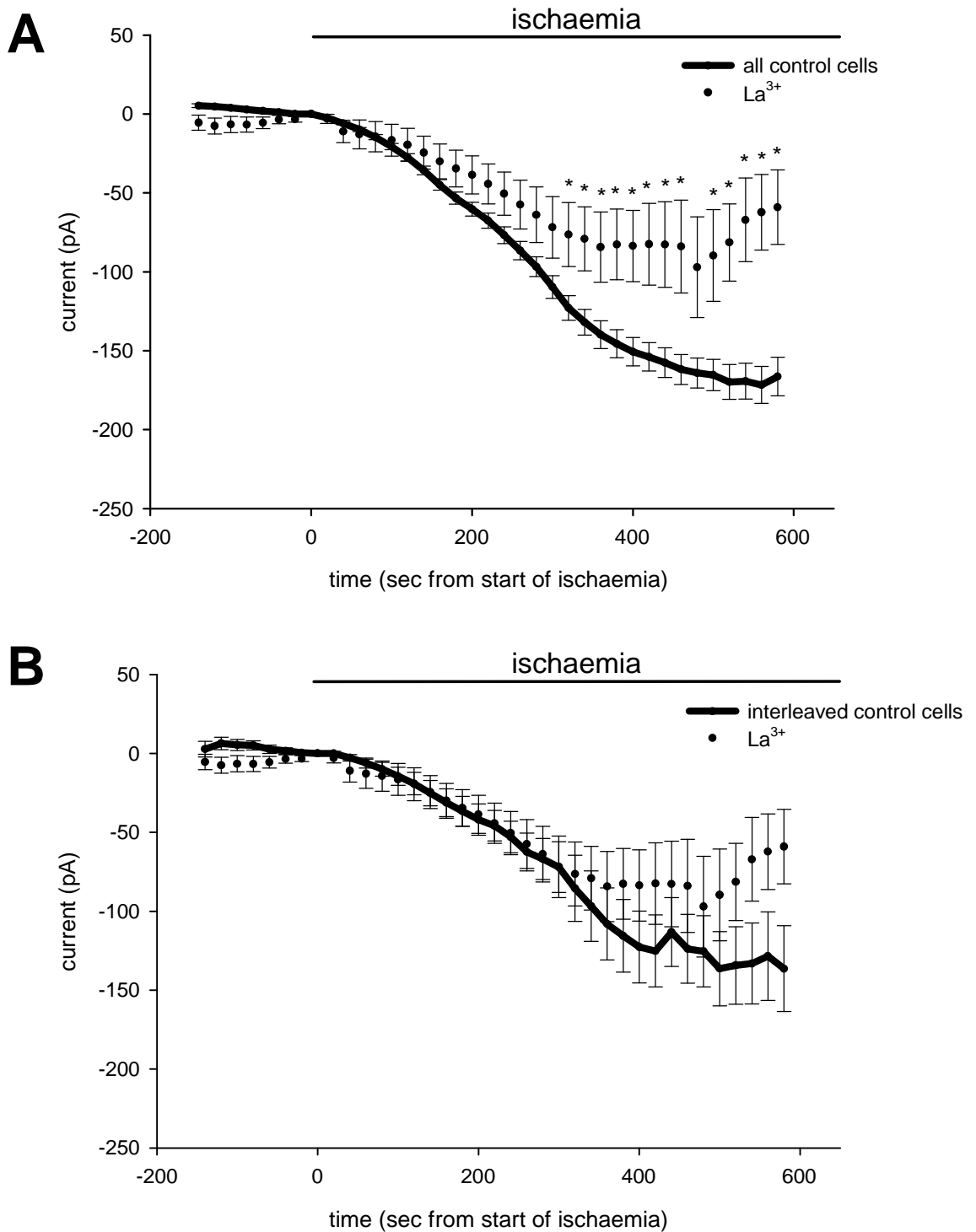


Figure 4.15

Effect of the gap junctional hemichannel blocker, lanthanum ($100 \mu\text{M}$) on the ischaemia-induced current in oligodendrocytes. **A** Averaged time courses of the ischaemia-evoked current in 11 cells from slices treated with La^{3+} and in all 179 control cells. **B** Averaged time courses of the ischaemia-evoked current in 11 cells from slices treated with La^{3+} and in 12 interleaved control cells (studied on the same day as La^{3+}). Both graphs show a late recovery of the current with the hemichannel blocker present that is absent in the control cells' current. Ischaemia starts at $t=0$. * indicates statistically significant difference at the time point indicated ($p<0.05$).

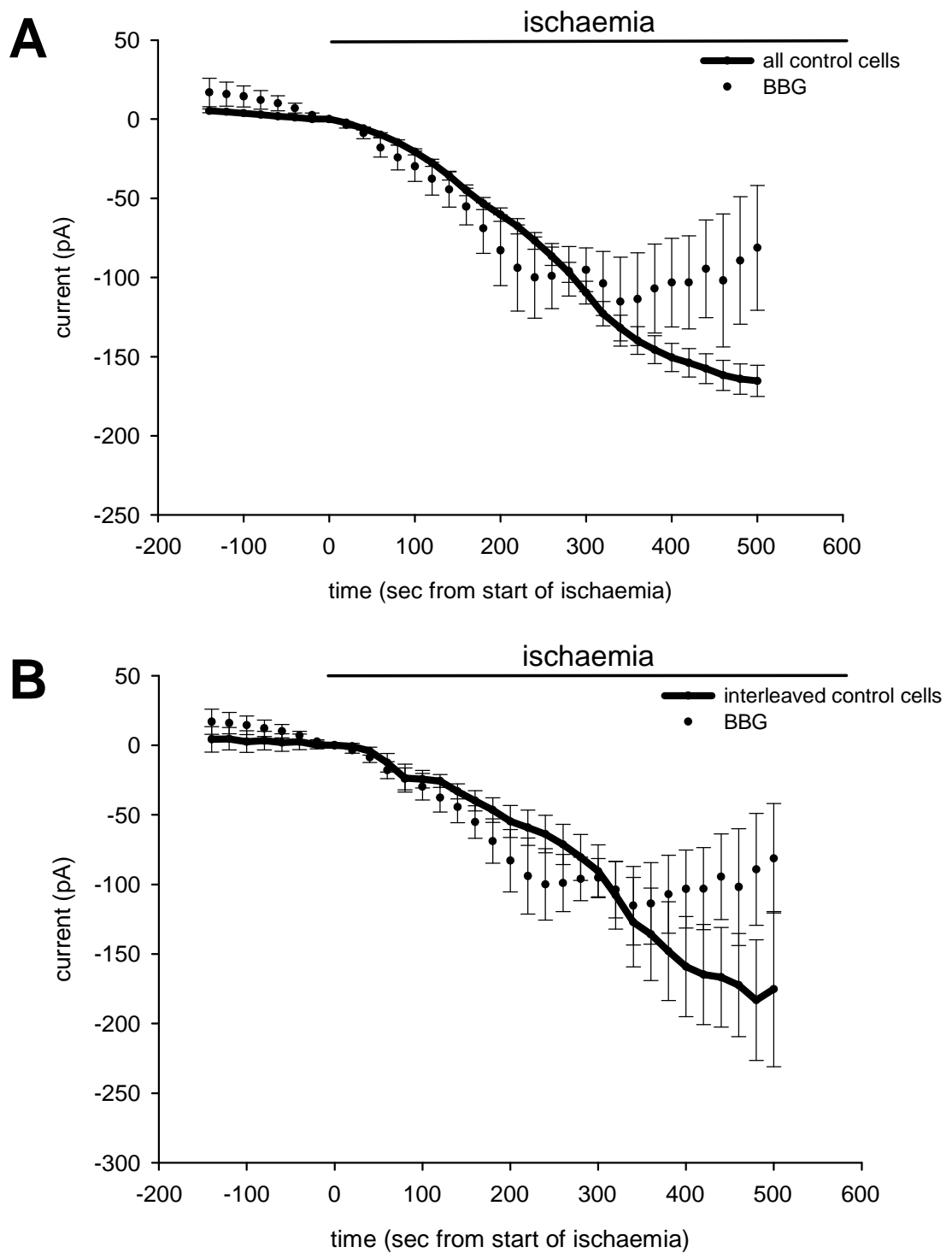


Figure 4.16

Effect of the P2X₇ receptor blocker, BBG (10 μM) on the ischaemia-induced current in oligodendrocytes. **A** Averaged time courses of the ischaemia-evoked current in 6 cells with BBG present and in all 179 control cells show that the current with BBG reaches an early peak and then shows a tendency to recovery which is not seen in the control current. **B** Averaged time courses of the ischaemia-evoked current in 6 cells with BBG and in 7 interleaved control cells (studied on the same day as BBG). Ischaemia starts at t=0.

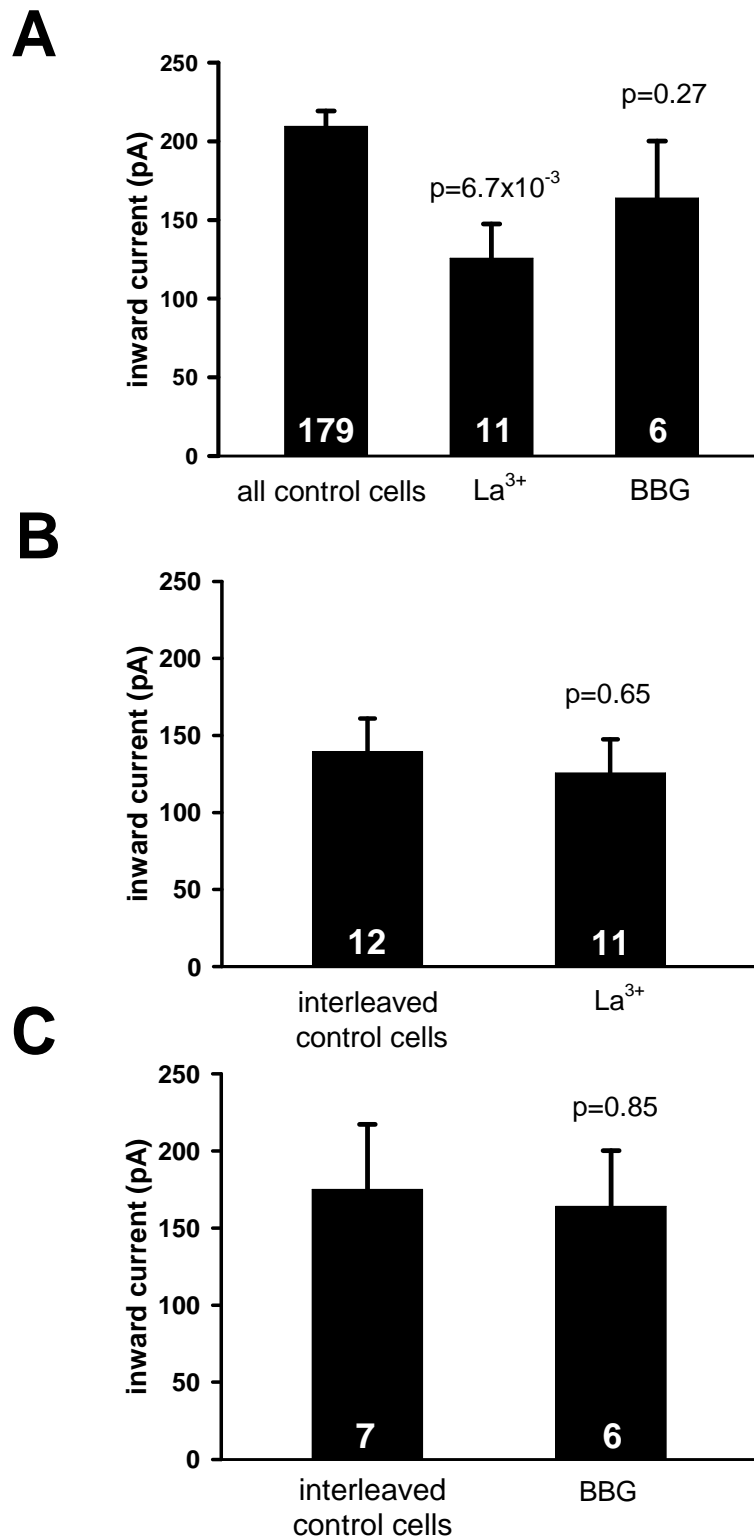


Figure 4.17

Effect of the gap junctional hemichannel blocker La³⁺ (100 μM) and the P2X₇ receptor blocker BBG (10 μM) on the peak ischaemia-evoked current (measured in each cell and then averaged across cells). **A** Average peak ischaemia-induced current in all 179 control cells, in 11 cells in the presence of La³⁺, and in 6 cells in BBG. **B** Average peak ischaemia-induced current in 11 cells studied with La³⁺ and in 12 interleaved control cells. **C** Average peak ischaemia-induced current in 6 cells studied with BBG and in 7 interleaved control cells.

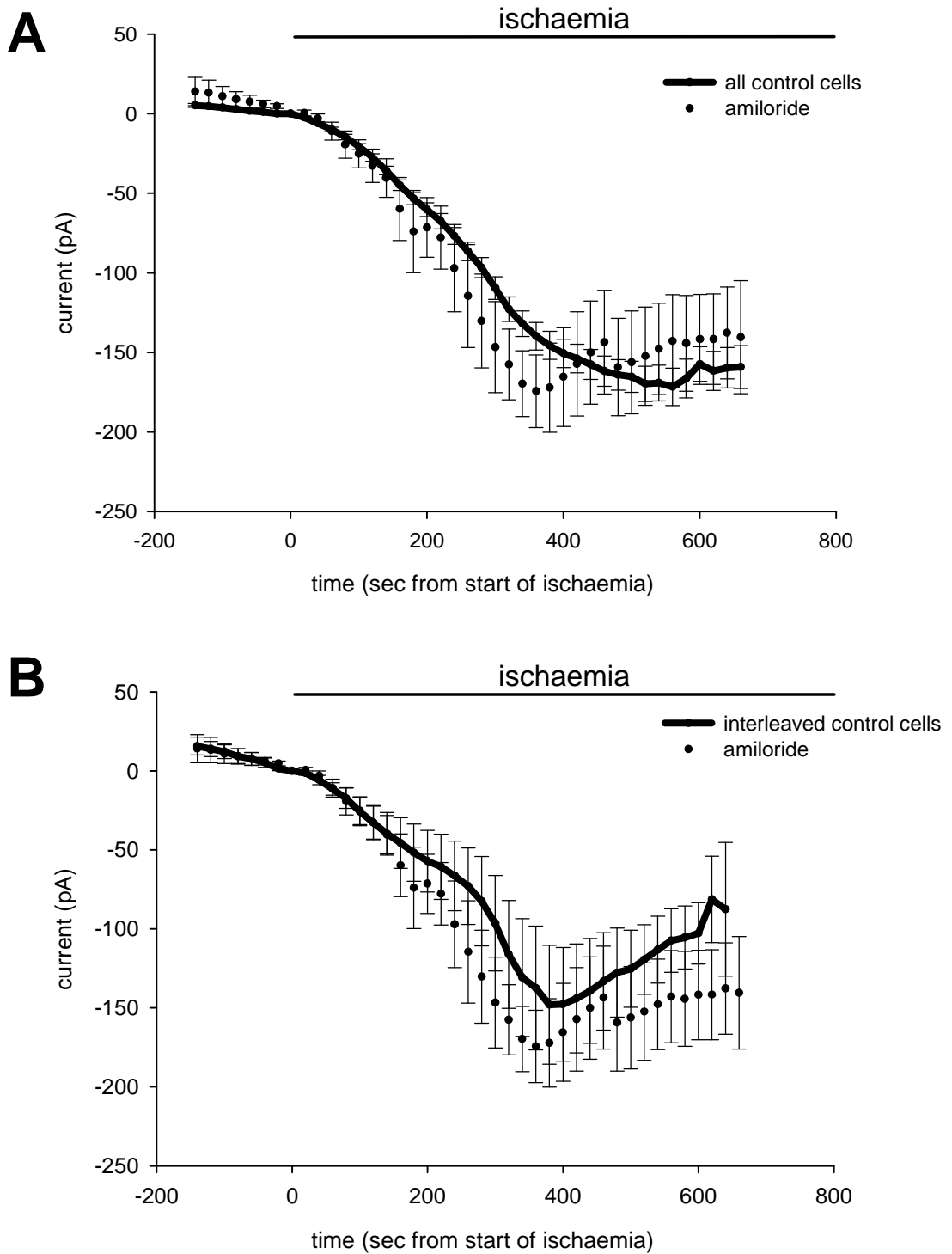


Figure 4.18

Effect of the ASIC blocker amiloride (100 μM) on the ischaemia-induced current in oligodendrocytes. **A** Averaged time courses of the ischaemia-evoked current in 6 cells studied with amiloride and in all 179 control cells. **B** Averaged time courses of the ischaemia-evoked current in 6 cells studied with amiloride and in 8 interleaved control cells studied on the same day as amiloride. Ischaemia starts at $t=0$.

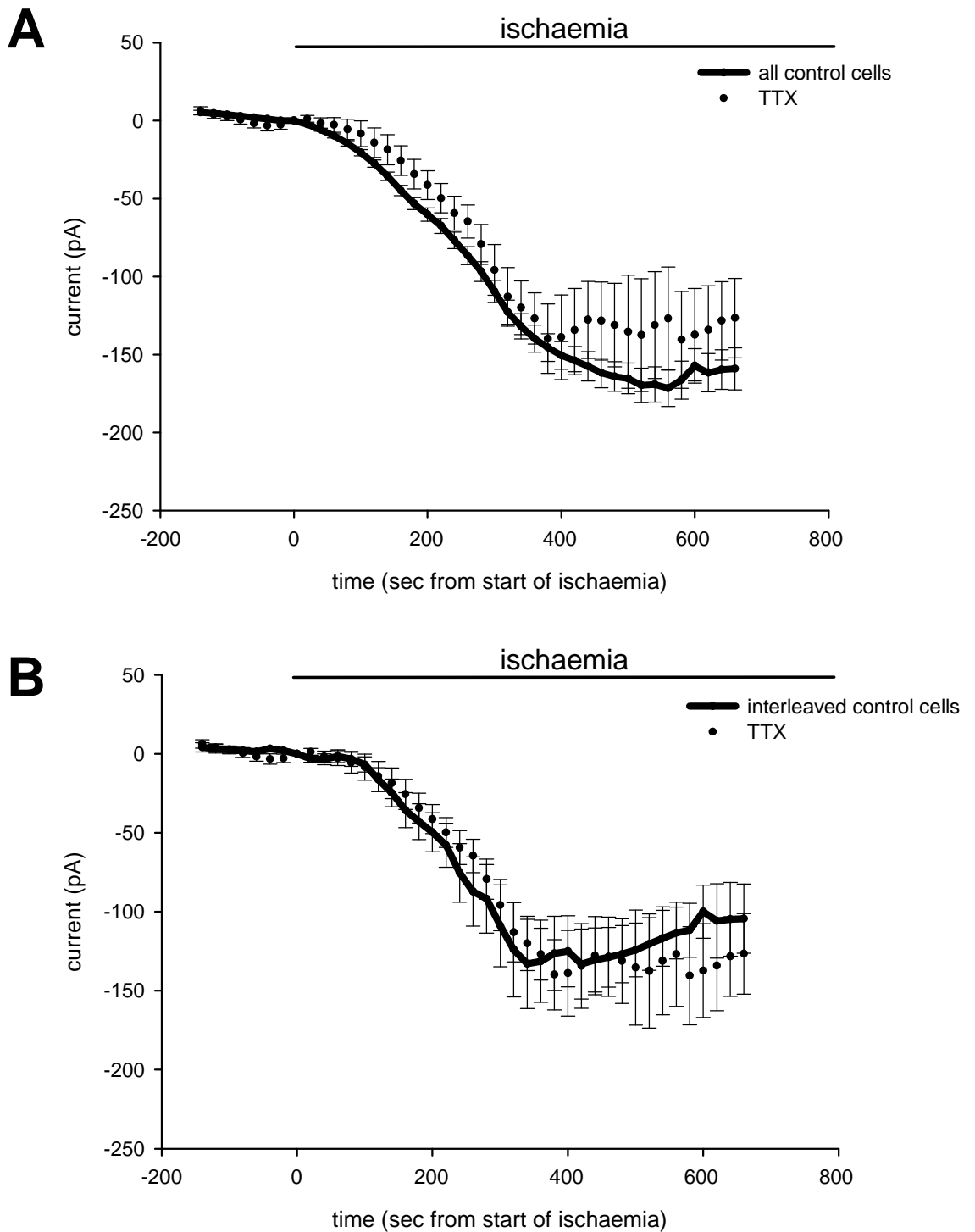


Figure 4.19

Effect of the action potential blocker TTX (1 μ M) on the ischaemia-induced current in oligodendrocytes. **A** Averaged time courses of the ischaemia-evoked current in 13 cells studied with TTX and in all 179 control cells. **B** Averaged time courses of the ischaemia-evoked current in 13 cells studied with amiloride and in 10 interleaved control cells studied on the same day as TTX. Ischaemia starts at $t=0$.

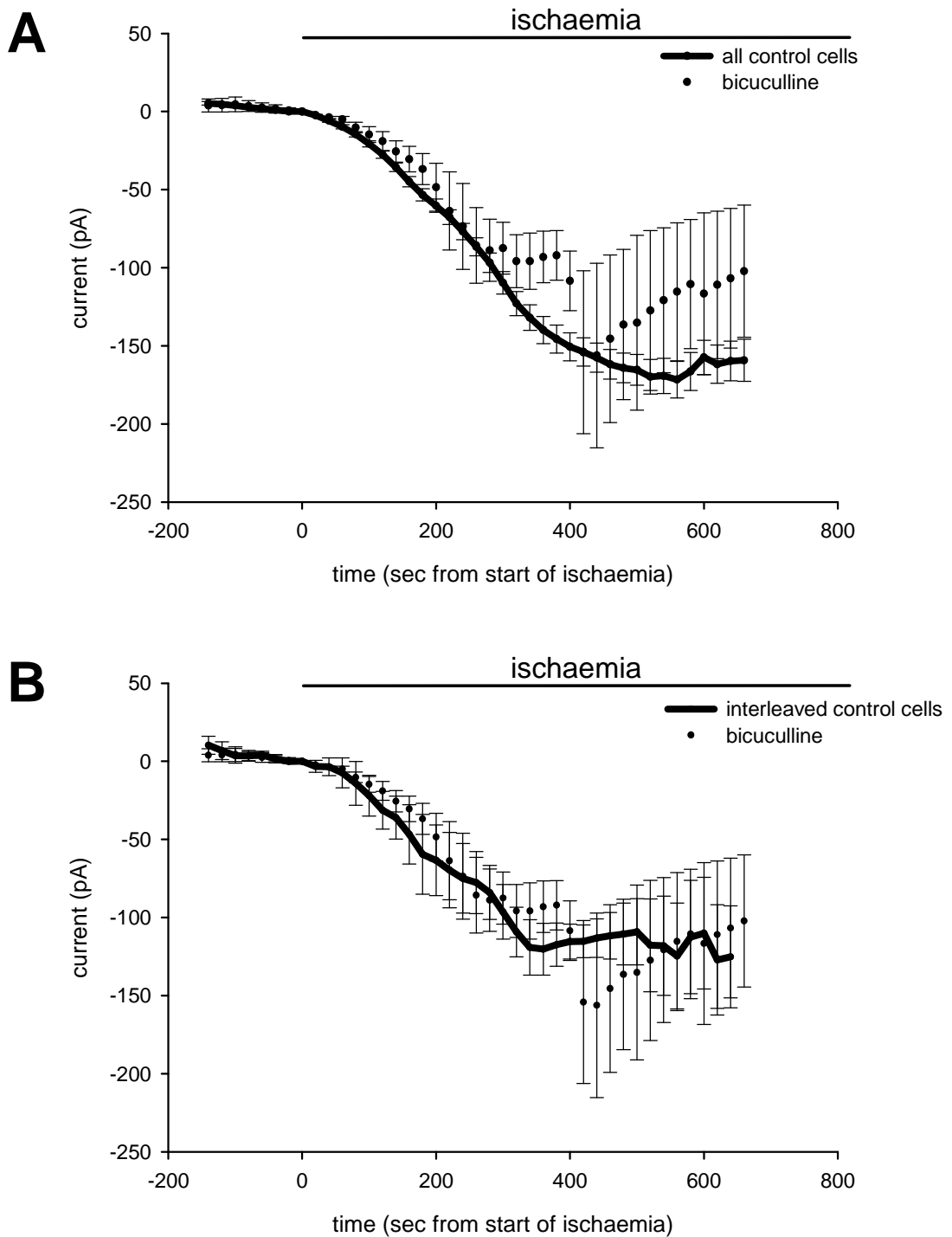


Figure 4.20

Effect of the GABA_A receptor blocker bicuculline (100 μM) on the ischaemia-induced current in oligodendrocytes. **A** Averaged time courses of the ischaemia-evoked current in 5 cells studied with bicuculline and in all 179 control cells. **B** Averaged time courses of the ischaemia-evoked control current in 5 cells studied with bicuculline and in 4 interleaved control cells studied on the same day as bicuculline. Ischaemia starts at t=0.

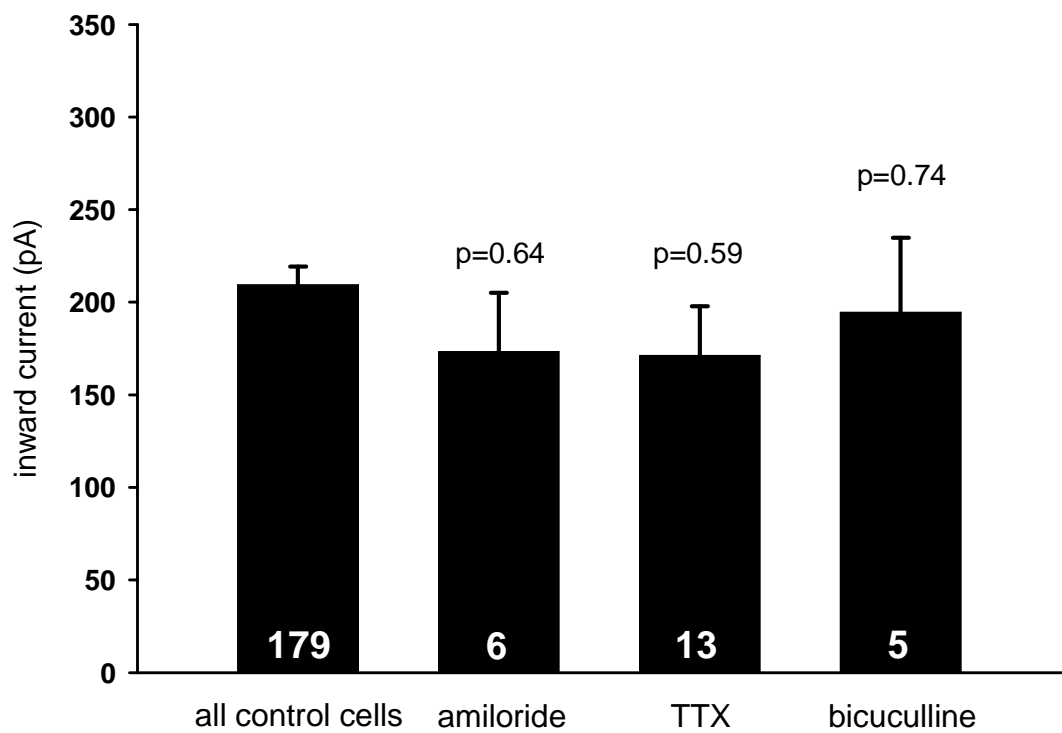


Figure 4.21

Comparison of the mean peak ischaemia-induced inward current of all 179 control cells with the mean peak current with the blockers applied shows that amiloride (100 μ M), TTX (1 μ M) and bicuculline (100 μ M) had no effect on the size of the peak of the ischaemic response.

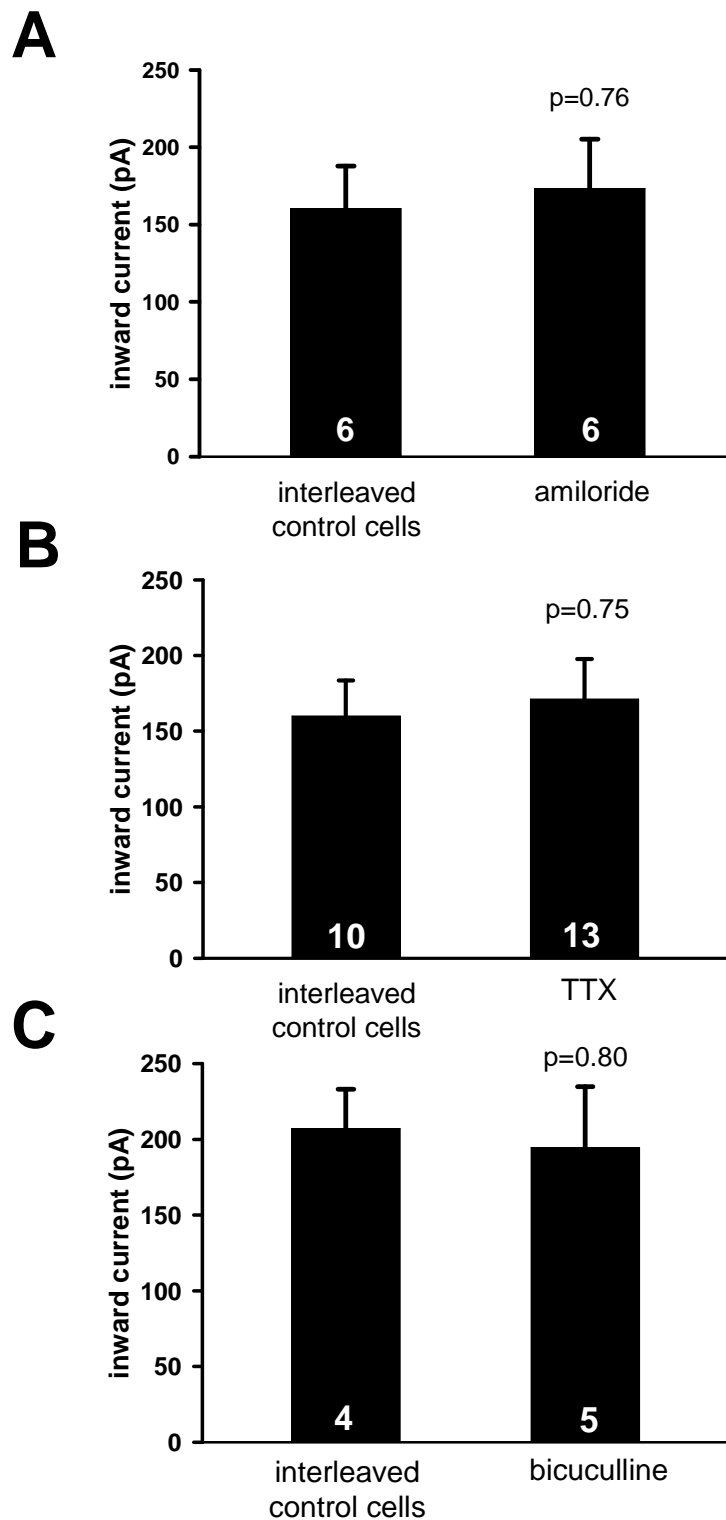


Figure 4.22

Comparison of the mean peak ischaemia-induced inward current in interleaved control cells (studied on the same day as the blockers) with the peak current evoked in the blockers shows that amiloride (100 μ M), TTX (1 μ M) and bicuculline (100 μ M) had no effect on the size of the peak ischaemia-evoked current. **A** Average peak ischaemia-induced current in 6 cells in amiloride and in 6 interleaved control cells. **B** Average peak ischaemia-induced current in 13 cells studied with TTX and in 10 interleaved control cells. **C** Averaged peak ischaemia-induced current in 5 cells studied in bicuculline and in 4 interleaved control cells.

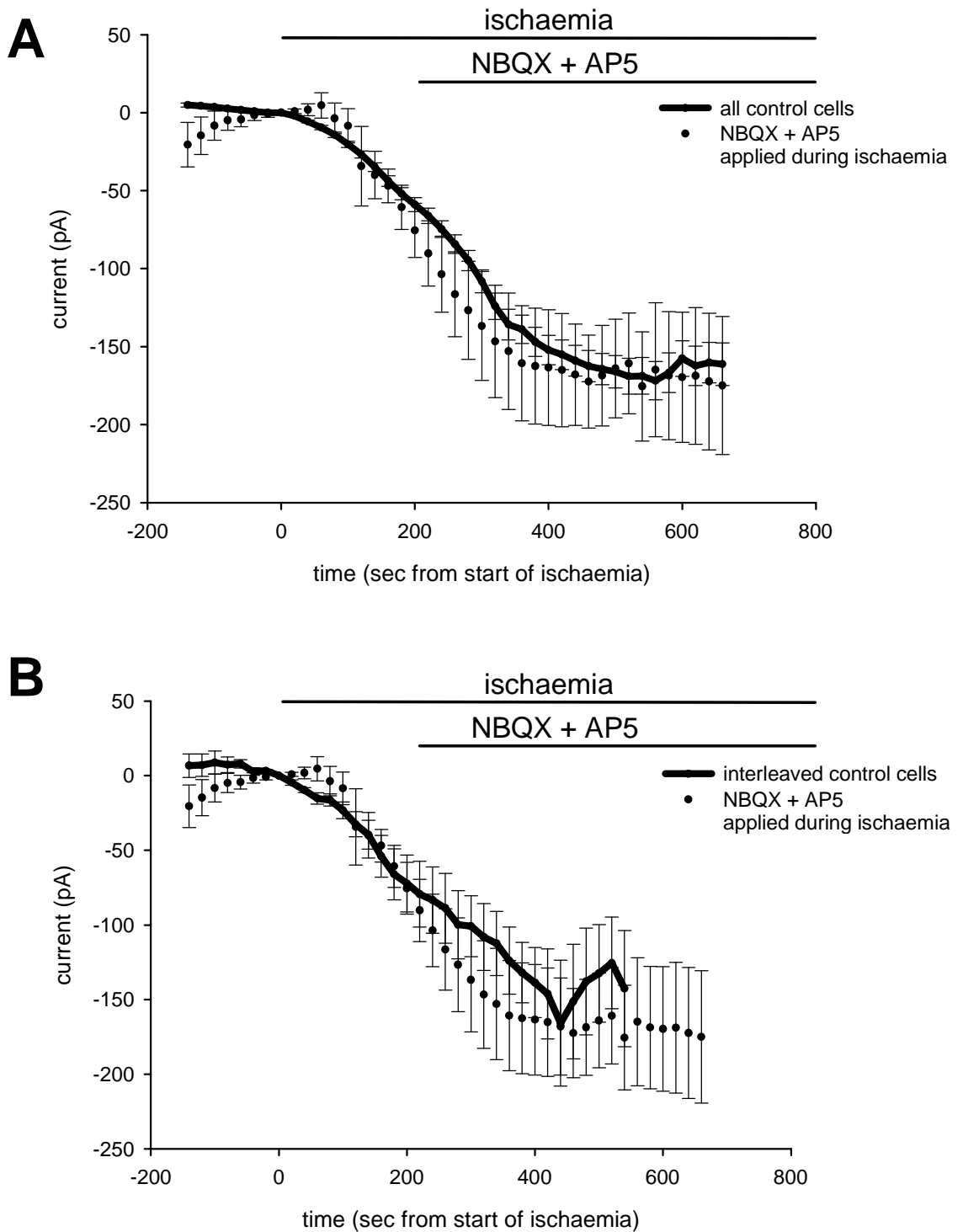


Figure 4.23

The AMPA/KA receptor blocker NBQX (25 μ M) and NMDA receptor blocker AP5 (50 μ M) do not block the ischaemia-induced current in oligodendrocytes once it has started. NBQX and AP5 were applied \sim 3.5 min after the start of ischaemia. **A** Averaged time courses of the ischaemia-evoked current in 6 cells to which NBQX and AP5 were applied \sim 3.5 min after the start of ischaemia and in all 179 control cells. **B** Averaged time courses of the ischaemia-evoked current in 6 cells to which NBQX and AP5 were applied \sim 3.5 min after the start of ischaemia and in 4 interleaved control cells. Ischaemia starts at $t=0$.

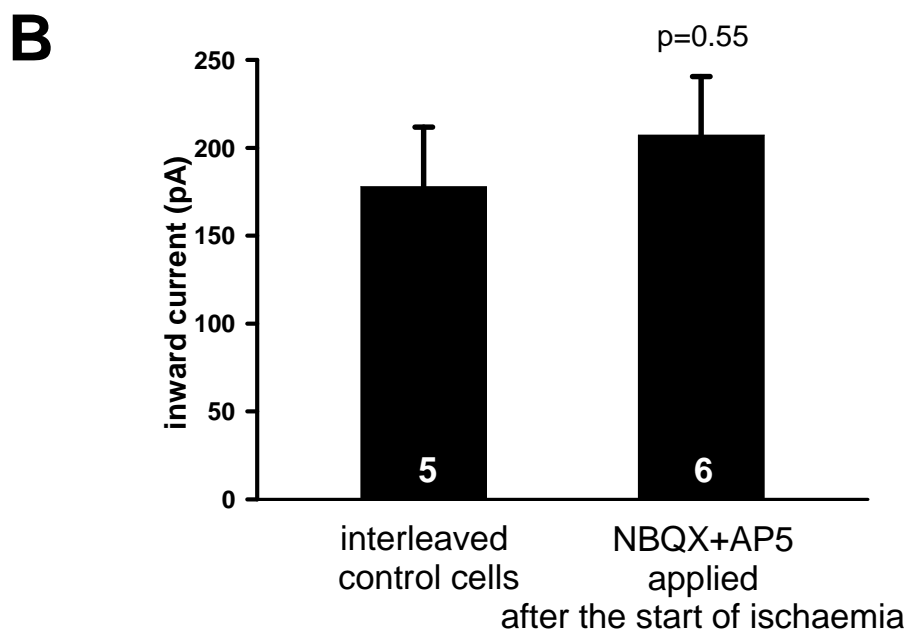
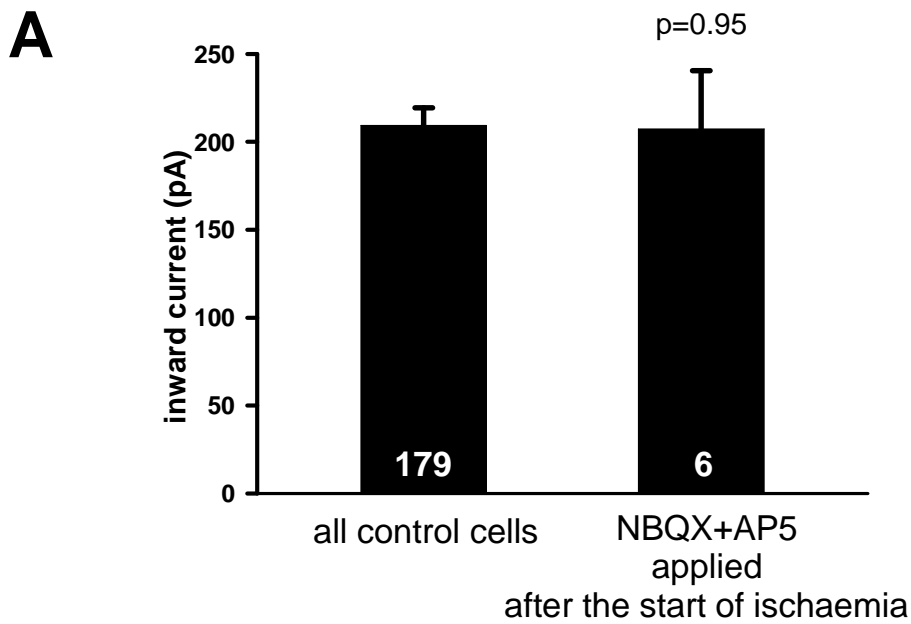


Figure 4.24

Comparison of the averaged peak ischaemia-induced current in control cells and in cells with NBQX (25 μ M) and AP5 (50 μ M) applied \sim 3.5 min after the start of ischaemia shows that the ionotropic receptor blockers had no effect on the peak response. **A** Average peak of the ischaemia-induced current in 6 cells to which NBQX and AP5 were applied after the start of ischaemia and in all 179 controls cells. **B** Average peak ischaemia-induced current in 6 cells to which NBQX and AP5 were applied \sim 3.5 min after the start of ischaemia and in 5 interleaved control cells studied on the same day.

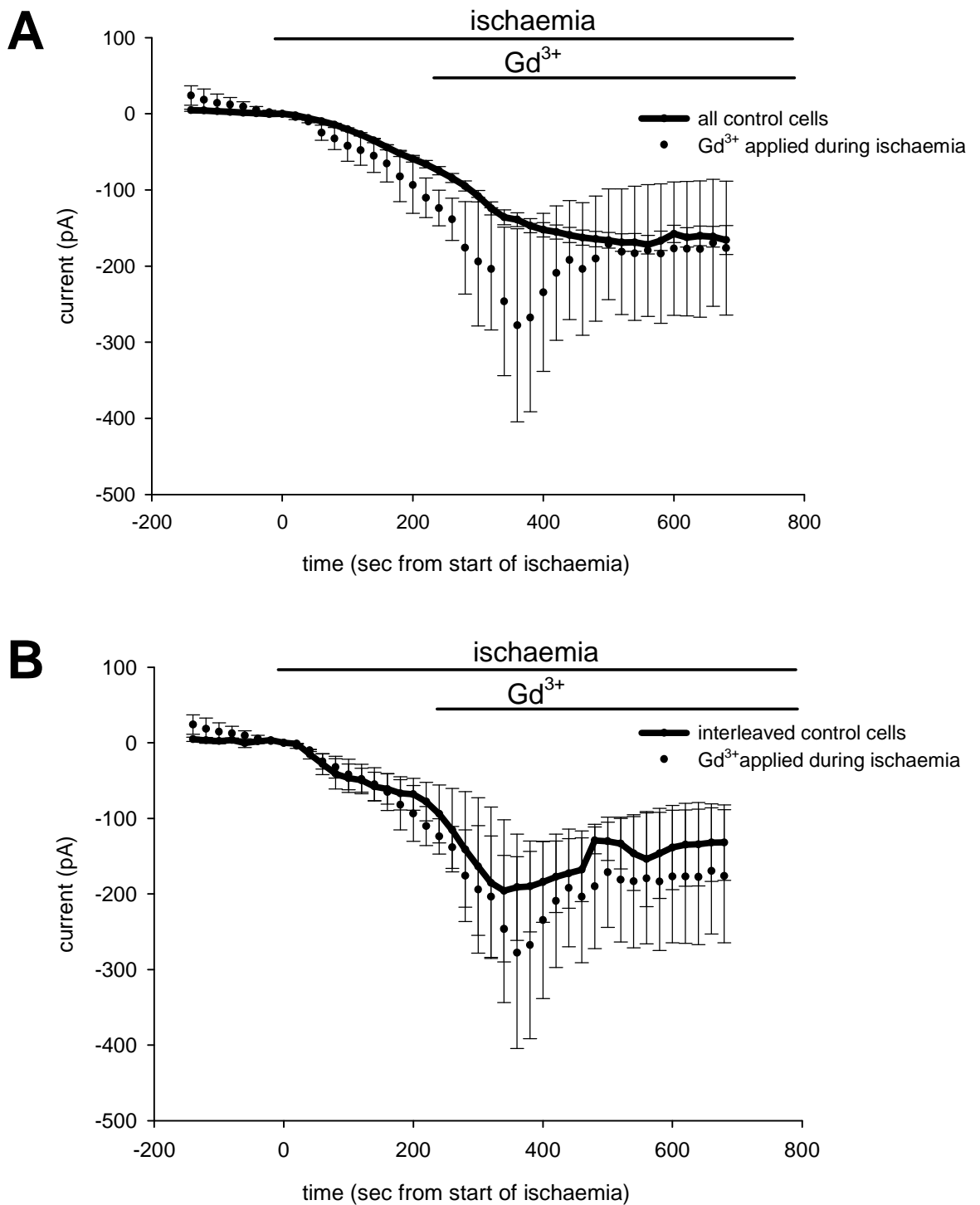


Figure 4.25

The extended neuronal depolarization (END) blocker, gadolinium (100 μ M), when applied from \sim 4 min after the start of ischaemia, does not block the ischaemia-induced current in oligodendrocytes. **A** Averaged time course of the ischaemia-evoked current in 3 cells studied with Gd³⁺ applied from \sim 4 min after the start of ischaemia and in all 179 control cells. **B** Averaged time course of the ischaemia-evoked current in 3 cells studied with Gd³⁺ applied from \sim 4 min after the start of ischaemia and in 3 interleaved control cells studied on the same day. Ischaemia starts at t=0.

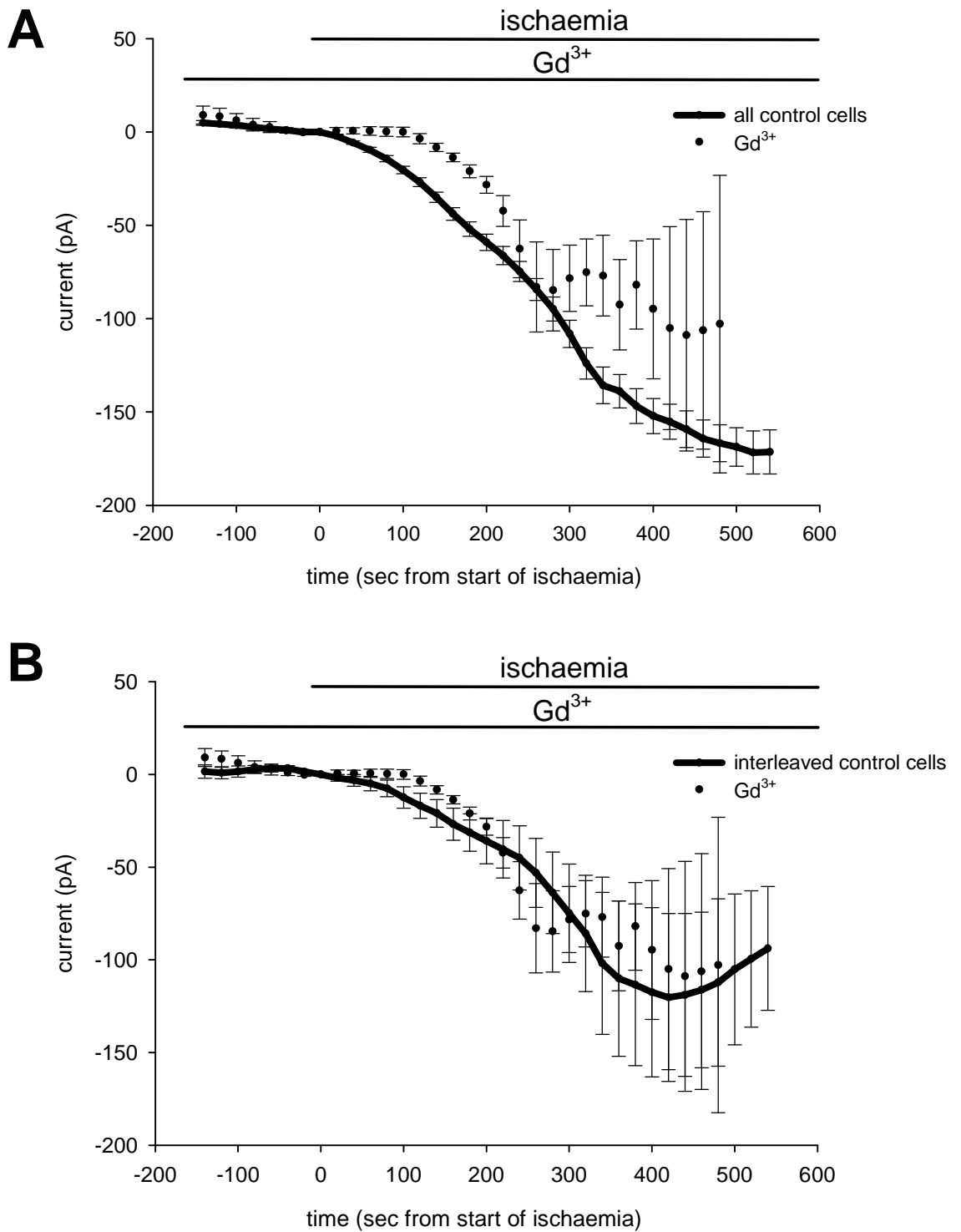


Figure 4.26

The extended neuronal depolarization (END) blocker, gadolinium (100 μM), when applied throughout ischaemia, does not block the ischaemia-induced current in oligodendrocytes. **A** Averaged time courses of the ischaemia-evoked current from 7 cells in Gd³⁺ and in all 179 control cells. **B** Averaged time courses of the ischaemia-evoked current in 7 cells in Gd³⁺ and in 6 interleaved control cells studied on the same day as Gd³⁺. Ischaemia starts at $t=0$.

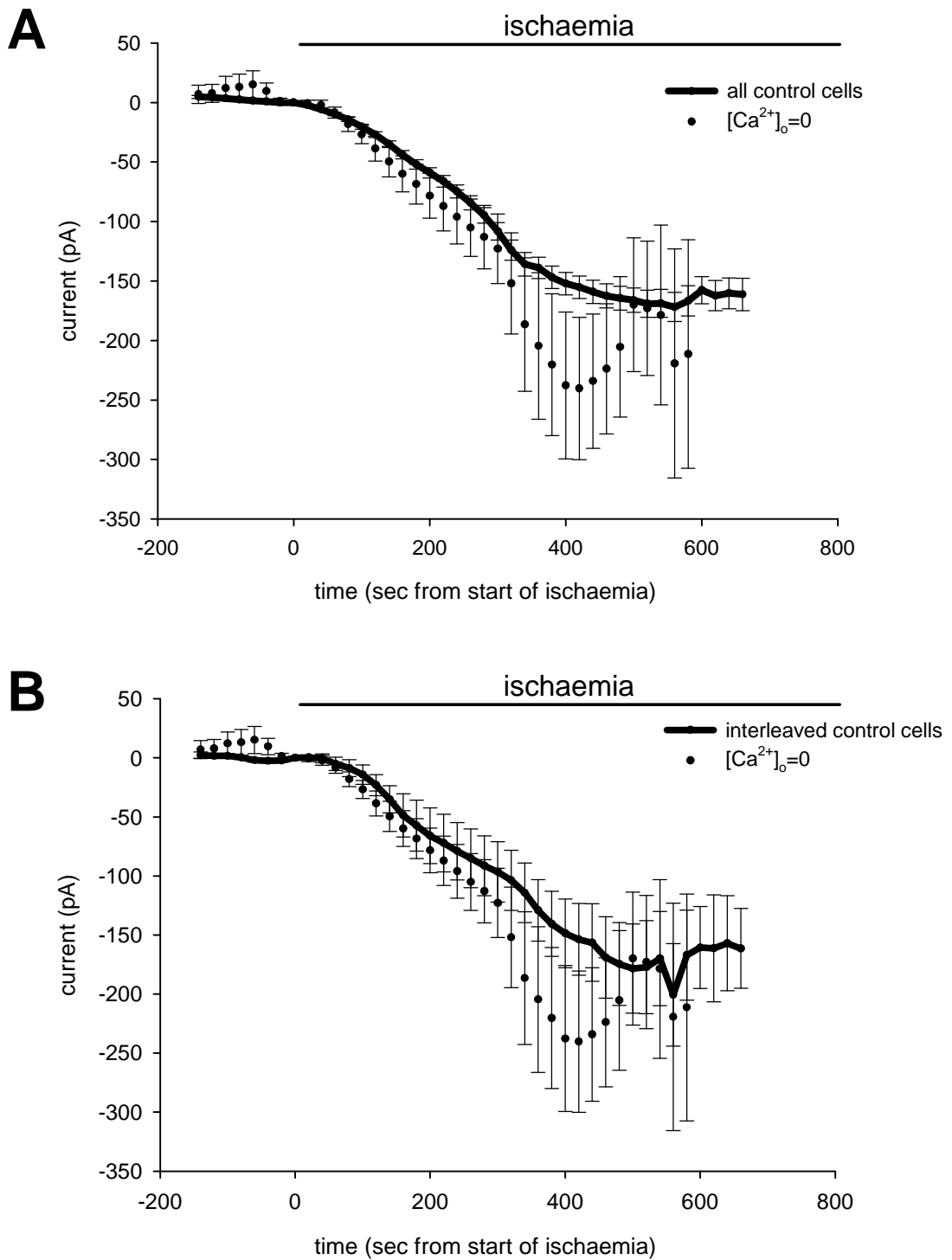


Figure 4.27

The omission of calcium (with 50 μ M EGTA added to bind trace calcium) throughout ischaemia, which blocks the extended neuronal depolarization in neurons, does not block the ischaemia-induced current in oligodendrocytes. **A** Averaged time courses of the ischaemia-evoked current in 6 cells in zero Ca^{2+} external solution and in all 179 control cells. **B** Averaged time courses of the ischaemia-evoked current in 6 cells in zero Ca^{2+} external solution and in 10 interleaved control cells studied on the same day as the omission of Ca^{2+} . Ischaemia starts at $t=0$.

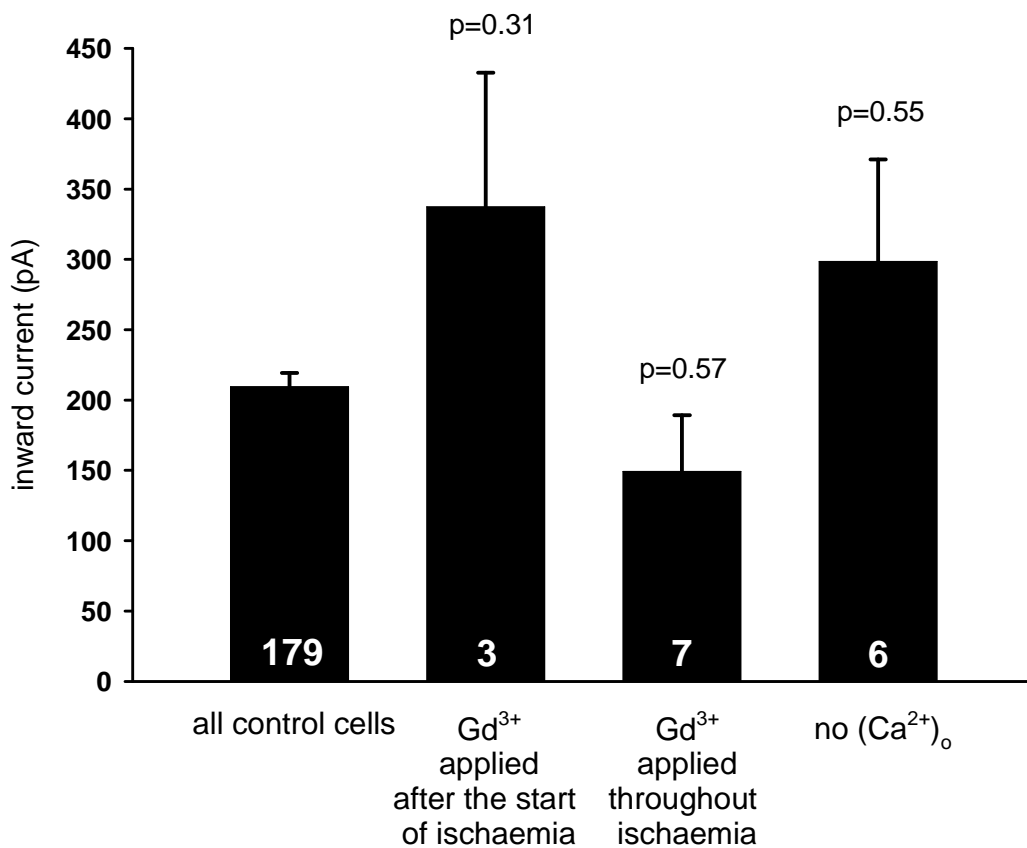


Figure 4.28

Average peak ischaemia-induced inward current for all 179 control cells and for 3 cells studied with Gd³⁺ present from ~4 min after the start of ischaemia, 7 cells studied with Gd³⁺ present throughout ischaemia and 6 cells studied in the absence of extracellular Ca²⁺ throughout ischaemia.

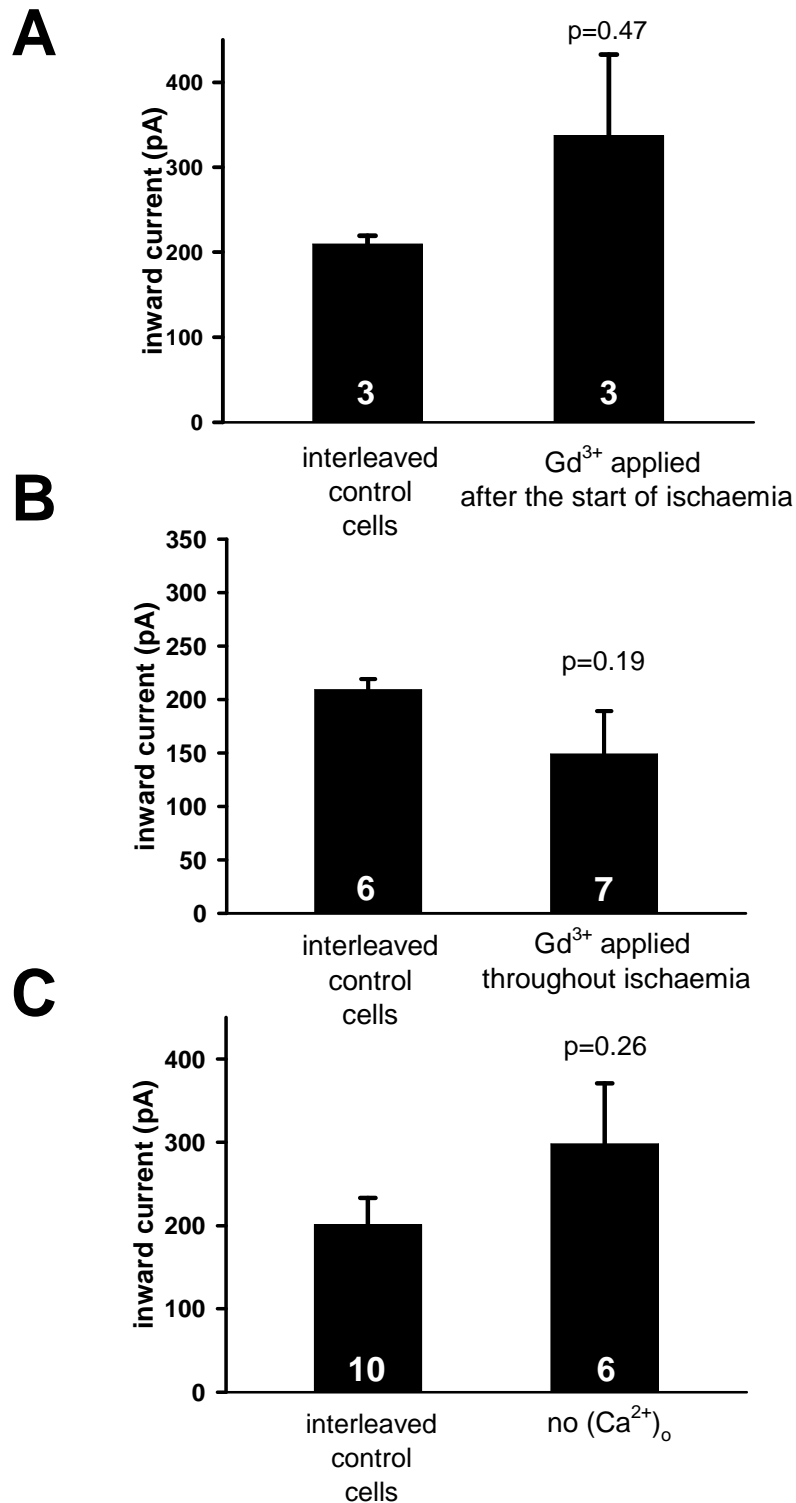


Figure 4.29

Comparing the peak ischaemia-induced inward current for manipulations that block the END and for interleaved control cells shows that Gd³⁺ (100 μM) applied after the start or throughout ischaemia, as well as the omission of extracellular Ca²⁺ throughout ischaemia (with EGTA, 50 μM), had no significant effect on the size of the peak ischaemia-evoked current. **A** Average peak ischaemia-induced current in 3 cells with Gd³⁺ applied ~4 min after the start of ischaemia and in 3 interleaved control cells. **B** Average peak ischaemia-induced current in 7 cells with Gd³⁺ present throughout ischaemia and in 6 interleaved control cells. **C** Average peak ischaemia-induced current in 6 cells recorded in zero external calcium solution throughout ischaemia and in 10 interleaved control cells.

Chapter 5: Oligodendroglial and neuronal electrical responses to NAA and NAAG

5.1 Introduction

Elevations of the levels of N-acetyl-aspartyl-glutamate (NAAG) and N-acetyl-aspartate (NAA) are associated with myelin loss in the leukodystrophies Canavan disease (CD) and Pelizaeus-Merzbacher-like Disease (PMLD) which, respectively, are caused by mutations in the genes for aspartoacylase (which converts NAA into aspartate and acetate: see Fig 1.16) and – in some cases of PMLD - by mutations in the gene for a gap junctional protein, Cx47 (which makes heterologous gap junctions with astrocytes; Pastor *et al.*, 1998; Orthmann-Murphy *et al.*, 2008). As reviewed in Chapter 1, NAAG and NAA have been reported to activate and antagonise neuronal NMDA receptors (Westbrook *et al.*, 1986; Sekiguchi *et al.*, 1992; Burlina *et al.*, 1994; Koenig *et al.*, 1994; Valivullah *et al.*, 1994; Rubinet *et al.*, 1995; Pliss *et al.*, 2000; Bergeron *et al.*, 2005), as well as to act on metabotropic glutamate receptors (NAAG acts on group II mGluRs (Wroblewska *et al.*, 1997; 1998), while NAA activates an unknown class of mGluRs to evoke a membrane current (Yan *et al.*, 2003)). Oligodendrocytes and their precursors have recently been shown to express NMDA receptors, the activation of which in ischaemia leads to the death of oligodendrocyte precursors and the loss of myelin (Káradóttir *et al.*, 2005; Salter and Fern, 2005; Micu *et al.*, 2006). This raises the possibility that the failure to develop myelin (dysmyelination) or the loss of already formed myelin (demyelination) occurring in the leukodystrophies could reflect an action of NAAG or NAA on oligodendrocyte NMDA receptors.

To examine this possibility, I performed electrophysiological recordings from mature oligodendrocytes in the cerebellar white matter and compared their responses to NAA and NAAG with those evoked in neurons (cerebellar granule cells). I wanted to characterise the oligodendrocyte and neuron membrane current responses to NAAG

and NAA, determine which receptor is responsible for any evoked current detected, and ascertain whether any current generated in oligodendrocytes reflects a direct action of NAAG and NAA on oligodendrocyte receptors or an indirect action mediated by neurons. Since the actions of NAA and NAAG on NMDA receptors have been reported at relatively high concentrations (Westbrook *et al.*, 1986; Valivullah *et al.*, 1994; Rubin *et al.*, 1995), a specific aim was to determine whether responses were evoked by pathologically-relevant concentrations of these substances, as are measured to occur in Canavan disease and Pelizaeus-Merzbacher-like disease.

5.2 Materials and methods

5.2.1 Brain slice preparation

Cerebellar slices were prepared from P12 rats as described in section 2.1. Slices were immersed and patch clamped in a HEPES-based solution (described in section 2.2.1) at room temperature with a flow rate of 2-4 ml/min. Usually MgCl_2 was omitted from the solution, and glycine (100 μM , to ensure activation of the glycine site of NMDA receptors) and strychnine (5 μM , to block glycine-gated chloride channels) were added. A single set of experiments, shown in Fig. 5.11, was performed in physiological (1 mM) Mg^{2+} and with no added glycine. NAA and NAAG were from Tocris, UK. HPLC data supplied by Tocris showed that 1 mM NAAG contained less than 0.2 μM contaminating glutamate.

5.2.2 Patch-clamping

White matter oligodendrocytes and cerebellar granule cells were identified (as described in section 2.5), and whole-cell patch-clamped (as described in section 2.6). Pipettes contained Cs^+ -based internal solution (see Table 2.1) to provide a better voltage-clamp quality. Series resistance was 10-30 $\text{M}\Omega$, and was not compensated. The membrane potential was held at -74 mV (including the junction potential of -14 mV).

5.2.3 Statistics

Data are presented as mean \pm s.e.m. P values are from Student's 2-tailed t-tests.

5.3 Results

5.3.1 The effect of NAA and NAAG on oligodendrocyte and granule cell currents

Both NAAG and NAA have been previously described to induce an inward current in neurons (Westbrook *et al.*, 1986; Yan *et al.*, 2003), and both can activate neuronal NMDA receptors (Westbrook *et al.*, 1986; Valivullah *et al.*, 1994; Rubin *et al.*, 1995). It was not known, however, whether these substances can activate the recently reported oligodendrocyte NMDA receptors that have an unusual subunit composition (Káradóttir *et al.*, 2005; Salter and Fern, 2005; Micu *et al.*, 2006).

To test if NAAG and NAA can induce a current in oligodendrocytes, I applied high concentrations of NAAG (1 mM) and NAA (1 mM), and used NMDA (60 μ M) as a positive control. These high concentrations of NAA and NAAG were used to determine whether there was any possibility of these agonists activating the cells' NMDA receptors, because earlier work (Westbrook *et al.*, 1986; Valivullah *et al.*, 1994; Rubin *et al.*, 1995) demonstrated a low potency for these compounds' action on neuronal NMDA receptors. NAA, NAAG and NMDA were usually applied in Mg²⁺-free solution containing glycine (100 μ M) to ensure adequate activation of the receptors' glycine/D-serine site (although, at least in the gray matter of the cerebellum, this site is saturated by endogenously released glycine or D-serine: Billups and Attwell, 2003).

NAAG (1 mM) evoked a significant inward current in oligodendrocytes of mean amplitude -11.4 ± 1.5 pA, which was $6.1 \pm 0.8\%$ of the current evoked by NMDA (60 μ M) in the same cells (this mean value also includes data for NMDA in a small number of cells to which NAA, but not NAAG, was applied). However, NAA evoked no detectable current (Figs. 5.1A and B). In contrast, in cerebellar granule neurons, NAAG evoked a current of -37.1 ± 8.3 pA which was $69 \pm 15\%$ of the current evoked by

NMDA in the same cells, and NAA also evoked a small but significant current of -2.6 ± 0.5 pA (Figs. 5.1C and D).

5.3.2 Pharmacology of the NAAG-evoked current

As mentioned above, in neurons NAAG has been found to be a low-potency NMDA receptor agonist (Westbrook *et al.*, 1986; Valivullah *et al.*, 1994; Rubin *et al.*, 1995). However, it was also reported that NAAG is a non-competitive antagonist of NMDA receptors (Burlina *et al.*, 1994; Yourick *et al.*, 2003; Bergeron *et al.*, 2005; 2007), as well as an agonist for metabotropic glutamate receptor type 3 (mGluR3) (Wroblewska *et al.*, 1997; 1998). Hence, it is still controversial which receptor is the main target for NAAG and NAA.

To investigate whether the NAAG-evoked inward current is caused by activation of NMDA receptors, I applied D-AP5 (100 μ M), a selective NMDA receptor blocker. D-AP5 reversibly blocked the current both in oligodendrocytes (by $76 \pm 24\%$, Figs. 5.2A and B) and in granule cells (by $108 \pm 14\%$, Figs. 5.2C and D). The incomplete block of the NAAG-evoked current in oligodendrocytes in Fig. 5.2B probably reflects the inaccuracies of measuring the very small current evoked by NAAG in the presence of small baseline current variations.

Since NAAG has also been reported to act on mGluR3 receptors (Wroblewska *et al.*, 1997; 1998), I tested the effect of EGLU ((2S)- α -ethylglutamic acid), a selective blocker of group II mGluR receptors, on the NAAG-evoked current. At a concentration of 200 μ M, i.e. 3 times the K_i value for mGluR3 receptor inhibition (Jane *et al.*, 1996), EGLU had no effect on the NAAG-evoked current in oligodendrocytes (Figs. 5.3A and B) and only caused a small (but significant block) in granule cells (Figs. 5.3C and D), leading to the conclusion that in both cells the current is mostly the result of NAAG activating NMDA receptors. The possible contribution of mGluR3 receptor activation to the NAAG-evoked current in granule cells is considered in the Discussion.

To test if the NAA-evoked current in granule cells was also a result of NMDA receptor activation, I applied D-AP5 (200 μ M). This completely blocked the NAA-evoked current (Fig. 5.4), confirming that this molecule has a low affinity for neuronal NMDA receptors.

5.3.3 Part of the oligodendrocyte NAAG response is produced by hydrolysis to glutamate

Extracellular NAAG, whether generated endogenously or applied exogenously, can be converted to glutamate by carboxypeptidases II and III on the extracellular surface of astrocytes (Fig. 1.16; Berger *et al.*, 1999; Bzdega *et al.*, 2004). To test whether the response of oligodendrocytes to NAAG was generated in part by secondarily derived glutamate, I blocked these enzymes with 10 μ M 2-PMPA (2-(phosphonomethyl)-pentanedioic acid (Jackson *et al.*, 1996): the IC₅₀ values for inhibition of GCP II and III are 6.7 and 0.9 nM respectively: Bzdega *et al.*, 2004). This concentration of 2-PMPA does not significantly block NMDA receptors (Tortella *et al.*, 2000).

I found an interesting variability in the effect of 2-PMPA. In some oligodendrocytes (Fig. 5.5A) the NAAG response was unaffected by blocking this enzyme, suggesting that the NAAG-evoked current was produced by NAAG itself (because HPLC data provided by Tocris showed that 1 mM NAAG solution contained less than 0.2 μ M contaminating glutamate), while in other cells the enzyme blocker significantly reduced the response (Fig. 5.5B) implying that part of the response was produced by conversion of NAAG to glutamate by endogenous carboxypeptidases. On average, 49 \pm 23% of the response was blocked by 2-PMPA (Fig. 5.5C), strongly suggesting that in part NAAG acts indirectly on oligodendrocytes due to its conversion to glutamate.

Surprisingly, when 2-PMPA was applied during NAAG-evoked response in granule cells, there was no significant block of the current (Fig. 5.6). This difference may stem from the difference in the methodological approach used in these experiments – in the experiments performed on oligodendrocytes, NAAG was first applied alone, then NAAG with 2-PMPA, followed by another application of NAAG alone, while in granule cells 2-PMPA was applied during a continuous NAAG response. With this protocol desensitisation of the current during the maintained presence of NAAG (Fig. 5.6A) may make it hard to observe a clear effect of the 2-PMPA, leading to the block of the current by 2-PMPA being underestimated. To check

this hypothesis, further experiments using the same method of drug application in both cell types would be required.

5.3.4 The NAAG response in oligodendrocytes is partly produced by neuronal action potentials

Superfusion of NAAG (or NMDA) could in principle evoke a current in oligodendrocytes either by acting directly on oligodendrocyte NMDA receptors, or by acting on neuronal NMDA receptors to increase neuronal firing and hence increase the release of factors like K^+ from axons which may generate a current in oligodendrocytes. The large NMDA-evoked current is not significantly affected by TTX (Káradóttir *et al.*, 2005), suggesting that essentially all of the NMDA-evoked current is generated by a direct action on oligodendrocytes. However, TTX (1 μ M) reduced the NAAG-evoked current by $76\pm 8\%$ (Figs. 5.7A and B), suggesting that much of the NAAG response is generated indirectly by NAAG activating neuronal NMDA receptors and increasing action potential firing (see Discussion). In contrast, TTX did not affect the NMDA-evoked current in granule cells (Figs. 5.7C and D).

5.3.5 NAAG and NAA are not strong blockers of NMDA receptors

Since the role of NMDA receptors in controlling and maintaining myelination is not yet known, it seemed possible that a demyelinating action of NAAG or NAA might occur if these agents blocked NMDA receptors and thus inhibited normal signalling from axons to oligodendrocytes or their precursors. Block of neuronal NMDA receptors by NAAG has been reported previously (Burlina *et al.*, 1994; Bergeron *et al.*, 2005; 2007).

However, when NAAG (1 mM) or NAA (1 mM) were applied during the response to NMDA in white matter oligodendrocytes, any reduction in the NMDA-evoked current they produced was small compared to the reduction occurring anyway as a result of receptor desensitisation (Fig. 5.8; the reduction of the response by NAAG/NAA was estimated by fitting a straight line to the desensitisation, and measuring the actual current at the end of the NAAG/NAA application relative to the interpolated value that would occur without NAAG/NAA). In some granule cells both

NAA and NAAG produced a small reduction of the NMDA-evoked current (Figs. 5.9A and B), but in others the reduction was minimal (the mean reduction is shown in Fig. 5.9C). Thus, even using 1 mM NAAG or NAA produced much less inhibition of the oligodendrocyte or granule cell NMDA response than the 80% block reported to be produced by NAAG concentrations above 20 μ M in hippocampal pyramidal neurons (Bergeron *et al.*, 2005).

5.3.6 The effect of pathologically relevant levels of NAAG

In Canavan disease the extracellular NAA concentration (assessed in the CSF) rises from its baseline value of \sim 1.5-100 μ M (Jakobs *et al.*, 1991; Sager *et al.*, 1997; Chakraborty *et al.*, 2001) to \sim 0.4-0.9 mM (Wevers *et al.*, 1995; Burlina *et al.*, 1999), i.e. less than the 1 mM concentration we have applied which produces no effect on oligodendrocytes, and the NAAG level rises from its normal value of 1-10 μ M to \sim 20 μ M (Burlina *et al.*, 1999). In Pelizaeus-Merzbacher-like disease the NAAG concentration has been reported to rise to \sim 50 μ M (Sartori *et al.*, 2008) or \sim 200 μ M (Wolf *et al.*, 2004). I therefore tested the effect of 50 and 200 μ M NAAG on the membrane current of oligodendrocytes and granule cells. In both oligodendrocytes (Figs. 5.10A and B) and granule cells (Figs. 5.10C and D) 50 μ M NAAG produced a barely detectable current, while 200 μ M NAAG evoked a significant current in 0 mM Mg^{2+} (in oligodendrocytes this measured -4.5 ± 1.0 pA). NAAG (200 μ M and 1 mM) also evoked a detectable current in some oligodendrocytes in the presence of physiological (1 mM) Mg^{2+} concentration (Fig. 5.11).

5.4 Discussion

The levels of NAA and NAAG rise in several leukodystrophies, and these agents have previously been shown to activate neuronal NMDA receptors. My data show, for the first time, that the rise of NAAG concentration occurring in the leukodystrophies should also evoke a small membrane current in oligodendrocytes.

The NAAG-evoked current, in both cerebellar granule cells and oligodendrocytes, was largely blocked by D-AP5 and was also blocked to a small extent by a blocker of mGluR3 receptors in granule cells, showing that the current is produced mainly by activation of NMDA receptors. However, my data show that NAAG and NAA have less effect on the type of NMDA receptor that generates the current in oligodendrocytes than on the NMDA receptors in granule cells, presumably because the oligodendrocyte receptors have a different subunit composition (Káradóttir *et al.*, 2005; Salter and Fern, 2005; Micu *et al.*, 2006). Thus, in granule cells 1 mM NAAG evokes a current which is about 3/4 the size of that evoked by 60 μ M NMDA, and 1 mM NAA evokes a detectable current, while in oligodendrocytes the NAAG-evoked current is only about 7% of the NMDA-evoked current, and NAA does not evoke a detectable current (Fig. 5.1).

The small effect exerted on the NAAG-evoked current by the mGluR3 receptor blocker EGLU in granule cells suggests a possible contribution of mGluRs to generating this current. It was shown before that activation of group II mGluR receptors causes a block of calcium channels (Chavis *et al.*, 1995), as well as an opening of potassium channels (Benarroch, 2008) and of non-specific cation channels (Guéridieu *et al.*, 1995). Opening of non-specific cation channels would result in an inward current upon NAAG application and so could possibly explain the partial block of the NAAG-evoked current by the mGluR3 receptor blocker.

The potency of NAAG at oligodendrocyte NMDA receptors is even less than is suggested by inspection of Fig. 5.1, because a significant fraction of the NAAG response in oligodendrocytes is generated indirectly. A major part of the response is blocked by TTX (Fig. 5.7), and so presumably reflects NAAG acting on neuronal NMDA receptors to increase neuronal firing, which then releases a substance, perhaps K^+ , which generates an inward current in the oligodendrocytes. Blocking carboxypeptidases also reduced the response to NAAG in oligodendrocytes (Fig. 5.5), implying that part of the NAAG-evoked current is generated by NAAG being converted to glutamate (see Fig. 1.16), and this will presumably also be the case for endogenously generated NAAG. Surprisingly, the blocker of carboxypeptidases had no effect on the NAAG-evoked current in granule cells – however, this lack of effect may

be explained by a difference in the methodological approach applied in this experiment (see section 5.3.3) and requires further investigation.

When assessing the effect of the pathologically-relevant concentrations of NAAG reported in Pelizeus-Merzbacher-like disease (Wolf *et al.*, 2004; Sager *et al.*, 1997), NAAG evoked a statistically significant current at a concentration of 200 μM , but only when no external magnesium was present (which removes the NMDA receptor channel block; compare Figs. 5.10 A,B and 5.11), while 1 mM NAA did not evoke a detectable current even in the absence of Mg^{2+} . These results suggest a very low affinity of NAAG and NAA for oligodendrocyte NMDA receptors, and thus very much lower the possibility of pathological consequences arising from these substances having a direct effect on oligodendrocytes.

In summary, I have tested the hypothesis that the elevation of NAAG and NAA concentrations that occurs in the leukodystrophies might damage oligodendrocytes by acting on oligodendrocyte NMDA receptors. My results show that NAAG evokes an inward current both in oligodendrocytes and granule cells, however, it is a much less effective agonist at oligodendrocyte NMDA receptors than at neuronal NMDA receptors, and the small current generated in oligodendrocytes by NAAG largely reflects a secondary consequence of its activation of neuronal NMDA receptors. Thus, if the elevation of NAAG concentration in the leukodystrophies causes white matter damage, this will most likely be initiated by a change of neuronal activity, not by acting on oligodendrocyte NMDA receptors. To further investigate the effect of NAAG and NAA on oligodendrocyte physiology, calcium-imaging and a cell death assay were employed, as described in Chapter 6.

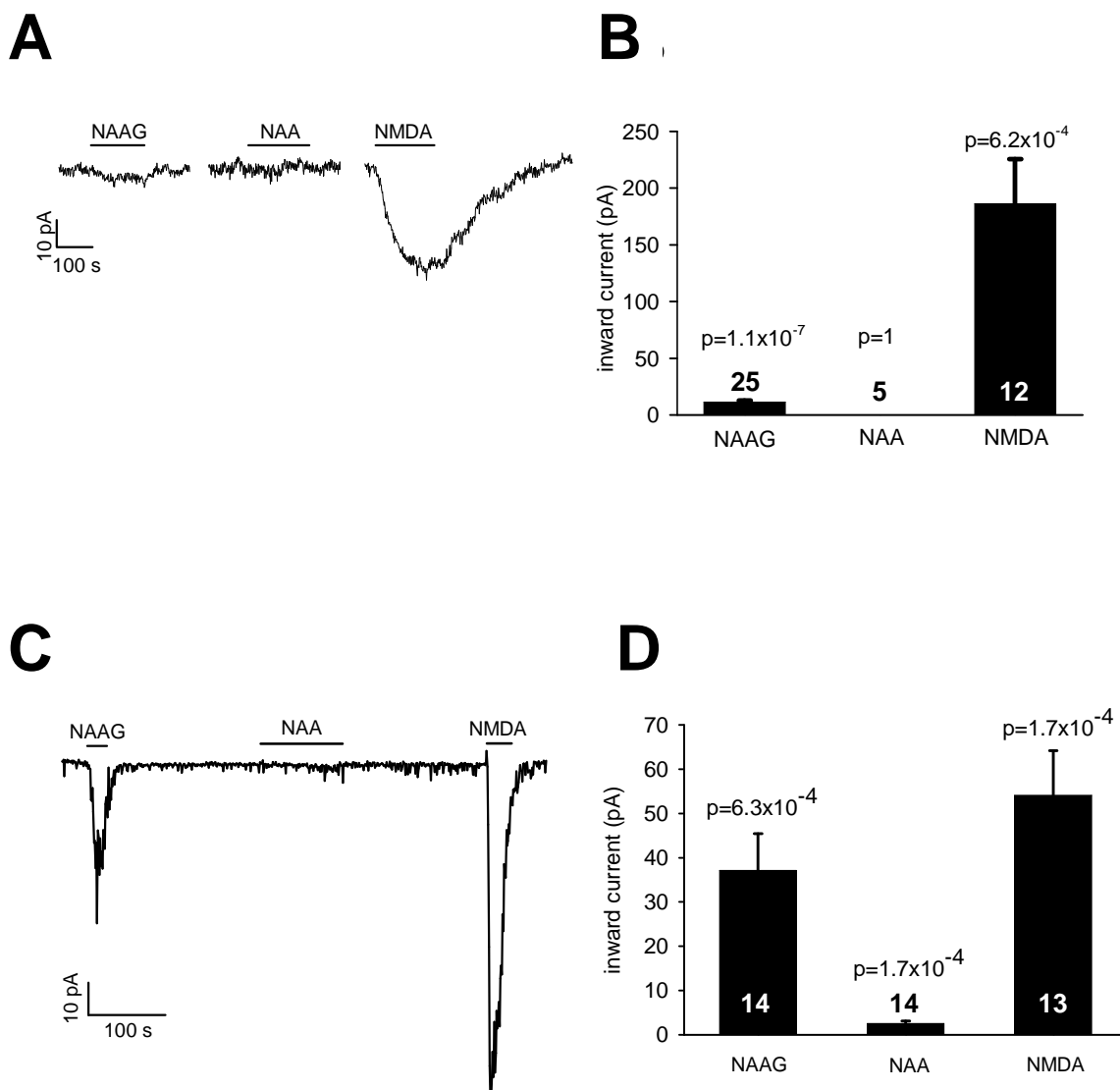


Figure 5.1

NAAG, NAA and NMDA-evoked whole cell currents at -74 mV in white matter oligodendrocytes and cerebellar granule cells. **A** Representative trace shows the current response to NAAG (1 mM), NAA (1 mM) and NMDA (60 μ M) in a single oligodendrocyte. **B** Average responses to NAAG (1 mM, n=20 cells), NAA (1 mM, n=5) and NMDA (60 μ M, n=12) in oligodendrocytes. **C** Representative trace shows the response to NAAG (1 mM), NAA (1 mM) and NMDA (60 μ M) in a single granule cell. **D** Average responses to NAAG (1 mM, n=14 cells), NAA (1 mM, n=14) and NMDA (60 μ M, n=13) in granule cells. P values compare with no response. All responses in this chapter are in 0 mM Mg²⁺ solution, apart from those in Fig. 5.11.

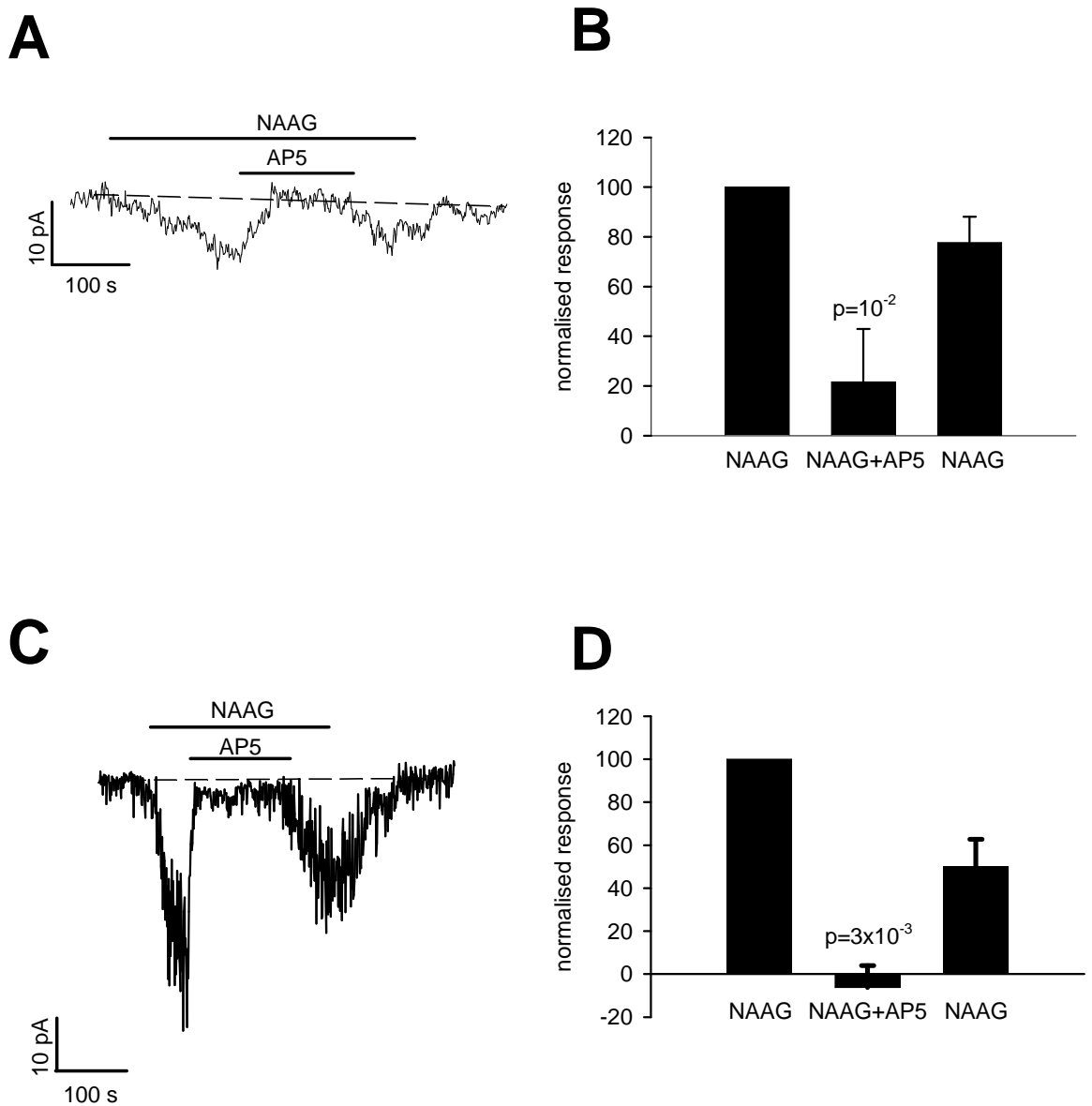


Figure 5.2

The NMDA receptor blocker, D-AP5 (100 μM), significantly reduces the oligodendrocyte response to NAAG. **A** Representative trace shows the response to NAAG (1 mM) and block of the response by AP5 (100 μM) in a white matter oligodendrocyte (dashed line shows the current baseline). **B** Mean effect on the NAAG response of AP5 in 10 white matter oligodendrocytes (dashed line shows the current baseline). The 2nd and 3rd bars are normalised to the initial NAAG response (as 100%), and show the response to NAAG in the presence of AP5 and the response to a subsequent application of NAAG alone. P value compares the response in NAAG + AP5 to the average of the preceding and subsequent responses without AP5. **C** Representative trace shows response to NAAG (1 mM) alone and block of the response by AP5 (100 μM) in a granule cell. **D** Mean effect on the NAAG response of AP5 in 4 granule cells. P values compare the response in AP5 with the average of the bracketing current values in the absence of AP5.

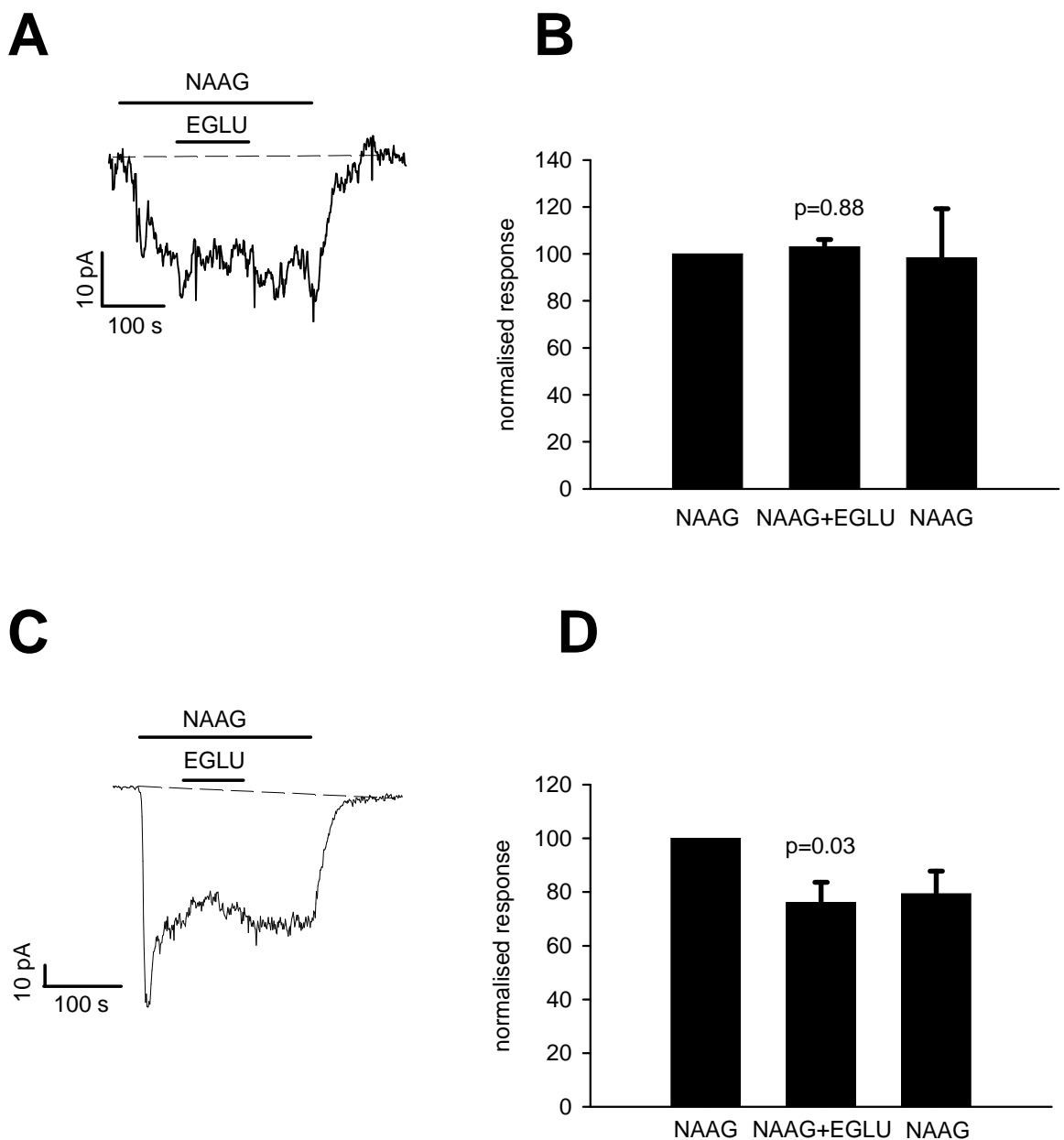
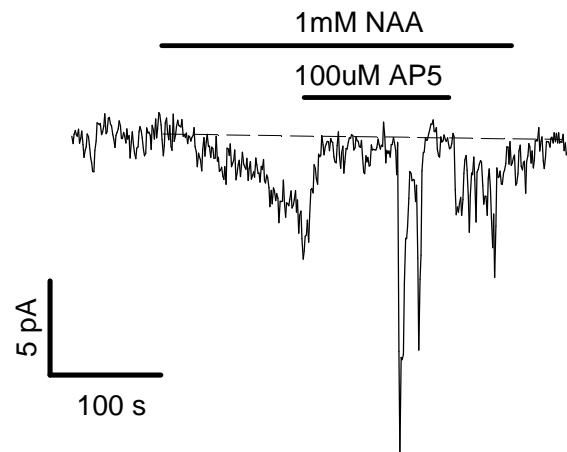
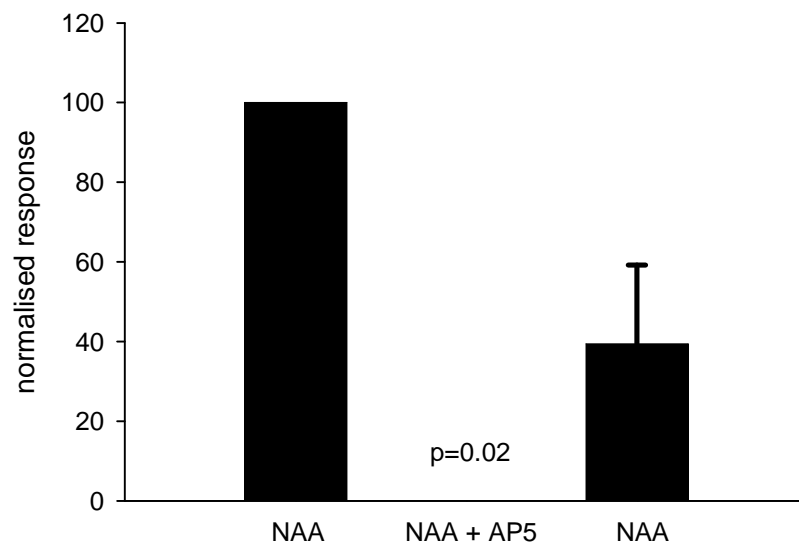


Figure 5.3

The metabotropic glutamate receptor type 3 blocker, EGLU, does not block the NAAG-evoked current in white matter oligodendrocytes, but to a small extent blocks the current in granule cells. **A** Representative trace shows the effect of EGLU (200 μ M) on the response to 1 mM NAAG in a white matter oligodendrocyte (dashed line shows the current baseline). **B** Mean effect of EGLU on the response to NAAG in 3 white matter oligodendrocytes. **C** Representative trace shows effect of EGLU (200 μ M) on the response to 1 mM NAAG in a granule cell (dashed line shows the current baseline). **D** Mean effect of EGLU on the response to NAAG in 4 granule cells. Response in EGLU was measured at the end of EGLU application, and response to NAAG after EGLU was measured at the end of NAAG application. The 2nd and 3rd bars are normalised to the initial NAAG response (as 100%), and show the response to NAAG in the presence of EGLU and the response to a subsequent application of NAAG alone. P values compare the response in EGLU with the average of the bracketing current values in the absence of EGLU.

A**B****Figure 5.4**

The NMDA receptor blocker, AP5, significantly blocked the response to NAA in cerebellar granule cells. **A** Representative trace shows response to NAA (1 mM) alone and block of the response by AP5 (100 μM) in a granule cell (dashed line shows the current baseline). **B** Mean effect on the response to NAA of AP5 in 3 granule cells. The initial response to NAA was measured just before the NAA + AP5 application, response in AP5 was measured at the end of NAA + AP5 application, and response to NAA after AP5 was measured at the end of NAA application. The 2nd and 3rd bars are normalised to the initial NAA response (as 100%), and show the response to NAA in the presence of AP5 and the response to a subsequent application of NAA alone. P value compares the response in NAA + AP5 to the average of the preceding and subsequent current values without AP5.

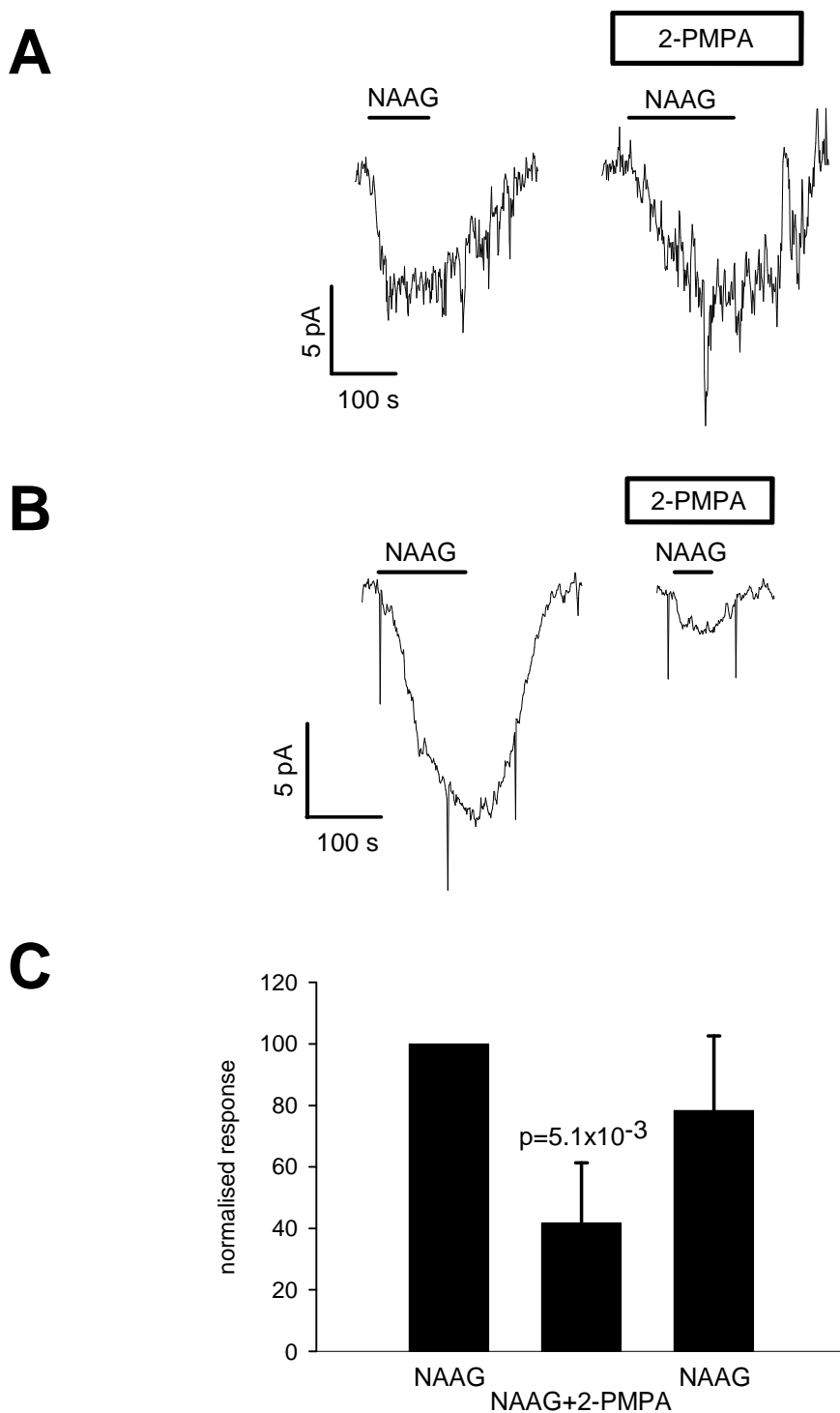


Figure 5.5

The effect of blocking carboxypeptidases on the NAAG-evoked current at -74 mV in white matter oligodendrocytes. **A** Specimen trace showing a cell where the carboxypeptidase blocker 2-PMPA (10 mM) had no effect on the NAAG-evoked current. **B** Specimen trace showing a cell where 2-PMPA reduced the NAAG-evoked current. **C** Mean effect of 2-PMPA on the NAAG-evoked current in 7 cells. The 2nd and 3rd bars are normalised to the initial NAAG response (as 100%), and show the response to NAAG in the presence of 2-PMPA and the response to a subsequent application of NAAG alone. P value compares the response in 2-PMPA to the average of bracketing responses without 2-PMPA.

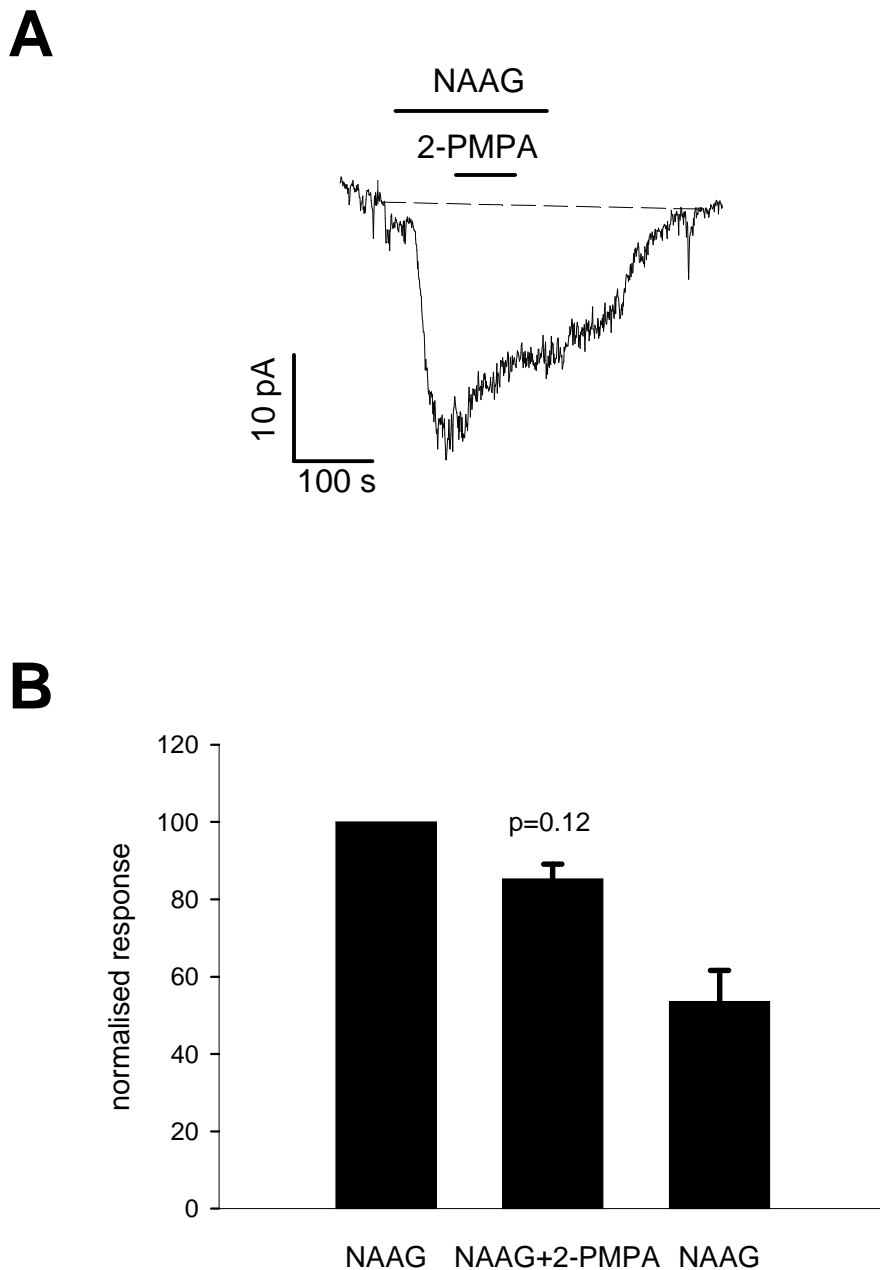


Figure 5.6

The carboxypeptidase blocker 2-PMPA does not significantly block the NAAG-evoked current at -74 mV in cerebellar granule cells. **A** Representative trace shows the response to NAAG (1 mM) and effect on the response of 2-PMPA (10 μ M) in a single granule cell (dashed line shows the current baseline). **B** Mean effect on the response to NAAG of 2-PMPA in 3 granule cells. The initial response to NAAG was taken as the current value just before the 2-PMPA was applied; the response in 2-PMPA was taken as the current value at the end of 2-PMPA application; the second response to NAAG was taken as the current at the end of the application of NAAG (after the 2-PMPA). The 2nd and 3rd bars are normalised to the initial NAAG response (as 100%), and show the response to NAAG in the presence of 2-PMPA and the response to a subsequent application of NAAG alone. P value compares the current in NAAG + 2-PMPA with the average of the bracketing current values in NAAG alone.

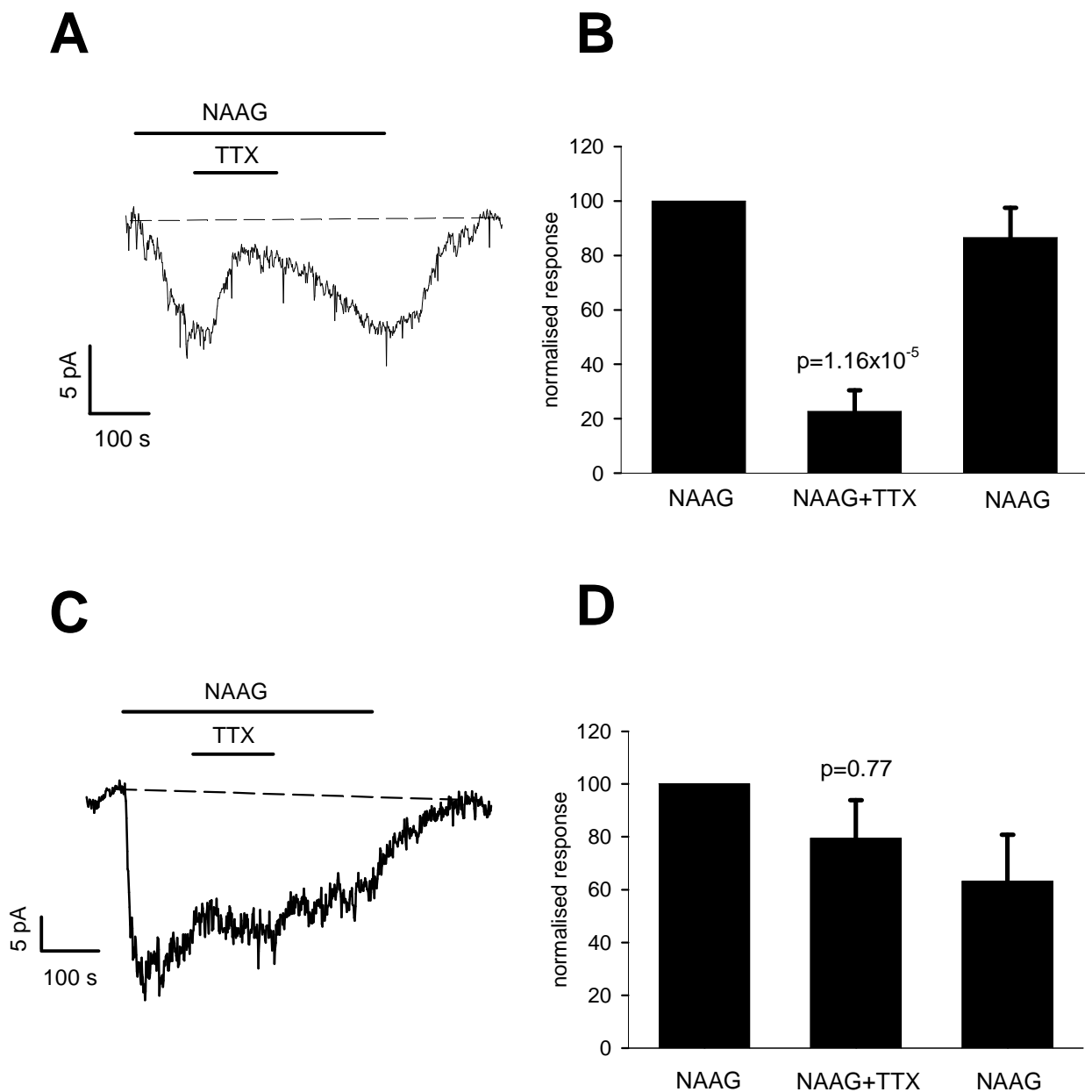


Figure 5.7

The action potential blocker, TTX, partially blocks the NAAG-evoked current at -74 mV in white matter oligodendrocytes, but has no effect on the current in cerebellar granule cells. **A** Representative trace shows effect of TTX (1 μ M) on the response evoked by 1 mM NAAG in a white matter oligodendrocyte (dashed line shows the current baseline). **B** Mean effect of TTX on the response to NAAG in 8 white matter oligodendrocytes. **C** Representative trace shows effect of TTX (1 μ M) on the response to 1 mM NAAG in a granule cell (dashed line shows the current baseline). **D** Mean effect of TTX on the response to NAAG in 4 granule cells. The initial response to NAAG was measured just before the NAAG + TTX application, response in TTX was measured at the end of NAAG + TTX application, and response to NAAG after TTX was measured at the end of NAAG application. The 2nd and 3rd bars are normalised to the initial NAAG response (as 100%), and show the response to NAAG in the presence of TTX and the response to a subsequent application of NAAG alone. P values show the response in TTX compared to the average of the bracketing current values without TTX.

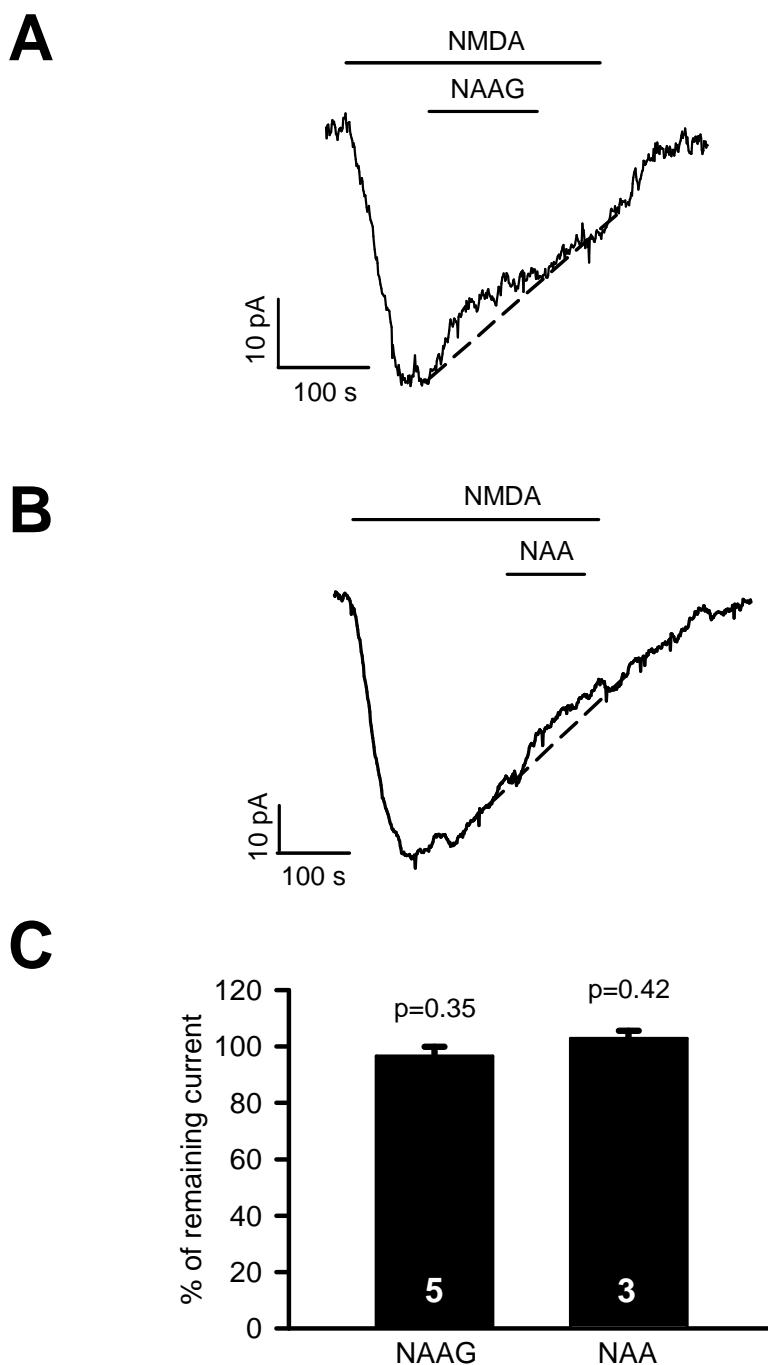


Figure 5.8

Test of block of the NMDA-evoked current at -74 mV by NAAG and NAA in white matter oligodendrocytes. **A** Representative trace shows block by NAAG (1 mM) of the response to $60 \mu\text{M}$ NMDA in an oligodendrocyte (dashed line shows the current baseline, i.e. current during NMDA application). **B** Representative trace shows block by NAA (1 mM) of the response to $60 \mu\text{M}$ NMDA in an oligodendrocyte (dashed line shows the current baseline, i.e. current during NMDA application). **C** Mean effect of NAAG (5 cells) and NAA (3 cells) on the NMDA-evoked current, calculated assuming for simplicity that desensitization of the NMDA-evoked current follows a linear time course (dashed lines in A and B: the NMDA-evoked current at the end of the NAAG or NAA application was divided by the interpolated current predicted assuming linear desensitization). P values assess the reduction in current compared with no reduction from 100%.

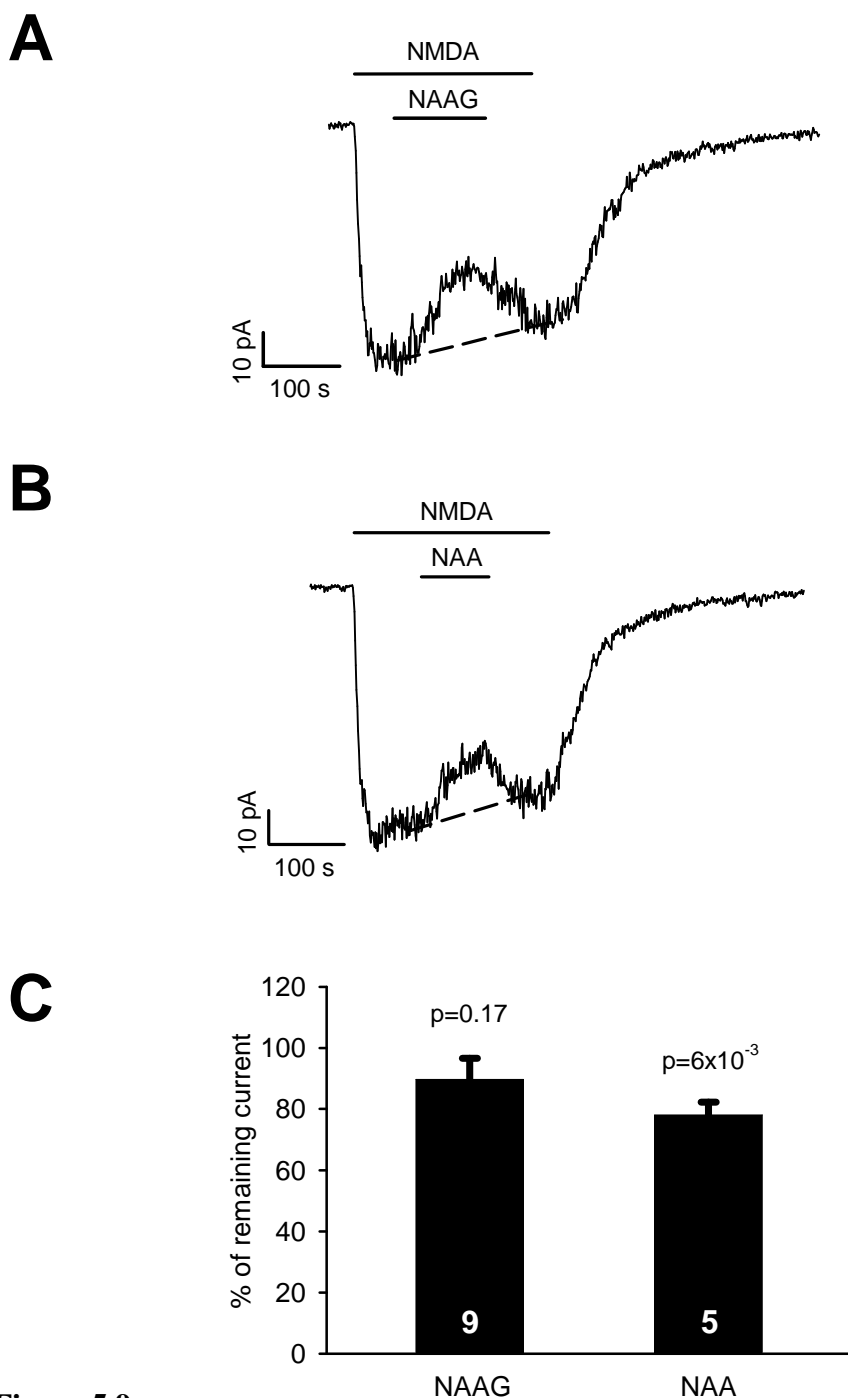


Figure 5.9

Test of block of the NMDA-evoked current at -74 mV by NAAG and NAA in cerebellar granule cells. **A** Representative trace shows block by NAAG (1 mM) of the response to 60 μ M NMDA in a granule cell (dashed line shows the current baseline, i.e. current during NMDA application). **B** Representative trace shows block by NAA (1 mM) of the response to 60 μ M NMDA in a granule cell (dashed line shows the current baseline, i.e. current during NMDA application). **C** Mean effect of NAAG (9 cells) and NAA (5 cells) on the NMDA-evoked current, calculated assuming for simplicity that desensitization of the NMDA-evoked current follows a linear time course (dashed lines in A and B: the NMDA-evoked current at the end of the NAAG or NAA application was divided by the interpolated current predicted assuming linear desensitization). P values assess the reduction in current compared with no reduction from 100%.

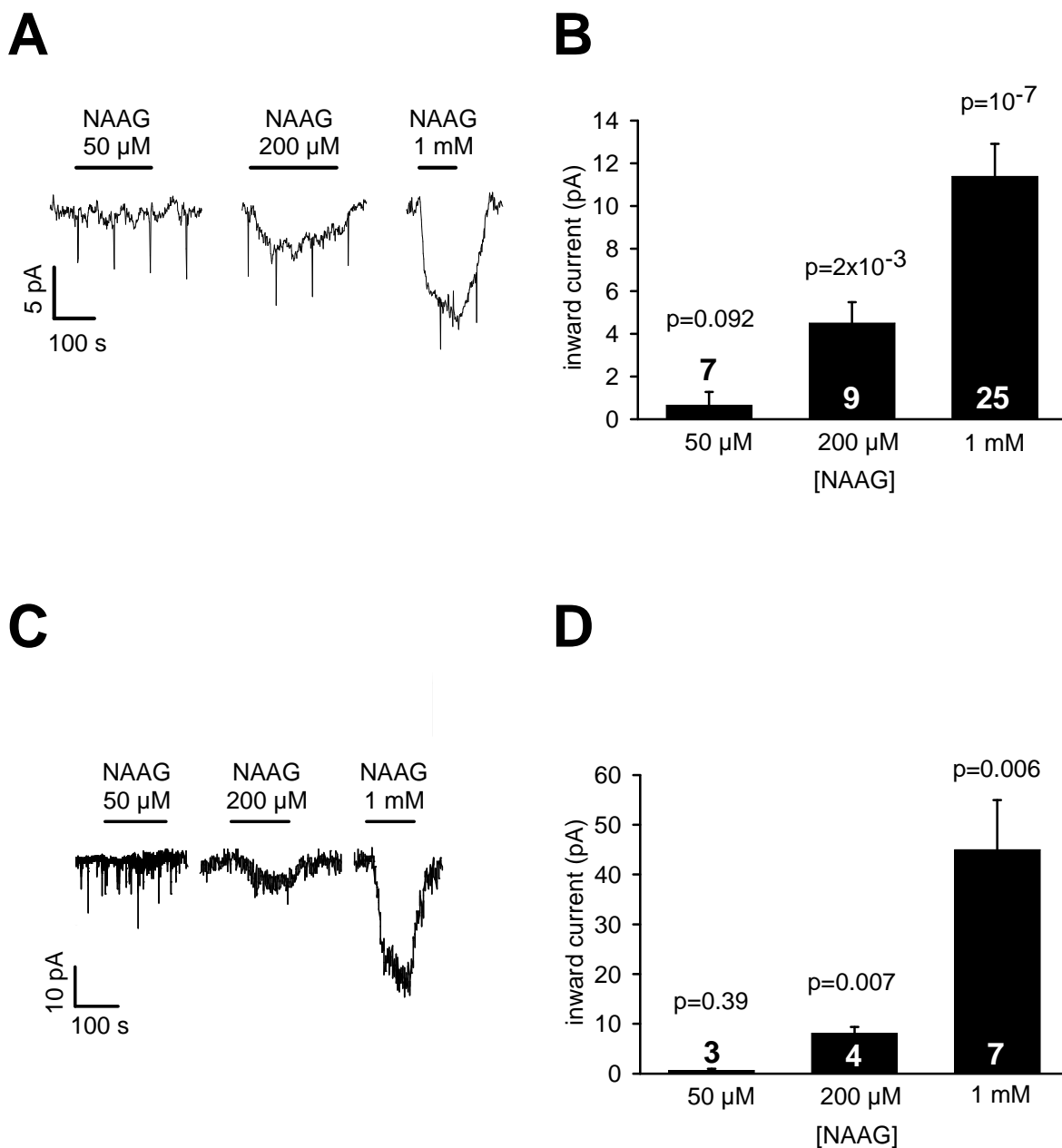
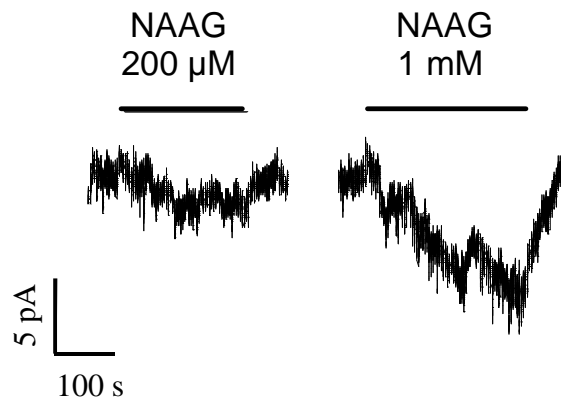
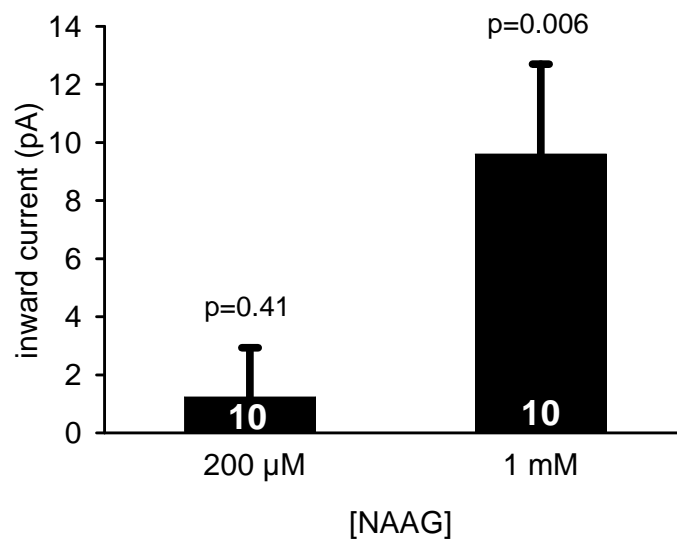


Figure 5.10

The current response of white matter oligodendrocytes and cerebellar granule cells to pathologically relevant concentrations of NAAG, 50 μ M, 200 μ M and 1 mM, in 0 mM Mg^{2+} solution. **A** Representative responses to 50 μ M, 200 μ M and 1 mM NAAG in a white matter oligodendrocyte. Vertical lines on trace are the response to voltage steps applied to monitor series resistance. **B** Mean responses to 50 μ M, 200 μ M and 1 mM NAAG in 7, 9 and 25 (respectively) white matter oligodendrocytes. **C** Representative responses to 50 μ M, 200 μ M and 1 mM NAAG in a granule cell. **D** Mean responses to 50 μ M, 200 μ M and 1 mM NAAG in 3, 4 and 7 (respectively) cerebellar granule cells. All *p* values are for comparison with zero response.

A**B****Figure 5.11**

The current response of white matter oligodendrocytes to pathologically relevant concentrations of NAAG, 200 μM and 1 mM, in 1 mM Mg²⁺ solution with no added glycine. **A** Representative responses to 200 μM and 1 mM NAAG in a single oligodendrocyte. **B** Mean response to 200 μM and 1 mM NAAG in 10 white matter oligodendrocytes. The p values are for comparison with zero response.

Chapter 6: Oligodendroglial and neuronal $[Ca^{2+}]_i$ changes in response to NAA and NAAG

6.1 Introduction

The intracellular calcium concentration rise that occurs upon opening of calcium-permeable channels or receptors, or after calcium release from the internal stores, can affect cell physiology by regulating processes ranging from transcription to neurotransmitter release. An excessive calcium influx is detrimental to the cell due to the activation of calcium-dependent proteases, lipases and endonucleases, and the induction of cell apoptosis. Oligodendrocyte NMDA receptors are assumed to be calcium-permeable and their overactivation in ischaemia leads to cell damage and death (Káradóttir *et al.*, 2005; Salter and Fern, 2005; Micu *et al.*, 2006). I showed in the previous chapter that high concentrations of NAAG evoke an inward current in both oligodendrocytes and neurons (and NAA evokes a small but significant current in neurons), by acting on their NMDA receptors. It is possible that these electrical changes are associated with a calcium influx into the cells, and that overactivation of NMDA receptors by NAAG in the leukodystrophies causes a calcium influx which, over a long period, might lead to death of the oligodendrocytes and a loss of myelin.

To investigate this, I recorded changes of intracellular calcium concentration in the white and grey matter of brain slices (loaded with the acetoxymethyl ester version of a calcium-sensing dye), determining whether they result solely from NMDA receptor activation or from an additional action on mGluR3 receptors (the activation of which might induce cellular responses undetected by electrical recordings, such as calcium release from the intracellular stores). I then whole-cell patch-clamped single oligodendrocytes or neurons, filling them with a calcium-sensing dye to simultaneously record the current and intracellular calcium changes. Finally, I performed a cell-death assay to examine if any $[Ca^{2+}]_i$ rise or current evoked in oligodendrocytes and neurons by NAAG might be the cause of myelin loss and cell death in the leukodystrophies.

6.2 Materials and methods

6.2.1 Brain slice preparation

Cerebellar slices were prepared from P12 rats as described in section 2.1. Slices were immersed in a HEPES-based solution (described in section 2.2.1) at room temperature with a flow rate of 2-4 ml/min. Usually MgCl_2 was omitted from the solution, and glycine (100 μM , to ensure activation of the glycine site of NMDA receptors) and strychnine (5 μM , to block glycine-gated chloride channels) were added. A single experiment, described in section 6.3.5, was performed using a physiological concentration of Mg^{2+} (1 mM) and with no added glycine.

6.2.2 Patch-clamping

White matter oligodendrocytes and cerebellar granule cells were identified (as described in section 2.5), and whole-cell patch-clamped (as described in section 2.6). Pipettes contained Cs^+ -based internal solution (see Table 2.1) to provide better voltage-clamp quality. The series resistance was 10-30 $\text{M}\Omega$, and was not compensated. The membrane potential was held at -74 mV (including the junction potential of -14 mV).

6.2.3 $[\text{Ca}^{2+}]_i$ imaging with Fluo-4-AM

Slices were loaded with the acetomethoxy ester of Fluo-4 (Fluo-4-AM) by incubating slices for 2 h in a 10 μM solution of Fluo-4-AM (for the preparation of the solution, see section 2.9.1). 95% O_2 /5% CO_2 solution was blown gently over the solution while loading. Fluorescence was excited at 488 nm and emitted light was collected at 535 nm. Regions of interest in the white and grey matter were identified from the morphology and anatomy of the slice. For slices that were not loaded with dye the baseline fluorescence was 2.99-fold lower for white matter and 3.37-fold lower for grey matter (comparing 12 loaded and 3 unloaded slices) and there was a negligible fluorescence (F) change in response to 1 mM NAAG ($\Delta\text{F}/\text{F} = -0.00146 \pm 0.00146$ in 3 unloaded slices, compared to 0.03611 ± 0.0095 in 12 loaded slices as described below).

6.2.4 Single cell $[Ca^{2+}]_i$ imaging

White matter oligodendrocytes and grey matter granule cells were patch-clamped with pipettes containing a Cs^+ -based solution including 1 mM of the calcium dye Fura-2 (see Table 2.1). Fluorescence was excited sequentially at 340 nm and 380 nm, and emitted light was collected at 510 nm. The ratio of the emission intensities (340 nm/380 nm) was used as a measure of increased $[Ca^{2+}]_i$, and only cells exhibiting both a decrease of fluorescence excited at 380 nm and an increase in fluorescence excited at 340 nm were used.

6.2.5 Cell death assay

Slices were bathed in a HEPES-buffered solution (see section 2.2.1) containing 1 mM NAAG, or 1 mM NAAG and 100 μ M AP5, or 100 μ M NMDA, or no added drug, at 36°C for 6 h. Propidium iodide (PI, Sigma, 37 μ M) was added to reveal a loss of membrane permeability associated with cell death (see section 2.10), as might be expected to occur when oligodendrocytes lose their myelinating processes during the first hour of ischaemia (Salter and Fern, 2005). Slices were then fixed and immunolabelled for myelin basic protein (MBP) to identify white matter (as described in section 2.11.1). Mounting solution containing DAPI was used to label nuclei and the images were acquired using a confocal microscope.

6.2.6 Confocal microscopy

Confocal images of slices were taken using Zeiss LSM 510 inverted microscope, with a 40x objective (as described in section 2.11.2). Suitable excitation and emission wavelengths for DAPI, AlexaFluor 488 and PI were used (see Table 2.3). The white matter was defined as being MBP-positive and grey matter as MBP-negative, and the percentage of dead cells was calculated as the number of PI-positive cells divided by the total number of cells with DAPI-labelled nuclei.

6.2.7 Statistics

Data are presented as mean \pm s.e.m. P values are from Student's 2-tailed t-tests.

6.3 Results

6.3.1 Effects of NAAG and NAA on $[Ca^{2+}]_i$ in the white matter and grey matter

To determine whether NAAG or NAA raise $[Ca^{2+}]_i$ in cells of the white matter, I initially used the Ca^{2+} -sensitive dye Fluo-4, which was loaded into the cells of cerebellar slices as its acetoxymethyl ester. Regions of interest were imaged that included, separately, the white matter and the grey matter (Fig. 6.1A).

In both the white and the grey matter, NAAG and NMDA evoked an increase in Fluo-4 fluorescence (NAAG: $\Delta F/F = 0.0361 \pm 0.0095$ in 12 regions of the white matter, $\Delta F/F = 0.2635 \pm 0.0475$ in 12 regions of the grey matter; NMDA: $\Delta F/F = 0.0888 \pm 0.0148$ in 10 regions of the white matter, $\Delta F/F = 0.1942 \pm 0.0365$ in 10 regions of the grey matter) while NAA did not (Figs. 6.1B-D). As for the membrane currents shown for grey matter granule cells and white matter oligodendrocytes in Chapter 5 (Fig. 5.1), the response to NAAG, relative to that for NMDA, was larger in the grey matter than in the white matter, which may in part reflect the oligodendrocyte NMDA receptors having a different subunit composition to those in neurons. Furthermore, in both areas the ratio of the NAAG response to that for NMDA tended to be larger for the calcium response than for the current response (NAAG/NMDA = 0.37 ± 0.14 in 9 regions for white matter $[Ca^{2+}]_i$ and 0.07 ± 0.01 in 10 cells for oligodendrocyte current, significantly different: $p=0.03$; NAAG/NMDA = 1.74 ± 0.57 in 9 regions for grey matter $[Ca^{2+}]_i$ and 0.77 ± 0.24 in 7 cells for granule cell current, not significantly different: $p=0.18$). The latter difference might in part be explained by the calcium dye bleaching and thus exhibiting a decreased sensitivity toward a subsequent agonist which most often was NMDA applied as a positive control after the NAAG had been applied.

6.3.2 Block of NAAG-evoked $[Ca^{2+}]_i$ rise in the white matter and grey matter

To investigate if the activation of NMDA receptors is responsible for the NAAG-evoked increase in $[Ca^{2+}]_i$, I applied D-AP5 (100 μM). This reduced the $[Ca^{2+}]_i$ rise evoked by NMDA (not shown) and by NAAG (Fig. 6.2). The NAAG-evoked $[Ca^{2+}]_i$ rise was reversibly reduced in the white matter by $78 \pm 5\%$ (Fig. 6.2B and C) and

in the grey matter by $86\pm 4\%$ (Fig. 6.2B and D), confirming that the observed changes in $[Ca^{2+}]_i$ are largely evoked by a calcium influx through NMDA receptors.

To exclude the possibility that mGluR3 receptors provide an additional contribution to the observed calcium changes by activating calcium-permeable channels, I applied EGLU (200 μ M), the blocker of group II mGluR receptors. There was no significant block of the NAAG-evoked rise in $[Ca^{2+}]_i$ in the white matter (Fig. 6.3B and C), and only a small but significant block in the grey matter (Fig. 6.3B and D). Note that the strong run down of the $[Ca^{2+}]_i$ response on repeated application of agonists means that the significance of the EGLU effect had to be assessed by comparing the response in EGLU with the average of bracketing responses to NAAG without EGLU, and if the run down was not linear with time this could result in an apparent block of the response by EGLU where one does not in fact exist. However, this result may also be consistent with the result obtained in the previous chapter (see section 5.3.2) where the NAAG-evoked current in granule cells (but not in oligodendrocytes) was slightly reduced by the application of the mGluR3 blocker, perhaps reflecting the opening of non-specific cation channels which might contribute to the rise in $[Ca^{2+}]_i$.

6.3.3 The effect of NAAG on $[Ca^{2+}]_i$ in oligodendrocytes and granule cells

Although AM-loading of the calcium dye Fluo-4 led to granule cells generating sufficient fluorescence for their calcium responses to be reliably distinguished from those generated in surrounding cells, this was not the case for the very fine processes of oligodendrocytes in the white matter. To determine whether the cells in the white matter that respond to NAAG with a $[Ca^{2+}]_i$ rise are oligodendrocytes, I therefore patch-clamped cells whose morphology (assessed after Lucifer yellow filling from the patch pipette) corresponded to mature oligodendrocytes, using pipettes containing the ratiometric Ca^{2+} -sensitive dye Fura-2. To confirm the results from the experiments in slices in grey matter, I also patch-clamped granule cells.

In oligodendrocytes, NAAG (1 mM) did not evoke a significant $[Ca^{2+}]_i$ rise in either the cell body or the processes (Fig. 6.4), despite NAAG evoking an inward current (Fig. 6.4B), and despite spontaneous $[Ca^{2+}]_i$ elevations being observed which

confirmed that the dye was working. Granule cells, however, responded to NAAG (1 mM) with a statistically significant $[Ca^{2+}]_i$ rise (both in their processes and cell body, Fig. 6.4C and 6.5B) that was blocked by D-AP5 (Fig. 6.5). The implications of these results are considered in the Discussion.

6.3.4 The effect of pathologically relevant levels of NAAG

As described in Chapter 5 (section 5.3.6), the NAAG concentration in Pelizaeus-Merzbacher-like disease (PMLD) rises to ~50 μ M (Sartori *et al.*, 2008) or ~200 μ M (Wolf *et al.*, 2004). These concentrations were shown to evoke significant currents in granule cells (see section 5.3.6), so to examine if they would also cause a $[Ca^{2+}]_i$ change in granule cells, I patch-clamped cells and filled them with Fura-2 and then applied 50 μ M and 200 μ M NAAG (and 1 mM NAAG as a positive control). Only 200 μ M NAAG evoked a detectable $[Ca^{2+}]_i$ rise (Fig. 6.6).

6.3.5 The effect of NAAG on cell death in white matter and grey matter

As NAAG evokes an inward current in oligodendrocytes of the cerebellar white matter, and an inward current and $[Ca^{2+}]_i$ rise in granule neurons of the grey matter, I decided to test if a direct effect or an indirect effect (e.g. via granule cells) of this molecule on oligodendrocytes may lead to their death and hence to the myelin loss observed in Canavan and Pelizaeus-Merzbacher-like diseases.

I bathed cerebellar slices in extracellular solution containing a physiological level of Mg^{2+} (1 mM), along with NAAG (1 mM), NAAG (1 mM) with AP5 (100 μ M), NMDA (100 μ M), or no added drug, at 37°C for 6 h. Afterwards, I immunolabelled the slices with antibody against MBP protein to define the white matter, and with DAPI to define cell nuclei, and quantified the percentage of dead cells (i.e. the ones that took up propidium iodide into their soma, divided by the total number of DAPI-labelled nuclei) in the white matter and the grey matter.

Although NMDA evoked significant death of granule cells in the grey matter ($p=0.004$), NAAG did not, and neither NAAG nor NMDA evoked significant cell death in the white matter (Fig. 6.7). The relevance of these data to the loss of myelin occurring in the leukodystrophies is discussed below.

6.4 Discussion

NAA and NAAG are two of the most abundant substances in CNS (Coyle, 1997; Sager *et al.*, 1997; Chakraborty *et al.*, 2001), but their physiological role remains elusive. NAA is mainly considered to be involved either in myelin formation (Chakraborty *et al.*, 2001) or in the regulation of cell osmolarity (Baslow, 2003), while NAAG has been suggested to be a co-transmitter at glutamatergic synapses (Bergeron *et al.*, 2005; 2007). In two types of leukodystrophy – Canavan disease and Pelizaeus-Merzbacher-like disease – the concentrations of NAA and NAAG are highly elevated, but their actual role in these diseases is unknown. In this chapter, I tested the possibility that these substances lead to an excessive influx of calcium into the oligodendrocytes or neurons, leading to cell damage, myelin loss and cell death.

I showed that cells in both the white and grey matter respond to NAAG, but not to NAA, with a significant intracellular calcium concentration ($[Ca^{2+}]_i$) rise that can be largely blocked by NMDA receptor blockers. Blocking mGluR3 receptors, another candidate for NAAG to act on, did not reduce the NAAG-evoked $[Ca^{2+}]_i$ change in the white matter, but decreased it slightly in the grey matter. This is similar to the result I obtained in Chapter 5, where I showed that mGluR3 receptors are not responsible for the NAAG-evoked inward current in oligodendrocytes, but that in granule cells their activation by NAAG may contribute a small but significant current. The small $[Ca^{2+}]_i$ rise and inward current contributed by NAAG acting on mGluR3 could be explained by the opening of cation channels downstream of mGluR3.

When calcium changes were recorded in single cells (along with electrical changes), oligodendrocytes did not respond to 1 mM NAAG, while granule cells responded to both 1 mM NAAG and to the pathologically-relevant NAAG concentration of 200 μ M (found in PMLD: Wolf *et al.*, 2004). The lack of response of oligodendrocytes suggests that the rise seen when imaging AM-loaded dyes in the white matter may reflect a calcium influx into astrocytes (rather than oligodendrocytes) through their NMDA receptors (Conti *et al.*, 1996; Schipke *et al.*, 2001; Lalo *et al.*, 2006). Finally, a cell death assay performed for 6 h showed no influence of NAAG on either oligodendrocyte or granule cell viability.

NMDA receptors on oligodendrocyte have been suggested to be calcium-permeable and actively involved in the cells' response to ischaemic insult, which leads to myelin loss and cell death (Káradóttir *et al.*, 2005; Salter and Fern, 2005; Micu *et al.*, 2006). NAAG, which was found to be either an agonist (Westbrook *et al.*, 1986) or an antagonist (Bergeron *et al.*, 2005; 2007) at NMDA receptor in neurons, in my experiments evoked calcium responses in cerebellar granule cells, but not in oligodendrocytes. This result may stem from the fact that much of the oligodendrocyte response to NAAG, as I show in Chapter 5, is an indirect one, with NAAG acting on neuronal NMDA receptors. This presumably increases neuronal firing and results in the release of a secondary substance (e.g. potassium) that induces the inward current in oligodendrocytes, so that most of the inward current recorded in a single oligodendrocyte is not associated with a calcium influx. In addition, the NMDA receptors that have been suggested to exist on oligodendrocyte lineage cells are suggested to include NR3 subunits (Káradóttir *et al.*, 2005; Salter and Fern, 2005; Micu *et al.*, 2006), which reduce the Ca^{2+} permeability of the receptors (Sasaki *et al.*, 2002).

The lack of cell death after 6 h of 1 mM NAAG application was initially surprising, especially in the case of granule cells which were found to respond to NAAG with both an inward current and a calcium influx through NMDA receptors. Conceivably 6 hours is simply not a long enough duration for a small calcium influx to damage the cells, especially in the absence of any metabolic compromise to inhibit Ca^{2+} pumping out of the cell. The lack of a large evoked membrane current and $[\text{Ca}^{2+}]_i$ rise evoked in oligodendrocytes by NAAG, and the lack of influence of NAAG on oligodendrocyte survival, make the hypothesis that this molecule contributes to myelin loss and cell death in Canavan and Pelizaeus-Merzbacher-like diseases much less probable, but cannot be entirely excluded. Patients with both CD and PMLD display their symptoms relatively late, around the first year of their life, and so it is possible that a constant high concentration of NAAG (and NAA) may lead to a slowly-developing damaging effect on cells which culminates in their damage, and thus eventually causes the severe demyelination observed in both of the leukodystrophies.

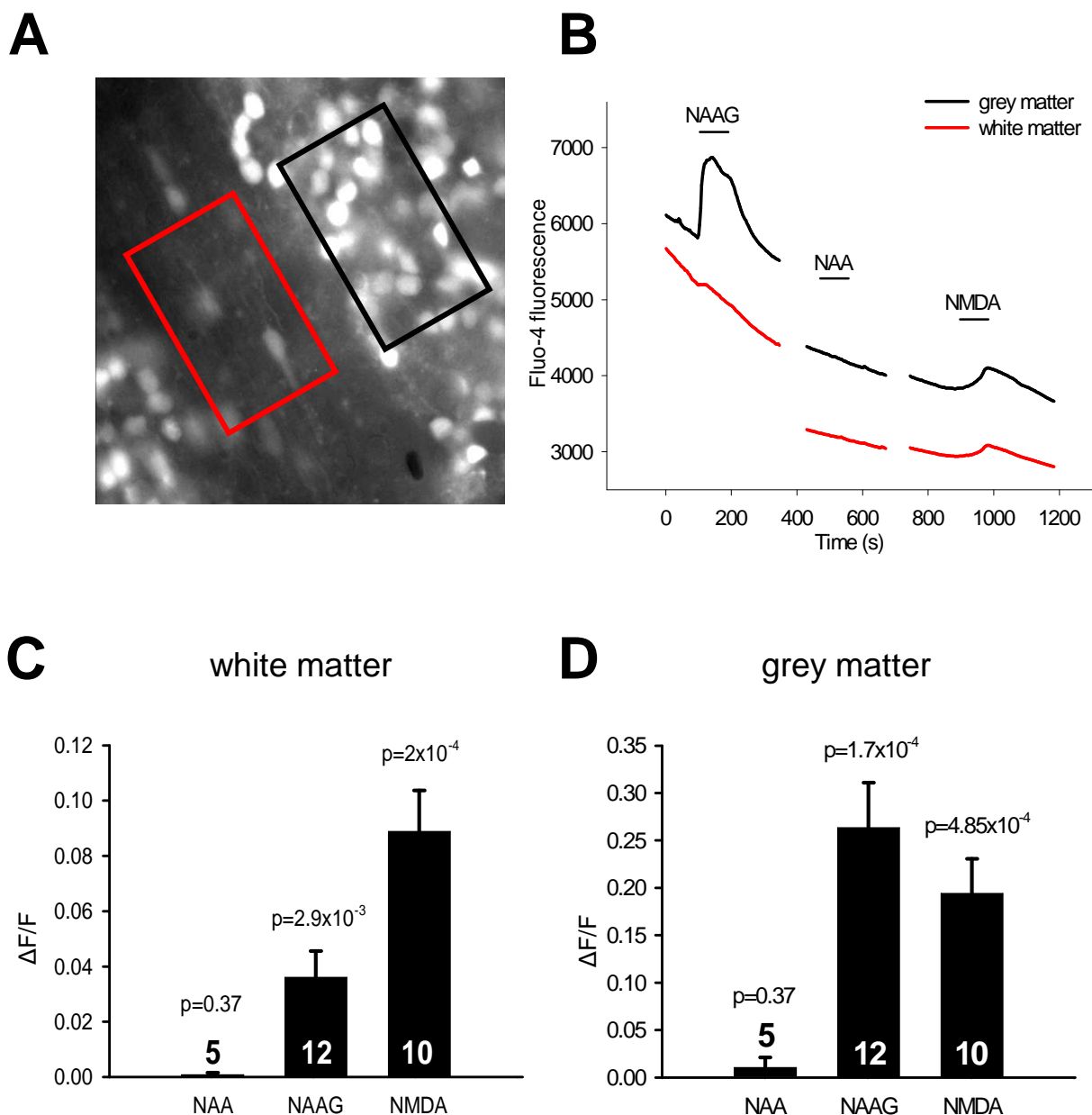


Figure 6.1

Change in $[Ca^{2+}]_i$ in the white and grey matter on application of NAA (1 mM), NAAG (1 mM) and NMDA (60 μ M). **A** Specimen image of cerebellar white matter (red region) and grey matter (black region) loaded with Fluo-4. **B** Rise of Fluo-4 fluorescence (F) in white matter and grey matter after application of NAAG and NMDA, and lack of a response after application of NAA. **C** Average responses of white matter to NAA, NAAG and NMDA. **D** Average responses of grey matter to NAA, NAAG and NMDA. Number on or above each bar indicates number of slices. P values are from one sample t-tests comparing with zero response.

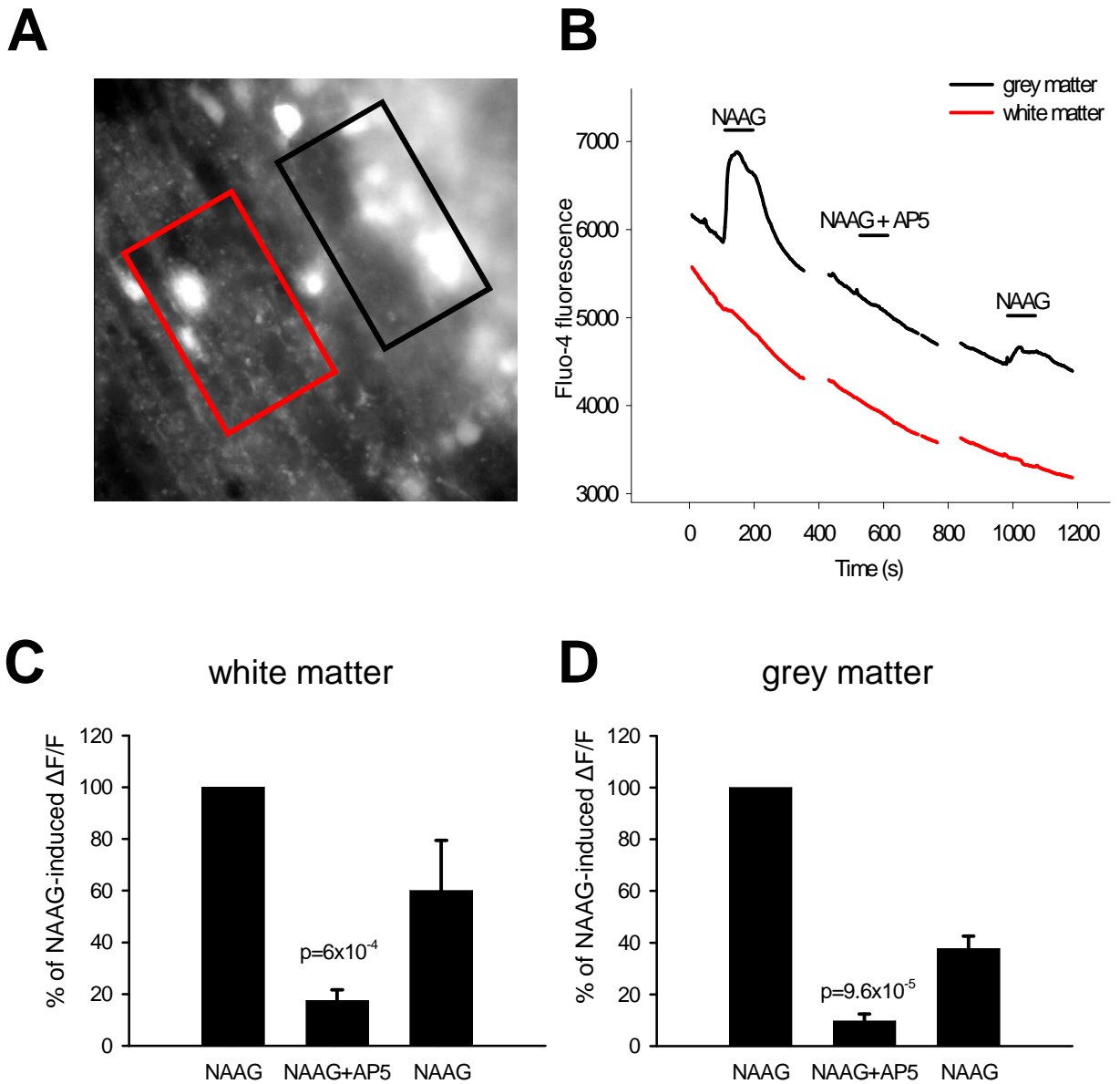


Figure 6.2

Block of NAAG-induced rise in $[Ca^{2+}]_i$ in white and grey matter by D-AP5 (100 μM). **A** Specimen image of cerebellar white matter (red region) and grey matter (black region) loaded with Fluo-4. **B** Block of NAAG-induced rise in Fluo-4 fluorescence in white matter and grey matter by AP5. **C** Average responses of white matter to NAAG, NAAG+AP5 and a subsequent application of NAAG, normalised to the amplitude of the first response. **D** Normalised average responses of grey matter to NAAG, NAAG+AP5, and a subsequent application of NAAG. All the experiments were performed in 4 slices. P values compare the response in AP5 with the average of the bracketing control responses without AP5.

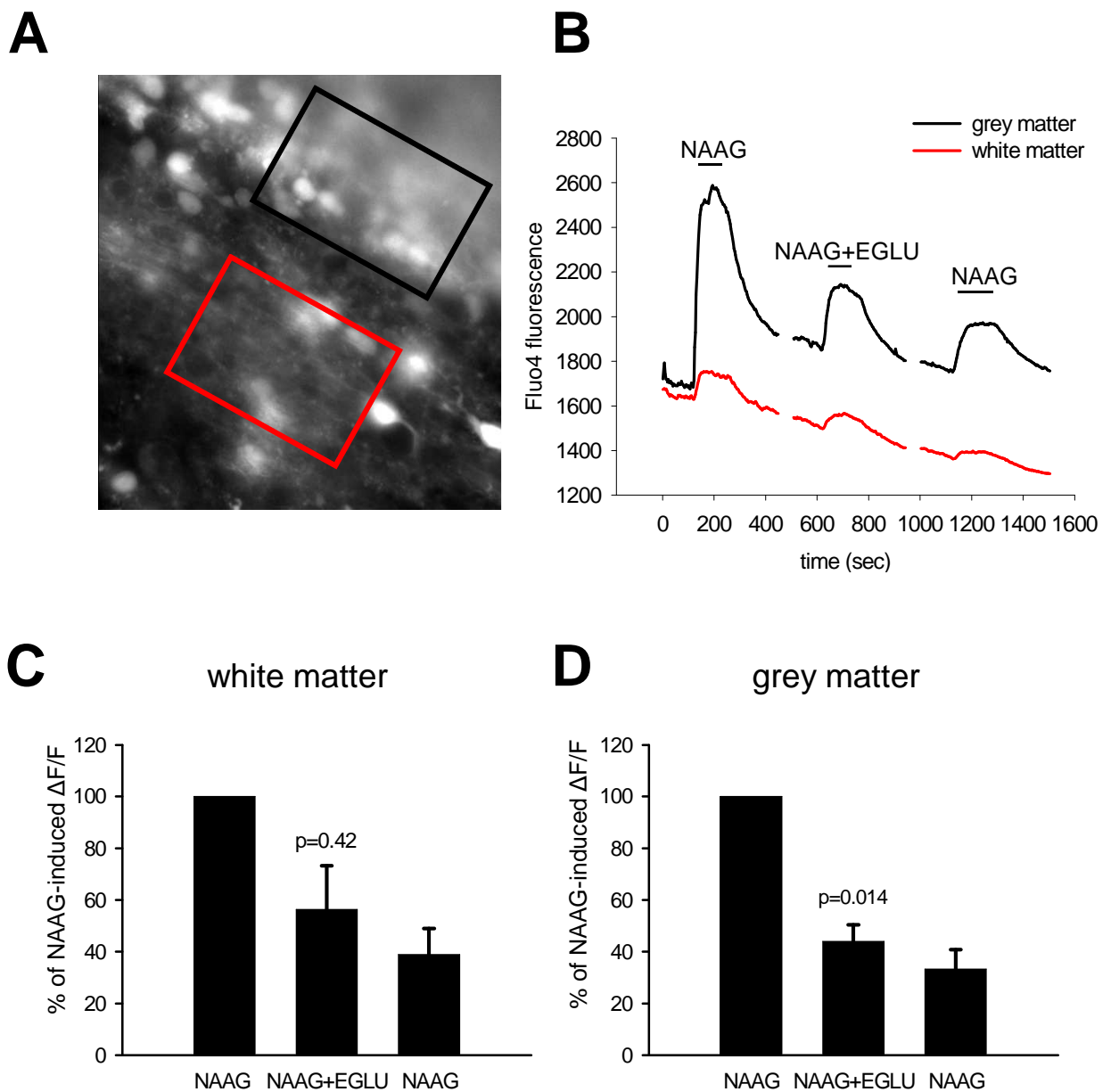


Figure 6.3

The group II mGluR blocker EGLU (200 μ M) did not reduce the NAAG-induced $[Ca^{2+}]_i$ rise in the white matter, but produced a small but significant decrease in the NAAG-evoked $[Ca^{2+}]_i$ rise in the grey matter. **A** Specimen image of cerebellar white matter (red region) and grey matter (black region) loaded with Fluo-4. **B** Effect of EGLU on the NAAG-induced rise in Fluo-4 fluorescence in white matter and grey matter (note that there is a strong run down of the responses to repeated agonist application, on which the EGLU effect will superimpose). **C** Average responses of white matter to NAAG, NAAG+EGLU and a subsequent application of NAAG, normalised to the amplitude of the first response. **D** Normalised average responses of grey matter to NAAG, NAAG+EGLU, and a subsequent application of NAAG. All the experiments were performed in 3 slices. P values compare the response in EGLU to the mean of the bracketing control responses (this procedure assumes that the rundown of the response in the absence of EGLU is linear with time).

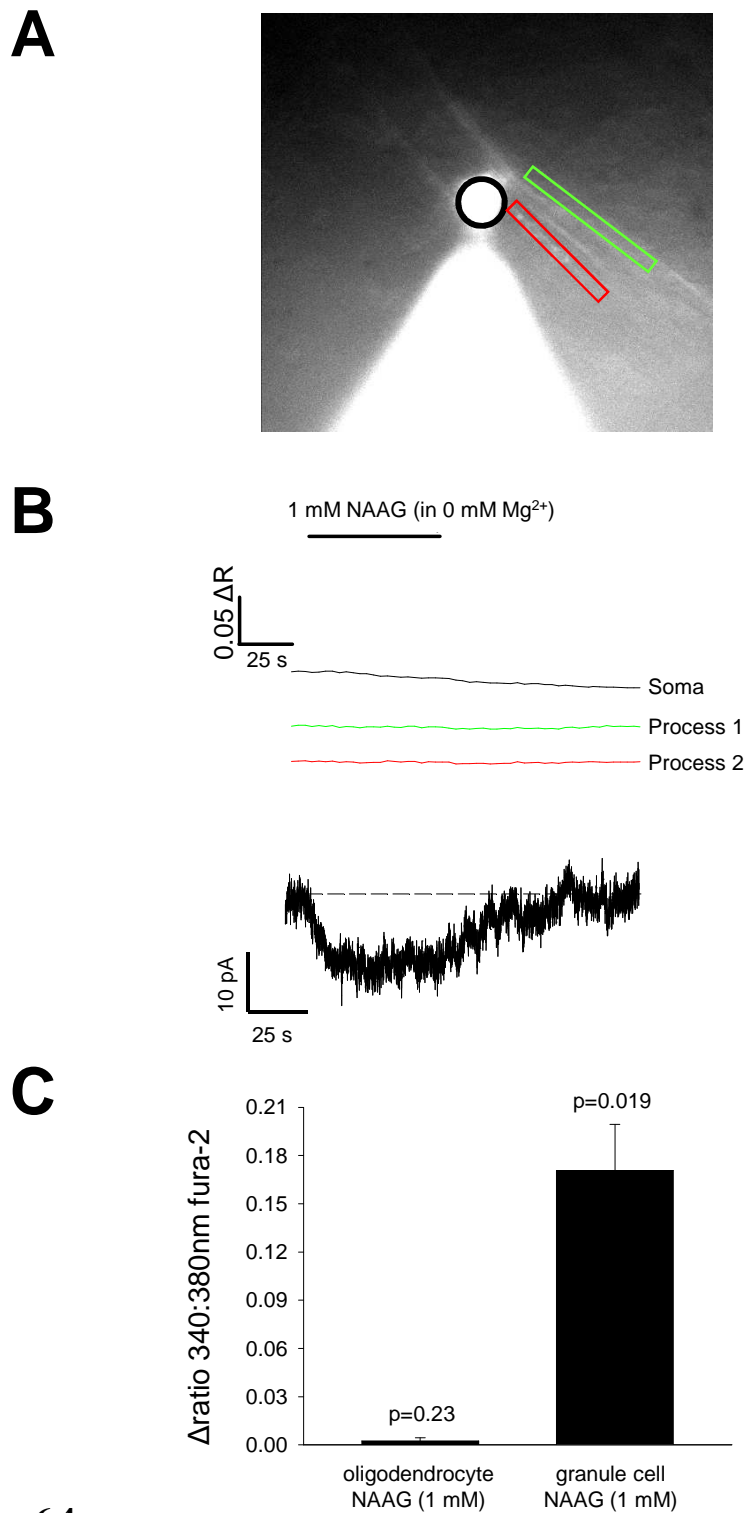


Figure 6.4

No detectable changes occurred in $[Ca^{2+}]_i$ in oligodendrocytes after NAAG (1 mM) application. **A** Specimen image of a cerebellar white matter oligodendrocyte, patch-clamped with a pipette containing Fura-2. Black line encircles soma, green and red rectangles are around processes aligned with axons. **B** Lack of change of Fura-2 fluorescence in both the soma and processes of the oligodendrocyte in **A** after application of 1mM NAAG (upper panel), despite NAAG evoking an inward current (lower panel). **C** Average responses of oligodendrocyte and granule cell somata (8 and 7 cells respectively). Granule cell data are from experiments as in Fig. 6.5. P values are from one sample t-tests comparing with zero response.

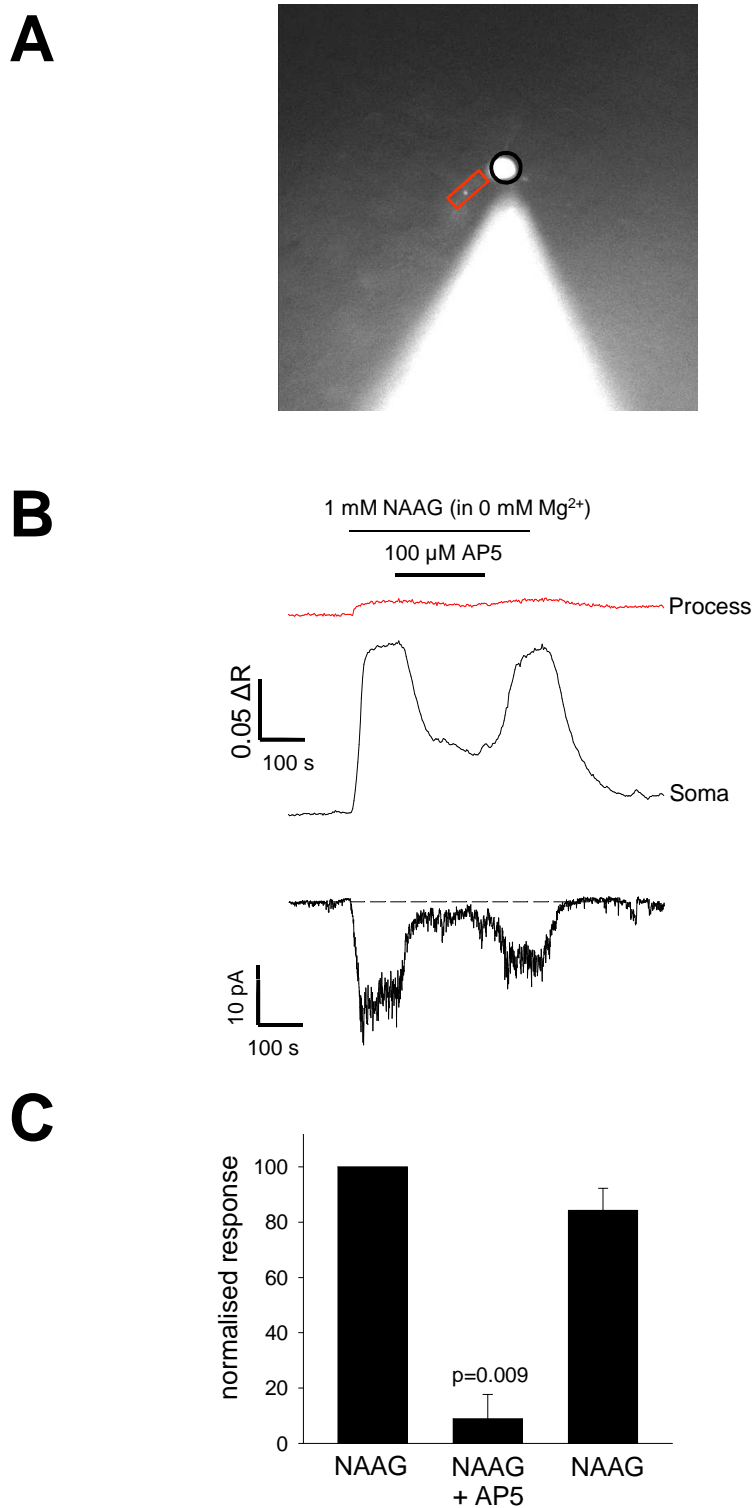


Figure 6.5

NAAG-evoked changes in $[Ca^{2+}]_i$ in cerebellar granule cells mediated by NMDA receptors. **A** Specimen image of a single granule cell patch-clamped with a pipette containing Fura-2. Black line encircles soma, red rectangle is around a single dendrite. **B** Change of Fura-2 fluorescence ($\Delta R =$ change of ratio 340nm/380nm) in the granule cell in B after application of 1mM NAAG, and block of this response by 100 μ M D-AP5 (upper panel), with the simultaneously evoked inward current (lower panel). **C** Average responses of granule cells to NAAG, NAAG+AP5, and a subsequent application of NAAG, normalised to the initial response (n=3 cells for each). P value compares the response in AP5 to the mean of the bracketing control responses.

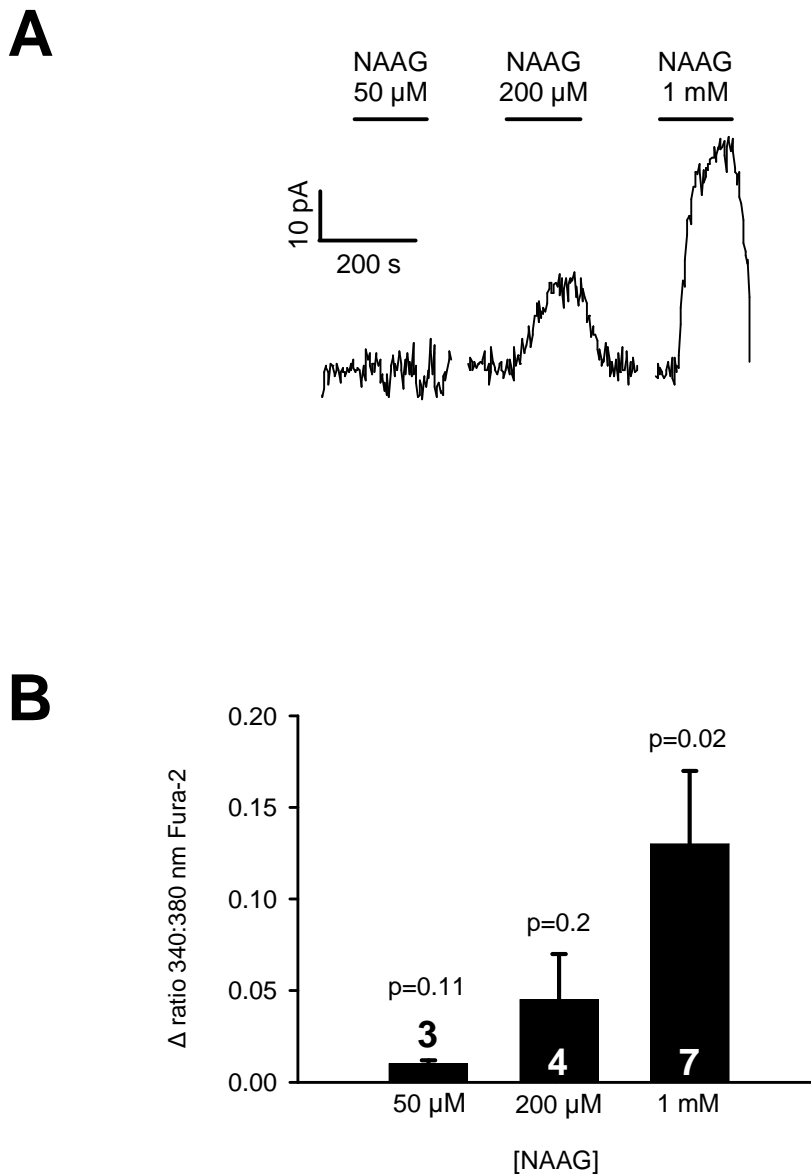
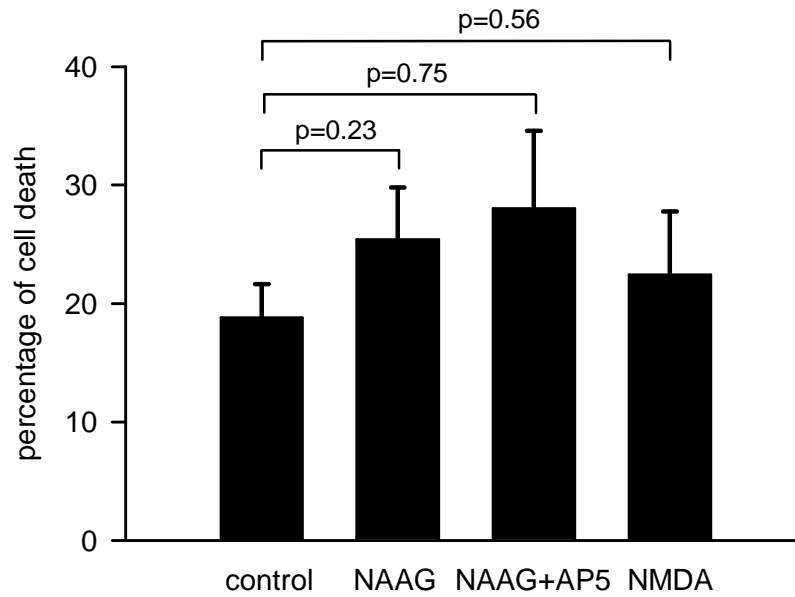
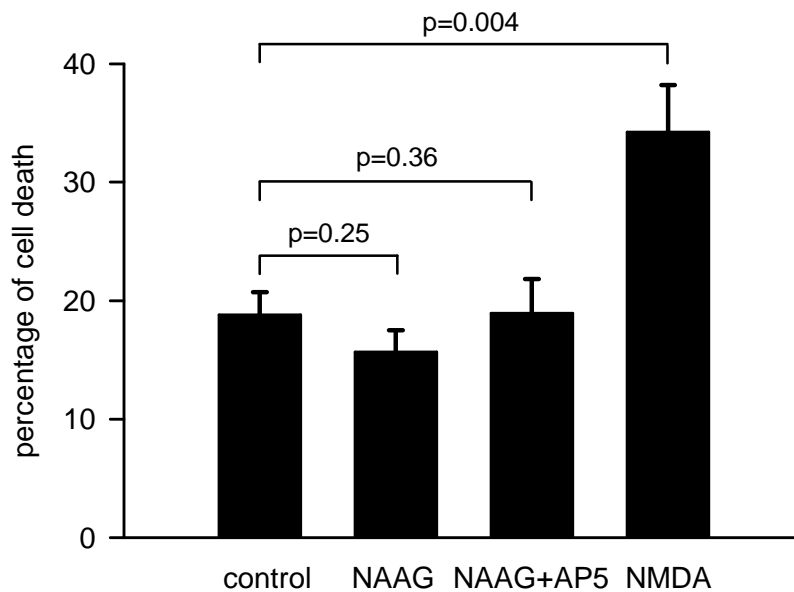


Figure 6.6

$[Ca^{2+}]_i$ rise in cerebellar granule cells, evoked by pathologically relevant concentrations of NAAG. **A** Representative image of a cerebellar granule cell patch-clamped with a pipette containing Fura-2. **B** $[Ca^{2+}]_i$ rise in a single granule cell upon application of 50 μ M, 200 μ M and 1 mM NAAG. **C** Average responses to 50, 200 and 1000 μ M NAAG in 3, 4 and 7 (respectively) granule cells. P values are from one sample t-tests comparing with zero response. The experiments were performed in 0 mM Mg^{2+} solution.

A**B****Figure 6.7**

The death of white matter (**A**) and grey matter (**B**) cells evoked by NAAG (1 mM; n=11 slices), NAAG+AP5 (1 mM and 100 μ M, respectively; n=6 slices), and NMDA (100 μ M; n=10 slices), compared with the death in control solution (n=10 slices). Slices were incubated at 36°C for 6 h, and data were averaged from 3 replicate experiments. The percentage of death was calculated by dividing the number of dead cells (labelled with PI) by the total number of cells (given by the number of nuclei labelled with DAPI).

Chapter 7: Discussion

In this chapter I will give a brief discussion of the results obtained in my PhD, and point out further experiments that could be done to address remaining interesting questions that I did not have time to address in the 3 year PhD.

7.1 The electrical response of white matter oligodendrocytes to simulated ischaemia

In Chapter 3 I characterised the membrane current changes evoked by ischaemia in oligodendrocytes.

7.1.1 Discussion

Mature oligodendrocytes responded to simulated ischaemia by generating an inward current which had a stereotypical waveform and an amplitude which increased as the cells developed. The amplitude and time course of the current were independent of the main ion used in the internal solution (Cs^+ or K^+).

When not voltage-clamped, oligodendrocytes responded to the stimulus with depolarisation that was much larger with Cs^+ inside than with K^+ inside, suggesting that K^+ channels generate an outward current at depolarised potentials, and/or at late times in ischaemia, which limits the depolarisation occurring, and that Cs^+ is not permeant through these channels. This suggests that, *in vivo*, oligodendrocytes will only undergo an ischaemia-evoked depolarization of less than 20 mV and then repolarise back towards their initial membrane potential. This feature is unique to oligodendrocytes as it was not observed in neurons (Hamann *et al.*, 2005) or astrocytes (Xie *et al.*, 2008).

During ischaemia the cell membrane resistance increased significantly. There was no capacitance decrease, which would have implied that this change could be attributed to a loss of the cell's myelinating processes. Interestingly, analysis of the I-V relation of the cells revealed that the increase in cell membrane resistance was induced by a closing of potassium channels. This phenomenon has not been reported previously, and is

dramatically different from the neuronal response to ischaemia, which is dominated by the opening of glutamate-gated cation channels.

7.1.2 Suggestions for the further work

The closing of potassium channels is apparently followed by the opening of voltage-gated K^+ channels that generate the membrane repolarisation. It would be interesting to identify the specific potassium channels that are involved in both of these processes. This is difficult, because of a lack of specific blockers for these channel types, and because any blockers applied will also affect channels in neurons and astrocytes, thus altering the change of $[K^+]_o$ occurring. Nevertheless, Gipson and Bordey (2002) showed that extracellular Cs^+ (5 mM) blocks inward rectifier currents in mature oligodendrocytes in corpus callosum slices, while Ba^{2+} (1 mM) blocks both inward and outward passive currents, and it would be interesting to assess the effect of these agents on the I-V relation of the oligodendrocytes in ischaemia to try to identify the channels which are closed in the initial part of the ischaemic response. Gipson and Bordey (2002) also reported the expression of a TEA-sensitive outward current in mature oligodendrocytes, which they attributed to the activation of delayed rectifier channels. Testing whether TEA inhibits the late repolarisation phase in ischaemia might therefore provide a test of my suggestion that this repolarisation is mediated by the activation of voltage-dependent (delayed rectifier) channels. Such channels would have to be activated by the relatively small depolarisation that is evoked by ischaemia in oligodendrocytes.

It would be interesting to test whether, at the time of the ischaemia-induced current in the oligodendrocytes, there is a rise of $[K^+]_o$ produced in the white matter. In order to do that, a K^+ -sensitive electrode could be used while simultaneously recording the ischaemia-evoked current from an oligodendrocyte. Of particular interest is whether the fast component of the inward current evoked after several minutes ischaemia reflects an increase of $[K^+]_o$ that is driven by the anoxic depolarization occurring in neurons in the nearby grey matter. This could be assessed by simultaneously recording (with two patch clamps) the current changes occurring in a granule or Purkinje cell and in an oligodendrocyte.

In all the experiments, ATP was one of the ingredients of the internal solution, added to better mimic the physiological intracellular solution. However, during ischaemia the intracellular ATP levels will fall due to the inhibition of glycolysis and oxidative phosphorylation, but this effect may not occur in the patch-clamped cell due to its constant perfusion by the ATP-containing pipette solution (in practice this will maintain the intracellular level better near the soma than at the ends of the long myelinating processes of the cells). It would be interesting, therefore, to test the oligodendrocyte's response to ischaemia using an internal solution devoid of ATP – although such an approach could induce a response unrelated to ischaemia and produced by ATP depletion even before the application of the ischaemic solution.

7.2 The role of glutamate in the oligodendrocyte response to ischaemia

In Chapter 4 I assessed the role of glutamate in generating the ischaemia-evoked current in oligodendrocytes.

7.2.1 Discussion

I showed that glutamate is released into the white matter in ischaemia primarily *via* the reversal of glutamate transporters, which confirmed a previous study by Li *et al.* (1999). Glutamate release as a result of the activity of astroglial NKCC1 co-transporters (Wilke *et al.*, 2006), synaptic release from unmyelinated axons (Kukley *et al.*, 2007; Ziskin *et al.*, 2007) or microglial system X_c⁻ (Domercq *et al.*, 2009) did not contribute significantly on the time scale that I investigated.

I also demonstrated that glutamate is the main trigger of the mature oligodendrocytes' response to ischaemia. Ionotropic glutamate receptor blockers (NBQX and AP5 applied together) and a metabotropic glutamate receptor blocker (MCPG), significantly reduced the inward current, unlike antagonists of P2X₇ receptors (Domercq *et al.*, 2010), hemichannel opening (Domercq *et al.*, 2010), ASICs (Feldman *et al.*, 2008), neuronal action potential, TRP channels or GABA_A receptors.

Interestingly, once initiated, the ischaemia-evoked inward current could not be blocked by ionotropic glutamate receptor blockers. This effect is different to that observed in neurons, where glutamate receptor blockers inhibited the current at any point of the cell response to ischaemia (Rossi *et al.*, 2000; Hamann *et al.*, 2005). Furthermore, this effect differs from the irreversible extended depolarization (END) observed in neurons (Sombati *et al.*, 1991; Limbrick *et al.*, 2003) in that it is not blocked by applying Gd^{3+} or removing external calcium. Thus, this response is specific to oligodendrocytes and has not been described in the literature before.

7.2.2 Suggestions for further work

As ionotropic and metabotropic glutamate receptor blockers reduced the ischaemia-induced current when applied separately, it would be interesting to test if the current was completely abolished with these blockers applied together, and if the current can be blocked by applying MCPG after the current has been initiated. Also, MCPG is a broad-spectrum mGluR blocker and so the use of the antagonists specific to the different groups of mGluRs would allow identification of the mGluR subtype involved.

It would be highly desirable to employ Ca^{2+} -imaging as an additional tool to characterise glutamate's effect on oligodendrocytes during ischaemia. A previous study, performed on the whole optic nerve, reported a continuous $[Ca^{2+}]_i$ rise in mature oligodendrocytes from the beginning of ischaemia, which was attributed to an NMDA-mediated Ca^{2+} influx into the cell processes (Micu *et al.*, 2006). However, neither blocking NMDA receptors alone (with 200 μ M AP5, i.e. a concentration twice as high as the one used by Micu *et al.*, 2006) nor omitting Ca^{2+} from the external solution (accompanied by 50 μ M EGTA, a Ca^{2+} chelator, to ensure a lack of free external Ca^{2+}) affected the shape or the amplitude of the ischaemia-evoked current and so it is highly unlikely that the current response reflects an NMDA receptor mediated Ca^{2+} entry into the cell. A study investigating the $[Ca^{2+}]_i$ changes evoked by ischaemia performed on a single cell loaded with Ca^{2+} dye from the patch pipette (i.e. not in a whole slice loaded with the AM ester form of the calcium dye), would provide a better approach to define the existence and source of an ischaemia-evoked $[Ca^{2+}]_i$ rise in oligodendrocytes.

The END-like effect in oligodendrocytes was not reported in the literature before. Such a response could be unique to oligodendrocytes, but it is also possible that the effect is more generally present in all glial cells, including astrocytes, Bergmann glia and Müller cells. It would be interesting to test this possibility, which could give us a better insight into the glial response to ischaemia, which seems to be significantly different to the one observed in neurons. Understanding this process could help with the development of therapies aiming, not only at neuronal, but also at glial cell survival in pathological conditions.

7.3 Oligodendroglial and neuronal electrical responses to NAA and NAAG

In Chapter 5 I tested whether NAA or NAAG act on glutamate receptors to evoke a membrane current in oligodendrocytes, to test the hypothesis that such an action might contribute to the cell damage occurring in certain leukodystrophies.

7.3.1 Discussion

The concentration of NAA and NAAG rises considerably in two types of leukodystrophy, Canavan Disease (CD) and Pelizaeus-Merzbacher-like Disease (PMLD). I showed for the first time that NAAG, but not NAA evoked an inward current in mature oligodendrocytes, by acting on NMDA receptors, although this current is small. The response was partially of an indirect nature, as blocking neuronal action potential significantly reduced the NAAG-evoked inward current. Additionally, there was a substantial reduction in the current upon the block of GCP II, the peptidase enzyme that cleaves NAAG to NAA and glutamate, suggesting that part of the response is caused by glutamate and not directly by NAAG. In comparison, the granule cell response to NAAG (which was significantly larger than the one observed in oligodendrocytes, despite the granule cells being smaller in membrane area) was not affected either by inhibition of action potentials or block of GCP II.

NAAG and NAA did not block the NMDA-induced current in oligodendrocytes, while NAA exerted a small blocking effect on the granule cell response to NMDA. This

block implies that NAA could antagonise granule cell NMDA receptor activation under pathological conditions, such as CD (where NAA levels rise to 0.4-0.9 mM (Burlina *et al.*, 1999), i.e. the concentration used in this study), and thus possibly affect the cell's excitability.

The pathologically-relevant concentration of NAAG, reported in Pelizeus-Merzbacher-like disease (Wolf *et al.*, 2004; Sartori *et al.*, 2008), evoked a statistically significant current in oligodendrocytes (and in granule cells) at a concentration of 200 μ M, but only when no external magnesium was present. This result further suggests a very low affinity of NAAG towards oligodendrocyte NMDA receptors and lowers the possibility of this substance having direct pathological effects on oligodendrocytes.

7.3.2 Suggestions for further work

I tested the effect of NAA and NAAG early in development on mature oligodendrocytes that had recently myelinated axons. This implicitly assumes a hypothesis in which the loss of myelin observed in CD and PMLD is caused by a process of demyelination, i.e. the loss of already formed myelin. However, it is also possible that the leukodystrophies develop due to an inability of the oligodendrocyte precursors to differentiate into mature oligodendrocyte and hence produce myelin. The fact that the NMDA receptor-mediated currents in OPCs (in particular their weak Mg^{2+} block) seem similar to those in mature cells (Karadottir *et al.*, 2005) suggests that it is unlikely that NAA and NAAG damage OPCs by acting on these receptors. However, OPCs could be affected by NAA or NAAG *via* a different mechanism, affecting their survival or their ability to develop into mature oligodendrocytes. This hypothesis should be tested, by applying NAA and NAAG to OPCs in the white matter and recording their membrane current and $[Ca^{2+}]_i$ changes.

7.4 Oligodendroglial and neuronal intracellular calcium concentration changes as a response to NAA and NAAG

Chapter 6 reports experiments testing whether NAA or NAAG evoke $[Ca^{2+}]_i$ elevations in oligodendrocytes or neurons.

7.4.1 Discussion

The application of NAAG, but not NAA, in both white and grey matter, evoked a significant increase in $[Ca^{2+}]_i$ (as assessed by AM-loading calcium dye into many cells in the tissue) suggesting an activation of NMDA receptors – a hypothesis that was confirmed by blocking the $[Ca^{2+}]_i$ rise with AP5. Application of a blocker of mGluR3, another candidate receptor by which these compounds might act, did not have an effect on the white matter response to NAAG, but reduced the response in the grey matter. This effect could be attributed to the opening of non-specific cation channels upon mGluR3 activation (Guérineau *et al.*, 1995).

Surprisingly, when single oligodendrocytes were patch-clamped, they did not exhibit a $[Ca^{2+}]_i$ change on NAAG application, either in the soma or in their processes (where oligodendrocyte NMDA receptors were suggested to be preferentially expressed; Salter and Fern, 2005; Micu *et al.*, 2006). This result might be explained by the oligodendrocyte NMDA receptors having a small Ca^{2+} permeability due to the presence in their structure of an NR3 subunit (Sasaki *et al.*, 2002), or by the action of NAAG being largely indirect and through activation of neuronal NMDA receptors (perhaps, for example, inducing an extracellular $[K^+]$ rise which leads to an inward current in oligodendrocytes that does not include a Ca^{2+} component). In comparison, single patch-clamped granule cells still displayed a $[Ca^{2+}]_i$ rise, like the bulk dye-loaded grey matter, confirming a direct action of NAAG on neuronal NMDA receptors. In some cells there was also a clear rise in $[Ca^{2+}]_i$ when the pathologically relevant concentration of 200 μM NAAG was applied, although this did not reach statistical significance when averaged across all cells studied.

The cell death assay performed after applying NAA and NAAG for 6 hours showed that these substances are unlikely to cause a substantial death of oligodendrocytes and neurons, at least on this time scale.

7.4.2 Suggestions for further work

As explained in section 7.3.2, it would be desirable to test the possibility that NAA and NAAG act on OPCs and inhibit their development in the leukodystrophies.

Ca²⁺-imaging studies should accompany the suggested electrophysiological experiments to more comprehensively describe the effect of NAA and NAAG on OPCs.

The white matter showed a [Ca²⁺]_i increase upon NAAG application, but this effect was not seen when single oligodendrocytes were studied. This implies that the change in [Ca²⁺]_i in the white matter is presumably occurring in another cell type within structure (into which the AM ester of the calcium dye has passed), presumably astrocytes. It would be interesting to test this hypothesis by applying NAAG to single patch-clamped astrocytes.

Finally, the cell death assay was performed for only 6 hours, and will probably mainly detect necrotic cell death. In contrast, the exposure of oligodendrocytes to highly elevated levels of NAA and NAAG in children who have the leukodystrophies is constant and lasts for a prolonged time. That implies that the experiments should be repeated on cultured slices, which could be exposed to NAA and NAAG for a considerably longer time than 6 hours, and (in addition to propidium iodide) caspase 3 labelling should be employed in order to assess both apoptotic and necrotic death caused by these two substances.

7.5 Conclusion

The experiments performed during my PhD and described in this thesis investigated the response of mature oligodendrocytes to pathological stimuli.

I showed that, in white matter ischaemia, the main origin of the excessive glutamate release occurring is the reversal of glutamate transporters (located, most probably, on axons and oligodendrocytes: Li *et al.*, 1999). Glutamate, acting on its ionotropic and metabotropic receptors, induces an inward current in oligodendrocytes that is a result of potassium channel closing. The direct cause of this phenomenon is not known. The sodium influx occurring through AMPA/KA receptors was previously shown to result in the closing of potassium channels in oligodendrocyte precursors (Knutson *et al.*, 1997) making plausible an explanation that sodium ions actively block the potassium channels' pore from its intracellular side. Another possibility is that an excessive

activation of glutamate receptors could trigger changes in the phosphorylation state of potassium channels. It has been shown previously that TASK and TREK channels are inhibited by the activation of G_q protein-coupled receptors (Mathie, 2007) that would also occur upon type I mGluR activation. Changes in the phosphorylation state of potassium channels could also cause their internalization: KCNQ1 channels were shown to undergo increased endocytosis upon G_q protein-coupled receptor activation (Kanda *et al.*, 2011), and Kv4.2 internalisation was reported to be an effect of the phosphorylation of these channels following AMPA receptor activation (Hammond *et al.*, 2008). Finally, the action of glutamate on oligodendrocyte potassium channels might be of an indirect nature, e.g. glutamate activating its receptors on astrocytes could cause a release of a secondary agent, such as 20-HETE, that would trigger the closing of oligodendrocyte potassium channels.

The closing of the potassium channels might eventually lead to oligodendrocyte damage or death in ischaemia. A loss of the potassium spatial buffering capabilities of oligodendrocytes will increase the rise of extracellular potassium concentration occurring in ischaemia. The resulting water efflux from the oligodendrocytes might disrupt the myelin and the attachment of the oligodendrocyte processes to the axons, possibly causing rupture of the oligodendrocyte membrane and thus, ultimately, death of the soma. The slow voltage repolarisation phase seen in current clamp experiments might occur due to the opening of slow outwardly rectifying calcium-activated potassium channels, caused by the opening of voltage-dependent calcium channels. Even a small calcium influx (that could be later amplified by calcium-induced calcium release), especially into the very compact intracellular space of the myelinating processes, could cause a detrimental effect to the processes and thus to the integrity of the whole cell. For a summary of the various contributions to the oligodendrocyte response to ischaemia, see Figure 7.1.

The ischaemia-induced response in oligodendrocytes differs substantially from that observed in neurons: unlike in neurons, the inward current is not primarily due to the opening of non-selective cation channels and, once triggered, it cannot be blocked by ionotropic glutamate receptor blockers (an effect similar to the END effect observed in neurons). These features make the oligodendrocyte response to ischaemia unique and are described in this thesis for the first time.

I also tested the hypothesis that high concentrations of NAA and NAAG can cause myelin damage and oligodendrocyte loss by acting on oligodendrocyte NMDA receptors in two types of leukodystrophy: Canavan Disease and Pelizaeus-Merzbacher-like Disease. I discovered that, although oligodendrocytes respond with a small current to NAAG (but not NAA), its effect on the cells is to a large extent secondary to an action of NAAG (or glutamate derived from NAAG) on neurons.

Further work is needed to describe the oligodendrocyte response to ischaemia in greater detail and to test the possibility of an action of NAA and NAAG on OPCs, with the long term aim of developing therapeutic strategies to prevent oligodendrocyte damage.

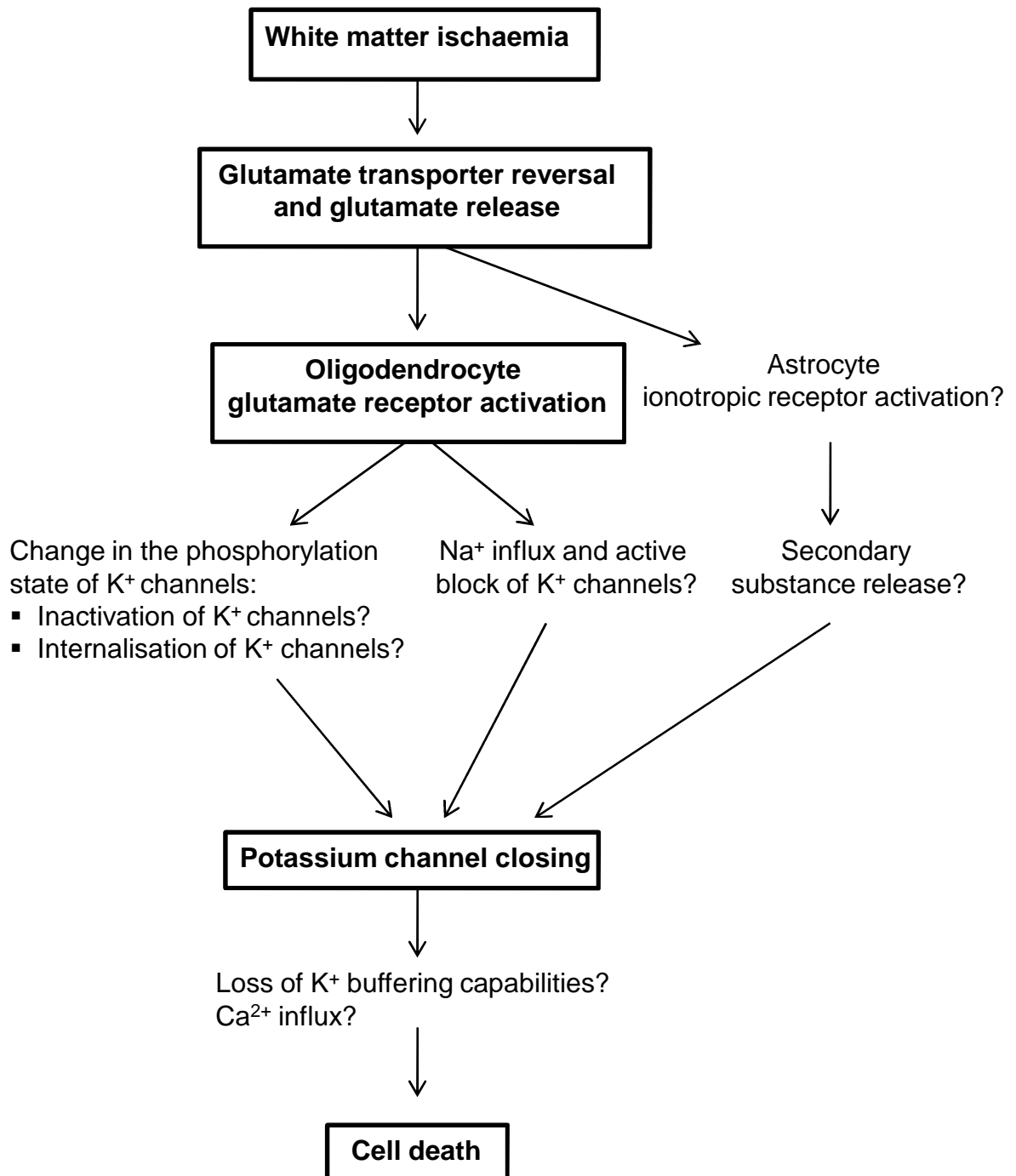


Figure 7.1

The possible sequence of events underlying the oligodendrocytes' response to ischaemia. In white matter ischaemia, cell membrane depolarisation causes the reversal of glutamate transporters and a release of glutamate which acts on oligodendrocyte glutamate receptors. The activation of the receptors triggers the irreversible closing of potassium channels, which may occur due to changes in the phosphorylation state of potassium channels and/or the active block of the channels by sodium ions. Alternatively, astrocytic glutamate receptor activation might lead to the release of a secondary substance that acts on oligodendrocytes. Closing of potassium channels may result in cell death as a result of a decrease of the oligodendrocytes' abilities to buffer potassium or an activation of a voltage-gated calcium influx into the cell, either of which could lead to process loss and damage to the soma.

Chapter 8: Bibliography

- Aarts M., Ihara K., Wei W.L., Xiong Z.G., Arundine M., Cerwinski W., MacDonald J.F. and Tymianski M., 2003. A key role for TRPM7 channels in anoxic neuronal death. *Cell*, 115(7), pp.863-877.
- Abbracchio M.P., Burnstock G., Verkhratsky A. and Zimmermann H., 2009. Purinergic signalling in the nervous system: an overview. *Trends Neurosci*, 32(1), pp.19-29.
- Agrawal S.K. and Fehlings M.G., 1997. Role of NMDA and non-NMDA ionotropic glutamate receptors in traumatic spinal cord axonal injury. *J Neurosci*, 17(3), pp.1055-1063.
- Agrawal S.K., Nashmi R. and Fehlings M.G., 2000. Role of L- and N-type calcium channels in the pathophysiology of traumatic spinal cord white matter injury. *Neuroscience*, 99(1), pp.179-188.
- Agresti C., Meomartini M.E., Amadio S., Ambrosini E., Volonté C., Aloisi F. and Visentin S., 2005. ATP regulates oligodendrocyte progenitor migration, proliferation, and differentiation: involvement of metabotropic P2 receptors. *Brain Res Brain Res Rev*, 48(2), pp.157-165.
- Allen N.J. and Attwell D., 2002. Modulation of ASIC channels in rat cerebellar Purkinje neurons by ischaemia-related signals. *J Physiol*, 543(Pt 2), pp.521-529.
- Allen N.J., Káradóttir R. and Attwell D., 2005. A preferential role for glycolysis in preventing the anoxic depolarization of rat hippocampal area CA1 pyramidal cells. *J Neurosci*, 25(4), pp.848-859.
- Allen N.J., Rossi D.J. and Attwell D., 2004. Sequential release of GABA by exocytosis and reversed uptake leads to neuronal swelling in simulated ischemia of hippocampal slices. *J Neurosci*, 24(15), pp.3837-3849.
- Alvarez-Leefmans F.J., Gamiño S.M., Giraldez F. and Noguerón I., 1988. Intracellular chloride regulation in amphibian dorsal root ganglion neurones studied with ion-selective microelectrodes. *J Physiol*, 406, pp.225-246.
- Arai K. and Lo E.H., 2009. Oligovascular signaling in white matter stroke. *Biol Pharm Bull*, 32(10), pp.1639-1644.
- Ariyannur P.S., Moffett J.R., Manickam P., Pattabiraman N., Arun P., Nitta A., Nabeshima T., Madhavarao C.N. and Namboodiri A.M., 2010. Methamphetamine-induced neuronal protein NAT8L is the NAA biosynthetic enzyme: implications for specialized acetyl coenzyme A metabolism in the CNS. *Brain Res*, 1335, pp.1-13.

- Armstrong R.C., Harvath L. and Dubois-Dalcq M.E., 1990. Type 1 astrocytes and oligodendrocyte-type 2 astrocyte glial progenitors migrate toward distinct molecules. *J Neurosci Res*, 27(3), pp.400-407.
- Arundine M. and Tymianski M., 2004. Molecular mechanisms of glutamate-dependent neurodegeneration in ischemia and traumatic brain injury. *Cell Mol Life Sci*, 61(6), pp.657-668.
- Attwell D. and Laughlin S.B., 2001. An energy budget for signaling in the grey matter of the brain. *J Cereb Blood Flow Metab*, 21(10), pp.1133-1145.
- Back S.A., Han B.H., Luo N.L., Chricton C.A., Xanthoudakis S., Tam J., Arvin K.L. and Holtzman D.M., 2002. Selective vulnerability of late oligodendrocyte progenitors to hypoxia-ischemia. *J Neurosci*, 22(2), pp.455-463.
- Bagayogo I.P. and Dreyfus C.F., 2009. Regulated release of BDNF by cortical oligodendrocytes is mediated through metabotropic glutamate receptors and the PLC pathway. *ASN neuro*, 1(1), p.e00001.
- Bakiri Y., Burzomato V., Frugier G., Hamilton N.B., Káradóttir R. and Attwell D., 2009. Glutamatergic signaling in the brain's white matter. *Neuroscience*, 158(1), pp.266-274.
- Bakiri Y., Hamilton N.B., Káradóttir R. and Attwell D., 2008. Testing NMDA receptor block as a therapeutic strategy for reducing ischaemic damage to CNS white matter. *Glia*, 56(2), pp.233-40.
- Bakiri Y., Káradóttir R., Cossell L. and Attwell D., 2011. Morphological and electrical properties of oligodendrocytes in the white matter of the corpus callosum and cerebellum. *J Physiol*, 589(3), pp.559-573.
- Baltan S., Besancon E.F., Mbow B., Ye Z., Hamner M.A. and Ransom B.R., 2008. White matter vulnerability to ischemic injury increases with age because of enhanced excitotoxicity. *J Neurosci*, 28(6), pp.1479-1489.
- Baron A., Waldmann R. and Lazdunski M., 2002. ASIC-like, proton-activated currents in rat hippocampal neurons. *J Physiol*, 539(Pt 2), pp.485-494.
- Barres B.A., Koroshetz W.J., Swartz K.J., Chun L.L. and Corey D.P., 1990. Ion channel expression by white matter glia: the O-2A glial progenitor cell. *Neuron*, 4(4), pp.507-524.
- Barres B.A. and Raff M.C., 1993. Proliferation of oligodendrocyte precursor cells depends on electrical activity in axons. *Nature*, 361(6409), pp.258-260.
- Barres B.A. and Raff M.C., 1994. Control of oligodendrocyte number in the developing rat optic nerve. *Neuron*, 12(5), pp.935-942.

- Barres B.A. and Raff M.C., 1999. Axonal control of oligodendrocyte development. *J Cell Biol*, 147(6), pp.1123-1128.
- Baslow M.H., 2002. Evidence supporting a role for N-acetyl-L-aspartate as a molecular water pump in myelinated neurons in the central nervous system. An analytical review. *Neurochem Int*, 40(4), pp.295-300.
- Baslow M.H., 2003. N-acetylaspartate in the vertebrate brain: metabolism and function. *Neurochem Res*, 28(6), pp.941-953.
- Baslow M.H., Suckow R.F., Sapirstein V. and Hungund B.L., 1999. Expression of aspartoacylase activity in cultured rat macroglial cells is limited to oligodendrocytes. *J Mol Neurosci*, 13(1-2), pp.47-53.
- Becker I., Lodder J., Gieselmann V. and Eckhardt M., 2010. Molecular characterization of N-acetylaspartylglutamate synthetase. *J Biol Chem*, 285(38), pp.29156-29164.
- Benarroch E.E., 2008. N-acetylaspartate and N-acetylaspartylglutamate: neurobiology and clinical significance. *Neurology*, 70(16), pp.1353-1357.
- Berent-Spillson A., Robinson A.M., Golovoy D., Slusher B., Rojas C. and Russell J.W., 2004. Protection against glucose-induced neuronal death by NAAG and GCP II inhibition is regulated by mGluR3. *J Neurochem*, 89(1), pp.90-9.
- Berger T., Schnitzer J. and Kettenmann H., 1991. Developmental changes in the membrane current pattern, K⁺ buffer capacity, and morphology of glial cells in the corpus callosum slice. *J Neurosci*, 11(10), pp.3008-3024.
- Berger T., Schnitzer J., Orkand P.M. and Kettenmann H., 1992a. Sodium and Calcium Currents in Glial Cells of the Mouse Corpus Callosum Slice. *Eur J Neurosci*, 4(12), pp.1271-1284.
- Berger T., Walz W., Schnitzer J. and Kettenmann H., 1992b. GABA- and glutamate-activated currents in glial cells of the mouse corpus callosum slice. *J Neurosci Res*, 31(1), pp.21-27.
- Berger U.V., Luthi-Carter R., Passani L.A., Elkabes S., Black I., Konradi C. and Coyle J.T., 1999. Glutamate carboxypeptidase II is expressed by astrocytes in the adult rat nervous system. *J Comp Neurol*, 415(1), pp.52-64.
- Bergeron R., Coyle J.T., Tsai G. and Greene R.W., 2005. NAAG reduces NMDA receptor current in CA1 hippocampal pyramidal neurons of acute slices and dissociated neurons. *Neuropsychopharmacology*, 30(1), pp.7-16.
- Bergeron R., Imamura Y., Frangioni J.V., Greene R.W. and Coyle J.T., 2007. Endogenous N-acetylaspartylglutamate reduced NMDA receptor-dependent current neurotransmission in the CA1 area of the hippocampus. *J Neurochem*, 100(2), pp.346-357.

- Bergles D.E., Roberts J.D., Somogyi P. and Jahr C.E., 2000. Glutamatergic synapses on oligodendrocyte precursor cells in the hippocampus. *Nature*, 405(6783), pp.187-191.
- Bhakoo K.K., Craig T.J. and Styles P., 2001. Developmental and regional distribution of aspartoacylase in rat brain tissue. *J Neurochem*, 79(1), pp.211-220.
- Billups D. and Attwell D., 2003. Active release of glycine or D-serine saturates the glycine site of NMDA receptors at the cerebellar mossy fibre to granule cell synapse. *Eur J Neurosci*, 18(11), pp.2975-2980.
- Bruzzone R., Hormuzdi S.G., Barbe M.T., Herb A. and Monyer H., 2003. Pannexins, a family of gap junction proteins expressed in brain. *Proc Natl Acad Sci USA*, 100(23), pp.13644-13649.
- Burlina A.P., Ferrari V., Divry P., Gradowska W., Jakobs C., Bennett M.J., Sewell A.C., Dionisi-Vici C., Burlina A.B., 1999. N-acetylaspartylglutamate in Canavan disease: an adverse effector? *Eur J Paediatr*, 158(5), pp.406-409.
- Burlina A.P., Schmitt B., Engelke U., Wevers R.A., Burlina A.B. and Boltshauser E., 2006. Hypoacetylaspartia: clinical and biochemical follow-up of a patient. *Adv Exp Med Biol*, 576, pp.283-287.
- Burlina A.P., Skaper S.D., Mazza MR., Ferrari V., Leon A. and Burlina A.B., 1994. N-acetylaspartylglutamate selectively inhibits neuronal responses to N-methyl-D-aspartic acid in vitro. *J Neurochem*, 63(3), pp.1174-1177.
- Burnstock G., 2006. Purinergic signalling. *Br J Pharmacol*, 147(1), pp.S172-181.
- Burzomato V., Frugier G., Pérez-Otaño I., Kittler J.T. and Attwell D., 2010. The receptor subunits generating NMDA receptor mediated currents in oligodendrocytes. *J Physiol*, 588(18), pp.3403-14.
- Bushell T., Clarke C., Mathie A. and Robertson B., 2002. Pharmacological characterization of a non-inactivating outward current observed in mouse cerebellar Purkinje neurones. *Br J Pharmacol*, 135(3), pp.705-712.
- Butt A.M. and Kalsi A., 2006. Inwardly rectifying potassium channels (Kir) in central nervous system glia: a special role for Kir4.1 in glial functions. *J Cell Mol Med*, 10(1), pp.33-44.
- Butt A.M. and Ransom B.R., 1989. Visualization of oligodendrocytes and astrocytes in the intact rat optic nerve by intracellular injection of lucifer yellow and horseradish peroxidase. *Glia*, 2(6), pp.470-475.
- Butt A.M. and Tutton M., 1992. Response of oligodendrocytes to glutamate and gamma-aminobutyric acid in the intact mouse optic nerve. *Neurosci Lett*, 146(1), pp.108-110.

- Bzdega T., Crowe S.L., Ramadan E.R., Sciarretta K.H., Olszewski R.T., Ojeifo O.A., Rafalski V.A., Wroblewska B. and Neale J.H., 2004. The cloning and characterization of a second brain enzyme with NAAG peptidase activity. *J Neurochem*, 89(3), pp.627-635.
- Bzdega T., Turi T., Wroblewska B., She D., Chung H.S., Kim H. and Neale J.H., 1997. Molecular cloning of a peptidase against N-acetylaspartylglutamate from a rat hippocampal cDNA library. *J Neurochem*, 69(6), pp.2270-2277.
- Cahoy J.D., Emery B., Kaushal A., Foo L.C., Zamanian J.L., Christopherson K.S., Xing Y., Lubischer J.L., Krieg P.A., Krupenko S.A., Thompson W.J. and Barres B.A., 2008. A transcriptome database for astrocytes, neurons, and oligodendrocytes: a new resource for understanding brain development and function. *J Neurosci*, 28(1), pp.264-278.
- Cai Z., Lin S. and Rhodes P.G., 2002. Neuroprotective effects of N-acetylaspartylglutamate in a neonatal rat model of hypoxia-ischemia. *Eur J Pharmacol*, 437(3), pp.139-145.
- Campanucci V.A., Fearon I.M. and Nurse C.A., 2003. A novel O₂-sensing mechanism in rat glossopharyngeal neurones mediated by a halothane-inhibitable background K⁺ conductance. *J Physiol*, 548(Pt 3), pp.731-743.
- Cavelier P. and Attwell D., 2005. Tonic release of glutamate by a DIDS-sensitive mechanism in rat hippocampal slices. *J Physiol*, 564(Pt 2), pp.397-410.
- Chakraborty G., Mekala P., Yahya D., Wu G. and Ledeen R.W., 2001. Intraneuronal N-acetylaspartate supplies acetyl groups for myelin lipid synthesis: evidence for myelin-associated aspartoacylase. *Journal of Neurochemistry*, 78(4), pp.736-745.
- Charles K.J., Calver A.R., Jourdain S. and Pangalos M.N., 2003. Distribution of a GABAB-like receptor protein in the rat central nervous system. *Brain Res*, 989(2), pp.135-146.
- Charles P., Reynolds R., Seilhean D., Rougon G., Aigrot M.S., Niezgodka A., Zalc B. and Lubetzki C., 2002. Re-expression of PSA-NCAM by demyelinated axons: an inhibitor of remyelination in multiple sclerosis? *Brain*, 125(Pt 9), pp.1972-1979.
- Chavis P., Fagni L., Bockaert J. and Lansman J.B., 1995. Modulation of calcium channels by metabotropic glutamate receptors in cerebellar granule cells. *Neuropharmacology*, 34(8), pp.929-937.
- Chen H. and Sun D., 2005. The role of Na-K-Cl co-transporter in cerebral ischemia. *Neurol Res*, 27(3), pp.280-286.
- Chen S., Ren Y.Q., Bing R. and Hillman D.E., 2000. Alpha 1E subunit of the R-type calcium channel is associated with myelinogenesis. *J Neurocytol*, 29(10), pp.719-728.

- Choi D.W., 1988. Glutamate neurotoxicity and diseases of the nervous system. *Neuron*, 1(8), pp.623-634.
- Choi D.W., Maulucci-Gedde M. and Kriegstein A.R., 1987. Glutamate neurotoxicity in cortical cell culture. *J Neurosci*, 7(2), pp.357-368.
- Chvátal A., Berger T., Vorísek I., Orkand R.K., Kettenmann H. and Syková E., 1997. Changes in glial K⁺ currents with decreased extracellular volume in developing rat white matter. *J Neurosci Res*, 49(1), pp.98-106.
- Colello R.J., Devey L.R., Imperato E. and Pott U., 1995. The chronology of oligodendrocyte differentiation in the rat optic nerve: evidence for a signaling step initiating myelination in the CNS. *J Neurosci*, 15(11), pp.7665-7672.
- Conn P.J. and Pin J.P., 1997. Pharmacology and functions of metabotropic glutamate receptors. *Annu Rev Pharmacol Toxicol*, 37, pp.205-237.
- Conti F., DeBiasi S., Minelli A. and Melone M., 1996. Expression of NR1 and NR2A/B subunits of the NMDA receptor in cortical astrocytes. *Glia*, 17(3), pp.254-258.
- Coulter D.A., Sombati S. and DeLorenzo R.J., 1992. Electrophysiology of glutamate neurotoxicity in vitro: induction of a calcium-dependent extended neuronal depolarization. *J Neurophysiol*, 68(2), pp.362-373.
- Coyle J.T., 1997. The nagging question of the function of N-acetylaspartylglutamate. *Neurobiol Dis*, 4(3-4), pp.231-238.
- Crang A.J., Gilson J.M., Li W.W. and Blakemore W.F., 2004. The remyelinating potential and in vitro differentiation of MOG-expressing oligodendrocyte precursors isolated from the adult rat CNS. *Eur J Neurosci*, 20(6), pp.1445-1460.
- Cull-Candy S.G. and Leszkiewicz D.N., 2004. Role of distinct NMDA receptor subtypes at central synapses. *Sci STKE*, 255, p.re16.
- Dawson M.R., Levine J.M. and Reynolds R., 2000. NG2-expressing cells in the central nervous system: are they oligodendroglial progenitors? *J Neurosci Res*, 61(5), pp.471-479.
- Dawson M.R., Polito A., Levine J.M. and Reynolds R., 2003. NG2-expressing glial progenitor cells: an abundant and widespread population of cycling cells in the adult rat CNS. *Mol Cell Neurosci*, 24(2), pp.476-488.
- De Biase L.M., Nishiyama A. and Bergles D.E., 2010. Excitability and synaptic communication within the oligodendrocyte lineage. *J Neurosci*, 30(10), pp.3600-3611.

- Demerens C., Stankoff B., Logak M., Anglade P., Allinquant B., Couraud F., Zalc B. and Lubetzki C., 1996. Induction of myelination in the central nervous system by electrical activity. *Proc Natl Acad Sci USA*, 93(18), pp.9887-92.
- Deng W., Rosenberg P.A., Volpe J.J. and Jensen F.E., 2003. Calcium-permeable AMPA/kainate receptors mediate toxicity and preconditioning by oxygen-glucose deprivation in oligodendrocyte precursors. *Proc Natl Acad Sci USA*, 100(11), pp.6801-6806.
- Deng W., Wang H., Rosenberg P.A., Volpe J.J. and Jensen F.E., 2004. Role of metabotropic glutamate receptors in oligodendrocyte excitotoxicity and oxidative stress. *Proc Natl Acad Sci USA*, 101(20), pp.7751-7756.
- Deshpande L.S., Limbrick D.D. Jr, Sombati S. and DeLorenzo R.J., 2007. Activation of a novel injury-induced calcium-permeable channel that plays a key role in causing extended neuronal depolarization and initiating neuronal death in excitotoxic neuronal injury. *J Pharmacol Exp Ther*, 322(2), pp.443-452.
- Dewar D., Underhill S.M. and Goldberg M.P., 2003. Oligodendrocytes and ischemic brain injury. *J Cereb Blood Flow Metab*, 23(3), pp.263-274.
- Dingledine R., Borges K., Bowie D. and Traynelis S.F., 1999. The glutamate receptor ion channels. *Pharmacol Rev*, 51(1), pp.7-61.
- Domercq M., Perez-Samartin A., Aparicio D., Alberdi E., Pampliega O. and Matute C., 2010. P2X7 receptors mediate ischemic damage to oligodendrocytes. *Glia*, 58(6), pp.730-740.
- Domercq M., Sánchez-Gómez M.V., Sherwin C., Etxebarria E., Fern R. and Matute C., 2007. System xc- and glutamate transporter inhibition mediates microglial toxicity to oligodendrocytes. *J Immunol*, 178(10), pp.6549-6556.
- Doyle J.P., Dougherty J.D., Heiman M., Schmidt E.F., Stevens T.R., Ma G, Bupp S., Shrestha P., Shah R.D., Doughty M.L., Gong S., Greengard P. and Heintz N., 2008. Application of a translational profiling approach for the comparative analysis of CNS cell types. *Cell*, 135(4), pp.749-762.
- Duprat F., Lesage F., Fink M., Reyes R., Heurteaux C. and Lazdunski M., 1997. TASK, a human background K⁺ channel to sense external pH variations near physiological pH. *EMBO J*, 16(17), pp.5464-5471.
- Edwards F.A., Konnerth A., Sakmann B. and Takahashi T., 1989. A thin slice preparation for patch clamp recordings from neurones of the mammalian central nervous system. *Pflugers Arch*, 414(5), pp.600-612.
- Fanarraga M.L., Griffiths I.R., Zhao M. and Duncan I.D., 1998. Oligodendrocytes are not inherently programmed to myelinate a specific size of axon. *J Comp Neurol*, 399(1), pp.94-100.

- Fancy S.P., Kotter M.R., Harrington E.P., Huang J.K., Zhao C., Rowitch D.H. and Franklin R.J., 2010. Overcoming remyelination failure in multiple sclerosis and other myelin disorders. *Exp Neurol*, 225(1), pp.18-23.
- Faull K.F., Rafie R., Pascoe N., Marsh L. and Pfefferbaum A., 1999. N-acetylaspartic acid (NAA) and N-acetylaspartylglutamic acid (NAAG) in human ventricular, subarachnoid, and lumbar cerebrospinal fluid. *Neurochem Res*, 24(10), pp.1249-1261.
- Feldman D.H., Horiuchi M., Keachie K., Mccauley E., Bannerman P., Itoh A., Itoh T. and Pleasure D., 2008. Characterization of acid-sensing ion channel expression in oligodendrocyte-lineage cells. *Glia*, 56(11), pp.1238-1249.
- Fenwick E.M., Marty A. and Neher E., 1982. A patch-clamp study of bovine chromaffin cells and of their sensitivity to acetylcholine. *J Physiol*, 331, pp.577-597.
- Fern R. and Möller T., 2000. Rapid ischemic cell death in immature oligodendrocytes: a fatal glutamate release feedback loop. *J Neurosci*, 20(1), pp.34-42.
- Fern R., Waxman S.G. and Ransom B.R., 1995. Endogenous GABA attenuates CNS white matter dysfunction following anoxia. *J Neurosci*, 15(1 Pt 2), pp.699-708.
- Fields R.D., 2008. White matter in learning, cognition and psychiatric disorders. *Trends Neurosci*, 31(7), pp.361-370.
- Fogal B., McClaskey C., Yan S., Yan H. and Rivkees S.A., 2010. Diazoxide promotes oligodendrocyte precursor cell proliferation and myelination. *PLoS One*, 5(5), p.e10906.
- Follett P.L., Rosenberg P.A., Volpe J.J. and Jensen F.E., 2000. NBQX attenuates excitotoxic injury in developing white matter. *J Neurosci*, 20(24), pp.9235-9241.
- Franklin R.J., 2002. Why does remyelination fail in multiple sclerosis? *Nat Rev Neurosci*, 3(9), pp.705-714.
- Franklin R.J. and Ffrench-Constant C., 2008. Remyelination in the CNS: from biology to therapy. *Nat Rev Neurosci*, 9(11), pp.839-855.
- Friese M.A., Craner M.J., Etzensperger R., Vergo S., Wemmie J.A., Welsh M.J., Vincent A. and Fugger L., 2007. Acid-sensing ion channel-1 contributes to axonal degeneration in autoimmune inflammation of the central nervous system. *Nat Med*, 13(12), pp.1483-1489.
- Fu Y., Sun W., Shi Y., Shi R. and Cheng J.X., 2009. Glutamate excitotoxicity inflicts paranodal myelin splitting and retraction. *PLoS One*, 4(8), p.e6705.
- Fujita T., Katsukawa H., Yodoya E., Wada M., Shimada A., Okada N., Yamamoto A. and Ganapathy V., 2005. Transport characteristics of N-acetyl-L-aspartate in rat

- astrocytes: involvement of sodium-coupled high-affinity carboxylate transporter NaC3/NaDC3-mediated transport system. *J Neurochem*, 93(3), pp.706-714.
- Fusco F.R., Martorana A., Giampà C., De March Z., Vacca F., Tozzi A., Longone P., Piccirilli S., Paolucci S., Sancesario G., Mercuri N.B. and Bernardi G., 2004. Cellular localization of TRPC3 channel in rat brain: preferential distribution to oligodendrocytes. *Neurosci Lett*, 365(2), pp.137-142.
- Gafurov B.S., Urazaev A.K., Grossfeld R.M. and Lieberman E.M., 2001. N-acetylaspartylglutamate (NAAG) is the probable mediator of axon-to-glia signaling in the crayfish medial giant nerve fiber. *Neuroscience*, 106(1), pp.227-235.
- Gallo V., Zhou J.M., McBain C.J., Wright P., Knutson P.L. and Armstrong R.C., 1996. Oligodendrocyte progenitor cell proliferation and lineage progression are regulated by glutamate receptor-mediated K⁺ channel block. *J Neurosci*, 16(9), pp.2659-2670.
- Gao T.M. and Fung M.L., 2002. Decreased large conductance Ca²⁺-activated K⁺ channel activity in dissociated CA1 hippocampal neurons in rats exposed to perinatal and postnatal hypoxia. *Neurosci Lett*, 332(3), pp.163-166.
- Gensert J.M. and Goldman J.E., 1997. Endogenous progenitors remyelinate demyelinated axons in the adult CNS. *Neuron*, 19(1), pp.197-203.
- Ghadge G.D., Slusher B.S., Bodner A., Canto M.D., Wozniak K., Thomas A.G., Rojas C., Tsukamoto T., Majer P., Miller R.J., Monti A.L. and Roos R.P., 2003. Glutamate carboxypeptidase II inhibition protects motor neurons from death in familial amyotrophic lateral sclerosis models. *Proc Natl Acad Sci USA*, 100(16), pp.9554-9559.
- Gilbert P., Kettenmann H. and Schachner M., 1984. gamma-Aminobutyric acid directly depolarizes cultured oligodendrocytes. *J Neurosci*, 4(2), pp.561-569.
- Gipson K. and Bordey A., 2002. Analysis of the K⁺ current profile of mature rat oligodendrocytes in situ. *J Membr Biol*, 189(3), pp.201-212.
- Girolamo F., Strippoli M., Errede M., Benagiano V., Roncali L., Ambrosi G. and Virgintino D., 2010. Characterization of oligodendrocyte lineage precursor cells in the mouse cerebral cortex: a confocal microscopy approach to demyelinating diseases. *Ital J Anat Embryol*, 115(1-2), pp.95-102.
- Globus M.Y., Busto R., Martinez E., Valdés I., Dietrich W.D. and Ginsberg M.D., 1991. Comparative effect of transient global ischemia on extracellular levels of glutamate, glycine, and gamma-aminobutyric acid in vulnerable and nonvulnerable brain regions in the rat. *J Neurochem*, 57(2), pp.470-478.

- Gudz T.I., Komuro H. and Macklin W.B., 2006. Glutamate stimulates oligodendrocyte progenitor migration mediated via an alpha v integrin/myelin proteolipid protein complex. *J Neurosci*, 26(9), pp.2458-2466.
- Guérineau N.C., Bossu J.L., Gähwiler B.H. and Gerber U., 1995. Activation of a nonselective cationic conductance by metabotropic glutamatergic and muscarinic agonists in CA3 pyramidal neurons of the rat hippocampus. *J Neurosci*, 15(6), pp.4395-4407.
- Hamann M., Rossi D.J., Mohr C., Andrade A.L. and Attwell D., 2005. The electrical response of cerebellar Purkinje neurons to simulated ischaemia. *Brain*, 128(Pt 10), pp.2408-2420.
- Hamill O.P., Marty A., Neher E., Sakmann B. and Sigworth F.J., 1981. Improved patch-clamp techniques for high-resolution current recording from cells and cell-free membrane patches. *Pflugers Arch*, 391(2), pp.85-100.
- Hamilton N., Vayro S., Wigley R. and Butt A.M., 2010. Axons and astrocytes release ATP and glutamate to evoke calcium signals in NG2-glia. *Glia*, 58(1), pp.66-79.
- Hamner M.A., Möller T. and Ransom B.R., 2011. Anaerobic function of CNS white matter declines with age. *J Cereb Blood Flow Metab*, 31(4), pp.996-1002.
- Hanaya R., Kiura Y., Kurisu K., Sakai N., Serikawa T. and Sasa M., 2008. N-acetyl-L-aspartate activates hippocampal CA3 neurons in rodent slice preparations. *Brain Res Bull*, 75(5), pp.663-667.
- Hansen A.J., 1985. Effect of anoxia on ion distribution in the brain. *Physiol Rev*, 65(1), pp.101-148.
- Hemmer B., Archelos J.J. and Hartung H.P., 2002. New concepts in the immunopathogenesis of multiple sclerosis. *Nat Rev Neurosci*, 3(4), pp.291-301.
- Henneke M., Combes P., Diekmann S., Bertini E., Brockmann K., Burlina A.P., Kaiser J., Ohlenbusch A., Plecko B., Rodriguez D., Boespflug-Tanguy O. and Gärtner J., 2008. GJA12 mutations are a rare cause of Pelizaeus-Merzbacher-like disease. *Neurology*, 70(10), pp.748-754.
- Hertz L., 2008. Bioenergetics of cerebral ischemia: a cellular perspective. *Neuropharmacology*, 55(3), pp.289-309.
- Hille B., 2001. *Ion channels of excitable membranes*. 3rd ed., Sunderland, Massachusetts, USA: Sinauer Associates, Inc.
- Hoffmann A., Grimm C., Kraft R., Goldbaum O., Wrede A., Nolte C., Hanisch U.K., Richter-Landsberg C., Brück W., Kettenmann H. and Harteneck C., 2010. TRPM3 is expressed in sphingosine-responsive myelinating oligodendrocytes. *J Neurochem*, 114(3), pp.654-665.

- Howell O.W., Palser A., Polito A., Melrose S., Zonta B., Scheiermann C., Vora A.J., Brophy P.J. and Reynolds R., 2006. Disruption of neurofascin localization reveals early changes preceding demyelination and remyelination in multiple sclerosis. *Brain*, 129(Pt 12), pp.3173-3185.
- Huang W., Wang H., Kekuda R., Fei Y.J., Friedrich A., Wang J., Conway S.J., Cameron R.S., Leibach F.H. and Ganapathy V., 2000. Transport of N-acetylaspartate by the Na(+)-dependent high-affinity dicarboxylate transporter NaDC3 and its relevance to the expression of the transporter in the brain. *J Pharmacol Exp Ther*, 295(1), pp.392-403.
- Iandiev I., Tenckhoff S., Pannicke T., Biedermann B., Hollborn M., Wiedemann P., Reichenbach A. and Bringmann A., 2006. Differential regulation of Kir4.1 and Kir2.1 expression in the ischemic rat retina. *Neurosci Lett*, 396(2), pp.97-101.
- Ishii A., Dutta R., Wark G.M., Hwang S.I., Han D.K., Trapp B.D., Pfeiffer S.E. and Bansal R., 2009. Human myelin proteome and comparative analysis with mouse myelin. *Proc Natl Acad Sci USA*, 106(34), pp.14605-14610.
- Itoh T., Beesley J., Itoh A., Cohen A.S., Kavanaugh B., Coulter D.A., Grinspan J.B. and Pleasure D., 2002. AMPA glutamate receptor-mediated calcium signaling is transiently enhanced during development of oligodendrocytes. *J Neurochem*, 81(2), pp.390-402.
- Jackman N., Ishii A. and Bansal R., 2009. Myelin biogenesis and oligodendrocyte development: parsing out the roles of glycosphingolipids. *Physiology (Bethesda)*, 24, pp.290-297.
- Jackson P.F., Cole D.C., Slusher B.S., Stetz S.L., Ross L.E., Donzanti B.A. and Trainor D.A., 1996. Design, synthesis, and biological activity of a potent inhibitor of the neuropeptidase N-acetylated alpha-linked acidic dipeptidase. *J Med Chem*, 39(2), pp.619-622.
- Jakobs C., ten Brink H.J., Langelaar S.A., Zee T., Stellaard F., Macek M., Srsnová K., Srsen S. and Kleijer W.J., 1991. Stable isotope dilution analysis of N-acetylaspartic acid in CSF, blood, urine and amniotic fluid: accurate postnatal diagnosis and the potential for prenatal diagnosis of Canavan disease. *J Inherit Metab Dis*, 14(5), pp.653-660.
- Jane D.E., Thomas N.K., Tse H.W. and Watkins J.C., 1996. Potent antagonists at the L-AP4- and (1S,3S)-ACPD-sensitive presynaptic metabotropic glutamate receptors in the neonatal rat spinal cord. *Neuropharmacology*, 35(8), pp.1029-1035.
- Jensen F.E., 2005. Role of glutamate receptors in periventricular leukomalacia. *J Child Neurol*, 20(12), pp.950-959.

- Kalsi A.S., Greenwood K., Wilkin G. and Butt A.M., 2004. Kir4.1 expression by astrocytes and oligodendrocytes in CNS white matter: a developmental study in the rat optic nerve. *J Anat*, 204(6), pp.475-485.
- Kandel E.R., Schwartz J.H. and Jessel T., 2000. The cerebellum. In *Principles of Neuroscience*. New York: McGraw-Hill Companies, Inc., pp. 832-851.
- Kang S.H., Fukaya M., Yang J.K., Rothstein J.D. and Bergles D.E., 2010. NG2+ CNS glial progenitors remain committed to the oligodendrocyte lineage in postnatal life and following neurodegeneration. *Neuron*, 68(4), pp.668-681.
- Kaplan M.R., Cho M.H., Ullian E.M., Isom L.L., Levinson S.R. and Barres B.A., 2001. Differential control of clustering of the sodium channels Na(v)1.2 and Na(v)1.6 at developing CNS nodes of Ranvier. *Neuron*, 30(1), pp.105-119.
- Kaplan M.R., Meyer-Franke A., Lambert S., Bennett V., Duncan I.D., Levinson S.R. and Barres B.A., 1997. Induction of sodium channel clustering by oligodendrocytes. *Nature*, 386(6626), pp.724-8.
- Káradóttir R. and Attwell D., 2006. Combining patch-clamping of cells in brain slices with immunocytochemical labeling to define cell type and developmental stage. *Nat Protoc*, 1(4), pp.1977-1986.
- Káradóttir R. and Attwell D., 2007. Neurotransmitter receptors in the life and death of oligodendrocytes. *Neuroscience*, 145(4), pp.1426-38.
- Káradóttir R., Cavelier P., Bergersen L.H. and Attwell D., 2005. NMDA receptors are expressed in oligodendrocytes and activated in ischaemia. *Nature*, 438(7071), pp.1162-6.
- Káradóttir R., Hamilton N.B., Bakiri Y. and Attwell D., 2008. Spiking and nonspiking classes of oligodendrocyte precursor glia in CNS white matter. *Nat Neurosci*, 11(4), pp.450-456.
- Katchman A.N. and Hershkowitz N., 1993. Early anoxia-induced vesicular glutamate release results from mobilization of calcium from intracellular stores. *J Neurophysiol*, 70(1), pp.1-7.
- Keirstead H.S. and Blakemore W.F., 1997. Identification of post-mitotic oligodendrocytes incapable of remyelination within the demyelinated adult spinal cord. *J Neuropathol Exp Neurol*, 56(11), pp.1191-1201.
- Kelland E.E. and Toms N.J., 2001. Group I metabotropic glutamate receptors limit AMPA receptor-mediated oligodendrocyte progenitor cell death. *Eur J Pharmacol*, 424(3), pp.R3-4.

- Kelley R.I. and Stamas J.N., 1992. Quantification of N-acetyl-L-aspartic acid in urine by isotope dilution gas chromatography-mass spectrometry. *J Inherit Metab Dis*, 15(1), pp.97-104.
- Kettenmann H. and Ransom B.R., 2005. Structure and function of oligodendrocytes. In *Neuroglia*. New York: Oxford University Press, Inc., pp. 36-47.
- Khwaja O. and Volpe J.J., 2008. Pathogenesis of cerebral white matter injury of prematurity. *Arch Dis Child Fetal Neonatal Ed*, 93(2), pp.F153-161.
- Kirchhoff F. and Kettenmann H., 1992. GABA Triggers a $[Ca^{2+}]_i$ Increase in Murine Precursor Cells of the Oligodendrocyte Lineage. *Eur J Neurosci*, 4(11), pp.1049-1058.
- Kirmani B.F., Jacobowitz D.M. and Namboodiri M.A., 2003. Developmental increase of aspartoacylase in oligodendrocytes parallels CNS myelination. *Brain Res Dev Brain Res*, 140(1), pp.105-115.
- Kleopa K.A., Orthmann-Murphy J. and Sargiannidou I., 2010. Gap junction disorders of myelinating cells. *Rev Neurosci*, 21(5), pp.397-419.
- Knutson P., Ghiani C.A., Zhou J.M., Gallo V. and McBain C.J., 1997. K^+ channel expression and cell proliferation are regulated by intracellular sodium and membrane depolarization in oligodendrocyte progenitor cells. *J Neurosci*, 17(8), pp.2669-2682.
- Koenig M.L., Rothbard P.M., DeCoster M.A. and Meyerhoff J.L., 1994. N-acetyl-aspartyl-glutamate (NAAG) elicits rapid increase in intraneuronal Ca^{2+} in vitro. *Neuroreport*, 5(9), pp.1063-1068.
- Kofuji P., Biedermann B., Siddharthan V., Raap M., Iandiev I., Milenkovic I., Thomzig A., Veh R.W., Bringmann A. and Reichenbach A., 2002. Kir potassium channel subunit expression in retinal glial cells: implications for spatial potassium buffering. *Glia*, 39(3), pp.292-303.
- Kołodziejczyk K., Hamilton N.B., Wade A., Káradóttir R. and Attwell D., 2009. The effect of N-acetyl-aspartyl-glutamate and N-acetyl-aspartate on white matter oligodendrocytes. *Brain*, 132(Pt 6), pp.1496-1508.
- Kraig R.P., Ferreira-Filho C.R. and Nicholson C., 1983. Alkaline and acid transients in cerebellar microenvironment. *J Neurophysiol*, 49(3), pp.831-850.
- Kukley M., Capetillo-Zarate E. and Dietrich D., 2007. Vesicular glutamate release from axons in white matter. *Nat Neurosci*, 10(3), pp.321-330.
- Kukley M., Nishiyama A. and Dietrich D., 2010. The fate of synaptic input to NG2 glial cells: neurons specifically downregulate transmitter release onto differentiating oligodendroglial cells. *J Neurosci*, 30(24), pp.8320-8331.

- Kulik A., Brockhaus J., Pedarzani P. and Ballanyi K., 2002. Chemical anoxia activates ATP-sensitive and blocks Ca²⁺-dependent K⁺ channels in rat dorsal vagal neurons in situ. *Neuroscience*, 110(3), pp.541-554.
- Kuner T. and Schoepfer R., 1996. Multiple structural elements determine subunit specificity of Mg²⁺ block in NMDA receptor channels. *J Neurosci*, 16(11), pp.3549-3558.
- Lalo U., Pankratov Y., Kirchhoff F., North R.A. and Verkhratsky A., 2006. NMDA receptors mediate neuron-to-glia signaling in mouse cortical astrocytes. *J Neurosci*, 26(10), pp.2673-2683.
- Lee M., Sakatani K. and Young W., 1993. A role of GABAA receptors in hypoxia-induced conduction failure of neonatal rat spinal dorsal column axons. *Brain Res*, 601(1-2), pp.14-19.
- Levine J.M. and Reynolds R., 1999. Activation and proliferation of endogenous oligodendrocyte precursor cells during ethidium bromide-induced demyelination. *Exp Neurol*, 160(2), pp.333-347.
- Levine J.M., Reynolds R. and Fawcett J.W., 2001. The oligodendrocyte precursor cell in health and disease. *Trends Neurosci*, 24(1), pp.39-47.
- Li S. and Stys P.K., 2000. Mechanisms of ionotropic glutamate receptor-mediated excitotoxicity in isolated spinal cord white matter. *J Neurosci*, 20(3), pp.1190-1198.
- Li S. and Stys P.K., 2001. Na⁺-K⁺-ATPase inhibition and depolarization induce glutamate release via reverse Na⁺-dependent transport in spinal cord white matter. *Neuroscience*, 107(4), pp.675-683.
- Li S., Mealing G.A., Morley P. and Stys P.K., 1999. Novel injury mechanism in anoxia and trauma of spinal cord white matter: glutamate release via reverse Na⁺-dependent glutamate transport. *J Neurosci*, 19(14), p.RC16.
- Liao Y., Kristiansen A.M., Oksvold C.P., Tuvnes F.A., Gu N., Rundén-Pran E., Ruth P., Sausbier M. and Storm J.F., 2010. Neuronal Ca²⁺-activated K⁺ channels limit brain infarction and promote survival. *PLoS One*, 5(12), p.e15601.
- Limbrick D.D. Jr, Sombati S. and DeLorenzo R.J., 2003. Calcium influx constitutes the ionic basis for the maintenance of glutamate-induced extended neuronal depolarization associated with hippocampal neuronal death. *Cell Calcium*, 33(2), pp.69-81.
- Lin S.C. and Bergles D.E., 2002. Physiological characteristics of NG2-expressing glial cells. *J Neurocytol*, 31(6-7), pp.537-549.

- Lin S.C. and Bergles D.E., 2004. Synaptic signaling between GABAergic interneurons and oligodendrocyte precursor cells in the hippocampus. *Nat Neurosci*, 7(1), pp.24-32.
- Lipski J., Park T.I., Li D., Lee S.C., Trevarton A.J., Chung K.K., Freestone P.S. and Bai J.Z., 2006. Involvement of TRP-like channels in the acute ischemic response of hippocampal CA1 neurons in brain slices. *Brain Res*, 1077(1), pp.187-199.
- Lipton P., 1999. Ischemic cell death in brain neurons. *Physiol Rev*, 79(4), pp.1431-1568.
- Losi G., Vicini S. and Neale J., 2004. NAAG fails to antagonize synaptic and extrasynaptic NMDA receptors in cerebellar granule neurons. *Neuropharmacology*, 46(4), pp.490-496.
- Lu Z.H., Chakraborty G., Ledeen R.W., Yahya D. and Wu G., 2004. N-Acetylaspartate synthase is bimodally expressed in microsomes and mitochondria of brain. *Brain Res Mol Brain Res*, 122(1), pp.71-78.
- Ludwin S.K., 2006. The pathogenesis of multiple sclerosis: relating human pathology to experimental studies. *J Neuropathol Exp Neurol*, 65(4), pp.305-318.
- Luyt K., Slade T.P., Dorward J.J., Durant C.F., Wu Y., Shigemoto R., Mundell S.J., Váradi A. and Molnár E., 2007. Developing oligodendrocytes express functional GABA(B) receptors that stimulate cell proliferation and migration. *J Neurochem*, 100(3), pp.822-40.
- Luyt K., Váradi A., Durant C.F. and Molnár E., 2006. Oligodendroglial metabotropic glutamate receptors are developmentally regulated and involved in the prevention of apoptosis. *J Neurochem*, 99(2), pp.641-656.
- Luyt K., Varadi A. and Molnar E., 2003. Functional metabotropic glutamate receptors are expressed in oligodendrocyte progenitor cells. *J Neurochem*, 84(6), pp.1452-1464.
- MacVicar B.A. and Thompson R.J., 2010. Non-junction functions of pannexin-1 channels. *Trends Neurosci*, 33(2), pp.93-102.
- Madhavarao C.N., Chinopoulos C., Chandrasekaran K. and Namboodiri M.A., 2003. Characterization of the N-acetylaspartate biosynthetic enzyme from rat brain. *J Neurochem*, 86(4), pp.824-835.
- Madry C., Haglerød C. and Attwell D., 2010. The role of pannexin hemichannels in the anoxic depolarization of hippocampal pyramidal cells. *Brain*, 133(12), pp.3755-3763.
- Maglione M., Tress O., Haas B., Karram K., Trotter J., Willecke K. and Kettenmann H., 2010. Oligodendrocytes in mouse corpus callosum are coupled via gap junction channels formed by connexin47 and connexin32. *Glia*, 58(9), pp.1104-1117.

- Magnotti L.M., Goodenough D.A. and Paul D.L., 2011. Deletion of oligodendrocyte Cx32 and astrocyte Cx43 causes white matter vacuolation, astrocyte loss and early mortality. *Glia*, [Epub ahead of print].
- Major G., 1993. Solutions for transients in arbitrarily branching cables: III. Voltage clamp problems. *Biophys J*, 65(1), pp.469-491.
- Matsuzawa A. and Ichijo H., 2005. Stress-responsive protein kinases in redox-regulated apoptosis signaling. *Antioxid Redox Signal*, 7(3-4), pp.472-481.
- Matute C., 2008. P2X7 receptors in oligodendrocytes: a novel target for neuroprotection. *Mol Neurobiol*, 38(2), pp.123-128.
- Matute C., Sánchez-Gómez M.V., Martínez-Millán L. and Miledi R., 1997. Glutamate receptor-mediated toxicity in optic nerve oligodendrocytes. *Proc Natl Acad Sci USA*, 94(16), pp.8830-8835.
- Matute C., Torre I., Pérez-Cerdá F., Pérez-Samartín A., Alberdi E., Etxebarria E., Arranz A.M., Ravid R., Rodríguez-Antigüedad A., Sánchez-Gómez M. and Domercq M., 2007. P2X(7) receptor blockade prevents ATP excitotoxicity in oligodendrocytes and ameliorates experimental autoimmune encephalomyelitis. *J Neurosci*, 27(35), pp.9525-9533.
- McCarran W.J. and Goldberg M.P., 2007. White matter axon vulnerability to AMPA/kainate receptor-mediated ischemic injury is developmentally regulated. *J Neurosci*, 27(15), pp.4220-4229.
- McDonald J.W., Althomsons S.P., Hyrc K.L., Choi D.W. and Goldberg M.P., 1998. Oligodendrocytes from forebrain are highly vulnerable to AMPA/kainate receptor-mediated excitotoxicity. *Nat Med*, 4(3), pp.291-297.
- Melani A., Cipriani S., Vannucchi M.G., Nosi D., Donati C., Bruni P., Giovannini M.G. and Pedata F., 2009. Selective adenosine A2a receptor antagonism reduces JNK activation in oligodendrocytes after cerebral ischaemia. *Brain*, 132(Pt 6), pp.1480-1495.
- Meuth S.G., Kleinschnitz C., Broicher T., Austinat M., Braeuninger S., Bittner S., Fischer S., Bayliss D.A., Budde T., Stoll G. and Wiendl H., 2009. The neuroprotective impact of the leak potassium channel TASK1 on stroke development in mice. *Neurobiol Dis*, 33(1), pp.1-11.
- Micu I., Jiang Q., Coderre E., Ridsdale A., Zhang L., Woulfe J., Yin X., Trapp B.D., McRory J.E., Rehak R., Zamponi G.W., Wang W. and Stys P.K., 2006. NMDA receptors mediate calcium accumulation in myelin during chemical ischaemia. *Nature*, 439(7079), pp.988-92.
- Miller R.H., 2002. Regulation of oligodendrocyte development in the vertebrate CNS. *Prog Neurobiol*, 67(6), pp.451-67.

- Mongin A.A., Aksentsev S.L., Orlov S.N., Slepko N.G., Kozlova M.V., Maximov G.V. and Konev S.V., 1994. Swelling-induced K⁺ influx in cultured primary astrocytes. *Brain Res*, 655(1-2), pp.110-114.
- Nave K.A., 2010. Myelination and support of axonal integrity by glia. *Nature*, 468(7321), pp.244-252.
- Nedergaard M., Kraig R.P., Tanabe J., Pulsinelli W.A., 1991. Dynamics of interstitial and intracellular pH in evolving brain infarct. *Am J Physiol*, 260(3 Pt 2), pp.R581-588.
- Nestler E.J., Hyman S.E. and Malenka R.C., 2008. *Molecular Neuropharmacology: A Foundation for Clinical Neuroscience* 2nd ed., McGraw-Hill Companies, Inc.
- Neusch C., Rozengurt N., Jacobs R.E., Lester H.A. and Kofuji P., 2001. Kir4.1 potassium channel subunit is crucial for oligodendrocyte development and in vivo myelination. *J Neurosci*, 21(15), pp.5429-5438.
- Ng B. and Barry P.H., 1995. The measurement of ionic conductivities and mobilities of certain less common organic ions needed for junction potential corrections in electrophysiology. *J Neurosci Methods*, 56(1), pp.37-41.
- Nichols C.G. and Lopatin A.N., 1997. Inward rectifier potassium channels. *Annu Rev Physiol*, 59, pp.171-191.
- Niwa M., Nitta A., Mizoguchi H., Ito Y., Noda Y., Nagai T. and Nabeshima T., 2007. A novel molecule “shati” is involved in methamphetamine-induced hyperlocomotion, sensitization, and conditioned place preference. *J Neurosci*, 27(28), pp.7604-7615.
- Oka A., Belliveau M.J., Rosenberg P.A. and Volpe J.J., 1993. Vulnerability of oligodendroglia to glutamate: pharmacology, mechanisms, and prevention. *J Neurosci*, 13(4), pp.1441-1453.
- Olney J.W. and de Gubareff T., 1978. Glutamate neurotoxicity and Huntington's chorea. *Nature*, 271(5645), pp.557-559.
- Olsen M.L. and Sontheimer H., 2008. Functional implications for Kir4.1 channels in glial biology: from K⁺ buffering to cell differentiation. *J Neurochem*, 107(3), pp.589-601.
- Olszewski R.T., Bukhari N., Zhou J., Kozikowski A.P., Wroblewski J.T., Shamimi-Noori S., Wroblewska B., Bzdega T., Vicini S., Barton F.B. and Neale J.H., 2004. NAAG peptidase inhibition reduces locomotor activity and some stereotypes in the PCP model of schizophrenia via group II mGluR. *J Neurochem*, 89(4), pp.876-885.

- Orthmann-Murphy J.L., Abrams C.K. and Scherer S.S., 2008. Gap junctions couple astrocytes and oligodendrocytes. *J Mol Neurosci*, 35(1), pp.101-116.
- Othman T., Yan H. and Rivkees S.A., 2003. Oligodendrocytes express functional A1 adenosine receptors that stimulate cellular migration. *Glia*, 44(2), pp.166-172.
- Paez P.M., Fulton D., Colwell C.S. and Campagnoni A.T., 2009a. Voltage-operated Ca(2+) and Na(+) channels in the oligodendrocyte lineage. *J Neurosci Res*, 87(15), pp.3259-3266.
- Paez P.M., Fulton D.J., Spreuer V., Handley V., Campagnoni C.W., Macklin W.B., Colwell C. and Campagnoni A.T., 2009b. Golli myelin basic proteins regulate oligodendroglial progenitor cell migration through voltage-gated Ca²⁺ influx. *J Neurosci*, 29(20), pp.6663-6676.
- Paez P.M., Spreuer V., Handley V., Feng J.M., Campagnoni C. and Campagnoni A.T., 2007. Increased expression of golli myelin basic proteins enhances calcium influx into oligodendroglial cells. *J Neurosci*, 27(46), pp.12690-12699.
- Pannicke T., Iandiev I., Uckermann O., Biedermann B., Kutzera F., Wiedemann P., Wolburg H., Reichenbach A. and Bringmann A., 2004. A potassium channel-linked mechanism of glial cell swelling in the postischemic retina. *Mol Cell Neurosci*, 26(4), pp.493-502.
- Pannicke T., Uckermann O., Iandiev I., Biedermann B., Wiedemann P., Perlman I., Reichenbach A. and Bringmann A., 2005. Altered membrane physiology in Müller glial cells after transient ischemia of the rat retina. *Glia*, 50(1), pp.1-11.
- Papadopoulos D., Pham-Dinh D. and Reynolds R., 2006. Axon loss is responsible for chronic neurological deficit following inflammatory demyelination in the rat. *Exp Neurol*, 197(2), pp.373-385.
- Park E., Velumian A.A. and Fehlings M.G., 2004. The role of excitotoxicity in secondary mechanisms of spinal cord injury: a review with an emphasis on the implications for white matter degeneration. *J Neurotrauma*, 21(6), pp.754-774.
- Pastor A., Chvátal A., Syková E. and Kettenmann H., 1995. Glycine- and GABA-activated currents in identified glial cells of the developing rat spinal cord slice. *Eur J Neurosci*, 7(6), pp.1188-1198.
- Pastor A., Kremer M., Möller T., Kettenmann H. and Dermietzel R., 1998. Dye coupling between spinal cord oligodendrocytes: differences in coupling efficiency between gray and white matter. *Glia*, 24(1), pp.108-120.
- Patneau D.K., Wright P.W., Winters C., Mayer M.L. and Gallo V., 1994. Glial cells of the oligodendrocyte lineage express both kainate- and AMPA-preferring subtypes of glutamate receptor. *Neuron*, 12(2), pp.357-371.

- Peretz A., Schottelndreier H., Aharon-Shamgar L.B. and Attali B., 2002. Modulation of homomeric and heteromeric KCNQ1 channels by external acidification. *J Physiol*, 545(Pt 3), pp.751-766.
- Phillis J.W., Smith-Barbour M. and O'Regan M.H., 1996. Changes in extracellular amino acid neurotransmitters and purines during and following ischemias of different durations in the rat cerebral cortex. *Neurochem Int*, 29(2), pp.115-120.
- Pignataro G., Simon R.P. and Xiong Z.G., 2007. Prolonged activation of ASIC1a and the time window for neuroprotection in cerebral ischaemia. *Brain*, 130(1), pp.151-158.
- Pitt D., Werner P. and Raine C.S., 2000. Glutamate excitotoxicity in a model of multiple sclerosis. *Nat Med*, 6(1), pp.67-70.
- Pliss L., FitzGibbon T., Balcar V.J. and St'astný F., 2000. Neurotoxicity of NAAG in vivo is sensitive to NMDA antagonists and mGluR II ligands. *Neuroreport*, 11(16), pp.3651-3654.
- Pohl H.B., Porcheri C., Mueggler T., Bachmann L.C., Martino G., Riethmacher D., Franklin R.J., Rudin M. and Suter U., 2011. Genetically induced adult oligodendrocyte cell death is associated with poor myelin clearance, reduced remyelination, and axonal damage. *J Neurosci*, 31(3), pp.1069-1080.
- Polito A. and Reynolds R., 2005. NG2-expressing cells as oligodendrocyte progenitors in the normal and demyelinated adult central nervous system. *J Anat*, 207(6), pp.707-716.
- Poopalasundaram S., Knott C., Shamotienko O.G., Foran P.G., Dolly J.O., Ghiani C.A., Gallo V. and Wilkin G.P., 2000. Glial heterogeneity in expression of the inwardly rectifying K(+) channel, Kir4.1, in adult rat CNS. *Glia*, 30(4), pp.362-372.
- Raff M.C., Abney E.R. and Fok-Seang J., 1985. Reconstitution of a developmental clock in vitro: a critical role for astrocytes in the timing of oligodendrocyte differentiation. *Cell*, 42(1), pp.61-69.
- Raichle M.E., 1983. The pathophysiology of brain ischemia. *Ann Neurol*, 13(1), pp.2-10.
- Rajan S., Wischmeyer E., Karschin C., Preisig-Müller R., Grzeschik K.H., Daut J., Karschin A. and Derst C., 2001. THIK-1 and THIK-2, a novel subfamily of tandem pore domain K⁺ channels. *J Biol Chem*, 276(10), pp.7302-7311.
- Ralevic V. and Burnstock G., 1998. Receptors for purines and pyrimidines. *Pharmacol Rev*, 50(3), pp.413-492.
- Ransom B.R., Walz W., Davis P.K. and Carlini W.G., 1992. Anoxia-induced changes in extracellular K⁺ and pH in mammalian central white matter. *J Cereb Blood Flow Metab*, 12(4), pp.593-602.

- Rehncrona S., 1985. Brain acidosis. *Ann Emerg Med*, 14(8), pp.770-776.
- Reiner P.B., Laycock A.G. and Doll C.J., 1990. A pharmacological model of ischemia in the hippocampal slice. *Neurosci Lett*, 119(2), pp.175-178.
- Richardson W.D., Kessaris N. and Pringle N., 2006. Oligodendrocyte wars. *Nat Rev Neurosci*, 7(1), pp.11-8.
- Rieger A.M., Nelson K.L., Konowalchuk J.D. and Barreda D.R., 2011. Modified annexin v/propidium iodide apoptosis assay for accurate assessment of cell death. *J Vis Exp*, (50), p.pii: 2597.
- Rio-Hortega P., 1928. *Tercera apotacion al conocimiento morfologica e interpretacion funcional de la oligodendroglia*, Madrid: Real Espaniola Sociedad de Histologia Natural.
- Rivers L.E., Young K.M., Rizzi M., Jamen F., Psachoulia K., Wade A., Kessaris N. and Richardson W.D., 2008. PDGFRA/NG2 glia generate myelinating oligodendrocytes and piriform projection neurons in adult mice. *Nat Neurosci*, 11(12), pp.1392-1401.
- Roettger V. and Lipton P., 1996. Mechanism of glutamate release from rat hippocampal slices during in vitro ischemia. *Neuroscience*, 75(3), pp.677-685.
- Rossi D.J., Oshima T. and Attwell D., 2000. Glutamate release in severe brain ischaemia is mainly by reversed uptake. *Nature*, 403(6767), pp.316-321.
- Rowitch D.H., 2004. Glial specification in the vertebrate neural tube. *Nat Rev Neurosci*, 5(5), pp.409-19.
- Rubin Y., LaPlaca M.C., Smith D.H., Thibault L.E. and Lenkinski R.E., 1995. The effect of N-acetylaspartate on the intracellular free calcium concentration in Ntera2-neurons. *Neuroscience letters*, 198(3), pp.209-212.
- Sáez J.C., Retamal M.A., Basilio D., Bukauskas F.F. and Bennett M.V., 2005. Connexin-based gap junction hemichannels: gating mechanisms. *Biochim Biophys Acta*, 1711(2), pp.215-224.
- Sager T.N., Fink-Jensen A. and Hansen A.J., 1997. Transient elevation of interstitial N-acetylaspartate in reversible global brain ischemia. *J Neurochem*, 68(2), pp.675-682.
- Salter M.G. and Fern R., 2005. NMDA receptors are expressed in developing oligodendrocyte processes and mediate injury. *Nature*, 438(7071), pp.1167-71.
- Sarantis M., Ballerini L., Miller B., Silver R.A., Edwards M. and Attwell D., 1993. Glutamate uptake from the synaptic cleft does not shape the decay of the non-NMDA component of the synaptic current. *Neuron*, 11(3), pp.541-549.

- Sartori S., Burlina A.B., Salviati L., Trevisson E., Toldo I., Laverda A.M. and Burlina A.P., 2008. Increased level of N-acetylaspartylglutamate (NAAG) in the CSF of a patient with Pelizaeus-Merzbacher-like disease due to mutation in the GJA12 gene. *Eur J Paediatr Neurol*, 12(4), pp.348-350.
- Sasaki Y.F., Rothe T., Premkumar L.S., Das S., Cui J., Talantova M.V., Wong H.K., Gong X., Chan S.F., Zhang D., Nakanishi N., Sucher N.J. and Lipton S.A., 2002. Characterization and comparison of the NR3A subunit of the NMDA receptor in recombinant systems and primary cortical neurons. *J Neurophysiol*, 87(4), pp.2052-2063.
- Schipke C.G., Ohlemeyer C., Matyash M., Nolte C., Kettenmann H. and Kirchhoff F., 2001. Astrocytes of the mouse neocortex express functional N-methyl-D-aspartate receptors. *FASEB J*, 15(7), pp.1270-1272.
- Schwartz E.A., 1993. L-glutamate conditionally modulates the K⁺ current of Müller glial cells. *Neuron*, 10(6), pp.1141-9.
- Seifert G., Hüttmann K., Binder D.K., Hartmann C., Wyczynski A., Neusch C. and Steinhäuser C., 2009. Analysis of astroglial K⁺ channel expression in the developing hippocampus reveals a predominant role of the Kir4.1 subunit. *J Neurosci*, 29(23), pp.7474-7488.
- Sekiguchi M., Wada K. and Wenthold R.J., 1992. N-acetylaspartylglutamate acts as an agonist upon homomeric NMDA receptor (NMDAR1) expressed in *Xenopus* oocytes. *FEBS Lett*, 311(3), pp.285-289.
- Shimada N., Graf R., Rosner G. and Heiss W.D., 1993. Ischemia-induced accumulation of extracellular amino acids in cerebral cortex, white matter, and cerebrospinal fluid. *J Neurochem*, 60(1), pp.66-71.
- Siesjö B.K., 1988. Mechanisms of ischemic brain damage. *Crit Care Med*, 16(10), pp.954-963.
- Sillitoe R.V. and Joyner A.L., 2007. Morphology, molecular codes, and circuitry produce the three-dimensional complexity of the cerebellum. *Annu Rev Cell Dev Biol*, 23, pp.549-577.
- Silver I.A. and Erecińska M., 1992. Ion homeostasis in rat brain in vivo: intra- and extracellular [Ca²⁺] and [H⁺] in the hippocampus during recovery from short-term, transient ischemia. *J Cereb Blood Flow Metab*, 12(5), pp.759-772.
- Sim F.J., Zhao C., Penderis J. and Franklin R.J., 2002. The age-related decrease in CNS remyelination efficiency is attributable to an impairment of both oligodendrocyte progenitor recruitment and differentiation. *J Neurosci*, 22(7), pp.2451-2459.

- Simons M. and Trajkovic K., S.M., 2006. Neuron-glia communication in the control of oligodendrocyte function and myelin biogenesis. *J Cell Sci*, 119(21), pp.4381-4389.
- Skatchkov S.N., Eaton M.J., Shuba Y.M., Kucheryavykh Y.V., Derst C., Veh R.W., Wurm A., Iandiev I., Pannicke T., Bringmann A. and Reichenbach A., 2006. Tandem-pore domain potassium channels are functionally expressed in retinal (Müller) glial cells. *Glia*, 53(3), pp.266-276.
- Smith P.L., Baukrowitz T. and Yellen G., 1996. The inward rectification mechanism of the HERG cardiac potassium channel. *Nature*, 379(6568), pp.833-836.
- Smith T., Groom A., Zhu B. and Turski L., 2000. Autoimmune encephalomyelitis ameliorated by AMPA antagonists. *Nat Med*, 6(1), pp.62-66.
- Sombati S., Coulter D.A. and DeLorenzo R.J., 1991. Neurotoxic activation of glutamate receptors induces an extended neuronal depolarization in cultured hippocampal neurons. *Brain Res*, 566(1-2), pp.316-319.
- Sontheimer H., Trotter J., Schachner M. and Kettenmann H., 1989. Channel expression correlates with differentiation stage during the development of oligodendrocytes from their precursor cells in culture. *Neuron*, 2(2), pp.1135-1145.
- Sosinsky G.E., Boassa D., Dermietzel R., Duffy H.S., Laird D.W., Macvicar B., Naus C.C., Penuela S., Scemes E., Spray D.C., Thompson R.J., Zhao H.B. and Dahl G., 2011. Pannexin channels are not gap junction hemichannels. *Channels (Austin)*, 5(3).
- Stevens B., Porta S., Haak L.L., Gallo V. and Fields R.D., 2002. Adenosine: a neuronal transmitter promoting myelination in the CNS in response to action potentials. *Neuron*, 36(5), pp.855-868.
- Stys P.K., 2004. White matter injury mechanisms. *Curr Mol Med*, 4(2), pp.113-30.
- Su G., Haworth R.A., Dempsey R.J. and Sun D., 2000. Regulation of Na(+)-K(+)-Cl(-) cotransporter in primary astrocytes by dibutyryl cAMP and high [K(+)](o). *Am J Physiol Cell Physiol*, 279(6), pp.C1710-1721.
- Su G., Kintner D.B. and Sun D., 2002. Contribution of Na(+)-K(+)-Cl(-) cotransporter to high-[K(+)](o)- induced swelling and EAA release in astrocytes. *Am J Physiol Cell Physiol*, 282(5), pp.C1136-1146.
- Sugawara T. and Chan P.H., 2003. Reactive oxygen radicals and pathogenesis of neuronal death after cerebral ischemia. *Antioxid Redox Signal*, 5(5), pp.597-607.
- Sugawara T., Fujimura M., Noshita N., Kim G.W., Saito A., Hayashi T., Narasimhan P., Maier C.M. and Chan P.H., 2004. Neuronal death/survival signaling pathways in cerebral ischemia. *NeuroRx*, 1(1), pp.17-25.

- Sugimoto Y., Taniguchi M., Yagi T., Akagi Y., Nojyo Y. and Tamamaki N., 2001. Guidance of glial precursor cell migration by secreted cues in the developing optic nerve. *Development*, 128(17), pp.3321-3330.
- Sun D. and Murali S.G., 1999. Na⁺-K⁺-2Cl⁻ cotransporter in immature cortical neurons: A role in intracellular Cl⁻ regulation. *J Neurophysiol*, 81(4), pp.1939-1948.
- Sun H.S., Feng Z.P., Barber P.A., Buchan A.M. and French R.J., 2007. Kir6.2-containing ATP-sensitive potassium channels protect cortical neurons from ischemic/anoxic injury in vitro and in vivo. *Neuroscience*, 144(4), pp.1509-1515.
- Sun H.S., Jackson M.F., Martin L.J., Jansen K., Teves L., Cui H., Kiyonaka S., Mori Y., Jones M., Forder J.P., Golde T.E., Orser B.A., Macdonald J.F. and Tymianski M., 2009. Suppression of hippocampal TRPM7 protein prevents delayed neuronal death in brain ischemia. *Nat Neurosci*, 12(10), pp.1300-1307.
- Szatkowski M., Barbour B. and Attwell D., 1990. Non-vesicular release of glutamate from glial cells by reversed electrogenic glutamate uptake. *Nature*, 348(6300), pp.443-446.
- Takeda M., Nelson D.J. and Soliven B., 1995. Calcium signaling in cultured rat oligodendrocytes. *Glia*, 14(3), pp.225-236.
- Tanaka E., Yamamoto S., Kudo Y., Mihara S. and Higashi H., 1997. Mechanisms underlying the rapid depolarization produced by deprivation of oxygen and glucose in rat hippocampal CA1 neurons in vitro. *J Neurophysiol*, 78(2), pp.891-902.
- Taoufik E. and Probert L., 2008. Ischemic neuronal damage. *Curr Pharm Des*, 14(33), pp.3565-3573.
- Targett M.P., Sussman J., Scolding N., O'Leary M.T., Compston D.A. and Blakemore W.F., 1996. Failure to achieve remyelination of demyelinated rat axons following transplantation of glial cells obtained from the adult human brain. *Neuropathol Appl Neurobiol*, 22(3), pp.199-206.
- Tekkök S.B. and Goldberg M.P., 2001. Ampa/kainate receptor activation mediates hypoxic oligodendrocyte death and axonal injury in cerebral white matter. *J Neurosci*, 21(12), pp.4237-4248.
- Tekkök S.B., Ye Z. and Ransom B.R., 2007. Excitotoxic mechanisms of ischemic injury in myelinated white matter. *J Cereb Blood Flow Metab*, 27(9), pp.1540-1552.
- Tessier-Lavigne M., Attwell D., Mobbs P. and Wilson M., 1988. Membrane currents in retinal bipolar cells of the axolotl. *J Gen Physiol*, 91(1), pp.49-72.

- Thomas A.G., Olkowski J.L. and Slusher B.S., 2001. Neuroprotection afforded by NAAG and NAALADase inhibition requires glial cells and metabotropic glutamate receptor activation. *Eur J Pharmacol*, 426(1-2), pp.35-38.
- Thompson R.J. and MacVicar B.A., 2008. Connexin and pannexin hemichannels of neurons and astrocytes. *Channels (Austin)*, 2(2), pp.81-86.
- Thompson R.J., Zhou N. and MacVicar B.A., 2006. Ischemia opens neuronal gap junction hemichannels. *Science*, 312(5775), pp.924-927.
- Tong G., Takahashi H., Tu S., Shin Y., Talantova M., Zago W., Xia P., Nie Z., Goetz T., Zhang D., Lipton S.A. and Nakanishi N., 2008. Modulation of NMDA receptor properties and synaptic transmission by the NR3A subunit in mouse hippocampal and cerebrotical neurons. *J Neurophysiol*, 99(1), pp.122-132.
- Tortella F.C., Lin Y., Ved H., Slusher B.S. and Dave J.R., 2000. Neuroprotection produced by the NAALADase inhibitor 2-PMPA in rat cerebellar neurons. *Eur J Pharmacol*, 402(1-2), pp.31-37.
- Trapp B.D., Nishiyama A., Cheng D. and Macklin W., 1997. Differentiation and death of premyelinating oligodendrocytes in developing rodent brain. *J Cell Biol*, 137(2), pp.459-468.
- Ueda H., Levine J.M., Miller R.H. and Trapp B.D., 1999. Rat optic nerve oligodendrocytes develop in the absence of viable retinal ganglion cell axons. *J Cell Biol*, 146(6), pp.1365-1374.
- Valivullah H.M., Lancaster J., Sweetnam P.M. and Neale J.H., 1994. Interactions between N-acetylaspartylglutamate and AMPA, kainate, and NMDA binding sites. *J Neurochem*, 63(5), pp.1714-1719.
- Vélez-Fort M., Maldonado P.P., Butt A.M., Audinat E. and Angulo M.C., 2010. Postnatal switch from synaptic to extrasynaptic transmission between interneurons and NG2 cells. *J Neurosci*, 30(20), pp.6921-6929.
- Venkatachalam K. and Montell C., 2007. TRP channels. *Annu Rev Biochem*, 76, pp.387-417.
- Vergo S., Craner M.J., Etzensperger R., Attfield K., Friese M.A., Newcombe J., Esiri M. and Fugger L., 2011. Acid-sensing ion channel 1 is involved in both axonal injury and demyelination in multiple sclerosis and its animal model. *Brain*, 134(Pt 2), pp.571-584.
- Volpe B.T., 2001. Palliative treatment for stroke. *Neurol Clin*, 19(4), pp.903-920.
- Volterra A., Bezzi P., Rizzini B.L., Trotti D., Ullensvang K., Danbolt N.C. and Racagni G., 1996. The competitive transport inhibitor L-trans-pyrrolidine-2, 4-dicarboxylate triggers excitotoxicity in rat cortical neuron-astrocyte co-cultures

- via glutamate release rather than uptake inhibition. *Eur J Neurosci*, 8(9), pp.2019-2028.
- Wagner M., Rudakova E., Schütz V., Frank M., Ehmke H. and Volk T., 2010. Larger transient outward K(+) current and shorter action potential duration in Galpha(11) mutant mice. *Pflugers Arch*, 459(4), pp.607-618.
- Waldmann R., Champigny G., Lingueglia E., De Weille J.R., Heurteaux C. and Lazdunski M., 1999. H(+)-gated cation channels. *Ann N Y Acad Sci*, 868, pp.67-76.
- Wang C., Pralong W.F., Schulz M.F., Rougon G., Aubry J.M., Pagliusi S., Robert A. and Kiss J.Z., 1996. Functional N-methyl-D-aspartate receptors in O-2A glial precursor cells: a critical role in regulating polysialic acid-neural cell adhesion molecule expression and cell migration. *J Cell Biol*, 135(6), pp.1565-1581.
- Wang H., Kunkel D.D., Martin T.M., Schwartzkroin P.A. and Tempel B.L., 1993. Heteromultimeric K⁺ channels in terminal and juxtaparanodal regions of neurons. *Nature*, 365(6441), pp.75-79.
- Wang H., Yan Y., Kintner D.B., Lytle C. and Sun D., 2003. GABA-mediated trophic effect on oligodendrocytes requires Na-K-2Cl cotransport activity. *J Neurophysiol*, 90(2), pp.1257-1265.
- Wang S., Sdrulla A.D., diSibio G., Bush G., Nofziger D., Hicks C., Weinmaster G. and Barres B.A., 1998. Notch receptor activation inhibits oligodendrocyte differentiation. *Neuron*, 21(1), pp.63-75.
- Wang X., Arcuino G., Takano T., Lin J., Peng W.G., Wan P., Li P., Xu Q., Liu Q.S., Goldman S.A. and Nedergaard M., 2004. P2X7 receptor inhibition improves recovery after spinal cord injury. *Nat Med*, 10(8), pp.821-827.
- Wasseff S.K. and Scherer S.S., 2011. Cx32 and Cx47 mediate oligodendrocyte:astrocyte and oligodendrocyte:oligodendrocyte gap junction coupling. *Neurobiol Dis*, 42(3), pp.506-513.
- Watanabe H. and Bannai S., 1987. Induction of cystine transport activity in mouse peritoneal macrophages. *J Exp Med*, 165(3), pp.628-640.
- Wen Q. and Chklovskii D.B., 2005. Segregation of the brain into gray and white matter: a design minimizing conduction delays. *PLoS Comput Biol*, 1(7).
- Westbrook G.L., Mayer M.L., Namboodiri M.A. and Neale J.H., 1986. High concentrations of N-acetylaspartylglutamate (NAAG) selectively activate NMDA receptors on mouse spinal cord neurons in cell culture. *J Neurosci*, 6(11), pp.3385-3392.

- Wevers R.A., Engelke U., Wendel U., de Jong J.G., Gabreëls F.J. and Heerschap A., 1995. Standardized method for high-resolution ¹H-NMR of cerebrospinal fluid. *Clin Chem*, 41(5), pp.744-751.
- Wiame E., Tyteca D., Pierrot N., Collard F., Amyere M., Noel G., Desmedt J., Nassogne M.C., Vikkula M., Octave J.N., Vincent M.F., Courtoy P.J., Boltshausen E. and van Schaftingen E., 2009. Molecular identification of aspartate N-acetyltransferase and its mutation in hypoaethylaspartia. *Biochem J*, 425(1), pp.127-136.
- Wilke S., Thomas R., Allcock N. and Fern R., 2004. Mechanism of acute ischemic injury of oligodendroglia in early myelinating white matter: the importance of astrocyte injury and glutamate release. *J Neuropathol Exp Neurol*, 63(8), pp.872-881.
- Williamson A.V., Mellor J.R., Grant A.L. and Randall A.D., 1998. Properties of GABA(A) receptors in cultured rat oligodendrocyte progenitor cells. *Neuropharmacology*, 37(7), pp.859-873.
- Williamson L.C. and Neale J.H., 1988a. Calcium-dependent release of N-acetylaspartylglutamate from retinal neurons upon depolarization. *Brain Res*, 475(1), pp.151-155.
- Williamson L.C. and Neale J.H., 1988b. Ultrastructural localization of N-acetylaspartylglutamate in synaptic vesicles of retinal neurons. *Brain Res*, 456(2), pp.375-381.
- Williamson L.C., Eagles D.A., Brady M.J., Moffett J.R., Namboodiri M.A. and Neale J.H., 1991. Localization and Synaptic Release of N-acetylaspartylglutamate in the Chick Retina and Optic Tectum. *Eur J Neurosci*, 3(5), pp.441-451.
- Windrem M.S., Schanz S.J., Guo M., Tian G.F., Washco V., Stanwood N., Rasband M., Roy N.S., Nedergaard M., Havton L.A., Wang S. and Goldman S.A., 2008. Neonatal chimerization with human glial progenitor cells can both remyelinate and rescue the otherwise lethally hypomyelinated shiverer mouse. *Cell Stem Cell*, 2(6), pp.553-565.
- Wolf N.I., Willemsen M.A., Engelke U.F., van der Knaap M.S., Pouwels P.J., Harting I., Zschocke J., Sistermans E.A., Rating D. and Wevers R.A., 2004. Severe hypomyelination associated with increased levels of N-acetylaspartylglutamate in CSF. *Neurology*, 62(9), pp.1503-1508.
- Wollmuth L.P. and Sobolevsky A.I., 2004. Structure and gating of the glutamate receptor ion channel. *Trends Neurosci*, 27(6), pp.321-328.
- Wolswijk G. and Balesar R., 2003. Changes in the expression and localization of the paranodal protein Caspr on axons in chronic multiple sclerosis. *Brain*, 126(Pt 7), pp.1638-1649.

- Wood P. and Bunge R.P., 1984. The biology of the oligodendrocyte. In *Oligodendroglia*. New York: Plenum Publishing Corp., pp. 1-46.
- Wrathall J.R., Choiniere D. and Teng Y.D., 1994. Dose-dependent reduction of tissue loss and functional impairment after spinal cord trauma with the AMPA/kainate antagonist NBQX. *J Neurosci*, 14(11 Pt 1), pp.6598-6607.
- Wroblewska B., Santi M.R. and Neale J.H., 1998. N-acetylaspartylglutamate activates cyclic AMP-coupled metabotropic glutamate receptors in cerebellar astrocytes. *Glia*, 24(2), pp.172-179.
- Wroblewska B., Wroblewski J.T., Pshenichkin S., Surin A., Sullivan S.E. and Neale J.H., 1997. N-acetylaspartylglutamate selectively activates mGluR3 receptors in transfected cells. *J Neurochem*, 69(1), pp.174-181.
- Wroblewska B., Wroblewski J.T., Saab O.H. and Neale J.H., 1993. N-acetylaspartylglutamate inhibits forskolin-stimulated cyclic AMP levels via a metabotropic glutamate receptor in cultured cerebellar granule cells. *J Neurochem*, 61(3), pp.943-948.
- Xie M., Wang W., Kimelberg H.K. and Zhou M., 2008. Oxygen and glucose deprivation-induced changes in astrocyte membrane potential and their underlying mechanisms in acute rat hippocampal slices. *J Cereb Blood Flow Metab*, 28(3), pp.456-467.
- Xiong Z.G., Zhu X.M., Chu X.P., Minami M., Hey J., Wei W.L., MacDonald J.F., Wemmie J.A., Price M.P., Welsh M.J. and Simon R.P., 2004. Neuroprotection in ischemia: blocking calcium-permeable acid-sensing ion channels. *Cell*, 118(6), pp.687-698.
- Xu Z.C., 1995. Neurophysiological changes of spiny neurons in rat neostriatum after transient forebrain ischemia: an in vivo intracellular recording and staining study. *Neuroscience*, 67(4), pp.823-836.
- Xu Z.C. and Pulsinelli W.A., 1996. Electrophysiological changes of CA1 pyramidal neurons following transient forebrain ischemia: an in vivo intracellular recording and staining study. *J Neurophysiol*, 76(3), pp.1689-1697.
- Yamamoto T., Saito O., Aoe T., Bartolozzi A., Sarva J., Zhou J., Kozikowski A., Wroblewska B., Bzdega T. and Neale J.H., 2007. Local administration of N-acetylaspartylglutamate (NAAG) peptidase inhibitors is analgesic in peripheral pain in rats. *Eur J Neurosci*, 25(1), pp.147-158.
- Yan H.D., Ishihara K., Serikawa T. and Sasa M., 2003. Activation by N-acetyl-L-aspartate of acutely dissociated hippocampal neurons in rats via metabotropic glutamate receptors. *Epilepsia*, 44(9), pp.1153-1159.

- Ye Z.C., Wyeth M.S., Baltan-Tekkok S. and Ransom B.R., 2003. Functional hemichannels in astrocytes: a novel mechanism of glutamate release. *J Neurosci*, 23(9), pp.3588-3596.
- Yenari M.A., Kauppinen T.M. and Swanson R.A., 2010. Microglial activation in stroke: therapeutic targets. *Neurotherapeutics*, 7(4), pp.378-391.
- Yodoya E., Wada M., Shimada A., Katsukawa H., Okada N., Yamamoto A., Ganapathy V. and Fujita T., 2006. Functional and molecular identification of sodium-coupled dicarboxylate transporters in rat primary cultured cerebrocortical astrocytes and neurons. *J Neurochem*, 97(1), pp.162-173.
- Yoshioka A., Ikegaki N., Williams M. and Pleasure D., 1996. Expression of N-methyl-D-aspartate (NMDA) and non-NMDA glutamate receptor genes in neuroblastoma, medulloblastoma, and other cells lines. *J Neurosci Res*, 46(2), pp.164-178.
- Yourick D.L., Koenig M.L., Durden A.V. and Long J.B., 2003. N-acetylaspartylglutamate and beta-NAAG protect against injury induced by NMDA and hypoxia in primary spinal cord cultures. *Brain Res*, 991(1-2), pp.56-64.
- Zhang H., Schools G.P., Lei T., Wang W., Kimelberg H.K. and Zhou M., 2008. Resveratrol attenuates early pyramidal neuron excitability impairment and death in acute rat hippocampal slices caused by oxygen-glucose deprivation. *Exp Neurol*, 212(1), pp.44-52.
- Zhang S.C., Ge B. and Duncan I.D., 1999. Adult brain retains the potential to generate oligodendroglial progenitors with extensive myelination capacity. *Proc Natl Acad Sci USA*, 96(7), pp.4089-4094.
- Zhang W., Murakawa Y., Wozniak K.M., Slusher B. and Sima A.A., 2006. The preventive and therapeutic effects of GCPII (NAALADase) inhibition on painful and sensory diabetic neuropathy. *J Neurol Sci*, 247(2), pp.217-223.
- Zhou M., Xu G., Xie M., Zhang X., Schools G.P., Ma L., Kimelberg H.K. and Chen H., 2009. TWIK-1 and TREK-1 are potassium channels contributing significantly to astrocyte passive conductance in rat hippocampal slices. *J Neurosci*, 29(26), pp.8551-8564.
- Zhu X., Bergles D.E. and Nishiyama A., 2008. NG2 cells generate both oligodendrocytes and gray matter astrocytes. *Development*, 135(1), pp.145-157.
- Ziskin J.L., Nishiyama A., Rubio M., Fukaya M. and Bergles D.E., 2007. Vesicular release of glutamate from unmyelinated axons in white matter. *Nat Neurosci*, 10(3), pp.311-320.